11. STATUS OF HIGGS BOSON PHYSICS

Revised May 2016 by M. Carena (Fermi National Accelerator Laboratory and the University of Chicago), C. Grojean (DESY, Hamburg, on leave from ICREA, Barcelona), M. Kado (Laboratoire de l'Accélérateur Linéaire, Orsay), and V. Sharma (University of California, San Diego).

I. Introduction

Understanding the mechanism that breaks the electroweak symmetry and generates the masses of the known elementary particles[1] has been one of the fundamental endeavors in particle physics. The discovery in 2012 by the ATLAS [1] and the CMS [2] Collaborations of a new resonance with a mass of approximately 125 GeV and the subsequent studies of its properties with a much larger data set have provided the first portrait of this mechanism. The mass of this boson has been precisely measured and its production

[1] In the case of neutrinos, it is possible that the electroweak symmetry breaking mechanism plays only a partial role in generating the observed neutrino masses, with additional contributions at a higher scale via the so called see-saw mechanism.

and decay rates are found to be consistent, within errors, with the standard model (SM) predictions. Nevertheless, many theoretical questions remain unanswered and new conundrums about what lies behind the Higgs boson have come to fore. Four years since its discovery, the Higgs boson has turned into a new tool to explore the manifestations of the SM and to probe the physics landscape beyond it.

In the SM [3] the electroweak interactions are described by a gauge field theory invariant under the $\mathrm{SU}(2)_L \times \mathrm{U}(1)_Y$ symmetry group. The mechanism of electroweak symmetry breaking (EWSB) [4] provides a general framework to keep untouched the structure of these gauge interactions at high energies and still generate the observed masses of the W and Z gauge bosons. The EWSB mechanism posits a self-interacting complex doublet scalar field, whose CP-even neutral component acquires a vacuum expectation value (VEV) $v \approx 246\,\mathrm{GeV}$, which sets the scale of electroweak symmetry breaking. Three massless Goldstone bosons are generated and are absorbed to give masses to the W and Z gauge bosons. The remaining component of the complex doublet becomes the Higgs boson – a new fundamental scalar particle. The masses of all fermions are also a consequence of EWSB since the Higgs doublet is postulated to couple to the fermions through Yukawa interactions.

The true structure behind the newly discovered boson – including the exact dynamics that triggers the Higgs VEV– and the corresponding ultraviolet completion is, however, still unsolved. Even if the discovered boson has weak couplings to all known SM degrees of freedom, it is not excluded that it is part of an extended symmetry structure or that it emerges from a light resonance of a strongly coupled sector. It needs to be established whether the Higgs boson is solitary or whether other states populate the EWSB sector.

Without the Higgs boson, the calculability of the SM would have been spoiled. In particular, perturbative unitarity [5, 6] would be lost at high energies as the longitudinal W/Z boson scattering amplitude would grow as the centre-of-mass energy increases. Moreover, the radiative corrections to the gauge boson self-energies would exhibit dangerous logarithmic divergences that would be difficult to reconcile with EW precision data. With the discovery of the Higgs boson, it has been experimentally established that the SM is based on a gauge theory that could a priori be consistently extrapolated to the Planck scale. The Higgs boson must have couplings to W/Z gauge bosons and fermions precisely as those in the SM to maintain the consistency of the theory at high energies, hence, formally there is no need for new physics at the EW scale. However, as the SM Higgs boson is a scalar particle, and therefore without a symmetry to protect its mass, at the quantum level it has sensitivity to the physics in the ultraviolet. Quite generally, the Higgs mass parameter m may be affected by the presence of heavy particles. Specifically, in presence of fermion and boson particles with squared masses $m_i^2 + \lambda_i^2\phi^2/2$, the running of the mass parameter from the scale μ to the scale Q reads

$$m^2(Q) = m^2(\mu) + \delta m^2, \tag{11.1}$$

$$\delta m^2 = \sum_i g_i(-1)^{2S_i}\frac{\lambda_i^2 m_i^2}{32\pi^2}\log(\frac{Q^2}{\mu^2}), \tag{11.2}$$

where the sum is over all particles and g_i and S_i correspond to the number of degrees of freedom and the spin of the particle i. Therefore, particles that couple to the Higgs and

have a large squared mass parameter m_i^2 would induce very large corrections to the Higgs mass parameter, demanding a large fine tuning to explain why m^2 remains small. Hence, in general, light scalars like the Higgs boson cannot naturally survive in the presence of heavy states at the grand-unification, string or Planck scales. This is known as the hierarchy or naturalness problem [7].

There are two broad classes of models addressing the naturalness problem[2]: one is based on a new fermion-boson symmetry in nature called supersymmetry (SUSY) [9–11]. This is a weakly coupled approach to EWSB, and in this case, the Higgs boson remains elementary and the corrections to its mass are screened at the scale at which SUSY is broken and remain insensitive to the details of the physics at higher scales. These theories predict at least three neutral Higgs particles and a pair of charged Higgs particles [12]. One of the neutral Higgs bosons, most often the lightest CP-even Higgs, has properties that resemble those of the SM Higgs boson. It is referred to as a SM-like Higgs boson, meaning that its VEV is predominantly responsible for EWSB, and hence has SM-like couplings to the W and Z gauge bosons.

The other approach invokes the existence of strong interactions at a scale of the order of a TeV or above and induces strong breaking of the electroweak symmetry [13]. In the original incarnation of this second approach, dubbed technicolor, the strong interactions themselves trigger EWSB without the need of a Higgs boson. Another possibility, more compatible with the ATLAS and CMS discovery, is that the strong interactions produce four light resonances identified with the Higgs doublet and EWSB proceeds through vacuum misalignment [14] (see Refs. [15, 16] for recent reviews).

Both approaches can have important effects on the phenomenology of the Higgs boson associated with EWSB. Also, in each case the Higgs role in unitarization is shared by other particles: additional Higgs bosons in supersymmetry, or new particles in the strong sector.

A third option has also been considered in the literature. It is also a variation of technicolor or Higgsless models [13, 17]. In light of the Higgs boson discovery these models are ruled out. Nevertheless, there still exists the possibility that the Higgs boson discovered at the LHC is in fact the Goldstone boson of the spontaneous breaking of scale invariance at a scale f [18, 19]. However, given the good agreement of the coupling measurements with the SM predictions, this dilaton/radion scenario now requires involved model-building.

The naturalness problem has been the prime argument for new physics at the TeV scale, and sizable effects on the Higgs boson properties were expected. But the apparent agreement of the Higgs couplings with the SM predictions, together with the strong bounds inherited from precision electroweak and flavor data leaves open the possibility that the Higgs boson may very well be elementary, weakly coupled and solitary up to the Planck scale. However, absence of evidence is not evidence of absence. It is possible that new states present at the TeV scale to stabilize the Higgs mass might simply be elusive at

[2] Another solution to the naturalness problem is to lower the fundamental scale of quantum gravity, like for instance in models with large extra-dimensions, see Ref. [8].

the LHC because they do not carry a color charge. Twin Higgs [20] models were the first incarnation of this neutral naturalness idea [21]. A more extreme recent proposal [22] relies on the cosmological evolution of the Universe to drive the Higgs boson mass to a value much smaller than the cutoff of the theory and alleviates the hierarchy problem without the need for TeV scale new physics.

Extensions of the SM Higgs sector without low-energy supersymmetry will also be discussed in this review. These type of models do not address the naturalness problem in a specific manner, but provide grounds to explore new Higgs boson signals in a more model-independent way, with different types of coupling structure to fermions and gauge bosons. Extended Higgs sectors are usually quite restricted by experimental constraints from precision electroweak measurements as well as constraints from flavor-changing neutral- and charged-current effects.

Section II is a review of the Higgs boson of the SM, discussing its properties and the production mechanisms and decay rates. In Section III, the SM Higgs boson analysis channels are described. In Section IV, the combination of the main analysis channels is discussed. In Section V, measurements of the main quantum numbers and the total width of the Higgs boson are given. In Section VI, a general theoretical framework to describe the deviations of the Higgs couplings from the SM predictions is introduced and the experimental measurements of these Higgs couplings is reviewed together with the analysis establishing the spin and CP-properties of the Higgs boson. Section VII presents, in detail, some of the most interesting models proposed for Higgs extensions of the SM and considers their experimental signatures. Section VIII provides a brief outlook.

II. The standard model and the mechanism of electroweak symmetry breaking

In the SM [3], electroweak symmetry breaking [4] is responsible for generating mass for the W and Z gauge bosons rendering the weak interactions short range. The SM scalar potential reads:

$$V(\Phi) = m^2\Phi^\dagger\Phi + \lambda(\Phi^\dagger\Phi)^2 \tag{11.3}$$

with the Higgs field Φ being a self-interacting SU(2) complex doublet (four real degrees of freedom) with weak hypercharge Y=1 (the hypercharge is normalized such that $Q = T_{3L} + Y/2$):

$$\Phi = \frac{1}{\sqrt{2}}\begin{pmatrix}\sqrt{2}\phi^+\\ \phi^0 + ia^0\end{pmatrix}, \tag{11.4}$$

where ϕ^0 and a^0 are the CP-even and CP-odd neutral components, and ϕ^+ is the complex charged component of the Higgs doublet, respectively. $V(\Phi)$ is the most general renormalizable scalar potential and if the quadratic term is negative the neutral component of the scalar doublet acquires a non-zero vacuum expectation value (VEV)

$$\langle\Phi\rangle = \frac{1}{\sqrt{2}}\begin{pmatrix}0\\ v\end{pmatrix}, \tag{11.5}$$

with $\phi^0 = H + \langle\phi^0\rangle$ and $\langle\phi^0\rangle \equiv v$, inducing the spontaneous breaking of the SM gauge symmetry $\mathrm{SU(3)}_C \times \mathrm{SU(2)}_L \times \mathrm{U(1)}_Y$ into $\mathrm{SU(3)}_C \times \mathrm{U(1)}_{\mathrm{em}}$. The global minimum of

the theory defines the ground state, and spontaneous symmetry breaking implies that there is a symmetry of the system (Lagrangian) that is not respected by the ground state. The Higgs field permeates the entire universe and through its self-interactions can cause spontaneous electroweak symmetry breaking (EWSB) in the vacuum. From the four generators of the $\mathrm{SU}(2)_L \times \mathrm{U}(1)_Y$ gauge group, three are spontaneously broken, implying that they lead to non-trivial transformations of the ground state and indicate the existence of three massless Goldstone bosons identified with three of the four Higgs field degrees of freedom. The Higgs field couples to the W_μ and B_μ gauge fields associated with the $\mathrm{SU}(2)_L \times \mathrm{U}(1)_Y$ local symmetry through the covariant derivative appearing in the kinetic term of the Higgs Lagrangian,

$$\mathcal{L}_{\mathrm{Higgs}} = (D_\mu \Phi)^\dagger (D^\mu \Phi) - V(\Phi)\,, \tag{11.6}$$

where $D_\mu \Phi = (\partial_\mu + i g \sigma^a W^a_\mu/2 + i g' Y B_\mu/2)\Phi$, g and g' are the SU(2) and U(1) gauge couplings, respectively, and $\sigma^a, a = 1,2,3$ are the usual Pauli matrices. As a result, the neutral and the two charged massless Goldstone degrees of freedom mix with the gauge fields corresponding to the broken generators of $\mathrm{SU}(2)_L \times \mathrm{U}(1)_Y$ and become the longitudinal components of the Z and W physical gauge bosons, respectively. The Z and W gauge bosons acquire masses,

$$M_W^2 = \frac{g^2 v^2}{4}\,, \quad M_Z^2 = \frac{(g'^2 + g^2)v^2}{4}. \tag{11.7}$$

The fourth generator remains unbroken since it is the one associated to the conserved $\mathrm{U}(1)_{\mathrm{em}}$ gauge symmetry, and its corresponding gauge field, the photon, remains massless. Similarly the eight color gauge bosons, the gluons, corresponding to the conserved $\mathrm{SU}(3)_C$ gauge symmetry with 8 unbroken generators, also remain massless. Hence, from the initial four degrees of freedom of the Higgs field, two are absorbed by the $W^\pm$ gauge bosons, one by the Z gauge boson, and there is one remaining degree of freedom, H, that is the physical Higgs boson — a new scalar particle. The Higgs boson is neutral under the electromagnetic interactions and transforms as a singlet under $\mathrm{SU}(3)_C$ and hence does not couple at tree level to the massless photons and gluons.

The fermions of the SM acquire mass through new renormalizable interactions between the Higgs field and the fermions: the Yukawa interactions,

$$\mathcal{L}_{\mathrm{Yukawa}} = -\hat{h}_{d_{ij}} \bar{q}_{L_i} \Phi\, d_{R_j} - \hat{h}_{u_{ij}} \bar{q}_{L_i} \tilde{\Phi} u_{R_j} - \hat{h}_{l_{ij}} \bar{l}_{L_i} \Phi\, e_{R_j} + h.c., \tag{11.8}$$

which respect the symmetries of the SM but generate fermion masses once EWSB occurs. In the above, $\tilde{\Phi} = i\sigma_2 \Phi^*$ and q_L (l_L) and u_R, d_R (e_R) are the quark (lepton) $\mathrm{SU}(2)_L$ doublets and singlets, respectively, while each term is parametrized by a 3×3 matrix in family space. The mass term for neutrinos is omitted, but could be added in an analogous manner to the up-type quarks when right-handed neutrinos are supplementing the SM particle content. Once the Higgs acquires a VEV, and after rotation to the fermion mass eigenstate basis that also diagonalizes the Higgs-fermion interactions, $\hat{h}_{f_{ij}} \to h_{f_i} \delta_{ij}$, all fermions acquire a mass given by $m_{f_i} = h_{f_i} v/\sqrt{2}$. The indices $i, j = 1,2,3$ refer to the

three families in the up-quark, down-quark or charged lepton sectors. It should be noted that the EWSB mechanism provides no additional insight on possible underlying reasons for the large variety of masses of the fermions, often referred to as the flavor hierarchy. The fermion masses, accounting for a large number of the free parameters of the SM, are simply translated into Yukawa couplings h_f.

II.1. The SM Higgs boson mass, couplings and quantum numbers

The SM Higgs boson is a CP-even scalar of spin 0. Its mass is given by $m_H = \sqrt{2\lambda}\, v$, where λ is the Higgs self-coupling parameter in $V(\Phi)$. The expectation value of the Higgs field, $v = (\sqrt{2}G_F)^{-1/2} \approx 246\,\text{GeV}$, is fixed by the Fermi coupling G_F, which is determined with a precision of 0.6 ppm from muon decay measurements [23]. The quartic coupling λ is a free parameter in the SM, and hence, there is no a priori prediction for the Higgs mass. Moreover the sign of the mass parameter $m^2 = -\lambda v^2$ is crucial for the EW symmetry breaking to take place, but it is not specified in the SM. The experimentally measured Higgs mass, $m_H \simeq$125 GeV, implies that $\lambda \simeq 0.13$ and $|m| \simeq 88.8\,\text{GeV}$. It is interesting to observe that in the SM one needs to assume that the mass term in the potential is negative in order to trigger EWSB. In other theories beyond the SM (BSM), such as supersymmetry, the analogue of the Higgs mass parameter can be made negative dynamically.

The Higgs boson couplings to the fundamental particles are set by their masses. This is a new type of interaction; very weak for light particles, such as up and down quarks, and electrons, but strong for heavy particles such as the W and Z bosons and the top quark. More precisely, the SM Higgs couplings to fundamental fermions are linearly proportional to the fermion masses, whereas the couplings to bosons are proportional to the square of the boson masses. The SM Higgs boson couplings to gauge bosons and fermions, as well as the Higgs boson self coupling, are summarized in the following Lagrangian:

$$\begin{aligned}\mathcal{L} = &- g_{Hff}\bar{f}fH + \frac{g_{HHH}}{6}H^3 + \frac{g_{HHHH}}{24}H^4 \\ &+ \delta_V V_\mu V^\mu \left(g_{HVV}H + \frac{g_{HHVV}}{2}H^2\right)\end{aligned} \tag{11.9}$$

with

$$g_{Hf\bar{f}} = \frac{m_f}{v}\,, \quad g_{HVV} = \frac{2m_V^2}{v}\,, \quad g_{HHVV} = \frac{2m_V^2}{v^2}\,, \tag{11.10}$$

$$g_{HHH} = \frac{3m_H^2}{v}\,, \quad g_{HHHH} = \frac{3m_H^2}{v^2}\,, \tag{11.11}$$

where $V = \text{W}^\pm$ or Z and $\delta_W = 1, \delta_Z = 1/2$. As a result, the dominant mechanisms for Higgs boson production and decay involve the coupling of H to W, Z and/or the third generation quarks and leptons. The Higgs boson coupling to gluons [24, 25] is induced at leading order by a one-loop process in which H couples to a virtual $t\bar{t}$ pair. Likewise, the Higgs boson coupling to photons is also generated via loops, although in this case the

one-loop graph with a virtual W^+W^- pair provides the dominant contribution [12] and the one involving a virtual $t\bar{t}$ pair is subdominant.

II.2. The SM custodial symmetry

The SM Higgs Lagrangian, $\mathcal{L}_{\rm Higgs} + \mathcal{L}_{\rm Yukawa}$ of Eq. (11.6) and Eq. (11.8), is, by construction, $\mathrm{SU}(2)_L \times \mathrm{U}(1)_Y$ gauge invariant, but it also has an approximate global symmetry. In the limit $g' \to 0$ and $h_f \to 0$, the Higgs sector has a global $\mathrm{SU}(2)_R$ symmetry, and hence in such a limit it is invariant under a global $\mathrm{SU}(2)_L \times \mathrm{SU}(2)_R$ symmetry, with $\mathrm{SU}(2)_L$ just being the global variant of the SM chiral gauge symmetry. This symmetry is preserved for non-vanishing Yukawa couplings, provided $h_u = h_d$. Once the Higgs acquires a VEV, both the $\mathrm{SU}(2)_L$ and $\mathrm{SU}(2)_R$ symmetry groups are broken but the subgroup $\mathrm{SU}(2)_{L+R}$ remains unbroken and is the subgroup that defines the custodial symmetry of the SM [26].

In the limit $g' \to 0$, the W and Z gauge bosons have equal mass and form a triplet of the $\mathrm{SU}(2)_{L+R}$ unbroken global symmetry. Using the expressions for the W and Z gauge boson masses in term of the gauge couplings, one obtains

$$\frac{M_W^2}{M_Z^2} = \frac{g^2}{g'^2 + g^2} = \cos^2\theta_W \quad \text{or} \quad \rho \equiv \frac{M_W^2}{M_Z^2 \cos^2\theta_W} = 1 \tag{11.12}$$

at tree level. The custodial symmetry protects the above relation between the W and Z masses under radiative corrections. All corrections to the ρ parameter are therefore proportional to terms that break the custodial symmetry. For instance, radiative corrections involving the Higgs are proportional to g'^2. Since $m_t \neq m_b$, there are also relevant radiative corrections generated by massive fermions. They are proportional to $m_t^2 + m_b^2 - 2(m_t^2 m_b^2)\,\log(m_t^2/m_b^2)/(m_t^2 - m_b^2)$ [27].

One can conceive of BSM theories in which the Higgs is a pseudo Nambu–Goldstone boson of a strongly interacting sector [28], and/or where there are additional degrees of freedom that may contribute to the W and Z mass via virtual loops, but in as much as the electroweak sector has a manifest custodial symmetry, the theory is protected from large radiative corrections. Precision measurements of electroweak observables are powerful in constraining such large radiative corrections. The custodial isospin symmetry is also a powerful probe of BSM physics. For a pedagogical discussion, see Ref. [29].

II.3. Stability of the Higgs potential

The discovery of a scalar particle with mass $m_H \approx 125\,\mathrm{GeV}$ has far reaching consequences within the SM framework. In particular, the precise value of m_H determines the value of the quartic coupling λ at the electroweak scale and makes it possible to study its behavior up to high energy scales. A larger value of m_H would have implied that the Higgs self-coupling would become non-perturbative at some scale Λ that could be well below the Planck scale. Specifically, from the measured values of the Higgs mass, the top-quark mass, the W and Z boson masses, and the strong gauge coupling, all within their experimental uncertainties, it follows that, as with the SM gauge and

Yukawa couplings, the Higgs quartic coupling remains perturbative all the way up to M_{Planck} [5, 6, 30], thereby rendering the SM a consistent, calculable theory.

The recently measured Higgs mass, however, generates an EW Higgs potential in which the vacuum state is at the edge between being stable and metastable. Indeed, allowing all relevant SM observables to fluctuate within their experimental and theoretical uncertainties, the metastability condition seems to be favored [31]. The high energy evolution of λ shows that it becomes negative at energies $\Lambda = \mathcal{O}(10^{10} - 10^{12})$ GeV, with a broader range if the top quark mass exceeds its current measured value by 3σ. When this occurs, the SM Higgs potential develops an instability and the long term existence of the EW vacuum is challenged. This behavior may call for new physics at an intermediate scale before the instability develops, i.e., below M_{Planck} or, otherwise, the electroweak vacuum remains metastable [32]. Reference [33] studied how new physics at M_{Planck} could influence the stability of the EW vacuum and possibly modify this conclusion. The consequences of the instability of the EW vacuum on high-scale inflation have been discussed in Refs. [34].

Within the SM framework, the relevant question is related to the lifetime of the EW metastable vacuum that is determined by the rate of quantum tunneling from this vacuum into the true vacuum of the theory. The running of the Higgs self coupling slows down at high energies with a cancellation of its β-function at energies just one to two orders of magnitude below the Planck scale [31, 35]. This slow evolution of the quartic coupling is responsible for saving the EW vacuum from premature collapse, allowing it to survive much longer times than those relevant from astrophysical considerations. It might help the Higgs boson to play the role of an inflaton [36] (see, however, Ref. [37] and references therein for potential issues with this Higgs-as-inflaton idea).

II.4. Higgs production and decay mechanisms

Reviews of the SM Higgs boson's properties and phenomenology, with an emphasis on the impact of loop corrections to the Higgs boson decay rates and cross sections, can be found in Refs. [38–45]. The state-of-the-art of the theoretical calculations in the main different production channels is summarized in Table 11.1.

II.4.1. Production mechanisms at hadron colliders

The main production mechanisms at the Tevatron collider and the LHC are gluon fusion, weak-boson fusion, associated production with a gauge boson and associated production with a pair of top/antitop quarks. Figure 11.1 depicts representative diagrams for these dominant Higgs production processes.

The cross sections for the production of a SM Higgs boson as a function of $\sqrt{s}$, the center of mass energy, for pp collisions, including bands indicating the theoretical uncertainties, are summarized in Fig. 11.2(left) [46]. A detailed discussion, including uncertainties in the theoretical calculations due to missing higher-order effects and experimental uncertainties on the determination of SM parameters involved in the calculations can be found in Refs. [42–45]. These references also contain state-of-the-art discussions on the impact of PDF's uncertainties, QCD scale uncertainties and uncertainties due to different matching

Table 11.1: State-of-the-art of the theoretical calculations in the main different Higgs production channels in the SM, and main MC tools used in the simulations

ggF	VBF	VH	$t\bar{t}H$
Fixed order:	Fixed order:	Fixed order:	Fixed order:
NNLO QCD + NLO EW	NNLO QCD	NLO QCD+EW	NLO QCD
(HIGLU, iHixs, FeHiPro, HNNLO)	(VBF@NNLO)	(V2HV and HAWK)	(Powheg)
Resummed:	Fixed order:	Fixed order:	(MG5_aMC@NLO)
NNLO + NNLL QCD	NLO QCD + NLO EW	NNLO QCD	
(HRes)	(HAWK)	(VH@NNLO)	
Higgs p_T:			
NNLO+NNLL			
(HqT, HRes)			
Jet Veto:			
N3LO+NNLL			

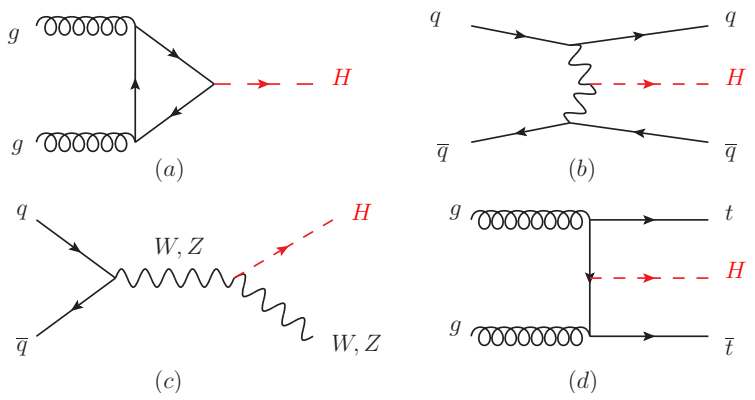

Figure 11.1: Generic Feynman diagrams contributing to the Higgs production in (a) gluon fusion, (b) weak-boson fusion, (c) Higgs-strahlung (or associated production with a gauge boson) and (d) associated production with top quarks.

procedures when including higher-order corrections matched to parton shower simulations as well as uncertainties due to hadronization and parton-shower events.

Table 11.2, from Refs. [42–45], summarizes the Higgs boson production cross sections and relative uncertainties for a Higgs mass of 125 GeV, for $\sqrt{s} = 7$, 8, 13 and 14 TeV. The Higgs boson production cross sections in $p\bar{p}$ collisions at $\sqrt{s} = 1.96$ TeV for the Tevatron are obtained from Ref. [47].

(i) Gluon fusion production mechanism

At high-energy hadron colliders, the Higgs boson production mechanism with the largest cross section is the gluon-fusion process, $gg \to H + X$, mediated by the exchange of a virtual, heavy top quark [48]. Contributions from lighter quarks propagating in the loop are suppressed proportional to m_q^2. QCD radiative corrections to the gluon-fusion

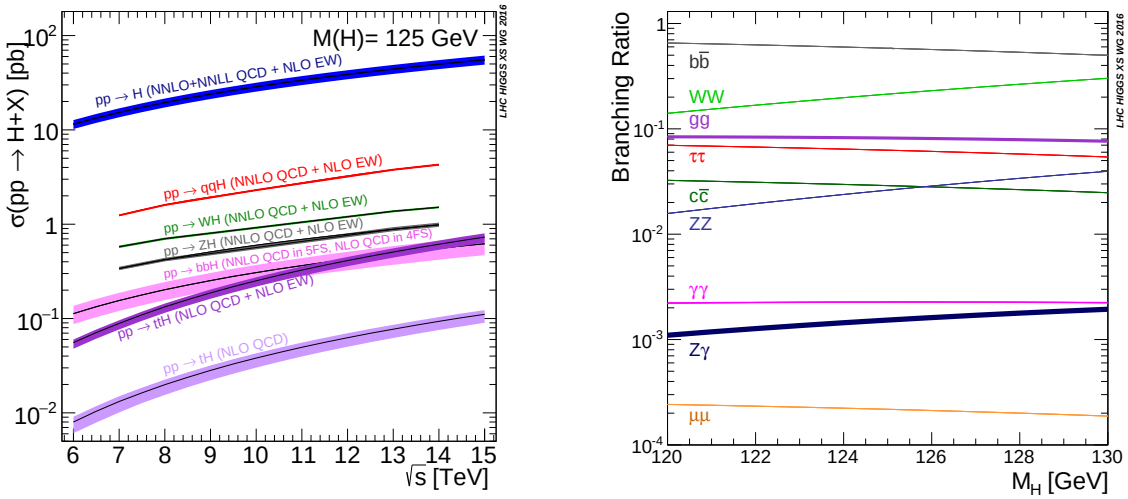

Figure 11.2: (Left) The SM Higgs boson production cross sections as a function of the center of mass energy, $\sqrt{s}$, for pp collisions. The theoretical uncertainties [46] are indicated as bands. (Right) The branching ratios for the main decays of the SM Higgs boson near $m_H = 125\,\text{GeV}$. The theoretical uncertainties [44, 45] are indicated as bands.

Table 11.2: The SM Higgs boson production cross sections for $m_H = 125\,\text{GeV}$ in pp collisions ($p\bar{p}$ collisions at $\sqrt{s} = 1.96\,\text{TeV}$ for the Tevatron), as a function of the center of mass energy, $\sqrt{s}$. The predictions for the LHC energies are taken from Refs. [42–45], the ones for the Tevatron energy are from Ref. [47]. The predictions for the ggF channel do not include the latest N3LO results which significantly reduce the theoretical uncertainties.

$\sqrt{s}$ (TeV)	Production cross section (in pb) for $m_H = 125\,\text{GeV}$					
	ggF	VBF	WH	ZH	$t\bar{t}H$	total
1.96	$0.95^{+17\%}_{-17\%}$	$0.065^{+8\%}_{-7\%}$	$0.13^{+8\%}_{-8\%}$	$0.079^{+8\%}_{-8\%}$	$0.004^{+10\%}_{-10\%}$	1.23
7	$15.3^{+10\%}_{-10\%}$	$1.24^{+2\%}_{-2\%}$	$0.58^{+3\%}_{-3\%}$	$0.34^{+4\%}_{-4\%}$	$0.09^{+8\%}_{-14\%}$	17.5
8	$19.5^{+10\%}_{-11\%}$	$1.60^{+2\%}_{-2\%}$	$0.70^{+3\%}_{-3\%}$	$0.42^{+5\%}_{-5\%}$	$0.13^{+8\%}_{-13\%}$	22.3
13	$44.1^{+11\%}_{-11\%}$	$3.78^{+2\%}_{-2\%}$	$1.37^{+2\%}_{-2\%}$	$0.88^{+5\%}_{-5\%}$	$0.51^{+9\%}_{-13\%}$	50.6
14	$49.7^{+11\%}_{-11\%}$	$4.28^{+2\%}_{-2\%}$	$1.51^{+2\%}_{-2\%}$	$0.99^{+5\%}_{-5\%}$	$0.61^{+9\%}_{-13\%}$	57.1

process are very important and have been studied in detail. Including the full dependence on the (top, bottom, charm) quark and Higgs boson masses, the cross section has been calculated at the next-to-leading order (NLO) in α_s [49, 50]. To a very good approximation, the leading top-quark contribution can be evaluated in the limit $m_t \to \infty$ by matching the SM to an effective theory. The gluon-fusion amplitude is then evaluated from an effective Lagrangian containing a local $HG^a_{\mu\nu}G^{a\,\mu\nu}$ operator [24, 25]. In this

approximation the cross section is known at NLO [51], at next-to-next-to-leading order (NNLO) [52], and recently the computation at next-to-next-to-next-to-leading order (N3LO) has been completed [53]. The validity of the large top-quark mass approximation in NNLO calculations has been established at the percent level by means of approximate calculations of the m_t dependence based on asymptotic expansions [54]. Moreover, the validity of the effective theory with infinite m_t is greatly enhanced by rescaling the result by the exact LO result: $\sigma = (\sigma^{LO}_{m_t}/\sigma^{LO}_{m_t=\infty}) \times \sigma_{m_t=\infty}$ [45].

The NLO QCD corrections increase the leading-order prediction for the cross section by about 80%, the NNLO corrections further enhance the cross section by approximately 30% (at $\mu_f = \mu_r = m_H/2$). Electroweak radiative corrections have been computed at NLO and increase the cross section by about 5% for $m_H \simeq 125\,\text{GeV}$ [55]. Mixed QCD-electroweak corrections of $O(\alpha\alpha_s)$ have been calculated in Ref. [56].

The NLO and NNLO fixed-order QCD predictions for the gluon-fusion cross section have been improved by resumming the soft, virtual and collinear gluon contributions to the cross section at next-to-next-to-leading logarithmic (NNLL) and partial NNNLL accuracy [57]. Precise predictions for the gluon-fusion cross section for different Higgs boson masses and LHC energies, and including detailed error estimates, have been obtained by combining the NNLO fixed-order QCD results with soft-gluon resummation at NNLL or NNNLL accuracy and two-loop electroweak corrections, and using the most recent sets of parton distribution functions [56, 58].

The perturbative QCD computation has been recently extended to N3LO. At this order the perturbation series is rather stable with a mere enhancement of 3% only, with a central value completely insensitive to threshold resummation effects with the scale choice mentioned above [53, 59, 45]. At the LHC with a center-of-mass energy of 13 TeV, the most up-to-date value for the production cross section of a 125 GeV Higgs boson amounts to [45]

$$\sigma^{N3LO}_{ggF} = 48.6\,\text{pb}^{+2.2\,\text{pb}(+4.6\%)}_{-3.3\,\text{pb}(-6.7\%)}(\text{theory}) \pm 1.6\,\text{pb}(3.2\%)(\text{PDF} + \alpha_s).$$

The difference between this result and the value quoted in Table 11.2 is due to several effects that include: the choice of optimal renormalization and factorization scales, the effect of the N3LO corrections, the different sets of parton distribution functions and value of α_s, as well as smaller differences due to the treatment of finite quark-mass effects [53].

Besides considering the inclusive Higgs boson production cross section at the LHC, it is important to study differential distributions in order to probe the properties of the Higgs boson in a detailed way. A more exclusive account of Higgs production is also required because experimental analyses often impose cuts on the final states in order to improve the signal-to-background ratio. To this end, it is useful to define benchmark cuts and compare the differential distributions obtained at various levels of theoretical accuracy (i.e., at NLO or NNLO) with Monte Carlo generators. Many search modes for the Higgs boson are carried out by separating the events according to the number of jets or the transverse momentum and rapidity of the Higgs boson. For $p_T < 30\,\text{GeV}$, predictions for the transverse-momentum distribution can only be trusted after large logarithms of the form $\alpha_s^n \ln^{2n-1}(m_H/p_T)$ have been resummed to all orders in perturbation theory [60].

This has been accomplished with NNLL accuracy [61], and the results have been matched onto the fixed-order prediction at NNLO [62]. Electroweak corrections have been studied in Ref. [63]. The effect of the non-zero quark mass on the pT spectrum has been considered in Refs. [64, 65], while the effect of the finite top mass on other differential observables has been studied in Refs. [66, 67]. There has been much activity in computing Higgs plus jet(s) production processes at NLO (see e.g. Refs. [68] and [69] for associated production with one and two jets, respectively), and even at NNLO [70]. In addition, efforts to improve the calculation of the Higgs production cross section with a jet veto (the "0-jet bin") by resumming large logarithms of the form $\alpha_s^n \ln^{2n-1}(m_H/p_T^{\rm veto})$ at NNLL order and beyond [71] have been made. Recently, reference results for the resummed cross section at NNLL have been combined with the N3LO result for the inclusive cross section to obtain accurate predictions for the jet-veto efficiency and zero-jet cross section [72]. Accurate predictions for the jet-veto cross section are required, e.g., to suppress the $t\bar{t}$ background in the $H \to WW$ channel [73].

(ii) Vector boson fusion production mechanism

The SM Higgs production mode with the second-largest cross section at the LHC is vector boson fusion (VBF). At the Tevatron collider, VBF also occurred, but for $m_H = 125\,\text{GeV}$ had a smaller cross section than Higgs production in association with a W or Z boson. Higgs production via VBF, $qq \to qqH$, proceeds by the scattering of two (anti-)quarks, mediated by t- or u-channel exchange of a W or Z boson, with the Higgs boson radiated off the weak-boson propagator. The scattered quarks give rise to two hard jets in the forward and backward regions of the detector. Because of the color-singlet nature of the weak-gauge boson exchange, gluon radiation from the central-rapidity regions is strongly suppressed. These characteristic features of VBF processes can be exploited to distinguish them from overwhelming QCD backgrounds, including gluon-fusion induced Higgs + 2 jet production, and from s-channel WH or ZH production with a hadronically decaying weak gauge boson. After the application of specific selection cuts, the VBF channel provides a particularly clean environment, not only for Higgs searches but also for the determination of Higgs boson couplings at the LHC [74].

Computations for total cross sections and differential distributions to Higgs production via VBF including NLO QCD and EW corrections have been presented in Refs. [39, 75] and are available in the form of flexible parton-level Monte-Carlo generators. Parton-shower effects have been considered in Ref. [76]. The NNLO QCD corrections to the total rate have been presented in Refs. [77]. They reduce the residual scale uncertainties on the inclusive cross section to approximately 2%. The uncertainties due to parton distributions are estimated to be at the same level. Fully differential predictions at NNLO have been computed recently [78], suggesting that the cross section under VBF cuts receives NNLO corrections that are larger than in the inclusive case and may reach O(5-6%).

(iii) WH and ZH associated production mechanism

The next most relevant Higgs boson production mechanisms after gluon fusion and VBF at the LHC, and the most relevant ones after gluon fusion at the Tevatron collider, are associated production with W and Z gauge bosons. The cross sections for the

associated production processes, $pp \to VH + X$, with $V = W^{\pm}, Z$ receive contributions at NLO given by NLO QCD corrections to the Drell–Yan cross section [79–81] and from NLO EW corrections. The latter, unlike the QCD corrections, do not respect the factorization into Drell–Yan production since there are irreducible box contributions already at one loop [82]. At NNLO, the Drell-Yan-like corrections to WH production also give the bulk of the corrections to ZH production [83]. For ZH production there are, however, gluon-gluon induced contributions that do not involve a virtual Z gauge boson but are such that the Z gauge boson and H boson couple to gluons via top-quark loops [84]. In addition, WH and ZH production receive non Drell–Yan-like corrections in the $q\bar{q}'$ and $q\overline{q}$ initiated channels, respectively, at the NNLO level, where the Higgs is radiated off top-quark loops [85]. The full QCD corrections up to NNLO order, the NLO EW corrections and the NLO corrections to the gluon-gluon channel are available in VH@NNLO [86].

As neither the Higgs boson nor the weak gauge bosons are stable particles, their decays also have to be taken into account. Providing full kinematical information for the decay products can furthermore help in the suppression of large QCD backgrounds. Differential distributions for the processes $pp \to WH \to \nu_\ell \ell H$ and $pp \to ZH \to \ell^+\ell^- H/\nu_\ell \bar{\nu}_\ell H$, including NLO QCD and EW corrections, have been presented in Ref. [87]. The NNLO QCD corrections to differential observables for WH production at the LHC, including the leptonic decays of the W boson and the decay of the Higgs boson into a $b\bar{b}$ pair, are presented in Ref. [88]. Calculations at the same level, including also the ZH process have been performed [89, 90]. The WH production mode has also been matched to a parton shower at NNLO accuracy [91]. The WH and ZH production modes, together with Higgs production in association with a top-quark pair, provide a relatively clean environment for studying the decay of the Higgs boson into bottom quarks.

(iv) Higgs production in association with $t\bar{t}$

Higgs radiation off top quarks, $pp \to t\bar{t}H$, can provide important information on the the top-Higgs Yukawa coupling and gives access to the Higgs decay into bottom quarks. The LO cross section for this production process was computed in Ref. [92]. Later, the NLO QCD corrections [93] were evaluated yielding a moderate increase in the total cross section of at most 20%, but reducing significantly the scale dependence of the inclusive cross section. The total theoretical errors, estimated by combining the uncertainties from factorization and renormalization scales, strong gauge coupling, and parton distributions, amount to 10–15% of the corresponding inclusive cross section. Interfaces between NLO QCD calculations for $t\bar{t}H$ production with parton-shower Monte Carlo programs have been provided in Ref. [94]. These programs provide the most flexible tools to date for the computation of differential distributions, including experimental selection cuts and vetoes on the final-state particles and their decay products.

(v) Other single Higgs production mechanisms at the LHC

The Higgs production in association with a single top quark, though subdominant, can bring valuable information, in particular regarding the sign of the top Yukawa coupling. This is due to an almost totally destructive interference between two large contributions, one where the Higgs couples to a space-like W boson and the other where it couples

to the top quark. This process has been computed at NLO in a five-flavor scheme [95] and amounts to about 90 fb at $\sqrt{s} = 14$ TeV (with the opposite sign of the top Yukawa coupling, the cross section increases by one order of magnitude).

The Higgs boson production in association with bottom quarks is known at NNLO in the case of five quark flavors [96–98]. The coupling of the Higgs boson to a b quark is suppressed in the SM by the bottom-quark mass over the Higgs VEV, m_b/v, implying that associated production of a SM Higgs boson with b quarks is small at the LHC. Yet, at high energy, large logarithms are present and need to be resummed, leading to an enhancement of the inclusive cross section. At $\sqrt{s} = 14$ TeV the bbH cross section can be as large as 600 fb, still two orders of magnitude below the ggF production cross section. In a two Higgs doublet model or a supersymmetric model, which will be discussed in Section VII, this coupling is proportional to the ratio of neutral Higgs boson vacuum expectation values, $\tan\beta$, and can be significantly enhanced for large values of this ratio. Consequently, the bbH mode can even become the dominant production process for the Higgs boson.

The Higgs production in association with charm quarks is also known at NNLO and is of the order of 85 fb at $\sqrt{s} = 13$ TeV.

(vi) Double Higgs production at the LHC

The main interest in the double Higgs production is that it provides invaluable information on the Higgs potential. In particular, it gives access to the Higgs cubic self-interaction. The dominant production is via gluon fusion $gg \to HH$. The NLO [99] and NNLO [100] fixed order corrections to $gg \to HH$ are known in the infinite top mass limit and, recently, the complete NLO corrections with all top quark mass effects also became available [101]. The QCD corrections are large, typically doubling the cross section from LO to NLO and further enhancing it by 20% from NLO to NNLO. At the differential level, the destructive interference between the box and the triangle contributions complicates the predictions made in the infinite top mass limit for both the HH invariant mass and the leading Higgs p_T distributions. With an inclusive cross section of about 40 fb at $\sqrt{s} = 13$ TeV and a difficult signal vs. background discrimination, the double Higgs production remains a challenging channel to probe and will greatly benefit from the high-luminosity run of the LHC.

II.4.2. Production mechanisms at e^+e^- colliders

The main Higgs boson production cross sections at an e^+e^- collider are the Higgs-strahlung process $e^+e^- \to ZH$ [6, 24, 102], and the WW fusion process [103] $e^+e^- \to \bar{\nu}_e\nu_e W^*W^* \to \bar{\nu}_e\nu_e H$. The cross-section for the Higgs-strahlung process scales as s^{-1} and is dominant at low energies, while the cross-section for the WW fusion process scales as $\ln(s/m_H^2)$ and dominates at high energies [104–106]. The ZZ fusion mechanism, $e^+e^- \to e^+e^-Z^*Z^* \to e^+e^-H$, also contributes to Higgs boson production, with a cross-section suppressed by an order of magnitude with respect to that of WW fusion. The process $e^+e^- \to t\bar{t}H$ [107, 108] becomes important for $\sqrt{s} \geq 500$ GeV. For a more detailed discussion of Higgs production properties at lepton colliders see, for example, Refs. [40, 41, 109, 110] and references therein.

II.4.3. SM Higgs branching ratios and total width

For the understanding and interpretation of the experimental results, the computation of all relevant Higgs decay widths is essential, including an estimate of their uncertainties and, when appropriate, the effects of Higgs decays into off-shell particles with successive decays into lighter SM ones. A Higgs mass of about 125 GeV provides an excellent opportunity to explore the Higgs couplings to many SM particles. In particular the dominant decay modes are $H \to b\bar{b}$ and $H \to WW^*$, followed by $H \to gg$, $H \to \tau^+\tau^-$, $H \to c\bar{c}$ and $H \to ZZ^*$. With much smaller rates follow the Higgs decays into $H \to \gamma\gamma$, $H \to \gamma Z$ and $H \to \mu^+\mu^-$. Since the decays into gluons, diphotons and $Z\gamma$ are loop induced, they provide indirect information on the Higgs couplings to WW, ZZ and $t\bar{t}$ in different combinations. The uncertainties in the branching ratios include the missing higher-order corrections in the theoretical calculations as well as the errors in the SM input parameters, in particular fermion masses and the QCD gauge coupling, involved in the decay. In the following the state-of-the-art of the theoretical calculations will be discussed and the reader is referred to Refs. [42, 43, 111] for detail.

The evaluation of the radiative corrections to the fermionic decays of the SM Higgs are implemented in HDECAY [112] at different levels of accuracy. The computations of the $H \to b\bar{b}$ and $H \to c\bar{c}$ decays include the complete massless QCD corrections up to N4LO, with a corresponding scale dependence of about 0.1% [113]. Both the electroweak corrections to $H \to b\bar{b}$, $c\bar{c}$ as well as $H \to \tau^+\tau^-$ are known at NLO [114] providing predictions with an overall accuracy of about 1-2% for $m_H \simeq 125$ GeV.

The loop induced decays of the SM Higgs are known at NLO and partially beyond that approximation. For $H \to gg$, the QCD corrections are known up to N3LO in the limit of heavy top quarks [115, 50] and the uncertainty from the scale dependence is about 3%. For the $H \to \gamma\gamma$, the full NLO QCD corrections are available [50, 116] and the three-loop QCD corrections have also been evaluated [117]. The NLO electroweak corrections to $H \to gg$ and $H \to \gamma\gamma$ have been computed in Ref. [118]. All these corrections are implemented in HDECAY [112]. For $m_H = 125$ GeV, the overall impact of known QCD and EW radiative effects turns out to be well below 1%. In addition, the contribution of the $H \to \gamma e^+e^-$ decay via virtual photon conversion has been computed in Ref. [119]. The partial decay width $H \to Z\gamma$ is only implemented at LO in HDECAY, including the virtual W, top-, bottom-, and τ-loop contributions. The QCD corrections have been calculated and are at the percent level [120], The theoretical uncertainty due to unknown electroweak corrections is estimated to be less than 5%, an accuracy that will be hard to achieve in measurements of this processes at the LHC.

The decays $H \to WW/ZZ \to 4f$ can be simulated with the Prophecy4f Monte-Carlo generator [121] that includes complete NLO QCD and EW corrections for Higgs decays into any possible four-fermion final state. All calculations are consistently performed with off-shell gauge bosons, without any on-shell approximation. For the SM Higgs boson the missing higher-order corrections are estimated to be roughly 0.5%. Such uncertainties will have to be combined with the parametric uncertainties, in particular those associated to the bottom-quark mass and the strong gauge coupling, to arrive at the full theory uncertainties. A detailed treatment of the differential distributions for a Higgs decay into four charged leptons in the final state is discussed in Refs. [44, 122].

The total width of a 125 GeV SM Higgs boson is $\Gamma_H = 4.07 \times 10^{-3}$ GeV, with a relative uncertainty of $^{+4.0\%}_{-3.9\%}$. The branching ratios for the most relevant decay modes of the SM Higgs boson as a function of m_H, including the most recent theoretical uncertainties, are shown in Fig. 11.2(right) and listed for $m_H = 125$ GeV in Table 11.3. Further details of these calculations can be found in Refs. [111, 123] and in the reviews [39–45].

Table 11.3: The branching ratios and the relative uncertainty [44, 45] for a SM Higgs boson with $m_H = 125$ GeV.

Decay channel	Branching ratio	Rel. uncertainty
$H \to \gamma\gamma$	2.27×10^{-3}	$^{+5.0\%}_{-4.9\%}$
$H \to ZZ$	2.62×10^{-2}	$^{+4.3\%}_{-4.1\%}$
$H \to W^+W^-$	2.14×10^{-1}	$^{+4.3\%}_{-4.2\%}$
$H \to \tau^+\tau^-$	6.27×10^{-2}	$^{+5.7\%}_{-5.7\%}$
$H \to b\bar{b}$	5.84×10^{-1}	$^{+3.2\%}_{-3.3\%}$
$H \to Z\gamma$	1.53×10^{-3}	$^{+9.0\%}_{-8.9\%}$
$H \to \mu^+\mu^-$	2.18×10^{-4}	$^{+6.0\%}_{-5.9\%}$

III. The experimental profile of the Higgs boson

An indirect experimental bound on the SM Higgs boson can be obtained by comparing precision electroweak data with SM predictions, that have a weak, logarithmic dependence on M_H. A global fit to electroweak data suggests $m_H = 96^{+22}_{-19}$ GeV, or $m_H < 134$ GeV at 90% confidence level [124].

The announcement on July 4, 2012 of the observation [1, 2] at the LHC of a narrow resonance with a mass of about 125 GeV was an important landmark in the decades-long direct search [125, 126] for the SM Higgs boson. Even as this discovery was being announced, ATLAS and CMS continued to accumulate pp collision data at $\sqrt{s} = 8$ TeV recording a total of about 20 fb^{-1} each at this energy. This data set together with about 5 fb^{-1} recorded at $\sqrt{s} = 7$ TeV comprised the LHC Run 1 pp collision data set. In the remainder of this section the focus will be on the final results on the measurements of Higgs boson properties with the LHC Run 1 data.

III.1. The principal discovery channels

For a given m_H, the sensitivity of a search channel depends on the production cross section of the Higgs boson, its decay branching fraction, reconstructed mass resolution,

selection efficiency and the level of background in the final state. For a low-mass Higgs boson ($110 < m_H(\text{GeV}) < 150$) where the natural width is only a few MeV, the five decay channels that play an important role at the LHC are listed in Table 11.4. In the $H \to \gamma\gamma$ and $H \to ZZ \to 4\ell$ channels, all final state particles can be very precisely measured and the reconstructed m_H resolution is excellent. While the $H \to W^+W^- \to \ell^+\nu_\ell\ell'^-\bar{\nu}_{\ell'}$ channel has relatively large branching fraction, the m_H resolution is poor due to the presence of neutrinos. The $H \to b\bar{b}$ and the $H \to \tau^+\tau^-$ channels suffer from large backgrounds and a poor mass resolution. For $m_H > 150\,\text{GeV}$, the sensitive search channels are $H \to WW$ and $H \to ZZ$ where the W or Z boson decays into a variety of leptonic and hadronic final states. These decay channels of the Higgs boson are searched for in the five Higgs boson production processes (ggF, VBF, WH, ZH and $t\bar{t}H$) described in Section II.4.1.

Table 11.4: The five principal decay channels for low mass SM Higgs boson searches at the LHC. The numbers reported are for $m_H = 125\,\text{GeV}$.

Decay channel	Mass resolution
$H \to \gamma\gamma$	1–2%
$H \to ZZ \to \ell^+\ell^-\ell'^+\ell'^-$	1–2%
$H \to W^+W^- \to \ell^+\nu_\ell\ell'^-\bar{\nu}_{\ell'}$	20%
$H \to b\bar{b}$	10%
$H \to \tau^+\tau^-$	15%

The candidate events in each Higgs boson decay channel are split into several mutually exclusive categories (or event tags) based on the specific topological, kinematic or other features present in the candidate event. The categorization of events increases the sensitivity of the overall analysis and allows a separation of different Higgs boson production processes. Most categories are dominated by signal from one Higgs decay mode but contain an admixture of various Higgs production processes. For example, a typical VBF category contains Higgs boson candidates accompanied by two energetic jets ($\geq 30\,\text{GeV}$) with a large dijet mass ($\geq 400\,\text{GeV}$) and separated by a large pseudorapidity ($\Delta\eta_{jj} \geq 3.5$). While such a category is enriched in Higgs bosons produced via VBF, the contamination from the gluon fusion production mechanism can be significant. Hence a measurement of the signal rate in the VBF category does not imply a measurement of VBF production cross-section. Simulations are used to determine the relative contributions of the various Higgs production modes in a particular category.

III.1.1. $H \to \gamma\gamma$

In the $H \to \gamma\gamma$ channel a search is performed for a narrow peak over a smoothly falling background in the invariant mass distribution of two high p_T photons. The background in this channel is conspicuous and stems from prompt $\gamma\gamma$, γ+jet and dijet processes. In order to optimize search sensitivity and also to separate the various Higgs production modes, ATLAS and CMS experiments split events into several mutually

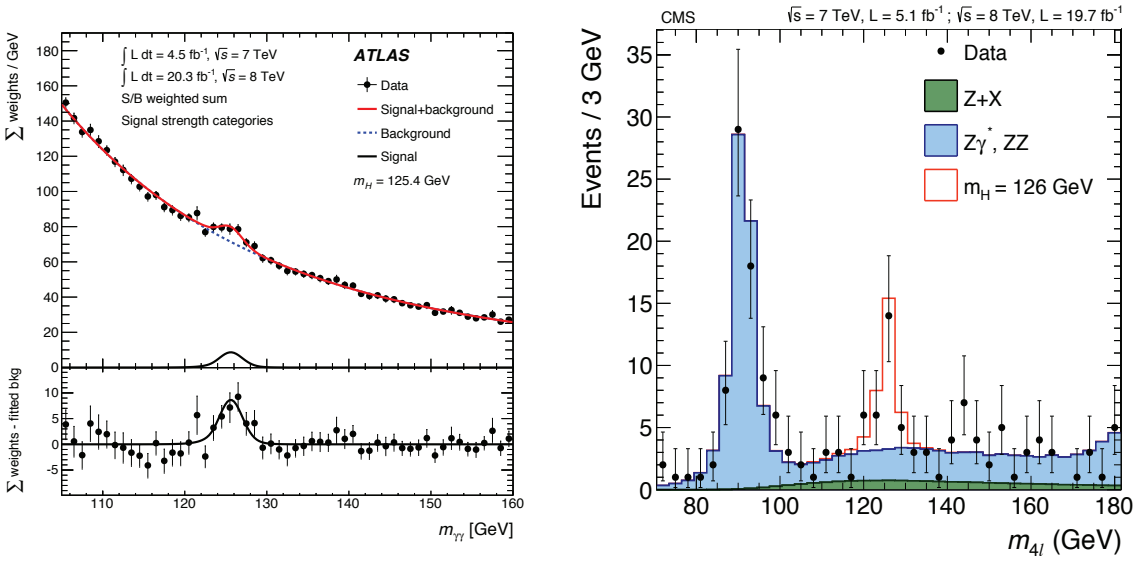

Figure 11.3: (Left) The invariant mass distribution of diphoton candidates, with each event weighted by the ratio of signal-to-background in each event category, observed by ATLAS [127]. The residuals of the data with respect to the fitted background are displayed in the lower panel. (Right) The combined $m_{4\ell}$ distribution from CMS [128] Run 1 data.

exclusive categories. Diphoton events containing a high p_T muon or electron, or missing energy ($E_T^{\rm miss}$) consistent with the decay of a W or Z boson are tagged in the VH production category. Diphoton events containing energetic dijets with a large mass and pseudorapidity difference are assigned to the VBF production category, and the remaining events are considered either in the VH category when the two jets are compatible with the hadronic decay of a W or a Z, or in the gluon fusion production category. While the leptonic VH category is relatively pure, the VBF category has significant contamination from the gluon fusion process. A summary of all categories used in this channel is given in Section IV.1 and in Table 11.9. Events which are not picked by any of the above selections are further categorized according to their expected $m_{\gamma\gamma}$ resolution and signal-to-background ratio. Categories with good m_H resolution and larger signal-to-background ratio contribute most to the sensitivity of the search.

Both ATLAS and CMS have studied in detail the calibration of the energy response of photons, in particular using $Z \to e^+e^-$, $Z \to \mu^+\mu^-\gamma$ and the response of muons in the calorimeter (for ATLAS) from $Z \to \mu^+\mu^-$ events. This information is used to correct the fully simulated signal mass lineshapes. In each category, parametric signal models are adjusted to these lineshape to provide a functional form for the signal. Simple monotonic functional forms of the backgrounds are determined by a fit to the full $m_{\gamma\gamma}$ distribution in each category. All categories are fitted simultaneously to determine the signal yield at a particular mass. In the full dataset, the $m_{\gamma\gamma}$ distribution after combining all categories is shown for the ATLAS experiment in Fig. 11.3. ATLAS observes [127] an excess over background at $m_H = 125.4\,\text{GeV}$ with a local significance of 5.2σ compared with 4.6σ

expected for SM Higgs boson at that mass. CMS observes [129] its largest excess at $m_H = 124.7\,\text{GeV}$ with a local significance of 5.7σ compared with 5.2σ expected for a SM Higgs boson of that mass.

The signal strength $\mu = (\sigma \cdot \text{BR})_{\text{obs}}/(\sigma \cdot \text{BR})_{\text{SM}}$, which is the observed product of the Higgs boson production cross section (σ) and its branching ratio (BR) in units of the corresponding SM values, is 1.17 ± 0.27 for ATLAS and $0.78^{+0.26}_{-0.23}$ for CMS at $m_H = 125.4$ and $124.7\,\text{GeV}$, respectively.

III.1.2. $H \to ZZ^* \to \ell^+\ell^-\ell'^+\ell'^-$

In the $H \to ZZ^* \to \ell^+\ell^-\ell'^+\ell'^-$ channel a search is performed for a narrow mass peak over a small continuous background dominated by non-resonant ZZ^* production from $q\overline{q}$ annihilation and gg fusion processes. The contribution and the shape of this background is taken from simulation. The subdominant and reducible backgrounds stem from $Z + b\bar{b}$, $t\bar{t}$ and $Z +$ jets events. Their contribution is suppressed by requirements on lepton isolation and lepton impact parameter and their yield is estimated from control samples in data.

To help distinguish the Higgs signal from the dominant non-resonant ZZ^* background, both ATLAS [130] and CMS [128] use a matrix element likelihood approach to construct a kinematic discriminant built for each 4ℓ event based on the ratio of complete leading-order matrix elements $|{\mathcal{M}_{sig}}^2/{\mathcal{M}_{bkg}}^2|$ for the signal ($gg \to H \to 4\ell$) and background($q\overline{q} \to ZZ \to 4\ell$) hypotheses. The signal matrix element $\mathcal{M}_{sig}$ is computed assuming $m_H = m_{4\ell}$. To further enhance the sensitivity to a signal, the ATLAS experiment uses the matrix element as an input variable to a Boosted Decision Tree, along with the transverse momentum and rapidity of the four-leptons system [130].

To enhance the sensitivity to VBF and VH production processes, the ATLAS and CMS experiments divide 4ℓ events into mutually exclusive categories. Events containing dijets with a large mass and pseudorapidity difference populate the VBF category. ATLAS requires the presence of an additional lepton in the VH category. In events with less than two jets, CMS uses the $p_T^{4\ell}$ to distinguish between production via the gluon fusion and the VH/VBF processes.

Since the $m_{4\ell}$ resolutions and the reducible background levels are different in the 4μ, $4e$ and $2e2\mu$ subchannels, they are analyzed separately and the results are then combined.

As shown in Fig. 11.3, the CMS experiment observes [128] its largest excess at $m_H = 125.6\,\text{GeV}$ with an observed local significance of 6.8σ to be compared with an expected significance of 6.7σ at that mass. In their combined $m_{4\ell}$ distribution, ATLAS observes [130] an excess at $m_H = 125.36\,\text{GeV}$ with a local significance of 8.1σ. The expected local significance for the SM Higgs boson at that mass is 6.2σ. Both experiments also observe a clear peak at $m_{4\ell} = 91\,\text{GeV}$ from Z/γ^* production at the expected SM rate [131].

The signal strength μ for the inclusive $H \to 4\ell$ production measured by the ATLAS and CMS experiments is $1.44^{+0.40}_{-0.33}$ at $m_H = 125.36\,\text{GeV}$ and $0.93^{+0.29}_{-0.25}$ at $m_H = 125.6\,\text{GeV}$, respectively.

III.2. Measurement of the Higgs boson mass

To measure the mass of the Higgs boson, ATLAS and CMS experiments rely on the two high mass resolution and sensitive channels, $\gamma\gamma$ and ZZ. The approaches are very similar in these two analyses for both experiments, with subtle differences on the use of categories, additional discriminating variables and per-event errors. These two channels are chosen for this precision measurement because they produce a narrow peak in mass with a resolution ranging from 1.4 GeV to 2 GeV for ATLAS and from 1.0 GeV to 2.8 GeV for CMS, where the best mass resolution is obtained for both experiments in the diphoton channel for central diphoton pairs (typically for events where both photons are not converted). For a model-independent mass measurement, the signal strengths in the $\gamma\gamma$ and ZZ channels are assumed to be independent and not constrained to the expected rate ($\mu = 1$) for the SM Higgs boson. The combined mass measured by ATLAS [132] and CMS [133] are $125.36 \pm 0.37(\text{stat.}) \pm 0.18(\text{syst.})$ GeV and $125.02^{+0.26}_{-0.27}(\text{stat.})^{+0.14}_{-0.15}(\text{syst.})$ GeV, respectively. In both experiments the measurements are dominated by the data statistics, however the systematic uncertainty is not negligible and is dominated by the precision in the knowledge of the photon energy or momentum scale. The ATLAS and CMS experiments have performed a combination of their mass measurements [134].

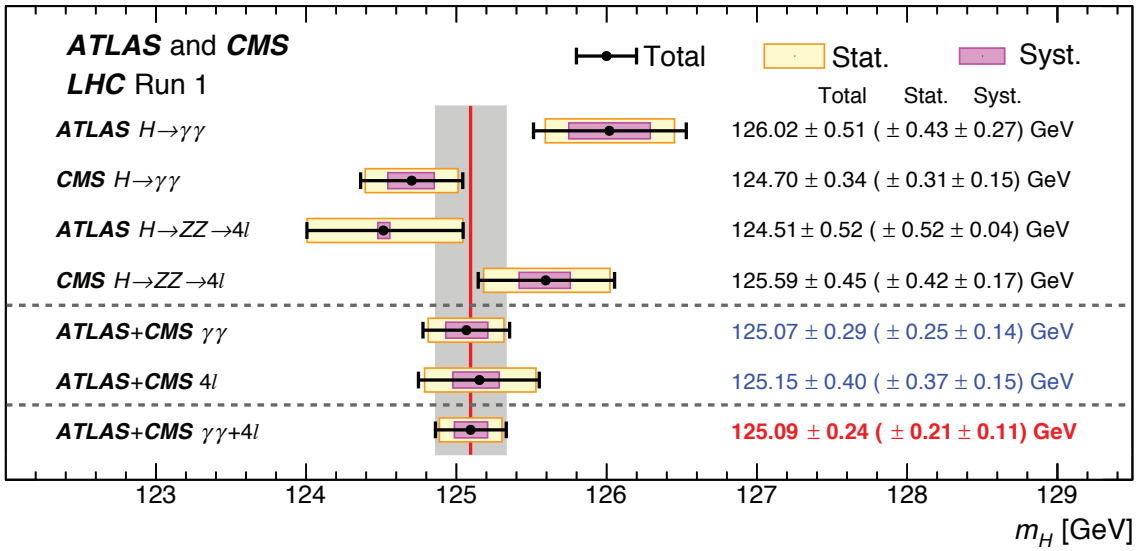

Figure 11.4: A compilation of the CMS and ATLAS mass measurements in the $\gamma\gamma$ and ZZ channels, the combined result from each experiment and their combination. From Ref. [134]

Figure 11.4 summarizes these measurements and their combination [134]. The significance of the difference between the measurements of the masses in the $\gamma\gamma$ and ZZ channels by the ATLAS experiment is 1.97σ [132]. The ATLAS and CMS combined mass measurement:

$$m_H = 125.09 \pm 0.21(\text{stat.}) \pm 0.11(\text{syst.})\ \text{GeV}$$

reaches a precision of 0.2% and is dominated by statistical uncertainties.

In the diphoton channel, as is discussed in Section V.3.2 a mass shift is expected to be induced by the deformation of the mass lineshape of the signal in presence of background, from the interference between the Higgs boson production and the continuum irreducible background. It is a small but non negligible effect of approximately 35 MeV for a Higgs boson width close to that of the SM, but this effect could be larger if the width of the discovered particle were to be completely different. This effect estimated by ATLAS with a full simulation is still relatively small with respect to the total uncertainty on the mass and is therefore neglected.

III.3. $H \to W^+W^- \to \ell^+\nu\ell^-\overline{\nu}$

While the production rate in the $H \to W^+W^- \to \ell^+\nu\ell^-\bar{\nu}$ channel is large, due to the presence of two neutrinos in the decay, the m_H resolution is quite poor ($\approx 20\%\ m_H$) so the search requires fitting in several characteristic kinematic variables.

Experiments search for an excess of events with two leptons of opposite charge accompanied by missing energy and up to two jets. Events are divided into several categories depending on the lepton flavor combination (e^+e^-, $\mu^+\mu^-$and $e^\pm\mu^\mp$) and the number of accompanying jets ($N_{\rm jet} = 0, 1, \geq 2$). The $N_{\rm jet} \geq 2$ category is optimized for the VBF production process by selecting two leading jets with a large pseudorapidity difference and with a large mass ($m_{jj} > 500\,\text{GeV}$).

Backgrounds contributing to this channel are numerous and depend on the category of selected events. Reducing them and accurately estimating the remainder is a major challenge in this analysis. For events with opposite-flavor lepton and no accompanying high p_T jets, the dominant background stems from non-resonant WW production. Events with same-flavor leptons suffer from large Drell–Yan contamination. The $t\bar{t}$, Wt and W + jets (with the jet misidentified as a lepton) events contaminate all categories. Non-resonant WZ, ZZ and $W\gamma$ processes also contribute to the background at a sub-leading level.

A requirement of large missing transverse energy ($E_T^{\rm miss}$) is used to reduce the Drell–Yan and multijet backgrounds. In the e^+e^- and $\mu^+\mu^-$ categories, events with $m_{\ell\ell}$ consistent with the Z mass are vetoed. The $t\bar{t}$ background is suppressed by a veto against identified b-jets or low p_T muons (assumed to be coming from semileptonic b-hadron decays within jets) and tight isolation requirements diminish the W+jets background. The scalar nature of the Higgs boson and the $V-A$ nature of the W boson decay implies that the two charged leptons in the final state are preferentially emitted at small angles with respect to each other. Therefore the dilepton invariant mass ($m_{\ell\ell}$) and the azimuthal angle difference between the leptons ($\Delta\phi_{\ell\ell}$) are used to discriminate between the signal and non-resonant WW events. The transverse mass, constructed from the dilepton p_T ($p_T^{\ell\ell}$), $E_T^{\rm miss}$ and the azimuthal angle between $E_T^{\rm miss}$ and $p_T^{\ell\ell}$, is defined as $m_T = \sqrt{2p_T^{\ell\ell}E_T^{\rm miss}(1-\cos\Delta\phi_{E_T^{\rm miss}\ell\ell})}$ and serves as an effective discriminant against backgrounds. The transverse mass variable also tracks the Higgs boson mass but with a poor mass resolution. All residual background rates except for the small contributions from non-resonant WZ, ZZ and $W\gamma$ are evaluated from control samples devised from data.

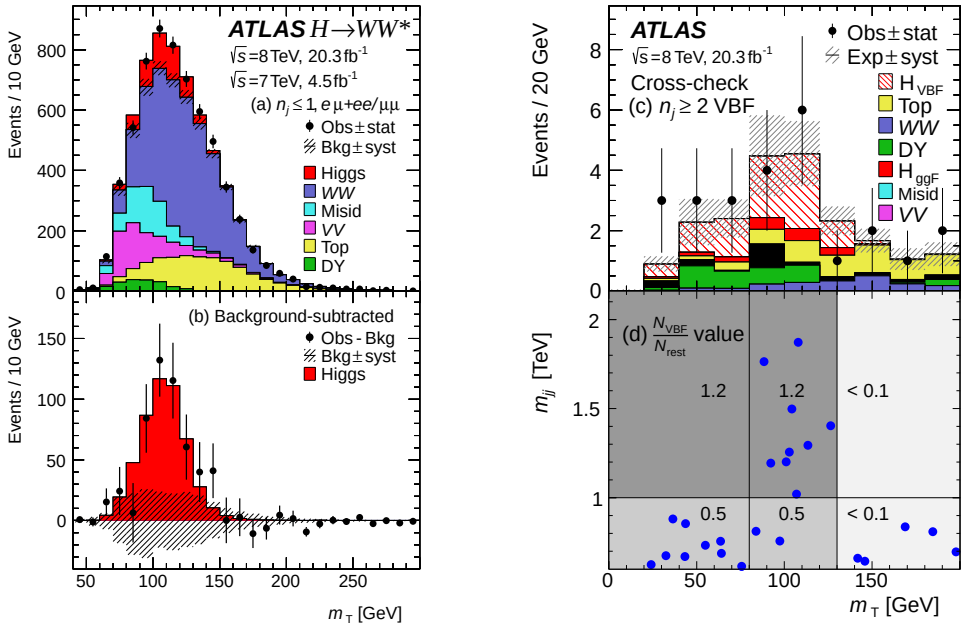

Figure 11.5: (a) The m_T distribution for selected events summed over all lepton flavors and with ≤ 1 associated jets. (b) The residual of the data over the estimated SM background and the expectation from a SM Higgs boson with $m_H = 125\,\text{GeV}$ indicating a clear excess with an event yield consistent with that from a SM Higgs boson [135]. The (c) m_T and (d) m_{jj} versus m_T distributions for the $N_{\text{jet}} \geq 2$ VBF-enriched category for the 8 TeV data analysis. For each region in (d), the ratio $N_{\text{VBF}}/N_{\text{rest}}$ is given (N_{rest} includes all production processes other than the VBF).

The m_T distributions of the selected events in Run 1 data are shown in Fig. 11.5 for the ATLAS experiment. The 0-jet category is dominated by non-resonant WW background while $t\bar{t}$ dominates the 1 and 2 jet categories. A clear excess over background expectation in the 0 and 1 jet categories is observed. An excess is also observed in the VBF-enrighed 2-jets category. The observed event yield is consistent with the expectation from a 125 GeV SM Higgs boson.

ATLAS fits the m_T distributions and observes [135] an excess at $m_H = 125.36\,\text{GeV}$ with a local significance of 6.1σ similar to that expected from a 125 GeV SM Higgs boson. The measured inclusive signal strength is $\mu = 1.09^{+0.23}_{-0.21}$. In the VBF category an excess with a significance of 3.2σ corresponding to a signal strength of $\mu = 1.27^{+0.53}_{-0.45}$ is observed [135]. The CMS analysis of 0 and 1 jet categories, using all lepton flavor combinations, shows [136] an excess with an observed significance of 4.3σ, lower than the expected sensitivity of 5.8σ for a 125.6 GeV SM Higgs boson. CMS observes [136] no significant excess in the VBF production mode and sets a 95% CL limit on the signal strength of $\mu_{\text{VBF}} < 1.7$ for $m_H = 125.6\,\text{GeV}$.

The ATLAS and CMS experiments have also searched for the associated Higgs boson production (VH) in this channel. The signal consists of up to three (WH) or four (ZH) high p_T isolated leptons with missing transverse energy and low hadronic activity.

The major backgrounds stem from triboson and diboson production where each boson decays leptonically. ATLAS observes [137] an excess at $m_H = 125.36\,\text{GeV}$ with a local significance of 2.5σ corresponding to a $\mu_{VH} = 3.0^{+1.6}_{-1.0}$. CMS instead sets [136] a 95% CL limit of $\mu_{VH} < 4.7$.

III.4. Decays to fermions

At hadron colliders, the most promising channel for probing the coupling of the Higgs field to the quarks and leptons are $H \to b\bar{b}$ and $H \to \tau^+\tau^-$, respectively. For a Higgs boson with $m_H \approx 125\,\text{GeV}$, the branching fraction to $b\bar{b}$ is about 57% and to $\tau^+\tau^-$ is about 6%. Nevertheless, the presence of very large backgrounds makes the isolation of a Higgs boson signal in these channels quite challenging.

III.4.1. $H \to \tau^+\tau^-$

In the $H \to \tau\tau$ search, τ leptons decaying to electrons (τ_e), muons (τ_μ) and hadrons (τ_{had}) are considered. The $\tau^+\tau^-$ invariant mass ($m_{\tau\tau}$) is reconstructed from a kinematic fit of the visible products from the two τ leptons and the missing energy observed in the event. Due to the presence of missing neutrinos, the $m_{\tau^+\tau^-}$ resolution is poor ($\approx 15\%$). As a result, a broad excess over the expected background in the $m_{\tau\tau}$ distribution is searched for. The major sources of background stem from Drell–Yan $Z \to \tau^+\tau^-$ and $Z \to e^+e^-$, W+jets, $t\bar{t}$ and multijet production. Events in all subchannels are divided into categories based on the number and kinematic properties of additional energetic jets in the event. The sensitivity of the search is generally higher for categories with one or more additional jets. The VBF category, consisting of a τ pair with two energetic jets separated by a large pseudorapidity, has the best signal-to-background ratio and search sensitivity, followed by the $\tau^+\tau^-$+1 jet category. The signal to background discrimination relies in part on the $m_{\tau\tau}$ resolution, which improves with the boost of the Higgs boson. The non-VBF categories are further subdivided according to the observed boost of the $\tau^+\tau^-$ system. The 0-jet category which has the poorest signal/background ratio is used to constrain the background yields, the reconstruction efficiencies, and the energy scales. CMS primarily uses the reconstructed $m_{\tau\tau}$ as the final discriminating variable [138] while the ATLAS experiment combines various kinematic properties of each event categories with multivariate techniques to build the final discriminant [139].

Searches for $H \to \tau^+\tau^-$ decays in the VH production mode are performed in final states where the W or Z boson decays into leptons or jets. The irreducible background in this search arises from non-resonant WZ and ZZ diboson production. The reducible backgrounds originate from W, Z, and $t\bar{t}$ events that contain at least one fake lepton in the final state due to a misidentified jet. The shape and yield of the major backgrounds in each category is estimated from control samples in data. Contributions from non-resonant WZ and ZZ diboson production are estimated from simulations but corrected for reconstruction efficiency using control samples formed from observed data.

Figure 11.6 shows the CMS [138] $m_{\tau\tau}$ distributions combining all categories, weighing the distributions in each category of each subchannel by the ratio between the expected signal and background yields for that category. The inset plot shows the difference

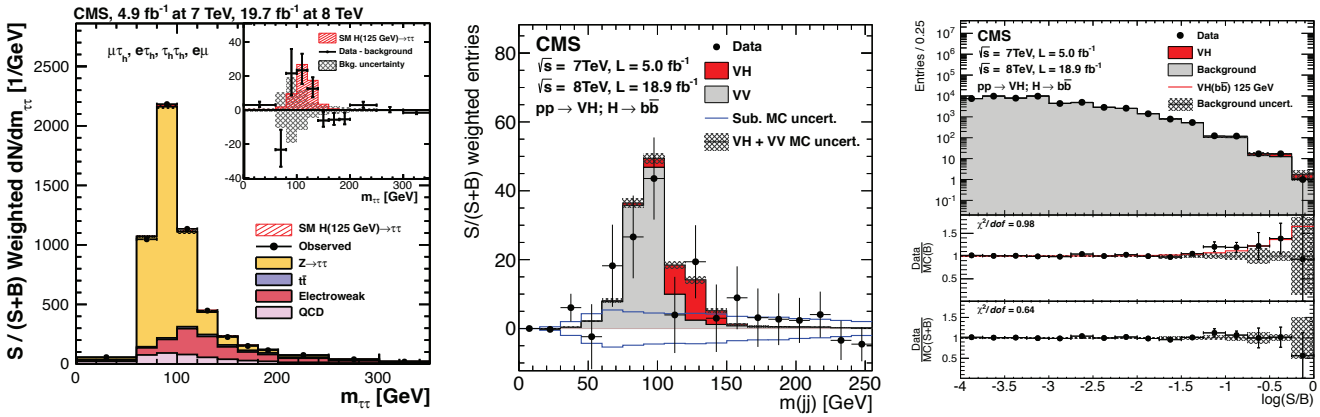

Figure 11.6: (Left) The observed and predicted $m_{\tau\tau}$ distributions for all $H \to \tau^+\tau^-$ subchannels combined by the CMS experiment. The inset shows the difference between the observed data and the expected SM background contributions, together with the expected signal distribution for a SM Higgs boson with $m_H = 125\,\text{GeV}$ [138]. (Center) The $m_{b\bar{b}}$ distribution for the $pp \to V(H \to b\bar{b})$ channels with all backgrounds except dibosons subtracted. The solid histograms for the backgrounds and the signal are summed cumulatively [140]. (Right) The combination of all $pp \to V(H \to b\bar{b})$ channels into a single multivariate distribution. The two bottom panels show the ratio of the data to the background-only prediction (above) and to the predicted sum of background and SM Higgs boson signal with a mass of 125 GeV (below).

between the observed and expected background distributions, together with the expected distribution for a SM Higgs boson signal with $m_H = 125\,\text{GeV}$. The significance of the observed excess at $m_H = 125\,\text{GeV}$ is 3.4 standard deviations, close to the expected sensitivity, and corresponds to a signal strength of $\mu = 0.86 \pm 0.29$. At $m_H = 125.36\,\text{GeV}$, the observed (expected) deviation from the background-only hypothesis in ATLAS corresponds to a local significance of 4.5 (3.4) standard deviations and the best fit value of the signal strength is $\mu = 1.43^{+0.43}_{-0.37}$ [139].

When the ATLAS and CMS $H \to \tau\tau$ measurements are combined [141], the significance of the observed excess corresponding to $m_H = 125.09\,\text{GeV}$ is 5.5 standard deviations and the combined signal strength is $\mu = 1.11^{+0.24}_{-0.22}$.

III.4.2. $H \to b\bar{b}$

The production mode $gg \to H$ with $H \to b\bar{b}$ is overwhelmed by the background from the inclusive production of $p\bar{p} \to b\bar{b} + X$ via the strong interaction. The associated production modes WH and ZH (collectively termed VH modes) allow use of the leptonic W and Z decays for triggering, and to purify the signal and reject QCD backgrounds. The W bosons are reconstructed via their leptonic decay $W \to \ell\bar{\nu}_\ell$ where $\ell = e, \mu$ or τ. The Z bosons are reconstructed via their decay into $e^+e^-, \mu^+\mu^-$ or $\nu\bar{\nu}$. The Higgs boson candidate mass is reconstructed from two b-tagged jets in the event. Backgrounds arise

from production of W and Z bosons in association with gluon, light and heavy-flavored jets (V+jets), $t\bar{t}$, diboson (ZZ and WZ with $Z \to b\bar{b}$) and QCD multijet processes. Due to the limited $m_{b\bar{b}}$ mass resolution, a SM Higgs boson signal is expected to appear as a broad enhancement in the reconstructed dijet mass distribution. The crucial elements in this search are b-jet tagging with high efficiency and low fake rate, accurate estimate of b-jet momentum and estimate of backgrounds from various signal depleted control samples constructed from data.

At the Tevatron, the $H \to b\bar{b}$ channel contributes the majority of the Higgs boson search sensitivity below $m_H = 130\,\text{GeV}$. The CDF and D0 experiments use multivariate analysis (MVA) techniques that combine several discriminating variables into a single final discriminant used to separate signal from background. Each channel is divided into exclusive subchannels according to various lepton, jet multiplicity, and b-tagging characteristics in order to group events with similar signal-to-background ratio and thus optimize the overall search sensitivity. The combined CDF and D0 data show [142, 126] an excess of events with respect to the predicted background in the 115–140 GeV mass range in the most sensitive bins of the discriminant distributions suggesting the presence of a signal. At $m_H = 125\,\text{GeV}$ the observed signal strength $\mu = 1.59^{+0.69}_{-0.72}$.

To reduce the dominant V+jets background, following Ref. [143], the LHC experiments select a region in VH production phase space where the vector boson is significantly boosted and recoils from the $H \to b\bar{b}$ candidate with a large azimuthal angle $\Delta\phi_{VH}$. For each channel, events are categorized into different $p_T(V)$ regions with varying signal/background ratios. Events with higher $p_T(V)$ have smaller backgrounds and better $m_{b\bar{b}}$ resolution. CMS uses [140] MVA classifiers based on kinematic, topological and quality of b-jet tagging and trained on different values of m_H to separate Higgs boson signal in each category from backgrounds. The MVA outputs for all categories are then fit simultaneously. Figure 11.6(right) shows the combined MVA output of all categories where events are gathered in bins of similar expected signal-to-background ratios as predicted by the MVA discriminants. The excess of events observed in bins with the largest signal-to-background ratios is consistent with the production of a 125 GeV SM Higgs boson with a significance of 2.1 standard deviations. The observed signal strength at 125 GeV is $\mu = 1.0 \pm 0.5$. Figure 11.6(center) shows the $m_{b\bar{b}}$ distribution for all categories combined, weighted by the signal-to-background ratio in each category, with all backgrounds except dibosons subtracted. The data show the clear presence of a diboson ($W/Z + \text{Z} \to b\bar{b}$) signal, with a rate consistent with the SM expectation, together with an excess that agrees with that expected from the production of a 125 GeV SM Higgs boson. The nominal results from ATLAS are also based on a combination [144] of (i) a multivariate analysis of their 8 TeV data, incorporating various kinematic variables in addition to $m_{b\bar{b}}$ and b-tagging information and (ii) a statistical analysis of their 7 TeV data centered on $m_{b\bar{b}}$ as the main discriminant. In both cases customized control samples devised from data are used to constrain the contributions of the dominant background processes. The net observed(expected) deviation from background-only hypothesis corresponds to a significance of 1.4(2.6) standard deviations and a signal strength of $\mu = 0.5 \pm 0.4$.

In their 8 TeV data, CMS has also searched for $H \to b\bar{b}$ in the VBF production mode [145]. The event topology consists of two "VBF-tagging" energetic light-quark jets in the forward and backward direction relative to the beam direction and two b-tagged jets in the central region of the detector. Due to the electroweak nature of the process, for the signal events, no energetic jet activity is expected in the rapidity gap between the two "VBF-tagging" jets. The dominant background in this search stems from QCD production of multijet events and the hadronic decays of vector bosons accompanied by additional jets. A contribution of Higgs boson events produced in the ggF process but with two or more associated jets is expected in the signal sample. The signal is expected as a broad enhancement in the $m_{b\bar{b}}$ distribution over the smoothly falling contribution from the SM background processes. The observed (expected) excess corresponding to $m_H = 125\,\text{GeV}$ was 2.2 (0.8) standard deviations corresponding to a signal strength of $\mu = 2.8^{+1.6}_{-1.4}$. Combining with the result of the CMS VH analysis yields a signal strength signal $\mu = 1.0 \pm 0.4$ and the local significance of the excess improves marginally to 2.6 standard deviations.

III.5. First results on the main production and decay channels at 13 TeV

After a period of long shutdown between 2013 and 2015 devoted to the consolidation of the machine, in Spring 2015 the LHC delivered pp collisions at an unprecedented centre-of-mass energy of 13 TeV. During this period the ATLAS and CMS experiments have collected datasets corresponding to integrated luminosities of 2.3 to 3.2 fb^{-1} for CMS and ATLAS, respectively. The first preliminary measurements of Higgs boson production at this increased centre-of-mass energy are arriving while this review is being finalized. Only a concise section and an update in the associated production with a top-quark pair are therefore devoted to these results.

The two high-resolution channels $H \to \gamma\gamma$ and $H \to ZZ^* \to \ell^+\ell^-\ell'^+\ell'^-$ have been measured both by the ATLAS and CMS experiments. With the increase in production cross sections, a fair sensitivity is expected in these two channels even with this limited amount of data. For the $H \to \gamma\gamma$ channel ATLAS has produced a fully inclusive analysis in order to measure a fiducial cross section with a sensitivity of 1.9σ and an observed excess of 1.8σ [146]. The measurement of the total cross section, as extrapolated from the fiducial region is shown in Fig. 11.7(left). CMS has produced an analysis with event classification that has reached a sensitivity of 2.7σ and has observed an overall excess of 1.7σ [147]. For the $H \to ZZ^*$ channel, ATLAS has also produced a fully inclusive analysis with a sensitivity of 2.8σ and no significant excess with respect to the background has been observed [148]. This outcome is however compatible with the presence of a signal at the 1.4σ level. The corresponding measurement of the total cross section is illustrated in Fig. 11.7(left). The CMS analysis in this channel is also inclusive and uses additional kinematic discriminants to reach a sensitivity of 3.4σ [149]. CMS observes an excess with a significance of 2.5σ. In this channel, CMS also measures a fiducial cross section as shown in Fig. 11.7(right). The ATLAS experiment has also performed a combination of the total cross sections in these two channel at 7, 8 and 13 TeV [150]. The results of these combinations are shown in Fig. 11.7(left).

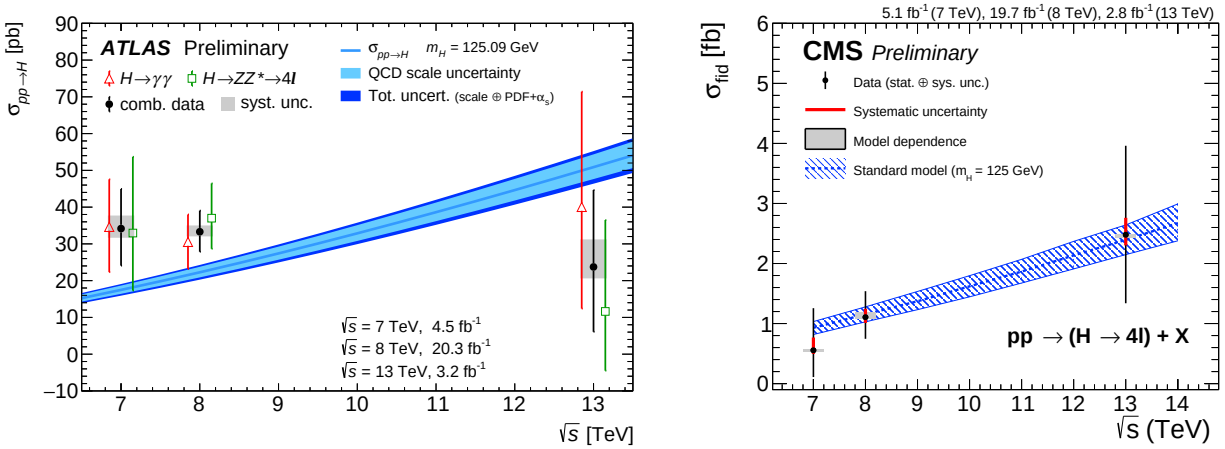

Figure 11.7: (Left) Total cross sections measured by ATLAS at 7, 8 and 13 TeV in the $H \to \gamma\gamma$ and $H \to ZZ^*$ channels and their combinations. (Right) The fiducial cross section measured in the $H \to ZZ^*$ channel by CMS at 7, 8 and 13 TeV.

The CMS experiment has investigated two additional channels. The first is the $H \to WW^* \to \ell\nu\ell\nu$ in categories of up to one jet, with a sensitivity of 2σ [151] and has observed only a very mild excess of 0.7σ. The second is the $H \to b\bar{b}$ decay mode in the VBF production sensitive only to approximately twice the SM production rate. The observation in this channel is compatible both with the background and the background in presence of a SM signal [152].

III.6. Higgs production in association with top quarks or in top decays

III.6.1. The associated production with top quark pairs

As discussed in Section II, the coupling of the Higgs particle to top quarks plays a special role in the electroweak breaking mechanism and in its possible extensions. Substantial indirect evidence of this coupling is provided by the compatibility of observed rates of the Higgs boson in the principal discovery channels, given that the main production process – the gluon fusion – is dominated by a top quark loop. Direct evidence of this coupling at the LHC and the future e^+e^- colliders will be mainly available through the $t\bar{t}H$ final state and will permit a clean measurement of the top quark-Higgs boson Yukawa coupling. The $t\bar{t}H$ production cross section at the LHC is tiny in comparison with the ggF or even VH production modes. The production cross section for a 125 GeV Higgs boson in pp collisions at $\sqrt{s} = 8$ TeV of about 130 fb makes it challenging to measure the $t\bar{t}H$ process with the LHC Run 1 dataset. It is thus imperative to target every accessible experimental signature. The analyses channels for such complex final states can be separated in four classes according to the decays of the Higgs boson. In each of these classes, most of the decay final states of the top quarks are considered. The topologies related to the decays of the top quarks are denoted 0L, 1L and 2L, for the fully hadronic, semi-leptonic and dilepton decay final states of the $t\bar{t}$, respectively.

The first analysis in this set is the search for $t\bar{t}H$ production in the $H \to \gamma\gamma$ channel. This analysis relies on the search for a narrow mass peak in the $m_{\gamma\gamma}$ distribution.

Table 11.5: Summary of the results of searches for a Higgs boson in association with a top quark pair by the ATLAS and CMS collaborations. The results are given in terms of measured signal strength. The results of subchannels including hadronically decaying taus, which are less sensitive, are not reported in this table but can be found in the corresponding references.

	ATLAS (7 and 8 TeV)	CMS (7 and 8 TeV)	CMS (13 TeV)
$t\bar{t}(H \to \gamma\gamma)$	$1.3\ ^{+2.6\ +2.5}_{-1.7\ -1.7}$	$1.2\ ^{+2.5\ +2.6}_{-1.7\ -1.8}$	—
$t\bar{t}(H \to b\bar{b})$-0L	$1.6\ \pm 0.8\ \pm 2.5$	—	
$t\bar{t}(H \to b\bar{b})$-1L	$1.2\ \pm 0.8\ \pm 0.8$	$1.7\ ^{+2.0}_{-1.8}$	$-0.4\ ^{+2.1}_{-2.1}$
$t\bar{t}(H \to b\bar{b})$-2L	$2.8; \pm 1.4\ \pm 2.0$	$1.0\ ^{+3.3}_{-3.0}$	$-4.7\ ^{+3.7}_{-3.8}$
$t\bar{t}(H \to b\bar{b})$	$1.4\ \pm 1.0\ \pm 0.6$	$1.6\ ^{+1.6}_{-1.5}$	$-2.0\ \pm 1.8$
$t\bar{t}(H \to 4\ell)$	$2.8\ ^{+2.0\ +0.9}_{-1.7\ -0.6}$	$-4.7\ ^{+5.0}_{-1.3}$	—
$t\bar{t}(H \to 3\ell)$	$2.8\ ^{+2.0\ +0.9}_{-1.7\ -0.6}$	$3.1\ ^{+2.4}_{-2.0}$	$5.8\ ^{+3.3}_{-2.7}$
$t\bar{t}(H \to SS2\ell)$	$2.8\ ^{+1.5\ +1.5}_{-1.4\ -1.3}$	$5.3\ ^{+2.1}_{-1.8}$	$-0.5\ ^{+1.0}_{-0.7}$
$t\bar{t}(H \to WW/\tau\tau/ZZ)$	$1.4\ \pm 0.6\ \pm 1.0$	—	$0.6\ ^{+1.4}_{-1.1}$
Combination	$1.7\ \pm 0.5\ \pm 0.8$	$2.8\ ^{+1.0}_{-0.9}$	—

The background is estimated from the $m_{\gamma\gamma}$ sidebands. The sensitivity in this channel is mostly limited by the available statistics. The second is the search in the $H \to b\bar{b}$ channel. This search is extremely intricate due to the large backgrounds, both physical and combinatorial in resolving the $b\bar{b}$ system related to the Higgs particle, in events with six jets and four b-tagged jets which are very hard to simulate. With the current dataset, the sensitivity of this analysis is severely impacted by the systematic uncertainties on the background predictions. The third channel is a specific search for $\tau^+\tau^-$ where the two tau leptons decay to hadrons. Finally, the W^+W^- , $\tau^+\tau^-$ and ZZ final states can be searched for inclusively in multilepton event topologies. The corresponding $t\bar{t}H$ modes can be decomposed in terms of the decays of the Higgs boson and those of the top quarks as having two b-quarks and four W bosons (or two W and two taus, or two W and two Z) in the final state.

CMS combines these four sets of measurements [153] and reports a 95% CL upper limit on the signal strength value of $\mu_{t\bar{t}H} < 4.5$. ATLAS reports [155–157] 95% CL upper limits on the signal strengths of 6.7, 6.4 and 4.7 for $H \to \gamma\gamma$, $H \to b\bar{b}$ and $H \to$ multilepton decay final states, respectively. The CMS experiment has also updated the $t\bar{t}H(\to b\bar{b})$ analysis using the matrix element method, aiming at an optimal separation between the signal and the dominant $t\bar{t}$ production in association with heavy flavor quarks in the final state [154].

III.6.2. The associated production with a single top quark

An additional production mode of the Higgs boson in association with a top quark is the single top associated production mode. There is an interesting similarity between this production mode and the $H \to \gamma\gamma$ decay mode. Both processes proceed through either the top Yukawa coupling or the interaction of the Higgs boson with the W-boson, with a negative interference between the two. Representative Feynman diagrams for this production process are shown in Fig. 11.8. Contrary to the diphoton decay channel, in this production mode the interference occurs at the tree level. This process can be used to further discriminate a negative relative sign between the couplings of the Higgs boson to fermions and its couplings to gauge bosons.

The ATLAS experiment has re-interpreted its Run 1 search of the diphoton decay channel in the ttH production in terms of tH production [155] and has produced 95% CL upper limits on the Higgs boson production cross section with respect to the rates expected for a given sign of the top Yukawa coupling. The result is not strong enough to exclude, at 95% CL, a negative top Yukawa coupling with an absolute strength equal to that of the SM. The excluded range in the ratio of the Higgs-top Yukawa coupling to that of the SM one, κ_t, at the 95% CL, is $]-\infty, -1.3] \cup [8, \infty[$.

The CMS experiment has produced a search with the Run 1 data exploiting a variety of Higgs boson decay modes resulting in final states with photons, bottom quarks, and multiple charged leptons, including tau leptons. The analysis is optimized for the opposite sign of the top Yukawa coupling with respect to that in the SM, and corresponding to a large enhancement of the signal cross section. The expected sensitivity of this analysis in terms of exclusion of the ratio of the cross section to the expected SM cross section is 2 for $\kappa_t = -1$, while the observed exclusion limit is 2.8.

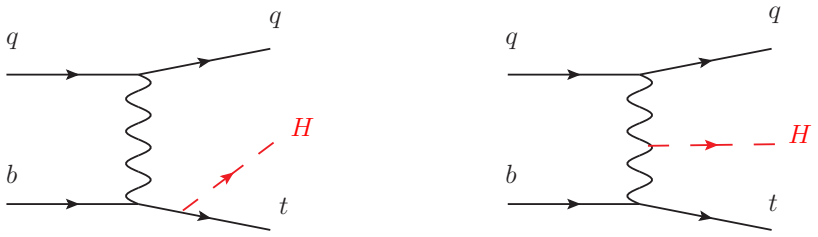

Figure 11.8: Feynman diagrams contributing to the Higgs production in association with a single top-quark through the top Yukawa coupling (left) and through the Higgs coupling to the W gauge boson (right).

III.6.3. Flavor changing neutral current decays of the top quark

The discovery of the Higgs boson at a mass smaller than the top quark mass opened a new decay channel for the top quark. The decays of the top quark to a Higgs boson and a charm or an up quark proceed through a Flavor Changing Neutral Current (FCNC) which are forbidden at the tree level and suppressed at higher orders through the Glashow–Iliopoulos–Maiani (GIM) mechanism [3]. The SM prediction for these branching

fractions is $\mathrm{BR}(t \to Hc) = 10^{-15}$ and two orders of magnitude less for the Hu final state. These decay channels of the top quark are, however, very interesting to probe possible FCNC interactions in the Higgs Yukawa couplings to the quark sector.

The ATLAS experiment has searched for FCNC top decays specifically in channels involving a Higgs boson with subsequent decays to two photons [158] and a pair of b-quarks [159]. It has also reinterpreted a search for the ttH production in the multilepton final state (discussed in Section III.6.1) [157]. The latter channel covers Higgs boson decays to a pair of W-bosons and a pair of taus. No significant excess was observed in any of the specific channels (as discussed in Section III.6.1, a slight excess is observed in the ttH multilepton channel) and 95% CL upper limits are set on $\mathrm{BR}(t \to Hc) < 0.46\%$ with an expected sensitivity of 0.25% and $\mathrm{BR}(t \to Hu) < 0.45\%$ with an expected sensitivity of 0.29%. The CMS experiment has performed a search for these FCNC top decays in the diphoton and multilepton channels [160], yielding a 95% CL upper limit on $\mathrm{BR}(t \to Hc) < 0.56\%$ with an expected sensitivity of 0.65%.

From these limits on branching fractions, constraints on non flavor-diagonal Yukawa couplings of a FCNC sector Lagrangian of the form:

$$\mathcal{L}_{FCNC} = \lambda_{tcH}\bar{t}Hc + \lambda_{tuH}\bar{t}Hu + h.c.$$

can be derived. The 95% CL observed (expected) upper limits from ATLAS on the $|\lambda_{tcH}|$ and $|\lambda_{tuH}|$ couplings are 0.13 (0.10) and 0.13 (0.10), respectively.

III.7. Searches for other rare production modes

III.7.1. Searches for Higgs boson pair production

Higgs boson pair production in the SM is rare. It is however a very interesting final state to search in two specific modes: (i) the search for non-resonant production of the Higgs boson pair and (ii) the search for resonant production of two Higgs bosons in the decay of a heavier particle.

Non-resonant Higgs pair production is an interesting milestone in the study of prospects for constraining Higgs self-couplings. In the SM the main non-resonant production mode of two Higgs bosons in the final state proceeds through a loop (mainly of top quarks) (Fig. 11.9a). Another production mode is via the trilinear coupling of the Higgs boson (Fig. 11.9b), whose amplitude is not negligible compared to the former. These diagrams interfere negatively making the overall production rate smaller than what would be expected in the absence of a trilinear coupling. The sensitivity to the trilinear coupling will be discussed in Section III.7.1.ii.

(i) Searches for Higgs boson pair production

The searches for Higgs boson pair production both resonant and non-resonant are very interesting probes for a variety of theories beyond the SM, and can be done in a large number of Higgs boson decay channels. The ATLAS collaboration has searched both for resonant and non resonant Higgs boson pair production in the following

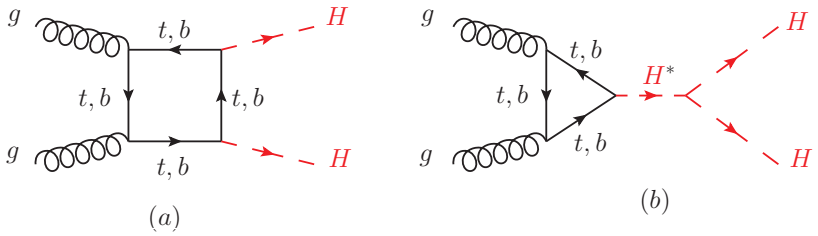

Figure 11.9: Feynman diagrams contributing to Higgs boson pair production through (a) a top- and b-quark loop and (b) through the self couplings of the Higgs boson.

Table 11.6: Summary of the final states investigated in the search for Higgs boson pair production by ATLAS (A) and CMS (C).

	$b\bar{b}$	$\tau^+\tau^-$	4ℓ	$\ell^+\nu\ell^-\overline{\nu}$	$\gamma\gamma$
$b\bar{b}$	A [163], C [166]	A [162], C [165]	C [164]	C [164]	A [161]
$\tau^+\tau^-$	–	C [164]	C [164]	C [164]	C [164]
4ℓ	–	–	C [164]	C [164]	C [164]
$\ell^+\nu\ell^-\overline{\nu}$	–	–	–	C [164]	A [162], C [164]

channels: (i) $HH \to b\bar{b}\gamma\gamma$ [161]; (ii) $HH \to b\bar{b}\tau^+\tau^-$ [162]; (iii) $HH \to b\bar{b}b\bar{b}$ [163]; and (iv) $HH \to WW^*\gamma\gamma$ [162]. The CMS collaboration has only performed searches for resonant Higgs boson pair production in a large variety of decay modes: (i) in final states containing multiple leptons (electrons or muons) covering the WW^*WW^*, WW^*ZZ^*, ZZ^*ZZ^*, $ZZ^*\tau^+\tau^-$, $WW^*\tau^+\tau^-$, $ZZ^*b\bar{b}$, $\tau^+\tau^-\tau^+\tau^-$ channels [164]; (ii) in final states with a di-photon pair compatible with being produced in the decay of the Higgs boson and one lepton covering the $\gamma\gamma WW^*$, $\gamma\gamma ZZ^*$, $\gamma\gamma\tau^+\tau^-$ channels [164]; (iii) in the $b\bar{b}\tau^+\tau^-$ channel [165]; and (iv) in the $b\bar{b}b\bar{b}$ channel [166]. A summary of the channels searched for at the LHC is given in Table 11.6. The results and interpretation of the search for resonant Higgs boson pair production are discussed in Section VII.8.i.d.

(ii) Measuring Higgs self couplings

The Higgs boson self coupling is an extremely important direct probe of the Higgs potential. The measurement of the quartic coupling in HHH final states is essentially deemed to be impossible at the HL-LHC. The possibility of measuring the trilinear coupling of the Higgs boson at the LHC in HH final states is studied in detail.

In the SM the Higgs boson pair production through the trilinear Higgs has an on-shell component and a large off-shell component. The on-shell $H \to H^*H^*$ is strongly disfavored, requiring two off-shell Higgs bosons in the final state. The sensitivity region to the trilinear coupling production as in Fig. 11.9-b, is mainly in the kinematic region where the two Higgs boson in the final state are on-shell and the Higgs boson acts as a propagator (off-shell). As discussed in the introduction to this section, this process interferes negatively with the background Higgs boson pair production (Fig. 11.9a). In the SM hypothesis sensitivity to the trilinear coupling requires the measurement of a

deficit in the Higgs boson pair production, in a similar way as the off-shell couplings measurement as explained in Section V.2. Given the current sensitivity of Higgs boson pair production measurements discussed in the previous Section III.7.1.i, only projections for the high Luminosity LHC are considered with an integrated luminosity of $3\,\text{ab}^{-1}$ and therefore in high pile-up conditions. Three channels have been investigated: (i) the $HH \to b\bar{b}\gamma\gamma$; (ii) the $HH \to b\bar{b}\tau^+\tau^-$; and (iii) the $HH \to b\bar{b}W^+W^-$. The prospects in channel (i) have been studied by both the ATLAS [167] and the CMS [168] collaborations, yielding a sensitivity of 1.3σ and 1.6σ respectively to overall Higgs boson pair production. The ATLAS and CMS collaborations have studied the channel (ii) yielding a sensitivity of 0.6σ [169] and 0.9σ [168] to Higgs boson pair production respectively. Only the CMS collaboration has studied the channel (iii) showing its low sensitivity [168]. It should be noted that there is a large uncertainty on these projections related both to the modeling of signal and the backgrounds, the very difficult high pile-up environment (both for reconstruction and trigger) and the design of the upgraded detectors. As discussed in Section III.7.1.i, more channels are possible and deserve to be studied in detail.

The measurements of the trilinear coupling requires to separate the contributions to the overall Higgs boson pair production and in particular measure the deficit expected in the case of SM couplings. The ATLAS collaboration has estimated the sensitivity to the trilinear λ_{HHH} coupling to exclusion regions of $\lambda_{HHH}/\lambda_{HHH}^{SM}$ at 95% CL of $]-\infty,-1.3]\cup[8.6,\infty[$ with the $b\bar{b}\gamma\gamma$ channel [167] and $]-\infty,-1.4]\cup[12.0,\infty[$ with the $b\bar{b}\tau^+\tau^-$ channel [169]. Measuring the Higgs boson trilinear coupling will be very difficult at the High Luminosity LHC.

III.8. Searches for rare decays of the Higgs boson

III.8.1. $H \to Z\gamma$

The search for $H \to Z\gamma$ is performed in the final states where the Z boson decays into opposite sign and same flavor leptons ($\ell^+\ell^-$), ℓ here refers to e or μ. While the branching fraction for $H \to Z\gamma$ is comparable to $H \to \gamma\gamma$ (about 10^{-3}) at $m_H = 125\,\text{GeV}$, the observable signal yield is brought down by the small branching ratio of $Z \to (e^+e^- + \mu^+\mu^-) = 6.7 \times 10^{-2}$. In these channels, the $m_{\ell\ell\gamma}$ mass resolution is excellent (1-3%) so the analyses search for a narrow mass peak over a continuous background. The major backgrounds arise from the $Z + \gamma$ final state radiation in Drell–Yan decays and $Z +$ jets processes where a jet is misidentified as a photon. The ratio of signal over background in this channel is typically of the order of 0.5%. In a narrow window of a few GeV around125 GeV, several hundreds of events are expected.

Events are divided into mutually exclusive categories on the basis of the expected $m_{\text{Z}\gamma}$ resolution and the signal-to-background ratio. A VBF category is formed for $H \to Z\gamma$ candidates which are accompanied by two energetic jets separated by a large pseudorapidity. While this category contains only about 2% of the total event count, the signal-to-noise is about an order of magnitude higher. The search for a Higgs boson is conducted independently in each category and the results from all categories are then combined.

No excess of events is observed in either ATLAS or CMS experiments. The CMS expected and observed 95% CL upper limits for $m_H = 125\,\text{GeV}$ [170] on the signal strength μ are 10 and 9.5 respectively. The ATLAS expected and observed upper limits [171] on the signal strength μ are 9 and 11 respectively for a SM $m_H = 125.5\,\text{GeV}$.

III.8.2. $H \to \mu^+\mu^-$

$H \to \mu^+\mu^-$ is the only channel where the Higgs coupling to second generation fermions can be measured at the LHC. The branching fraction in this channel for a 125 GeV SM Higgs boson is 2.2×10^{-4}, about ten times smaller than that for $H \to \gamma\gamma$. The dominant and irreducible background arises from the $Z/\gamma^* \to \mu^+\mu^-$ process which has a rate several orders of magnitude larger than that from the SM Higgs boson signal. Due to the precise muon momentum measurement achieved by ATLAS and CMS, the $m_{\mu^+\mu^-}$ mass resolution is excellent ($\approx 2-3\%$). A search is performed for a narrow peak over a large but smoothly falling background. For optimal search sensitivity, events are divided into several categories. To take advantage of the superior muon momentum measurement in the central region, the two experiments subdivide events by the pseudorapidity of the muons. To suppress the Drell–Yan background, ATLAS requires $p_T^{\mu^+\mu^-} > 15\,\text{GeV}$ while CMS separates them into two $p_T^{\mu^+\mu^-}$ based categories. CMS further categorizes events by the number and the topology of additional energetic jets in the event.

No excess in the $m_{\mu^+\mu^-}$ spectrum is observed near 125 GeV. From an analysis of their Run 1 data, ATLAS sets [172] an observed (expected) 95% CL upper limit on the signal strength $\mu < 7.0$ (7.2). The CMS analysis [173] of their 7 and 8 TeV data sets an observed (expected) limit of $\mu < 7.4$ (6.5).

III.8.3. $H \to e^+e^-$

A search similar to the $H \to \mu^+\mu^-$, is performed by CMS in the di-electron channel [173]. In this search channel there the contribution from the peaking background from Higgs boson decays to diphoton mis-identified as di-electrons (when mostly converted photons are faking electrons) needs to be assessed. The sensitivity to the SM Higgs decays is negligible given the extremely small branching fraction to e^+e^-, approximately 40,000 times smaller than the branching fraction to dimuons. It is nevertheless interesting to probe this decay channel to search for potential large anomalous couplings. Assuming a SM Higgs boson production cross section, the observed limit on the branching fraction at the 95% CL is 0.0019 [173], five orders of magnitude larger than the expected SM prediction.

III.8.4. Lepton flavor violating (LFV) Higgs boson decays

Given the Yukawa suppression of the couplings of the Higgs boson to quarks and leptons of the first two generations and the small total width of the Higgs boson, new physics contributions could easily have sizable branching fractions. One very interesting possibility is the Lepton Flavor Violating (LFV) decays of the Higgs boson, in particular in the $\tau\mu$ and τe modes. These decays are suppressed in the SM but could be enhanced in theories such as two-Higgs-doublet models (discussed in Section VII).

Table 11.7: Summary of the results of searches for lepton flavor violating decays of the Higgs boson in the $\tau\mu$ channel from ATLAS and CMS.

	ATLAS $\tau_{\rm had}\mu$	ATLAS $\tau_{\rm lep}\mu$	ATLAS $\tau\mu$	CMS $\tau\mu$
BR($H \to \tau\mu$)	$(0.77 \pm 0.62)\%$	$(0.03^{+0.88}_{-0.86})\%$	$(0.53 \pm 0.51)\%$	$(0.84^{+0.39}_{-0.37})\%$
95% CL Expected limit	1.24%	1.73%	1.01%	0.75%
95% CL Observed limit	1.85%	1.79%	1.43%	1.51%

There are already fairly strong constraints on LFV Yukawa couplings $|Y_{\tau\mu}|$ from channels such as the $\tau \to 3\mu$ or $\tau \to \mu\gamma$, or a re-interpretation of the search for Higgs decays to $\tau^+\tau^-$. A direct search at the LHC however complements these indirect limits. The search for LFV decays in the $\tau\mu$ channel have been done with the Run 1 dataset in several channels according to the subsequent decay of the τ. The results from CMS [174] and for ATLAS for the hadronic [175], the leptonic [176] decays of the tau, and their combination [176] are reported in Table 11.7. It is interesting to note that the analysis strategies for the di-lepton $\tau_{lep}\mu$ channel are very different between the ATLAS [176] and CMS [174].

As shown in Table 11.7 a small excess in this channel is observed by CMS with a significance of 2.5σ, while in ATLAS the excess is smaller and of the order of 1σ.

The ATLAS collaboration has also reported results on the search for the LFV Higgs boson decays in the τe channel [176], yielding an observed (expected) limit of 1.04% (1.21%).

III.8.5. Probing charm- and light-quark Yukawa couplings

Probing the Yukawa couplings to quarks of the second or even the first generation is extremely challenging given the overwhelming background and the much smaller signal rates. The possibility of probing the Yukawa coupling to the charm has been discussed in [177] where indirect bounds on the charm Yukawa coupling are estimated from a combined fit to the Higgs data. The direct impact of Higgs decays to a pair of charm quarks on the direct search for $H \to b\overline{b}$ is also investigated.

Another possibility to access the Higgs Yukawa coupling has been discussed in [178], through the decays of the Higgs boson to a final state with charmonium: $H \to J/\Psi\gamma$. Higgs decays in this final state have been searched for by the ATLAS collaboration [179]. The sensitivity of this analysis is however several orders of magnitude above the branching fraction estimated for the SM coupling BR($H \to J/\Psi\gamma$) $= (2.8 \pm 0.2) \times 10^{-6}$ [178]. The ATLAS collaboration [179] has also searched for Higgs decays to $\Upsilon(nS)\gamma$ where $(n = 1, 2, 3)$, a channel with much lower sensitivity than the $H \to b\overline{b}$ to the Yukawa coupling to b-quarks.

More recently the ATLAS collaboration has searched for another quarkonia final state where the Higgs boson decays to $\phi\gamma$ [180] at the LHC Run 2 and a center-of-mass energy of 13 TeV, with a specific trigger. This channel could probe deviations from the strange-quark Yukawa coupling of the Higgs boson. Its sensitivity is several orders of magnitude above the expectation from the SM Higgs boson. Other quarkonia final states,

such as the $\rho\gamma$, which could potentially probe the Yukawa coupling to light quarks, can also be searched for.

III.8.6. Rare decays outlook

Rare decays such as those described in the above sections have a clearly limited sensitivity. They however already deliver interesting messages. For example, if the coupling of the Higgs boson was as strong in the dimuon channel as it is for the top quark, this mode would have been observed already with large significance. The observed Higgs boson couplings are manifestly non-universal. Further developing these rare decay modes is an important component of the high luminosity program of the LHC to directly probe the couplings of the Higgs boson, and to potentially measure the Yukawa coupling of the Higgs boson to fermions of the second generation, in particular to muons.

III.9. Searches for non-standard model decay channels

The main decay and production properties of the observed Higgs boson are consistent with predictions of the SM. It may however have other decay channels beyond those anticipated in the SM. Among these and of great interest are the invisible decays into stable particles that interact very weakly with the detector, and that are undetected, such as Dark Matter particle candidates. Other non standard decay channels that have been investigated are the decays of the Higgs particle to hidden valley or dark particles.

III.9.1. Invisible decays of the Higgs boson

The discovery of the Higgs boson immediately raised the question of its couplings to dark matter and how it could be used to reveal its existence at colliders, using the Higgs boson as a portal to dark matter (see Ref. [181] and references therein). If kinematically accessible and with a sufficiently large coupling to the Higgs boson, dark matter particles, such as, e.g., neutralinos in SUSY models, graviscalars in models with extra dimensions or heavy neutrinos in the context of four-generation fermion models, would manifest themselves as invisible decays of the Higgs boson, thus strongly motivating searches for the invisible decays of the Higgs boson.

To identify an invisibly decaying Higgs boson at the LHC, it must be produced in association with other particles. Searches for invisible decays of the Higgs particle at the LHC have been carried out in three associated production modes of the Higgs boson with the highest SM cross sections and target events with large missing energy.

The ggF production mode has the largest SM cross section but it usually results in the Higgs boson being created alone and hence leaving no characteristic signature in the detector of its invisible decay. One way to search for invisible decays in ggF production mode is to look for events with the "monojet" topology arising from initial state gluon radiation and containing missing energy. The major irreducible background in such searches stems from Z + jets events where the Z boson decays into a pair of neutrinos. The analysis with the best sensitivity targets the VBF production topology but suffers from large backgrounds arising from events with two jets and large missing energy. The VH mode has much smaller cross section but the presence of a W or Z boson allows a variety of final states that can be tagged with relatively low background.

Table 11.8: Summary of the channels searched for and the corresponding 95% CL limits from ATLAS and CMS on the branching fraction for the Higgs boson decay to invisible particles assuming a SM Higgs boson production cross section. The results in parentheses are the expected exclusions. [*] indicates analyses based only on 8 TeV data. When combining Run 1 results and the results from the $\approx 2\,\text{fb}^{-1}$ of 13 TeV data acquired in 2015, the CMS observed (expected) limit improves to < 32 (26) % at 95% CL.

	ATLAS (Run 1)	CMS (Run 1)	CMS (13 TeV, 2015)
ggF (monojet); $H \to$ inv.	–	67 (71) % [*]	-
VBF; $H \to$ inv.	28 (31) %	57 (40) % [*]	69 (62) %
$Z \to \ell^+\ell^-$; $H \to$ inv.	75 (62)%	75 (91) %	125 (125)%
$Z \to b\bar{b}$; $H \to$ inv.	–	182 (189) % [*]	-
$Z \to jj$; $H \to$ inv.	78 (86)%	–	-
Combination of all direct searches	25 (27)%	36 (30) %	-

ATLAS [182–185], and CMS [186–189] have searched for such final states but have observed no significant excess over predicted backgrounds. Table 11.8 summarizes the 95% CL limits on the invisible decays of the Higgs boson assuming SM Higgs boson production cross section and corresponding detector acceptances.

III.9.2. Exotic Higgs boson decays

The 125 GeV Higgs boson not only serves as a probe for potential dark matter candidates, but also to search for other exotic particles arising from fields associated with a low-mass hidden sector. Such hidden sectors are composed of fields that are singlets under the SM group $\text{SU}(3) \times \text{SU}(2) \times U(1)$. These models are referred to as hidden valley models [190, 191]. Since a light Higgs boson is a particle with a narrow width, even modest couplings to new states can give rise to a significant modification of Higgs phenomenology through exotic decays. Simple hidden valley models exist in which the Higgs boson decays to an invisible fundamental particle, which has a long lifetime to decay back to SM particles through small mixings with the SM Higgs boson; Ref. [191] describes an example. The Higgs boson may also decay to a pair of hidden valley "v-quarks," which subsequently hadronize in the hidden sector, forming "v-mesons." These mesons often prefer to decay to the heaviest state kinematically available, so that a possible signature is $H \to 4b$. Some of the v-mesons may be stable, implying a mixed missing energy plus heavy flavor final state. In other cases, the v-mesons may decay to leptons, implying the presence of low mass lepton resonances in high- H_T events [192]. Other scenarios have been studied [193] in which Higgs bosons decay predominantly into light hidden sector particles, either directly, or through light SUSY states, and with subsequent cascades that increase the multiplicity of hidden sector particles. In such scenarios, the high multiplicity hidden sector particles, after decaying back into the SM, appear in the detector as clusters of collimated leptons known as lepton jets.

A variety of models have been investigated searching for final states involving dark photons and hidden valley scalars. The resulting topologies searched for are prompt

electron jets in the WH production process [194], displaced muonic jets [195], four muons final state, and long lived weakly interacting particles [196]. The latter occur not only in hidden valley scenarios, but also in gauge-mediated extensions of the minimal supersymmetric standard model (MSSM), the MSSM with R-parity violation, and inelastic dark matter [197]. Finally the CMS collaboration has performed a search for pair production of light bosons [198]. Such a scenario can occur in supersymmetric models with additional hidden (or dark) valleys.

IV. Combining the main channels

As described in Section II, there are five main production modes of a SM Higgs boson at the LHC. In the LHC Run 1 dataset the predicted numbers of SM Higgs bosons produced per experiment are approximately 0.5 million, 40,000, 20,000 and 3,000 in the gluon fusion, vector boson fusion, the associated VH and $t\bar{t}H$ production modes respectively[3]. There are also five main decay channels: the $\gamma\gamma$, ZZ, WW, $\tau^+\tau^-$ and $b\bar{b}$. Analyses using exclusive categories according to production modes have been designed to maximize the sensitivity of the analyses to the presence of a signal using known characteristic features of these modes. These categories can also be used to further separate production modes for each decay channel. The typical number of events selected eventually in each decay channel ranges from a fraction of an event to O(100) events per experiment.

The analysis strategy used by the LHC and Tevatron experiments to perform the searches for the Higgs boson has been based on the Higgs decay modes. It is a natural choice given that it focusses on the decay products of the object searched for. However, for each channel, exclusive subchannels have been defined according to the Higgs production processes and in the results presented these subchannels have been combined. The natural extension of this approach in order to probe further the production and decay modes of the Higgs boson is to combine the analysis channels together. Such a combination is also used in Section VI to further measure the coupling properties of the Higgs boson.

At the LHC or the Tevatron, the total cross section cannot be measured in any of the production modes. As a consequence, neither the absolute branching fractions nor the total natural width of the Higgs boson can be directly measured. However, a combined measurement of the large variety of categories described in Section III, with different sensitivities to various production and decay modes permits a wide variety of measurements of the production, decay or in general coupling properties. These measurements require, in general, a limited but nevertheless restrictive number of assumptions.

[3] Similarly at the Tevatron where the CDF and D0 experiments have gathered approximately $10\,\mathrm{fb}^{-1}$ of data at 1.96 TeV, the predicted numbers of SM Higgs boson events produced per experiment are approximately 10,000 and 2,000 events in the gluon fusion and VH associated production, respectively.

In this section, results will be given combining not only different channels, but also the ATLAS and CMS results together [141]. These results were derived by the two collaborations, taking rigorously into account all correlations in the systematic uncertainties and in the large number of channels and their categories. This combination has led the two collaborations to a more precise experimental portrait of the Higgs boson. This work also concludes and synthesizes the analyses of the main production and decay channels of the Higgs boson at the Run 1 of the LHC.

In this section, only the results on the main Higgs boson production and decay modes will be discussed. The combination framework described herein will also be used in Section VI, to discuss the measurements of the coupling properties of the Higgs boson.

IV.1. Principles of the combination

The combination of the Higgs boson analysis channels in each experiment and for the two experiments together is done using a fit of a signal and background model to the data. As described above the data is made of a large number of categories, aiming at reconstructing exclusive production and decay modes. In the combination of ATLAS and CMS [141] there are approximately 600 categories. The combination is a simultaneous fit to all these categories, using a reduced number of parameters of interest and a Higgs boson mass fixed at its measured value (see Section III.2). A synoptic view of the main production categories is illustrated in Table 11.9. The much larger number of categories present in the ATLAS and CMS combination [141], is due to additional separation in terms of finer exclusive production regions, decay channels of the Z and the W bosons, and taus, control regions where little-to-no signal is present, and different center-of-mass energies. It should be noted that the individual combination performed by ATLAS [199] included two additional decay channels: the $\mu^+\mu^-$ and $Z\gamma$, for the sake of simplicity these channels were omitted in the ATLAS-CMS combination. In addition, a $H \to b\overline{b}$ analysis performed by CMS [133] and included in its own combination, has been omitted from the ATLAS-CMS combination.

The key to understanding how the combination of channels works relies on the combination master formula, which expresses for each category, indexed by c, of a given channel (typically a category covers mostly one decay mode, but possibly various production modes), the measured number of signal events n_s^c as a function of a limited number of parameters as follows:

$$n_s^c = (\sum_{i,f} \mu_i \, \sigma_i^{SM} \times A_{if}^c \times \varepsilon_{if}^c \times \mu_f \, \mathrm{BR}_f^{SM}) \times \mathcal{L}^c \tag{11.13}$$

The production index is defined as $i \in \{ggH, VBF, VH, ttH\}$ and the decay index is defined as $f \in \{\gamma\gamma, WW, ZZ, bb, \tau\tau\}$ while σ_i^{SM} and BR_f^{SM} are the corresponding production cross sections and decay branching fractions, estimated as described in Section II, assuming that the Higgs boson is that of the SM. A_{if}^c and ε_{if}^c are the signal acceptance and the reconstruction efficiency for given production and decay modes in

Table 11.9: Summary of the main production categories used in the analysis channels involved in the combined measurement of the coupling properties of the Higgs boson. (A) and (C) indicate respectively when ATLAS and CMS include the specific exclusive category in the combination. For the ttH channel, note that the number of leptons (ℓ) indicates typically the type of decay of the two top quarks.

	$\gamma\gamma$	ZZ (4ℓ)	WW ($\ell\nu\ell\nu$)	$\tau^+\tau^-$	$b\overline{b}$
ggF (high p_T^H)	A	A	—	A	—
ggF (incl. or low p_T^H)	A - C	A - C	A - C	—	—
ggF 1-jet	—	C	A - C	C	—
VBF	A - C	A - C	A - C	A - C	C
WH (1-ℓ)	A - C	A	A - C	C	A - C
WH (two jets)	A - C	A - C	A - C	—	—
ZH (0-ℓ)	A - C	A	—	—	A - C
ZH (2-ℓ)	A - C	A	A - C	C	A - C
ZH (two jets)	A - C	A - C	A - C	—	—
ttH (1-ℓ)	A - C	—	A - C	A - C	A - C
ttH (2-ℓ)	—	—	A - C	A - C	A - C
ttH (hadronic)	A - C	—	—	—	A

the category c. $\mathcal{L}^c$ is the integrated luminosity used for that specific category. For the purpose of this review, these parameters can be considered as fixed[4].

The parameters of interest in the master formula are the signal strength parameters μ_i and μ_f. It is important to note that the formula relies on the factorization of the production cross section and decay branching fraction, which assumes the narrow width approximation. The width of the Higgs boson will be discussed in Section V, however for the precision needed here, the fact that the Higgs boson has been observed in decay channels with high mass resolution as a resonance is sufficient to validate this hypothesis. It is also manifest in the above equation that the ten parameters for the production modes (μ_i) and decay modes (μ_f) cannot be determined simultaneously. This illustrates that total cross sections or branching fractions cannot be measured without further assumptions in this fit.

The master formula also illustrates an important caveat to the measurement of signal

[4] In the combination performed by the ATLAS and CMS experiments the systematic uncertainties on these parameters are taken into account by allowing these parameters to vary in the fit.

Table 11.10: Summary of the combined measurements of the $\sigma \times$ BR for the five main production and five main decay modes. When uncertainties are separated into two components, the first is the statistical uncertainty and the second is the systematic uncertainty. When only one uncertainty is reported, it is the total uncertainty.

	$\gamma\gamma$	ZZ (4ℓ)	WW ($\ell\nu\ell\nu$)	$\tau^+\tau^-$	$b\bar{b}$	Comb.
ggF	$1.10^{+0.22+0.07}_{-0.21-0.05}$	$1.13^{+0.33+0.09}_{-0.30-0.07}$	$0.84^{+0.12+0.12}_{-0.12-0.11}$	$1.00^{+0.4+0.4}_{-0.4-0.4}$	—	$1.03^{+0.16}_{-0.14}$
VBF	$1.3 \pm 0.5^{+0.2}_{-0.1}$	$0.1^{+1.1+0.2}_{-0.6-0.2}$	$1.2^{+0.4+0.2}_{-0.3-0.2}$	$1.3^{+0.3+0.2}_{-0.3-0.2}$	—	$1.18^{+0.25}_{-0.23}$
WH	$0.5^{+1.3+0.2}_{-1.2-0.1}$	—	$1.6^{+1.0+0.6}_{-0.9-0.5}$	$-1.4^{+1.2+0.7}_{-1.1-0.8}$	$1.0^{+0.4+0.3}_{-0.4-0.3}$	$0.89^{+0.40}_{-0.38}$
ZH	$0.5^{3.0\ +0.5}_{-2.5-0.2}$	—	$5.9^{+2.3+1.1}_{-2.1-0.8}$	$2.2^{+2.2+0.8}_{-1.7-0.6}$	$0.4^{+0.3+0.2}_{-0.3-0.2}$	$0.79^{+0.38}_{-0.36}$
ttH	$2.2^{1.6\ +0.2}_{-1.3-0.1}$	—	$5.0^{+1.5+1.0}_{-1.5-0.9}$	$-1.9^{+3.2+1.9}_{-2.7-1.8}$	$1.1^{+0.5+0.8}_{-0.5-0.8}$	$2.3^{+0.7}_{-0.6}$
Comb.	$1.14^{+0.19}_{-0.18}$	$1.29^{+0.26}_{-0.23}$	$1.09^{+0.18}_{-0.16}$	$1.11^{+0.24}_{-0.22}$	$0.70^{+0.29}_{-0.27}$	$1.09^{+0.11}_{-0.10}$

strength parameters. In case these are interpreted as scale factors of the production cross sections or branching fractions, then all the other quantities such as the acceptances and efficiencies, A^c_{if} and ε^c_{if}, need to be assumed as independent and fixed to their estimated values for the SM Higgs boson. An additional important caveat to note concerning these combined results is that only the normalizations are varied, while the discriminating variables for the signal are not modified and are still used in the fit. These caveats are of particular importance in the use of the combination to measure the coupling properties of the Higgs boson as discussed in Section VI. For relatively small perturbations of the couplings of the Higgs boson from the SM values, this hypothesis is valid.

However the 25 products, $\mu_i \times \mu_f$, can be considered as free parameters and in principle measurable (if there is sufficient sensitivity from specific categories). Measuring the products of signal strengths can be viewed as the measurements of the cross sections times the branching fraction, $\sigma \cdot$ BR. The results are reported in Table 11.10 for the combination of ATLAS and CMS and they are illustrated in Fig. 11.10.

It is remarkable that of the 25 possible combinations of production and decay modes in the main channels, the fit to ATLAS and CMS data allows the measurement of 20. A coherent picture emerges with an excellent consistency between the observation in each channel and the expectation for a SM Higgs boson.

This 20 parameter fit quantifies, with very little theoretical input, the current experimental knowledge of the main production and decays modes. It is also a very useful tool to further understand the influential channels in the measurements of the Higgs couplings. Without a loss of independence of the theoretical predictions, a less general fit allowing for further interpretations concerning production cross sections and branching fractions is possible. In this fit a reference process, measured with high precision and significance, is used to parametrize all the other processes. In the ATLAS-CMS combination [141] the gluon fusion production mechanism in the $H \to ZZ$ decay mode is

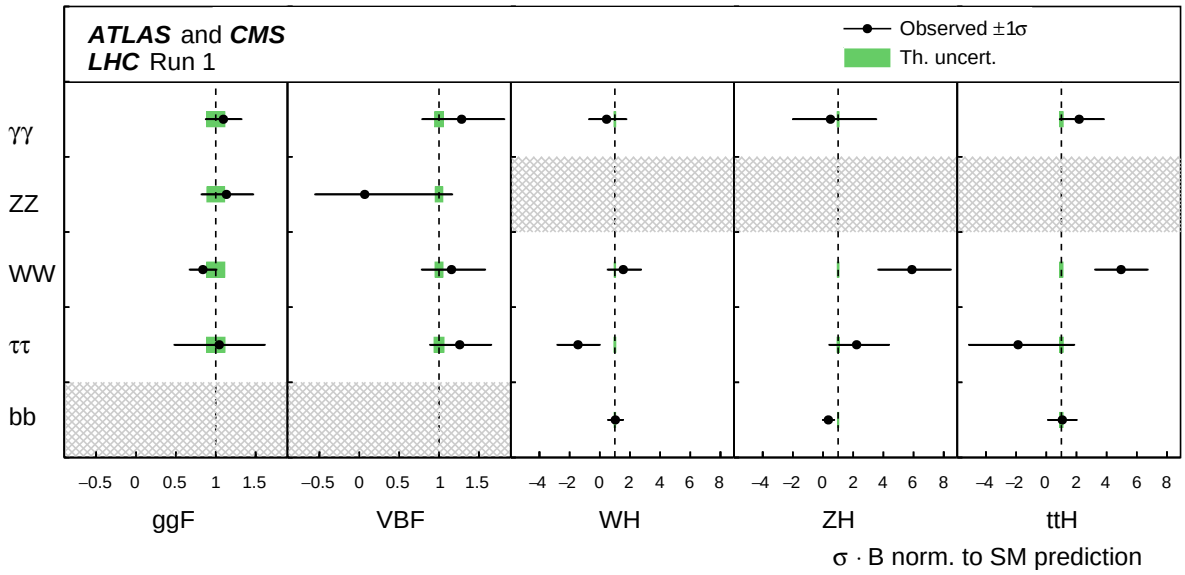

Figure 11.10: Combined measurements of the products $\sigma \cdot \mathrm{BR}$ for the five main production and five main decay modes.

chosen. Then, the master formula applies with the following parameters for all i and f indices except when both $i = ggF$ and $f = ZZ$

$$\begin{aligned} \mu_i &= \frac{\sigma_i}{\sigma_{ggF}\sigma_i^{SM}} \times \mu_{gg\to H\to ZZ} \\ \mu_f &= \frac{\mathrm{BR}_i}{\mathrm{BR}_{ZZ}\mathrm{BR}_i^{SM}} \\ \mu_{gg\to H\to ZZ} &= \mu_{ggF} \times \mu_{ZZ} \times \sigma_i^{SM} \times \mathrm{BR}_f^{SM} \end{aligned} \tag{11.14}$$

The result of the combination with these 9 parameters is illustrated in Fig. 11.11. It allows interesting conclusions on the production and decay properties of the Higgs boson. It shows that the ratio of the decay rates to Z and W bosons is as expected from the SM, a direct illustration of the custodial symmetry, and also quantifies the relative precision at which the ttH coupling is currently measured. It also shows that with the improved precision stemming from the combination, no significant deviations from the SM is observed.

Finally, the most constrained fit in this combination, and historically the first made, allows for only one single parameter to vary *i.e.* $\forall(i,f), \mu_i = \mu_f = \mu$. This global signal strength model provides the most precise and simple probe of the compatibility of the signal with the SM Higgs boson. This model is sensitive to any deviation from the SM Higgs boson couplings provided that these deviations do not cancel overall. The combined global signal strength is

$$\mu = 1.09 \pm 0.07\ (\mathrm{stat})\ \pm 0.04\ (\mathrm{expt})\ \pm 0.03\ (\mathrm{th.\,bkg})\ \pm 0.07\ (\mathrm{th.\,sig})$$

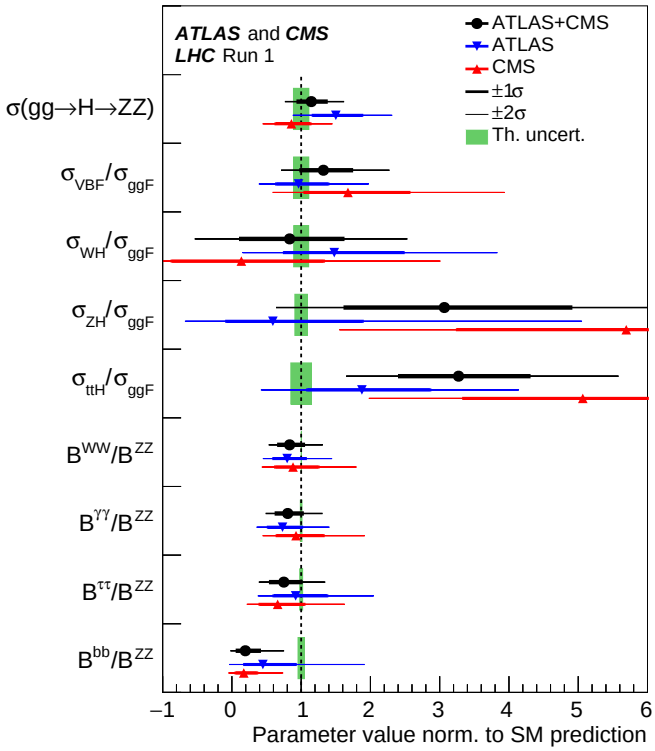

Figure 11.11: Measurement of the $\sigma(gg \to H \to ZZ)$ cross section and of the ratios of cross sections and branching fractions from the combination of the ATLAS and CMS measurements. The results from each experiment are also shown. The results are normalised to the SM predictions for the various parameters. The shaded bands indicate the theoretical uncertainties in these predictions.

This overall signal strength is fully compatible with the SM expectation of 1, with a precision of 10%. It is interesting to note that the major uncertainties in this first measurement arises from the limited precision in the theoretical predictions for the signal production processes.

IV.2. Characterization of the main decay modes and observation of Higgs decays to taus

Despite the large number of decay channels, since the cross sections cannot be independently measured, from the measurements described in this section it is impossible to measure decay branching fractions without a loss of generality. The simplest assumption that can be made is that the production cross sections are those of the SM Higgs boson, which is equivalent to assuming that for all i indices $\mu_i = 1$. All branching fractions μ_f can then be measured in a simple 5 parameter fit. The result of this fit is illustrated in Fig. 11.12, and the measured signal strengths are reported in Table 11.11.

Table 11.11 also reports the results of a similar combination by each experiment from their data. For the main discovery modes $\gamma\gamma$, ZZ and WW, the combined significance is not computed as these decay modes have been firmly established by each experiment

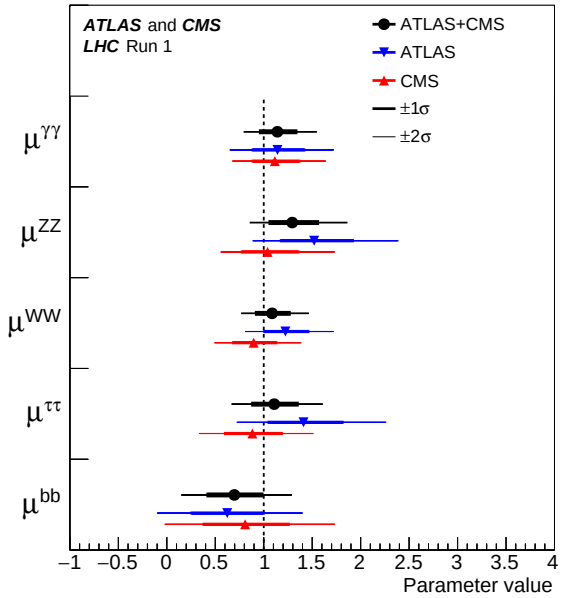

Figure 11.12: The signal strengths μ measured by the ATLAS and CMS experiments [141] for the five principal Higgs boson decay channels assuming that the production cross sections are those of the SM.

independently. However for the $\tau^+\tau^-$ and $b\bar{b}$ decay modes these results shed new combined light on the observation significance in these channels.

For the $\tau^+\tau^-$ channel, ATLAS and CMS are both sensitive and have observed excesses in their data. The individual results are not sufficiently significant to claim an observation, but combined they are. This conclusion can be made also in a more generic manner using the ratio of branching fractions model described above. It should be noted that in the search for $H \to \tau\tau$ decay, the most sensitive production mode is the VBF process, the experimental evidence for which is discussed in Section IV.3.

As illustrated in Table 11.11, ATLAS and CMS are both much less sensitive to the $H \to b\bar{b}$ decay mode. The available sensitivity comes mostly from the VH process, as discussed earlier in this section. The combined significance of 3.7σ is sufficient to suggest evidence, however ATLAS and CMS observations are both low with respect to the rate expected for the SM Higgs boson. With the increased production cross sections at 13 TeV and the much larger dataset expected, this channel will undoubtedly be followed with great attention at the Run 2 of the LHC.

IV.3. Characterization of the main production modes and evidence for VBF production

As discussed earlier, most analysis channels are divided into several exclusive categories allowing for an increased overall sensitivity and to measure the various Higgs production modes. The cross sections of the main production modes can be measured assuming that the branching fractions are those of the SM Higgs boson, *i.e.* for all f indices $\mu_f = 1$. These assumptions lead to a 5 parameter combination. The result is illustrated

Table 11.11: Summary of the significances of the excesses observed for the main decay processes. The $\gamma\gamma$, ZZ, and W^+W^- decay modes have been established at more than 5σ by both the ATLAS and CMS experiments individually, the combined observation significance therefore exceeds 5σ and is not reported here.

	Expected Z	Observed Z
$\gamma\gamma$	4.6σ (ATLAS) 5.3σ (CMS)	5.2σ (ATLAS) 4.6σ (CMS)
ZZ	6.2σ (ATLAS) 6.3σ (CMS)	8.1σ (ATLAS) 6.5σ (CMS)
WW	5.9σ (ATLAS) 5.4σ (CMS)	6.5σ (ATLAS) 4.7σ (CMS)
$\tau^+\tau^-$	3.4σ (ATLAS) 3.9σ (CMS)	4.5σ (ATLAS) 3.8σ (CMS)
$b\bar{b}$	2.6σ (ATLAS) 2.5σ (CMS)	1.4σ (ATLAS) 2.1σ (CMS)
$\tau^+\tau^-$ (Combined)	5.0σ	5.5σ
$b\bar{b}$ (Combined)	3.7σ	2.6σ

Table 11.12: Summary of the combined significance of observation for the main production processes. The ggF process has been established at more than 5σ by both the ATLAS and CMS experiments individually, the combined observation significance far exceeds 5σ and is not reported here.

	Expected Z		Observed Z	
ggF	Ind.	Obs.	Ind.	Obs.
VBF	4.6σ		5.4σ	
WH	2.7σ		2.4σ	
ZH	2.9σ		2.3σ	
VH	4.2σ		3.5σ	
ttH	2.0σ		4.4σ	

in Fig. 11.13 for the ATLAS-CMS combination [141]. The significance of observation of the production modes are reported in Table 11.12.

The gluon fusion production process is the dominant production mode. Although no numerical estimate of combined significance of observation for this process has been given by the experiments, it is considered as established due to the overwhelming evidence from the three main discovery channels. None of the other production modes have been firmly established by the experiments individually. These show that for the VBF mode, the combination has a large sensitivity and produced a combined observation of 5.4σ, establishing this process with a rate compatible with that expected from the SM Higgs boson. A similar conclusion can be reached but with assumptions from the fit to the ratio $\sigma_{VBF}/\sigma_{ggF}$ discussed earlier in this section.

It is interesting to note that despite the low sensitivity to the ttH production mode, the excesses observed in several ttH channels (discussed in Section III.6.1), lead to a significance of direct observation for ttH production in excess of 4σ. The compatibility of this observation with the SM production rate is at the 2.3σ level. Given the increased sensitivity expected at the higher center-of-mass energy of 13 TeV, a great attention will undoubtedly be devoted to this channel.

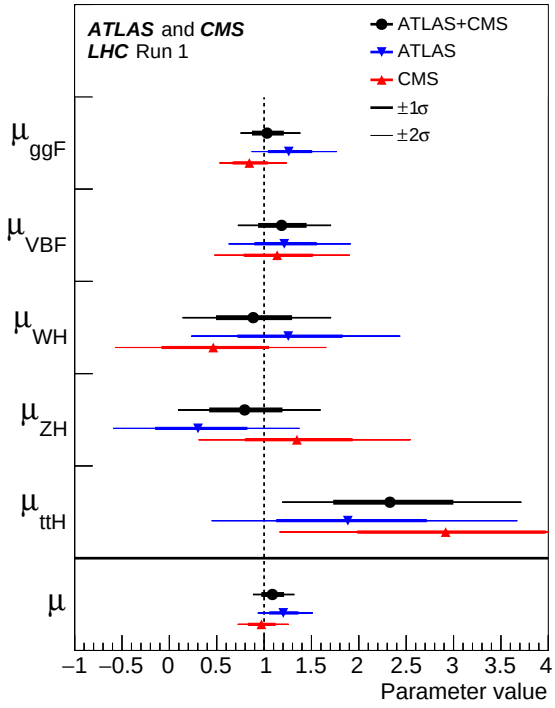

Figure 11.13: The signal strengths μ measured by the ATLAS and CMS experiments [141] in the five principal production modes and their combination, assuming that the decay branching fractions are those of the SM Higgs boson.

One can further reduce the number of parameters of interest by grouping the ggF and ttH production modes together, as they both originate in the SM from the Yukawa coupling to the top quark and the VH and VBF processes together as they both originate from the coupling of the Higgs boson to massive vector bosons. Grouping here means that the two production cross sections are scaled by a single parameter of interest, which is equivalent to fixing their ratio to the expected ratio for a SM Higgs boson. The 2-dimensional profile of the likelihood for each main decay channel individually is shown in Fig. 11.14, illustrating the relative constraint that each decay channel is imposing on the production process and the correlation between the grouped processes. This correlation stems from the cross contamination of the exclusive categories with processes from the two groups. Concerning the VBF production mode, these results show its manifest predominance in the $\tau^+\tau^-$ channel and the importance of the $\gamma\gamma$ and WW channels in constraining it. While in most cases the $ggF + ttH$ group is mostly

constrained by the indirect gluon fusion process, in the case of the $b\bar{b}$ channel, the bulk of the constraint comes from the ttH process.

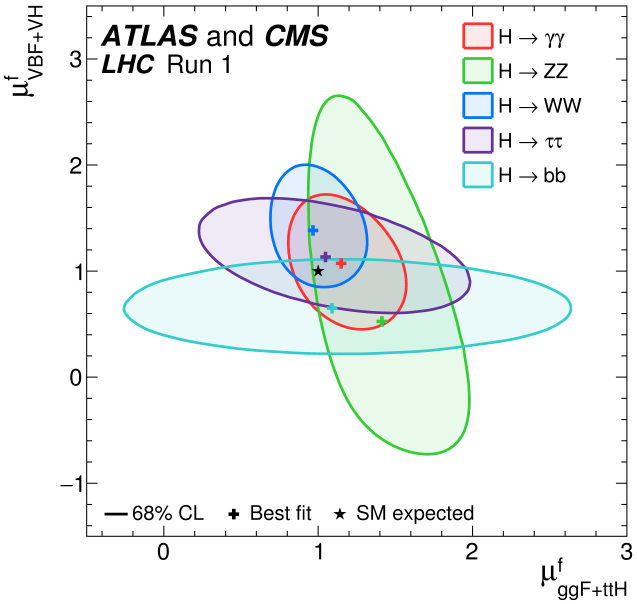

Figure 11.14: Two dimensional likelihood contours for individual production signal strengths for the $VBF + VH$ versus $ggF + ttH$ processes for various Higgs boson decay modes for the ATLAS and CMS experiment combination.

V. Main quantum numbers and width of the Higgs boson

V.1. Main quantum numbers J^{PC}

Probing the Higgs boson quantum numbers is essential to further unveiling its coupling properties. The measurements of the signal event yields of the observed new state in all the channels discussed in Sections III and IV and their compatibility with the SM Higgs boson predictions, give a qualitative, but nonetheless compelling indication of its nature. This qualitative picture is further complemented by the implications of the observation of the particle in the diphoton channel. According to the Landau–Yang theorem [200], the observation made in the diphoton channel excludes the spin-1 hypothesis and restricts possibilities for the spin of the observed particle to 0 or 2.

The Landau–Yang theorem does not apply if the observed state is not decaying to a pair of photons but to a pair of scalars subsequently decaying to two very collimated pairs of photons (as for example in the case of $H \to a_1 a_1 \to 4\gamma$). This possibility has not been rigorously excluded but is not experimentally favored since tight selection criteria are applied on the electromagnetic shower shapes of the reconstructed photons. A more systematic analysis of shower shapes and the fraction of conversions could be performed to

further discriminate between the single prompt photon and the two overlapping photons hypotheses. There are also potential theoretical loopholes concerning the applicability of the Landau–Yang theorem [200], such as off-shell vector boson decays. However, for the observed particle not to be of spin 0 and +1 parity would require an improbable conspiracy of effects. It is nevertheless important that this hypothesis be independently tested, in particular since the measurements of coupling properties of the Higgs boson assume that the observed state is CP-even.

V.1.1. Charge conjugation

The charge conjugation quantum number is multiplicative, therefore given that the Higgs-like particle is observed in the $H \to \gamma\gamma$ channel, and given that photons are C-odd eigenstates, assuming C conservation, the observed neutral particle should be C-even.

V.1.2. Spin and parity

To probe the spin and parity quantum numbers of the discovered particle, a systematic analysis of its production and decay processes is performed in several analyses, designed to be independent of the event yields measured and relying instead on the production and the decay angles, and on the threshold distributions as long as a significant signal is observed (*i.e.* an excess over the expected background that can be used to further discriminate between signal hypotheses) of the produced particle. These analyses are based on probing various alternative models of spin and parity. These models can be expressed in terms of an effective Lagrangian [201] or in terms of helicity amplitudes [202, 203]. The two approaches are equivalent. In the following, the effective Lagrangian formalism is chosen to describe the models considered and a restricted number of models are discussed [201]. In the analysis performed by CMS [202] a larger number of models have been investigated, however the main channels studied by both experiments are essentially the same and the main conclusions are similar and fully consistent.

(i) Spin-0 model

The interaction Lagrangian relevant for the analysis of spin-0 particle interaction with a pair of W- or Z-boson with either fixed or mixed SM and BSM CP-even couplings or CP-odd couplings, is the following:

$$\begin{aligned}\mathcal{L}_0^{W,Z} \supset \Big\{ & \cos(\alpha)\kappa_{SM}[\frac{1}{2}g_{HZZ}Z_\mu Z^\mu + g_{HWW}W_\mu^+ W^{-\mu}] \\ & - \frac{1}{4\Lambda}[\cos(\alpha)\kappa_{HZZ}Z_{\mu\nu}Z^{\mu\nu} + \sin(\alpha)\kappa_{AZZ}Z_{\mu\nu}\tilde{Z}^{\mu\nu}] \\ & - \frac{1}{2\Lambda}[\cos(\alpha)\kappa_{HWW}W_{\mu\nu}^+ W^{-\mu\nu} + \sin(\alpha)\kappa_{AWW}W_{\mu\nu}^+ \tilde{W}^{-\mu\nu}]\Big\} H_0\end{aligned} \tag{11.15}$$

Where $V^\mu = Z^\mu, W^{+\mu}$ are the vector boson fields, $V^{\pm\mu\nu}$ are the reduced field tensors and $\tilde{V}^{\pm\mu\nu} = 1/2\,\varepsilon^{\mu\nu\rho\sigma}V_{\rho\sigma}$ are the dual tensor fields. Here, Λ defines an effective theory energy scale. The factors $\kappa_{SM}, \kappa_{HZZ}, \kappa_{HWW}, \kappa_{AZZ}, \kappa_{AWW}$ denote the

coupling constants corresponding of the coupling of the SM, BSM CP-even and CP-odd components of the Higgs field H_0 to the W and Z fields. The mixing angle α allows for the production of CP-mixed state and the CP-symmetry is broken when $\alpha \neq 0, \pi$.

This formalism can be used to probe both CP-mixing for a spin-0 state or specific alternative hypotheses such as a pure CP-odd state ($J^P = 0^-$) corresponding to $\alpha = \pi/2$, $\kappa_{SM} = \kappa_{HVV} = 0$ and $\kappa_{AVV} = 1$. A BSM CP-even state $J^P = 0_h^+$ corresponds to $\alpha = 0$, $\kappa_{SM} = \kappa_{AVV} = 0$ and $\kappa_{HVV} = 1$. These hypotheses are compared to the SM Higgs boson hypothesis corresponding to $\alpha = 0$ and $\kappa_{HVV} = \kappa_{AVV} = 0$ and $\kappa_{SM} = 1$.

(ii) Spin-2 model

The graviton inspired interaction Lagrangian for a spin-2 boson $X^{\mu\nu}$ for a color, weak and electromagnetic singlet spin-2 resonance uniquely interacting with the energy momentum tensor $\mathcal{T}^{V,f}$ of vector bosons V or fermions f, can be written as follows [204]:

$$\mathcal{L}_2 \supset \frac{1}{\Lambda}\left[\sum_V \xi_V \mathcal{T}^V_{\mu\nu} X^{\mu\nu} + \sum_f \xi_f \mathcal{T}^f_{\mu\nu} X^{\mu\nu}\right]$$

Where the strength of the interaction is determined by the couplings ξ_V and ξ_f. The simplest scenario, referred to as the universal couplings (UC), corresponds to $\xi_V = \xi_f$. These models predict a large branching ratio to photons (of approximately 5%) and negligible couplings to massive gauge bosons (W and Z). Such scenarios are therefore disfavored and other models are investigated where the couplings of the W, Z and γ are assumed to be independent. Universality of the couplings refers to $\xi_g = \xi_q$. Two other scenarios are considered with low light-quark fraction where $\xi_q = 0$ and the low gluon-fraction where $\xi_q = 2\xi_g$. In these scenarios a large enhancement of the tail of the transverse momentum of the spin-2 state is expected and requires a further selection requirement in order to probe the models within the range of validity of the effective field theory. Two requirements are considered, $p_T^X < 300\,\text{GeV}$ and $p_T^X < 125\,\text{GeV}$ [201].

V.1.3. Probing fixed J^P scenarios

At the LHC, the determination of the spin and *CP* properties of the Higgs boson is done independently from the total rates measurement, it uses a global angular helicity analysis and, when applicable, the study of threshold effects. The channels used for this analysis, $H \to \gamma\gamma$, $H \to W^{(*)}W^{(*)} \to \ell\nu\ell\nu$ and $H \to Z^{(*)}Z^{(*)} \to 4\ell$, are those where the observation of a signal is unambiguous.

At the Tevatron, an analysis using the threshold distribution of the production of the discovered state [205] in the associated production mode VH with subsequent decay to a pair of b-quarks was performed by the D0 collaboration.

(i) The VH production at D0

The mass of the VH system is a powerful discriminant to distinguish a $J^P = 0_m^+$, with a threshold behavior in $d\sigma/dM^2 \sim \beta$ from 0^- or 2^+ with threshold behaviors respectively in $\sim \beta^3$ and $\sim \beta^5$ (for a graviton like spin 2) [205]. The VH mass observable, not only

discriminates signal hypotheses, but also has an increased separation between the 0^- and 2^+ hypotheses with respect to the backgrounds, thus allowing, with a small and not yet significant signal yield, to exclude that the observed state is 0^- at 98% CL [206] and 2^+ at the 99.9% CL [207].

(ii) The $\gamma\gamma$ channel at the LHC

In the $H \to \gamma\gamma$ channel, the analysis is performed inclusively using the production angle $\cos\theta^*_{CS}$ and the transverse momentum of the diphoton pair [201]. The definition chosen for the polar angle in the rest frame is the Collins–Soper frame, which is defined as the bisector axis of the momenta of the incoming protons in the diphoton rest frame. The SM Higgs signal distribution is expected to be uniform with a cutoff due to the selection requirements on the photons transverse momentum. The $H \to \gamma\gamma$ channel is mostly sensitive to the gluon-initiated spin-2 production scenarios, which yield a $\cos\theta^*_{CS}$ distribution peaking at values close to 1. The limits are derived from a fit of the signal in bins of $\cos\theta^*_{CS}$ and diphoton transverse momentum and are summarized in Fig. 11.15 for ATLAS, only combined results are shown. The data shows a good compatibility with the SM 0^+ hypothesis and contributes strongly to the exclusion of several Spin-2 scenarios. The conclusions are the same from CMS results [202].

(iii) The $H \to W^{(*)}W^{(*)} \to \ell\nu\ell\nu$ channel at the LHC

In the $H \to W^{(*)}W^{(*)} \to \ell\nu\ell\nu$ channel, the production and decay angles cannot be easily reconstructed due to the presence of neutrinos in the final state, however sensitivity arises from the V-A structure of the decay of the W bosons. A scalar state thus yields a clear spin correlation pattern that implies that the charged leptons e or μ from the decays of the W bosons are produced close to one another in the transverse plane. This feature, which impacts observables such as the azimuthal angle between the two leptons $\Delta\Phi_{\ell\ell}$ or their invariant mass $M_{\ell\ell}$ in addition of the threshold behavior of the decay which is used in kinematic variables such as the transverse mass defined in Section III, can be used to discriminate between various spin and parity hypotheses. The approach adopted by ATLAS uses a multivariate discriminant, whereas CMS uses a 2D-fit of the dilepton mass and the transverse mass. The results of the $H \to W^{(*)}W^{(*)} \to \ell\nu\ell\nu$ analyses alone are summarized in Fig. 11.15 for ATLAS and in combination with other channels. Spin-1 hypotheses (1^+ and 1^-) have also been tested with this channel by ATLAS and CMS. ATLAS and CMS exclude the 1^+ and 1^- hypotheses at more than 95% CL.

(iv) The $H \to Z^{(*)}Z^{(*)} \to 4\ell$ channel at the LHC

The $H \to Z^{(*)}Z^{(*)} \to 4\ell$ coupling analysis, as described in Section III, also uses a discriminant based on the 0^+ nature of the Higgs boson to further discriminate the signal from the background. In this analysis this feature is used to discriminate between signal hypotheses. The observables sensitive to the spin and parity are [208] the masses of the two Z bosons (due to the threshold dependence of the mass of the off-shell Z boson), two production angle θ^* and ϕ_1, and three decay angles, ϕ, θ_1 and θ_2. The production and decay angles defined as:

– θ_1 and θ_2, the angles between the negative final state lepton and the direction of flight of Z_1 and Z_2 in the rest frame.

– ϕ, the angle between the decay planes of the four final state leptons expressed in the four lepton rest frame.

– ϕ_1, the angle defined between the decay plane of the leading lepton pair and a plane defined by the vector of the Z_1 in the four lepton rest frame and the positive direction of the proton axis.

– θ^*, the production angle of the Z_1 defined in the four lepton rest frame with respect to the proton axis.

These angles are illustrated in Fig. 11.15. There are two approaches to this analysis. The first, used by CMS, is a matrix element likelihood approach where a kinematic discriminant is defined based on the ratio of the signal and background probabilities. These probabilities are defined using the leading-order matrix elements. A similar approach is also performed by ATLAS as a cross check of their main result. The main approach adopted by ATLAS is the combination of sensitive observables with a Boosted Decision Tree. These analyses are sensitive to various J^P hypotheses and in particular discriminate the 0^+ hypothesis from the 0^-. In all scenarios investigated and for both the ATLAS and CMS experiments, the data are compatible with the 0^+ hypothesis. ATLAS [203] and CMS [202] exclude a pseudoscalar nature of the observed boson at CL_S levels of 98% and 99.8%.

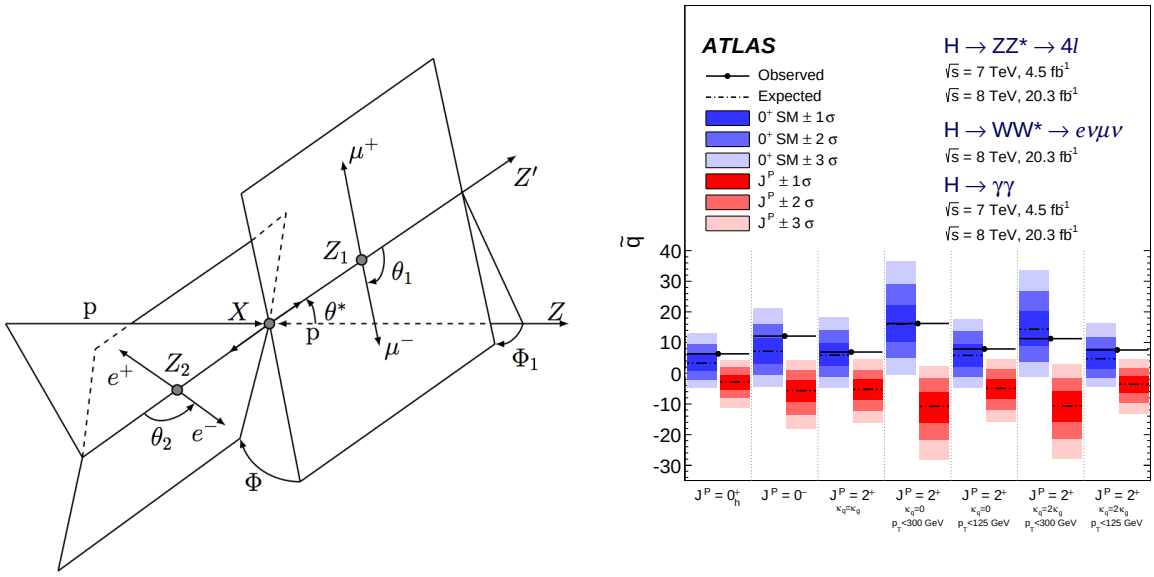

Figure 11.15: (Left) Definition of the production and decay angles defined for the $H \to Z^{(*)}Z^{(*)} \to 4\ell$ final state [202]. Expected distributions of the test statistic for the SM hypothesis (in blue) and several alternative spin and parity hypotheses (in red).

V.1.4. Probing anomalous HVV couplings

The careful study of the kinematic properties of the events observed in the

$H \to Z^{(*)}Z^{(*)} \to 4\ell$ and $H \to W^{(*)}W^{(*)} \to \ell\nu\ell\nu$ channel, and in particular the angular distributions described above, allows one to further probe the HVV coupling beyond testing fixed hypotheses. Assuming that the observed particle is a spin-0 state, and using several discriminating observables in the $H \to Z^{(*)}Z^{(*)} \to 4\ell$ and $H \to W^{(*)}W^{(*)} \to \ell\nu\ell\nu$ channels, the anomalous terms in the formalism of Eq. (11.15) can be probed. In the approach of helicity amplitudes used by CMS [202], all terms are essentially equivalent, except for one additional phase which is neglected in Eq. (11.15).

Results are derived in terms of the parameters $\tilde{\kappa}_{HVV} = v/\Lambda\,\kappa_{HVV}$ and $\tilde{\kappa}_{AVV} = v/\Lambda\,\kappa_{AVV}$, and more precisely as measurements of $\tilde{\kappa}_{HVV}/\kappa_{SM}$ and $\tan\alpha\,.\,\tilde{\kappa}_{AVV}/\kappa_{SM}$ as shown in Fig. 11.16. These parameters can be interpreted as mixing parameters of a tensor anomalous CP-even coupling and a CP-odd component. The measurements are made in the $H \to Z^{(*)}Z^{(*)} \to 4\ell$ and $H \to W^{(*)}W^{(*)} \to \ell\nu\ell\nu$ channels independently and then combined assuming that the $\tilde{\kappa}_{HVV}/\kappa_{SM}$ and $\tan\alpha\,.\,\tilde{\kappa}_{AVV}/\kappa_{SM}$ are the same for the W and Z vector bosons. Only the combination of the WW and ZZ channels is shown in Fig. 11.16. The asymmetric shape of the likelihood as a function of $\tilde{\kappa}_{HWW,HZZ}/\kappa_{SM}$ is mainly due to the interference between the BSM and the SM contributions that give a maximal deviation from the SM predictions for negative relative values of the BSM couplings. In Fig. 11.16 the expected likelihood profiles for a SM Higgs boson are also displayed. While no significant deviation from the SM Higgs boson expectation is observed, the precision of the measurements of the mixing parameters is fairly low. The results from the CMS measurements [202] are very similar and the conclusions the same.

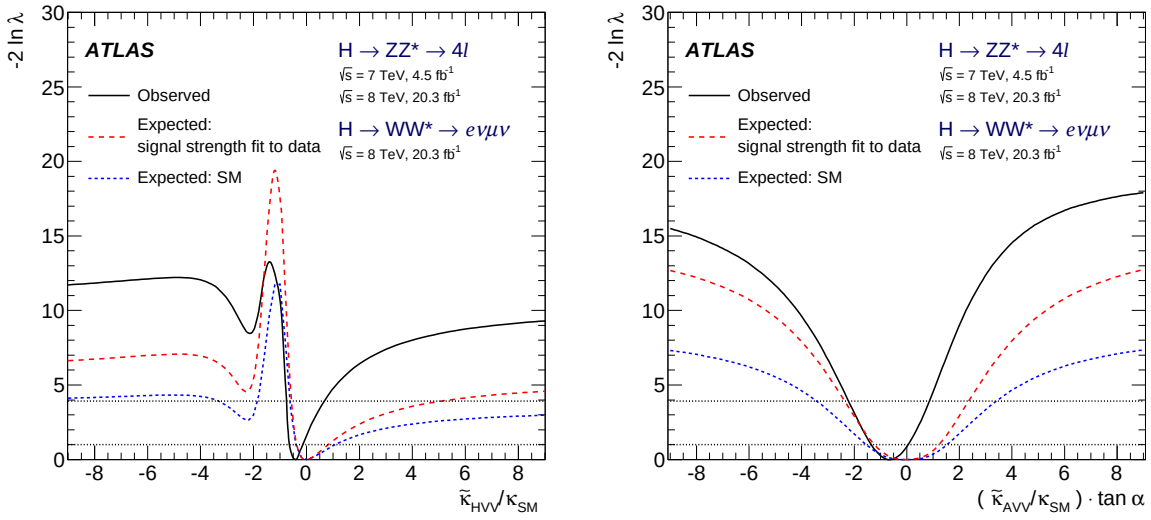

Figure 11.16: Likelihood profiles for the $\tilde{\kappa}_{HVV}$ and $\tilde{\kappa}_{AVV}\,.\,\tan\alpha$ parameters, representing respectively CP-even and CP-odd anomalous couplings of the Higgs boson.

V.2. Off-shell couplings of the Higgs boson

In the dominant gluon fusion production mode, the production cross section of a off-shell Higgs boson is known to be sizable. This follows as a consequence of the enhanced couplings of the Higgs boson to the longitudinal polarizations of the massive vector bosons at high energy.

The off-shell to on-shell cross section ratio is approximately 8% in the SM. Still the Higgs contribution to VV production at large invariant mass remains small compared to the background. It is nevertheless interesting to probe Higgs production in this regime as it is sensitive to new physics beyond the SM.

The difficulty in the off-shell VV analysis, beyond the small signal-to-background ratio, is due to a large negative interference between the signal and the $gg \to VV$ background. boson signal in the far off-shell domain results in a deficit of events with respect to the expectation from background only events. It is only when the off-shell couplings of the Higgs boson are larger than expected in the SM that the presence of a signal appears as an excess over the background expectation. One additional intricacy arises from the precision in the prediction of the rate for $gg \to VV$, a loop process at lowest order, and its interference with the signal. At the time of the publications of the results from the ATLAS [209] and CMS [210] a full NLO prediction had not been computed.

It is interesting to note that in this regime the Higgs boson is studied as a propagator and not as a particle. The measurement of its off-shell couplings is therefore absolute and does not rely on the knowledge of the total Higgs boson width. The off-shell couplings constraints can then be used to indirectly constrain the natural width of the Higgs boson, under specific assumptions detailed in Section V.3.3.

This measurement has been carried out in the $H \to ZZ \to 4\ell$, $H \to ZZ \to \ell\ell\nu\nu$ and $H \to WW \to \ell\nu\ell\nu$ channels. To enhance the sensitivity of the analysis the knowledge of the full kinematics of the events is important. In particular the signal and the background can be further distinguished by the invariant mass of the VV system, which is more accurately accessible in the $H \to ZZ \to 4\ell$ channel. Angular distributions also play an important role in this analysis. For these reasons the $H \to Z^{(*)}Z^{(*)} \to 4\ell$ channel is significantly more sensitive than $H \to W^{(*)}W^{(*)} \to \ell\nu\ell\nu$. The CMS results in Refs. [210] and [211] include the VBF and VH processes through the selection of two additional jets in the final state. The ATLAS results do not have a specific selection for the VBF or VH production processes, but their contributions are taken into account.

Limits on the off-shell rates have been reported for the two channels by ATLAS [209] and CMS [211]. The combined results assuming that the off-shell rates in the ZZ and WW channels scale equally, are given for two different hypotheses on the VBF production rate: fixing it to its SM value or scaling it as the gluon fusion rate. The observed (expected) limits on the off-shell rate fraction with respect to its SM expectation is 6.7 (9.1) for ATLAS [209] with the VBF rate fixed to its SM value and 2.4 (6.2) for CMS [211] where no assumption is made on the relative production rates of gluon-fusion and VBF. In both cases the custodial symmetry is assumed and the ratio of the rates in the ZZ and WW decays are fixed to those of the Standard Model. Results without this assumption have also been reported in Ref.[211].

V.3. The Higgs boson width

In the SM, the Higgs boson width is very precisely predicted once the Higgs boson mass is known. For a mass of 125.1 GeV, the Higgs boson has a very narrow width of 4.2 MeV. It is dominated by the fermionic decays partial width at approximately 75%, while the vector boson modes are suppressed and contribute 25% only.

Table 11.13: The observed (expected) direct 95% CL constraints on the natural width of the 125 GeV resonance from fits to the $\gamma\gamma$ and ZZ mass spectra and to the 4ℓ vertex lifetime.

Experiment	$M_{\gamma\gamma}$ mass spectrum	$M_{4\ell}$ spectrum	4ℓ vertex lifetime
ATLAS	$< 5.0(6.2)\,\text{GeV}$	$< 2.6(6.2)\,\text{GeV}$	—
CMS	$< 2.4(3.1)\,\text{GeV}$	$< 3.4(2.8)\,\text{GeV}$	$> 3.5 \times 10^{-12}\,\text{GeV}$

At the LHC or the Tevatron, in all production modes, only the cross sections times branching fractions can be measured. As a consequence, the total natural width of the Higgs boson cannot be inferred from measurements of Higgs boson rates. Direct constraints on the Higgs boson width are much larger than the expected natural width of the SM Higgs boson.

V.3.1. Direct constraints

Analysis of the reconstructed mass lineshape in the two channels with a good mass resolution, the $H \to \gamma\gamma$ and $H \to Z^{(*)}Z^{(*)} \to 4\ell$, allow for a direct measurement of the width of the SM Higgs boson. The intrinsic mass resolution in these channels is about 1-2 GeV, much larger than the expected width of the SM Higgs boson. As a result only upper limits on the Higgs boson width have been measured by ATLAS [132] and CMS [133]. The two main challenges of direct constraints on the width through the measurement of the lineshape are: (i) the modeling of resolution uncertainties and (ii) the modeling of the interference between the signal and the continuum background which can be sizable for large widths, in particular in the range where direct constraints are set. Given that these interference effects are small with respect to the individual channels sensitivity, they are neglected in deriving constraints on the total width. The combined constraints however, being more precise could be affected by the interference. ATLAS [132] has therefore not combined the constraints on the width from the two channels. The results are reported in Table 11.13. These constraints are still three orders of magnitude larger than the expected SM width and are fully compatible with the SM hypothesis.

Another direct constraint on the Higgs boson width can be obtained in the $H \to Z^{(*)}Z^{(*)} \to 4\ell$ channel, from the measurement of the average lifetime of the Higgs boson calculated from the displacement of the four-lepton vertex from the beam spot. This analysis has been carried out by CMS [210], using the measured decay length. The measured $c\tau_H$ is $2^{+25}_{-2}\,\mu$m, yielding an observed (and expected) limit at the 95% CL of $c\tau_H < 57(56)\,\mu$m. From this upper limit on the lifetime of the Higgs boson. The 95% CL lower limit on its natural width is $\Gamma_H > 3.5 \times 10^{-12}\,\text{GeV}$.

V.3.2. Indirect constraints from mass shift in the diphoton channel

In the diphoton channel, it was noticed in [212], that the effect of the interference between the main signal $gg \to H \to \gamma\gamma$ and the continuum irreducible background $gg \to \gamma\gamma$, taking into account detector resolution effects, is responsible for a non negligible mass shift. The size of the mass shift depends on the total width of the Higgs boson

and it was suggested that measuring this mass shift could provide a constraint on the width [212]. Comparing the mass measured in the diphoton channel with the mass measured in the four-leptons channel is subject to non negligible detector calibration systematic uncertainties, however it was further noticed that the mass shift has a dependence also on the diphoton transverse momentum. The total width of the Higgs boson could therefore be constrained using the diphoton channel alone.

Further studies were performed by the ATLAS collaboration to estimate the size of the expected mass shift [213]. The expected shift in mass in the diphoton channel is 35 ± 9 MeV for the SM Higgs boson. Very preliminary studies of the sensitivity of this method to estimate the width of the Higgs boson in the high-luminosity regime have been made by ATLAS [214] and yield an expected 95% CL upper limit on the total width of approximately 200 MeV from 3 ab^{-1} of 14 TeV data.

V.3.3. Indirect constraints from off-shell couplings

Using simultaneously on-shell and off-shell measurements in the VV channels, it was noticed [215] that the total width of the Higgs could be constrained. This can be illustrated from the parametrization of the signal strength measurements both on-shell ($\mu_{\text{on-shell}}$) and off-shell ($\mu_{\text{off-shell}}$) as a function of the couplings modifiers κ_g and κ_V parameterizing the main process $gg \to H \to VV$. The on-shell signal strength can be written as:

$$\mu_{\text{on-shell}} = \frac{\kappa^2_{g,\,\text{on-shell}}\,\kappa^2_{V,\,\text{on-shell}}}{\Gamma_H/\Gamma_{SM}}$$

while in the case of the off-shell signal strength where the Higgs boson is a propagator:

$$\mu_{\text{on-shell}} = \kappa^2_{g,\,\text{off-shell}}\,\kappa^2_{V,\,\text{off-shell}}$$

Then, with the following assumption

$$\kappa^2_{g,\,\text{on-shell}}\,\kappa^2_{V,\,\text{on-shell}} \leq \kappa^2_{g,\,\text{off-shell}}\,\kappa^2_{V,\,\text{off-shell}}\,,$$

from the on-shell and off-shell constraints. This assumes that no new physics alters the Higgs boson couplings in the off-shell regime, i.e. that the running of its couplings is negligible in the off-shell regime. Both ATLAS [209] and CMS [210, 211] have used their off-shell production limits to constrain the width of the Higgs boson.

Both ATLAS and CMS analyses use the kinematic event characteristics to further gain in sensitivity to discriminate between the signal and background. The ATLAS analysis assumes that there are no anomalous couplings of the Higgs boson to vector bosons, and obtains 95% CL observed (expected) upper limit on the total width of $5.7\times\Gamma_{SM}$ ($9.0\times\Gamma_{SM}$) [209]. In the CMS approach, results are also derived allowing for anomalous couplings of the Higgs boson, therefore reducing the discriminating power of the kinematic variables used in the analysis but reducing the model dependence. When standard couplings are assumed for the Higgs boson, the observed (expected) limit on the total width is $6.2\times\Gamma_{SM}$ ($9.8\times\Gamma_{SM}$) for the ZZ channel only [210]. Without assumptions

on the anomalous couplings of the Higgs boson, the observed (expected) limit on the total width is $10.9\times\Gamma_{SM}$ ($17.4\times\Gamma_{SM}$) [210].

The CMS experiment has also combined the ZZ and W^+W^- channels while keeping the gluon-fusion and VBF production processes separate. For the gluon fusion mode the observed (expected) combined upper limit at the 95% CL on the total width of the Higgs boson is $2.4\times\Gamma_{SM}$ ($6.2\times\Gamma_{SM}$) [211], while for the VBF production mode the exclusion limits are $19.3\times\Gamma_{SM}$ ($34.4\times\Gamma_{SM}$) [211].

ATLAS has also performed a study of the prospects for measuring the Higgs width in the four lepton channel alone, in the high luminosity phase of the LHC for and projects that for a LHC luminosity of $3\,\mathrm{ab}^{-1}$, the width of the Higgs boson could be measured with the following precision [216]:

$$\Gamma_H = 4.2^{+1.5}_{-2.1}\,\mathrm{MeV}$$

VI. Probing the coupling properties of the Higgs boson

As discussed in Section II, within the SM, all the Higgs couplings are fixed unambiguously once all the particle masses are known. Any deviation in the measurement of the couplings of the Higgs boson could therefore signal physics beyond the SM.

Measuring the Higgs couplings without relying on the SM assumption requires a general framework treating deviations from the SM coherently at the quantum level in order to provide theoretical predictions for relevant observables to be confronted with experimental data. The first attempt in that direction was the development of the so-called κ-formalism where the SM Higgs couplings are rescaled by factors κ_f, keeping the same Lorentz structure of the interactions. This formalism allows for simple interpretation of the signal strengths μ measured in the various Higgs channels and it has been used to test various physics scenarios, like the existence of additional new particles contributing to the radiative Higgs production and decays, or to probe various symmetries of the SM itself, in particular the custodial symmetry. But the κ-formalism has obvious limitations and certainly does not capture the most general deformations of the SM, even under the assumptions of heavy and decoupling new physics. A particularly acute shortcoming at the time Higgs physics is entering a precision era is the lack of proficiency of the κ's to assert the richness of kinematical distributions beyond simple signal strength measurements. Several extensions and alternative approaches are being developed as part of the activities of the Higgs cross-section working group.

The Higgs Pseudo-Observable (HPO) approach [217] is providing a particularly elegant formalism to report the data in terms of a finite set of on-shell form factors parametrizing amplitudes of physical processes subject to constraints from Lorentz invariance and other general requirements like analyticity, unitarity, and crossing symmetry. These form factors are expanded in powers of kinematical invariants of the process around the known poles of SM particles, assuming that poles from BSM particles are absent in the relevant energy regime. A set of HPOs have been proposed to characterize both the Higgs decays

and the EW Higgs production channels, thus exploring different kinematical regimes. Prospective studies concluded that these HPOs can be measured/bounded at the percent level at the HL-LHC and could therefore be used to constrain some explicit models of New Physics.

Another promising approach to characterize the possible Higgs coupling deviations induced by physics beyond the SM is the use of Effective Field Theories (EFT). This approach assumes again that the new physics degrees of freedom are sufficiently heavy to be integrated out and they simply give rise to effective interactions among the light SM particles. By construction the effective Lagrangians cannot account for deviations in Higgs physics induced by light degrees of freedom, unless they are added themselves as extra fields in the effective Lagrangians. In Section VII, several examples of models with light degrees of freedom affecting Higgs production and decay rates will be presented. The main advantage of EFTs is their prowess to relate different observables in different sectors and at different energies to constrain a finite set of effective interactions among the SM degrees of freedom. In an EFT, the SM Lagrangian is extended by a set of higher-dimensional operators, and it reproduces the low-energy limit of a more fundamental UV description. It will be assumed that the Higgs boson is part of a CP-even EW doublet. This is motivated by the apparent relation between the Higgs couplings and the masses of the various particles which naturally follows under this assumption of a linear realization of the $\mathrm{SU}(2)_L \times \mathrm{U}(1)_Y$ symmetry of the SM. There have been some recent attempts to write the most general EFT bypassing this assumption, see for instance [218].

VI.1. Effective Lagrangian framework

The EFT has the same field content and the same linearly-realized $\mathrm{SU}(3)_C \times \mathrm{SU}(2)_L \times \mathrm{U}(1)_Y$ local symmetry as the SM. The difference is the presence of operators with canonical dimension D larger than 4. These are organized in a systematic expansion in D, where each consecutive term is suppressed by a larger power of a high mass scale. Assuming baryon and lepton number conservation, the most general Lagrangian takes the form

$$\mathcal{L}_{\rm eff} = \mathcal{L}_{\rm SM} + \sum_i c_i^{(6)} \mathcal{O}_i^{(6)} + \sum_j c_j^{(8)} \mathcal{O}_j^{(8)} + \cdots . \tag{11.16}$$

The list of dimension-6 operators was first classified in a systematic way in Ref. [219] after the works of Ref. [220]. Subsequent analyses pointed out the presence of redundant operators, and a minimal and complete list of operators was finally provided in Ref. [221][5]. For a single family of fermions, there are 76 real ways to deform the SM generated by 59 independent operators (with the 3 families of fermions of the SM, flavor indices can be added to these 59 operators, and furthermore, new operator structures, that have been dismissed by means of Fierz transformations in the single family case, have to be

[5] Complete classifications of D=8 operators have recently appeared in the literature, see Ref. [222]. Still, in this review, the EFT Lagrangians will be truncated at the level of dimension-6 operators.

Table 11.14: List of 17 CP-even operators affecting, at tree-level, only Higgs production and decay rates (left) as well as EW observables (right). See text for notations.

Ops. affecting Higgs physics only	Ops. affecting Higgs and EW physics
$\mathcal{O}_r = \lvert\Phi\rvert^2 \lvert D_\mu\Phi\rvert^2$	$\mathcal{O}_W = \frac{ig}{2}\big(\Phi^\dagger\sigma^i \overleftrightarrow{D}^\mu\Phi\big)(D^\nu W_{\mu\nu})^i$
$\mathcal{O}_6 = \lambda\lvert\Phi\rvert^6$	$\mathcal{O}_B = \frac{ig'}{2}\big(\Phi^\dagger \overleftrightarrow{D}^\mu\Phi\big)(\partial^\nu B_{\mu\nu})$
$\mathcal{O}_{BB} = \frac{g'^2}{4}\lvert\Phi\rvert^2 B_{\mu\nu}B^{\mu\nu}$	$\mathcal{O}_T = \frac{1}{2}\big(\Phi^\dagger \overleftrightarrow{D}^\mu\Phi\big)^2$
$\mathcal{O}_{WW} = \frac{g^2}{4}\lvert\Phi\rvert^2 W^i_{\mu\nu}W^{i\,\mu\nu}$	$\mathcal{O}_{HB} = ig'\,(D^\mu\Phi)^\dagger(D^\nu\Phi)B_{\mu\nu}$
$\mathcal{O}_{GG} = \frac{g_S^2}{4}\lvert\Phi\rvert^2 G^A_{\mu\nu}G^{A\mu\nu}$	$\mathcal{O}_{Hu} = i\,(\bar{u}_R\gamma^\mu u_R)\,\big(\Phi^\dagger\overleftrightarrow{D}_\mu\Phi\big)$
$\mathcal{O}_{yu} = y_u\,\lvert\Phi\rvert^2\,\bar{q}_L\tilde{\Phi}u_R$	$\mathcal{O}_{Hd} = i\,\big(\bar{d}_R\gamma^\mu d_R\big)\,\big(\Phi^\dagger\overleftrightarrow{D}_\mu\Phi\big)$
$\mathcal{O}_{yd} = y_d\,\lvert\Phi\rvert^2\,\bar{q}_L\Phi d_R$	$\mathcal{O}_{He} = i\,\big(\bar{l}_R\gamma^\mu l_R\big)\,\big(\Phi^\dagger\overleftrightarrow{D}_\mu\Phi\big)$
$\mathcal{O}_{ye} = y_e\,\lvert\Phi\rvert^2\,\bar{L}_L\Phi e_R$	$\mathcal{O}_{Hq} = i\,(\bar{q}_L\gamma^\mu q_L)\,\big(\Phi^\dagger\overleftrightarrow{D}_\mu\Phi\big)$
	$\mathcal{O}^{(3)}_{Hq} = i\,\big(\bar{q}_L\gamma^\mu\sigma^i q_L\big)\,\big(\Phi^\dagger\sigma^i\overleftrightarrow{D}_\mu\Phi\big)$

Table 11.15: List of 8 dipoles operators. See text for notations.

Dipoles ops.
$\mathcal{O}_{uB} = g'\,(\bar{q}_L\tilde{\Phi}\sigma^{\mu\nu}u_R)\,B_{\mu\nu}$
$\mathcal{O}_{uW} = g\,(\bar{q}_L\sigma^i\tilde{\Phi}\sigma^{\mu\nu}u_R)\,W^i_{\mu\nu}$
$\mathcal{O}_{uG} = g_S\,(\bar{q}_L\tilde{\Phi}\sigma^{\mu\nu}t^A u_R)\,G^A_{\mu\nu}R$
$\mathcal{O}_{dB} = g'\,(\bar{q}_L\Phi\sigma^{\mu\nu}d_R)\,B_{\mu\nu}$
$\mathcal{O}_{dW} = g\,(\bar{q}_L\sigma^i\Phi\sigma^{\mu\nu}d_R)\,W^i_{\mu\nu}$
$\mathcal{O}_{dG} = g_S\,(\bar{q}_L\Phi\sigma^{\mu\nu}t^A d_R)\,G^A_{\mu\nu}$
$\mathcal{O}_{lB} = g'\,(\bar{L}_L\Phi\sigma^{\mu\nu}l_R)\,B_{\mu\nu}$
$\mathcal{O}_{lW} = g\,(\bar{L}_L\sigma^i\Phi\sigma^{\mu\nu}l_R)\,W^i_{\mu\nu}$

considered, for a total of 2499 real deformations [223]). Of particular interest are the 17 CP-invariant operators, in addition to 8 dipole operators, that affect, at tree-level, the Higgs production and decay rates [224–226]. A convenient list of these operators can be found in Table 11.14, and Table 11.15. The other operators completing the basis of dimension-6 operators can be found in Ref. [226].

The SM gauge couplings are denoted by g', g, g_S while $y_{u,d,e}$ are the SM Yukawa couplings (in the mass eigenstate basis that diagonalizes the general Yukawa coupling matrices $Y_{u,d,l}$) and λ is the SM Higgs quartic coupling. We denote by $i\Phi^\dagger\overleftrightarrow{D}^\mu\Phi$ the Hermitian derivative $i\Phi^\dagger(D^\mu\Phi) - i(D^\mu\Phi)^\dagger\Phi$, $\sigma^{\mu\nu} \equiv i[\gamma^\mu,\gamma^\nu]/2$ and $\tilde{\Phi}$ is the Higgs charge-conjugate doublet: $\tilde{\Phi} = i\sigma^2\Phi^*$. Each operator $\mathcal{O}_{yu,yd,ye}$ is further assumed to be

flavor-aligned with the corresponding fermion mass term, as required in order to avoid large Flavor-Changing Neutral Currents (FCNC) mediated by the tree-level exchange of the Higgs boson. This implies one coefficient for the up-type quarks (c_{yu}), one for down-type quarks (c_{yd}), and one for the charged leptons (c_{ye}), i.e. the $c_{yu,ud,ye}$ matrices should be proportional to the identity matrix in flavor space.

The choice of the basis of operators is not unique and using the equations of motion, i.e., performing field redefinitions, different dimension-6 operators can be obtained as linear combinations of the operators in the previous tables and of four-fermion operators. Some relations between common bases of operators can be found for instance in Refs. [225, 223]. Different bases have different advantages. For instance the so-called SILH basis [224] better captures the low-energy effects of universal theories in which new physics couples to SM bosons only. The Warsaw basis [221] on the other hand mostly includes vertex corrections and easily connects operators to observables [226]. The basis defined in Table 11.14, and Table 11.15 is particularly well suited for an analysis of the Higgs data. The reason is that the eight operators of the left-hand side of Table 11.14, in the vacuum with $|\Phi|^2 = v^2/2$, merely redefine the SM input parameters and therefore were left unconstrained at tree-level before Higgs data are considered. These eight operators modify the physical Higgs vertices and can be probed via the decay processes $H \to \gamma\gamma, Z\gamma, \bar{b}b, \bar{\tau}\tau$ and the production channels $gg \to H, VV \to H, pp \to \bar{t}tH$ and $gg \to HH$. Section VI.2 illustrates how the Higgs data accumulated at the LHC can (partially) constrain these eight operators, following the initial phenomenological study of Ref. [226]. The other nine operators of Table 11.14 are tightly constrained by the LEP EW precision measurements (the measurements of the Z-boson couplings to quarks and leptons on the Z-pole) and by diboson production.[6]

The minimal flavor violation assumption imposes Yukawa dependences in the eight dipole operators. For the light generations of fermions, this dependence lowers the induced deviations in the Higgs rates below the experimental sensitivity reachable in any foreseeable future. The corresponding operators in the top sector are not suppressed but they are already constrained by the limit of the top dipole operators imposed by the bounds on the neutron electric dipole moment, on the $b \to s\gamma$ and $b \to s\ell^+\ell^-$ rates and on the $t\bar{t}$ cross section [229, 225].

Automatic tools [225, 204] are being developed to analyze the experimental data within an EFT framework.

VI.2. Probing coupling properties

As described in Section III a framework was developed by the ATLAS and CMS collaboration [141], individually and together, to combine the very large number of exclusive categories aimed at reconstructing the five main decay modes and the five main production modes of the Higgs boson. The general conclusions of this combination in

[6] There remains an accidental flat direction [227] in the fit of anomalous gauge boson couplings using LEP2 data on diboson production alone. This flat direction can be lifted when LHC Higgs data are considered [228].

terms of production cross sections and decay modes, illustrating the compatibility of the observation with the expectation from the SM Higgs boson is given in Section III. The same framework with its master formula Eq. (11.13) can be used to further measure coupling properties of the Higgs boson under specific additional assumptions.

VI.2.1. Combined measurements of the coupling properties of H

(i) From effective Lagrangians to Higgs observables

All 8 operators of the effective Lagrangian that were unconstrained before the Higgs data induce, at tree-level, deviations in the Higgs couplings that either respect the Lorentz structure of the SM interactions, or generate simple new interactions of the Higgs boson to the W and Z field strengths, or induce some contact interactions of the Higgs boson to photons (and to a photon and a Z boson) and gluons that take the form of the ones that are generated by integrating out the top quark. In other words, the Higgs couplings are described, in the unitary gauge, by the following effective Lagrangian [230, 44]

$$\begin{aligned}\mathcal{L} = {} & \kappa_3 \frac{m_H^2}{2v} H^3 + \kappa_Z \frac{m_Z^2}{v} Z_\mu Z^\mu H + \kappa_W \frac{2m_W^2}{v} W_\mu^+ W^{-\mu} H \\ & + \kappa_g \frac{\alpha_s}{12\pi v} G^a_{\mu\nu} G^{a\mu\nu} H + \kappa_\gamma \frac{\alpha}{2\pi v} A_{\mu\nu} A^{\mu\nu} H + \kappa_{Z\gamma} \frac{\alpha}{\pi v} A_{\mu\nu} Z^{\mu\nu} H \\ & + \kappa_{VV} \frac{\alpha}{2\pi v} \left(\cos^2\theta_W Z_{\mu\nu} Z^{\mu\nu} + 2\, W^+_{\mu\nu} W^{-\mu\nu} \right) H \\ & - \left(\kappa_t \sum_{f=u,c,t} \frac{m_f}{v} f\overline{f} + \kappa_b \sum_{f=d,s,b} \frac{m_f}{v} f\overline{f} + \kappa_\tau \sum_{f=e,\mu,\tau} \frac{m_f}{v} f\overline{f} \right) H. \end{aligned} \tag{11.17}$$

The correspondence between the effective coefficients of the dimension-6 operators and the κ's can be found for instance in Ref. [45]. In the SM, the Higgs boson does not couple to massless gauge bosons at tree level, hence $\kappa_g = \kappa_\gamma = \kappa_{Z\gamma} = 0$. Nonetheless, the contact operators are generated radiatively by SM particles loops. In particular, the top quark gives a contribution to the 3 coefficients $\kappa_g, \kappa_\gamma, \kappa_{Z\gamma}$ that does not decouple in the infinite top mass limit. For instance, in that limit $\kappa_\gamma = \kappa_g = 1$ [24, 25, 231].

The coefficient for the contact interactions of the Higgs boson to the W and Z field strengths is not independent but obeys the relation

$$(1 - \cos^4\theta_W)\kappa_{VV} = \sin 2\theta_W \kappa_{Z\gamma} + \sin^2\theta_W \kappa_{\gamma\gamma}. \tag{11.18}$$

This relation is a general consequence of the custodial symmetry [225], which also imposes $\kappa_Z = \kappa_W$ at leading order ($\kappa_Z/\kappa_W - 1$ is a measure of custodial symmetry breaking and as such is already constrained by electroweak precision data and the bounds on anomalous gauge couplings). When the Higgs boson is part of an $\mathrm{SU}(2)_L$ doublet, the custodial symmetry could only be broken by the $\mathcal{O}_T = \frac{1}{2}\left(\Phi^\dagger \overleftrightarrow{D}^\mu \Phi\right)^2$ operator at the level of dimension-6 operators and it is accidentally realized among the interactions with four derivatives, like the contact interactions considered.

The coefficient κ_3 can be accessed directly only through double Higgs production processes, hence it will remain largely unconstrained at the LHC. The LHC will also have a limited sensitivity on the coefficient κ_τ since the lepton contribution to the Higgs production cross section remains subdominant and the only way to access the Higgs coupling is via the $H \to \tau^+\tau^-$ and possibly $H \to \mu^+\mu^-$ channels. Until the associated production of a Higgs with a pair of top quarks is observed, the Higgs coupling to the top quark is only probed indirectly via the one-loop gluon fusion production or the radiative decay into two photons. However, these two processes are only sensitive to the combinations of couplings $(\kappa_t + \kappa_g)$ and $(\kappa_t + \kappa_\gamma)$ and not to the individual couplings. Therefore a deviation in the Higgs coupling to the top quark can in principle always be masked by new contact interactions to photons and gluons (and this is precisely what is happening in minimal incarnations of composite Higgs models). The current limited sensitivity in the $t\bar{t}H$ channel leaves elongated ellipses in the direction $\kappa_g = \kappa_\gamma = 1 - \kappa_t$.

The operators already bounded by EW precision data and the limits on anomalous gauge couplings modify in general the Lorentz structure of the Higgs couplings and hence induce some modifications of the kinematical differential distributions [232, [233]. A promising way to have a direct access to the effective coefficients of these operators in Higgs physics is to study the VH associated production with a W or a Z at large invariant mass of the VH system [232, 234]. It has not been estimated yet whether the sensitivity on the determination of the effective coefficients in these measurements can compete with the one derived for the study of anomalous gauge couplings. In any case, these differential distributions could also be a way to directly test the hypothesis that the Higgs boson belongs to an $\mathrm{SU}(2)_L$ doublet together with the longitudinal components of the massive electroweak gauge bosons.

(ii) Interpretations of the experimental data

The measurements of the coupling properties of the Higgs boson are entirely based on the formalism of the effective Lagrangian described in Section V.6.2.i. Measurements of coupling properties in this framework means measurements of the parameters of the model Eq. (11.17) or combinations of these parameters with different sets of assumptions.

These measurements are carried out with the combination framework described in Section IV where the μ_i and μ_f signal strength parameters are further interpreted in terms of modifiers of the SM couplings κ_k where $k \in \{Z, W, f, g, \gamma, Z\gamma\}$ as in Eq. (11.17). These coupling modifiers κ are fully motivated as leading order coupling scale factors defined such that the cross sections σ_j and the partial decay widths Γ_j associated with the SM particle j scale with the factor κ_j^2 when compared to the corresponding SM prediction. The number of signal events per category for the various production modes are typically estimated at higher orders in the analyses but are scaled by these single LO-inspired factors, thus not taking into account possible intricacies and correlations of these parameters through the higher order corrections. This approximation is valid within the level of precision of current results and their compatibility with the SM expectation.

In this formalism further assumptions are explicitly made: (i) the signals observed in the different search channels originate from a single narrow resonance with a mass of 125 GeV; (ii) similarly to the combination described in Section IV the narrow width

approximation is assumed (to allow the decomposition of signal yields); (iii) the tensor structure of the couplings is assumed to be the same as that of a SM Higgs boson. This means in particular that the observed state is assumed to be a CP-even scalar as in the SM.

Loop-level couplings such as the $gg \to H$, $H \to \gamma\gamma$ and $H \to Z\gamma$ can either be treated effectively, with The κ_g, κ_γ and $\kappa_{Z\gamma}$ as free parameters in the fit or these parameters can be expressed in terms of the know SM field content and as a function of the SM coupling modifiers, in the following way:

$$\begin{aligned} \kappa_g^2(\kappa_t, \kappa_b) &= 1.06\,\kappa_t^2 - 0.07\,\kappa_t\kappa_b + 0.01\,\kappa_b^2 \\ \kappa_\gamma^2(\kappa_F, \kappa_V) &= 1.59\,\kappa_V^2 - 0.66\,\kappa_V\kappa_F + 0.07\,\kappa_F^2 \\ \kappa_{Z\gamma}^2(\kappa_F, \kappa_V) &= 1.12\,\kappa_V^2 - 0.15\,\kappa_V\kappa_F + 0.03\,\kappa_F^2 \end{aligned} \tag{11.19}$$

The $\kappa_{Z\gamma}$ parametrization is used only in the ATLAS combined measurements of the coupling properties of the Higgs boson [199]. Neither the $Z\gamma$ nor the $\mu^+\mu^-$ channels are included in the CMS [133] and the ATLAS-CMS combinations [141], which therefore do not use the $\kappa_{Z\gamma}$ or κ_μ parameters explicitly. The parametrizations are given for a Higgs boson mass hypothesis of 125.09 GeV (and in the last two expressions, all the Higgs-fermion couplings are assumed to be rescaled by an universal multiplicative factor κ_F). It can be noted from the expression of κ_γ that the coupling of the Higgs boson to photons is dominated by the loop of W bosons, and it is affected by the top quark loop mostly through its interference with the W loop. The sensitivity of the current measurements to the relative sign of the fermion and vector boson couplings to the Higgs boson is due to this large negative interference term. The κ_g parameter is expressed in terms of the scaling of production cross sections and therefore also depends on the pp collisions centre-of-mass energy. The parametrizations of κ_γ and $\kappa_{Z\gamma}$ are obtained from the scaling of partial widths and are only dependent on the Higgs boson mass hypothesis. Experiments use a more complete parametrization with the contributions from the b-quarks, τ-leptons in the loop [230, 44].

The global fit is then performed expressing the μ_i and μ_f parameters in terms of a limited number of κ_k parameters or their ratios, under various assumptions. The parametrization for the main production modes are: $\mu_{ggF} = \kappa_g^2$ for the gluon fusion and an effective coupling of the Higgs boson to the gluons; $\mu_{VBF,VH} = \kappa_V^2$ for the VBF and VH processes when the W and Z couplings are assumed to scale equally, and the following expression for the VBF production mode is used:

$$\mu_{VBF}^2(\kappa_W, \kappa_Z) = \frac{\kappa_W^2\sigma_{WWH} + \kappa_Z^2\sigma_{ZZH}}{\sigma_{WWH} + \sigma_{ZZH}} \tag{11.20}$$

when the couplings to the W and Z bosons are varied independently (σ_{WWH} and σ_{ZZH} denote the VBF cross sections via the fusion of a W and a Z boson respectively, the small interference term is neglected); $\mu_{ttH} = \kappa_t^2$ for the $t\bar{t}$H production mode.

Numerically the production modes signal strengths as a function of the coupling modifiers to the SM fields are:

$$\mu_{ggF} = 1.06\kappa_t^2 + 0.01\kappa_b^2 - 0.07\kappa_t\kappa_b$$
$$\mu_{VBFF} = 0.74\kappa_W^2 + 0.26\kappa_Z^2$$

The decay mode signal strengths are parametrized as $\mu_k = \kappa_k^2/\kappa_H^2$ where $k \in \{Z, W, f, g, \gamma, Z\gamma\}$ denotes the decay mode and κ_H the overall modifier of the total width. Similarly to the combinations reported in Section IV, when parametrizing signal yields per categories using the combination master formula, it is again manifest that parametrizations as a function of coupling modifiers (κ) cannot be obtained is κ_H is considered effective, since it is a common factor to all signal yields. However, κ_H can also be treated as an effective parameter or expressed in terms of the coupling modifiers to the SM field content. Its general expression as a function of the Standard Model field content is:

$$\begin{aligned}\kappa_H^2 =& 0.57\kappa_b^2 + 0.06\kappa_\tau^2 + 0.03\kappa_c^2 \\ &+ 0.22\kappa_W^2 + 0.03\kappa_Z^2 + 0.09\kappa_g^2 + 0.0023\kappa_\gamma^2\end{aligned} \tag{11.21}$$

The general expression of the total width of the Higgs boson can be written as follows:

$$\Gamma_H = \frac{\kappa_H^2 \Gamma_H^{SM}}{1 - \mathrm{BR}_{\mathrm{BSM}}}$$

where Γ_H^{SM} is the total width of the SM Higgs boson and $\mathrm{BR}_{\mathrm{BSM}}$ is the branching fraction of the Higgs boson to new particles beyond the SM.

Specific parametrizations will be made in order to address the following aspects of the coupling properties of the Higgs boson under different assumptions: (i) the relative couplings of the Higgs boson to fermions and bosons; (ii) the potential impact of the presence of new particles beyond the SM either in the loops or both in the loops and the decay of the H; and (iii) also, more general models either of coupling modifiers or their ratios, under different assumptions.

(iii) Relative couplings to bosons and fermions

As will be discussed in Section VII.6.3, it is interesting to probe a model where no additional field content is considered in the decay width of the Higgs boson and where the relative couplings of the Higgs boson to W- and Z-bosons is fixed to its SM value and where all Yukawa couplings scale with one coupling modifier. In this model only SM particles are assumed to contribute to the gluon fusion and the diphoton loops, all fermion couplings modifiers are required to scale simultaneously with a unique factor κ_F and all vector boson couplings modifiers must scale simultaneously with a unique factor κ_V. This parametrization assumes that no new particles affect the direct decays or the loops. It is a two parameters fit with κ_V and κ_F as parameters of interest. The ATLAS-CMS combined results for each channel independently, the combinations of all channels for the two experiments separately and the results and the overall combination are shown in Fig. 11.17.

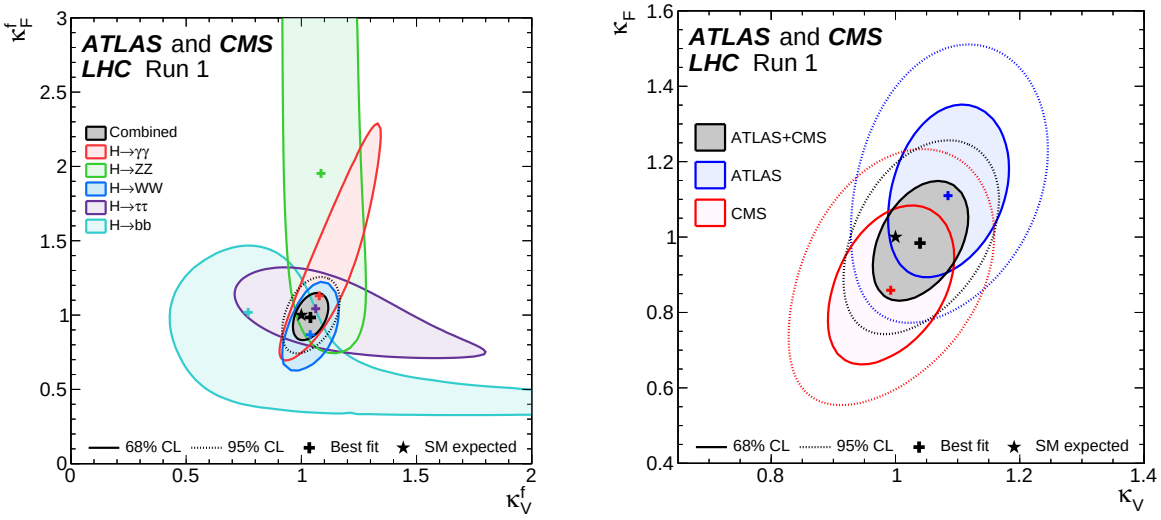

Figure 11.17: Likelihood contours in the (κ_F, κ_V) plane for the ATLAS-CMS combination for the main decay channels separately (left) and for the individual combination of all channels for ATLAS and CMS separately and the complete combined contour (right) [141].

The global fit is only sensitive to the relative sign of κ_V and κ_F. By convention negative values of κ_F can be considered. Such values are not excluded a priori, but would imply the existence of new physics at a light scale and would also raise questions about the stability of such a vacuum [235]. Among the five low mass Higgs channels, only the $\gamma\gamma$ is sensitive to the sign of κ_F through the interference of the W and t loops as shown in Eq. (11.19). The current global fit disfavors a negative value of κ_F at more than five standard deviations. A specific analysis for the Higgs boson production in association with a single top quark has been proposed [236, 237] in order to more directly probe the sign of κ_F. All available experimental data show a fair agreement of the SM prediction of the couplings of the Higgs boson to fermions and gauge bosons. The results shown in Fig. 11.17 assume that $\kappa_F \geq 0$, however in Ref. [141], a similar combination is done without this assumption. The combined sensitivity to the exclusion of a negative relative sign, is approximately 5σ in this model. It is interesting to note that although none of the channels have a significant sensitivity to resolve the sign ambiguity, the combination can, mainly through the $W-t$ interference in the $H \to \gamma\gamma$ channel and the $H \to W^+W^-$ channel. The observed exclusion is fully compatible with the expectation [141]. The combined measurements of these parameters:

$$\kappa_V = 1.04 \pm 0.05$$
$$\kappa_F = 0.98^{+0.11}_{-0.10}$$

Is already at the 5% level for the κ_V parameter with the Run 1 dataset.

(iv) Coupling measurements and probing new physics beyond the SM in loops and in the decay

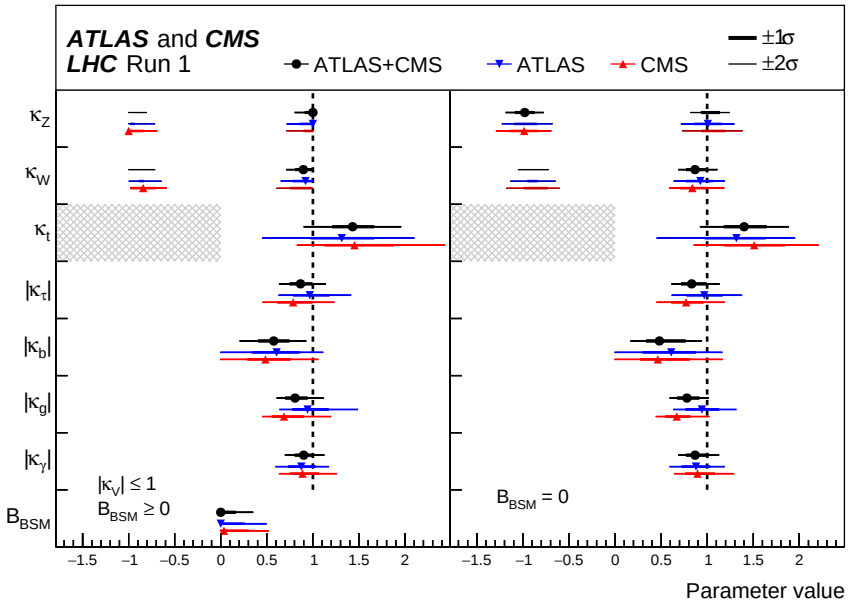

Figure 11.18: ATLAS-CMS combined measurements of coupling modifiers.

In the model described above in Section VI.2.1.iii the assumption is that no new fields distort in a perceptible way the loop contributions in the couplings of the H to gluons and photons and the total width, its couplings to known SM particles are then probed. In a first approach to simultaneously probe new physics beyond the SM in the loops and not in the decay and the couplings of the Higgs boson to SM particles, only one assumption is needed *i.e.* that $\mathrm{BR}_{\mathrm{BSM}} = 0$. In this model the coupling of the H to photons and gluons is effective and κ_Z, κ_W, κ_t, $|\kappa_\tau|$, and $|\kappa_b|$ are measured simultaneously. The absolute value of certain coupling modifiers only indicates the complete degeneracy of combined likelihood for the two signs. It can be noted that when the coupling to gluons is not considered effective, there is some sensitivity to the sign of κ_b through the interference between the top and bottom quarks loops in the gluon fusion process. In this model it is interesting to note that the constraints on the top quark Yukawa coupling comes from the ttH direct search channels. The expected precision on κ_t is approximately 40%. As discussed in Section III the excesses observed in the ttH channel yield a large value of $\kappa_t = 1.40^{+0.24}_{-0.21}$. The complete set of results from this model is given in Fig. 11.18.

This model, which assumes that no new particles enter the decay of the Higgs boson, also yields very interesting constraints on new physics in the loops through the effective coupling modifiers κ_g and κ_γ. The measured values of these parameters:

$$\kappa_g = 0.78^{+0.13}_{-0.10}$$
$$\kappa_\gamma = 0.87^{+0.14}_{-0.09}$$

are fully compatible with the expectation for the SM Higgs boson.

A more constrained model fully focussing on BSM scenarios with new heavy particles contributing to the loops (and not directly in the decays *i.e.* $\mathrm{BR_{BSM}} = 0$) and where all couplings to the SM particles are assumed to be the same as in the Standard Model ($\kappa_W = \kappa_Z = \kappa_t = \kappa_b = \kappa_\tau = 1$) is also used to constrain the κ_g and κ_γ parameters only. The contours of the combined likelihood in the $(\kappa_\gamma, \kappa_g)$ plane for the ATLAS and CMS experiments and their combination are shown in Fig. 11.19.

This general model requires the strong assumption that the the Higgs boson decays only to SM particles. This assumption is necessary due to the degeneracy of solutions given that κ_H is a common factor to all measured signals. The degeneracy can however be resolved using a constraint on the width of the Higgs boson as the one from the Off-Shell couplings measurements. This approach was used by the ATLAS experiment [199], thus yielding a absolute measurement of the couplings of the Higgs boson.

Another well motivated constraint to resolve the aforementioned degeneracy is unitarity. Simply requiring that $\kappa_V \leq 1$ allows to free the $\mathrm{BR_{BSM}}$ parameter and further probe new physics in the decay of the Higgs boson. An intuitive understanding of how this constraint works can be given by a simple example *e.g.* VBF $H \to W^+W^-$ production where the number of signal events will be parametrized by $(1 - \mathrm{BR_{BSM}})\kappa_W^4/\kappa_H^2$, where for a number of signal events observed close to the SM expectation, large values of $\mathrm{BR_{BSM}}$ cannot be compensated by a large value of κ_W and is thus limited. Or in other terms, if $\kappa_W \sim 1$ is preferred from other channels, a low signal in the VBF $H \to W^+W^-$ channel would be a sign of the presence of new physics beyond the SM in the Higgs decays. From this general model all the above parameters can be measured in addition to $\mathrm{BR_{BSM}}$. The results of this combination are shown in Fig. 11.18. The results for all parameters do not change significantly with respect to the previous model. A limit can however be set on the beyond the SM branching fraction of the Higgs boson at the 95% CL:

$$\mathrm{BR_{BSM}} < 34\%$$

In the second approach, new physics is considered also in the decay thus affecting the total width of the H through decays to particles which are either "invisible" and escape detection in the experiments, or "undetected" which are not distinctive enough to be seen in the current analyses. This approach is complementary to the direct search for invisible decays of the Higgs boson described in Section III. The two approaches can be combined assuming that the undetected branching fraction is negligible. this combination was performed by the ATLAS experiment [238] and yields a limit on the invisible decays of the Higgs boson of $\mathrm{BR}_{inv} < 25\%$ at the 95% CL.

This constraint can then be further used to probe Higgs portal models to Dark Matter [239], where an additional weakly interacting particle χ with mass typically lower than $m_H/2$ is introduced as Dark Matter candidate and where the Higgs boson is considered as the only mediator between the SM particles and Dark Matter. In this model it is interesting to express the limit on the invisible branching fraction in terms of strength of interaction of Dark Matter with standard matter, *i.e.* in terms of it interaction cross section with nucleons $\sigma_{\chi-N}$. In this model the couplings of the Higgs boson to SM particles are assumed to be those of the SM and the interaction of the Higgs

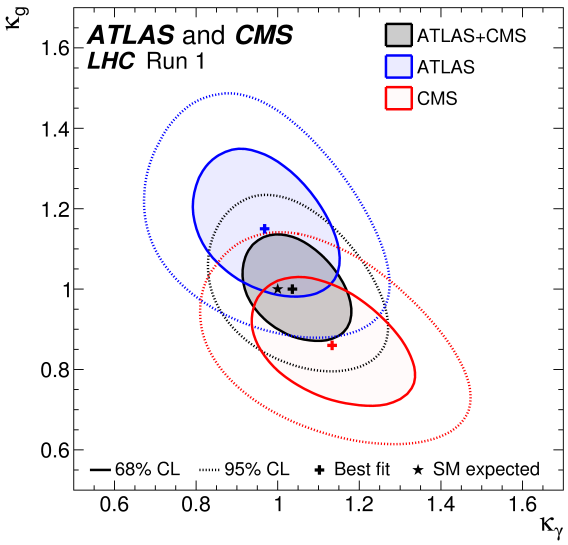

Figure 11.19: Likelihood contours of the global in the $(\kappa_g, \kappa_\gamma)$ plane for the ATLAS-CMS combination for the individual combination of all channels for ATLAS and CMS separately and the complete combined contour [141].

boson with the nucleon is parametrized in Higgs-Nucleon form factor estimated using lattice QCD calculations [239]. The exclusion limits from the constraints on invisible Higgs decays, both direct and indirect from the measurement of the coupling properties of the Higgs boson can be compared to direct detection experiments. For comparison the limit at 90% CL on the invisible branching fraction of $\mathrm{BR}_{inv} < 22\%$ [238] is used and converted into limits on $\sigma_{\chi-N}$ under several hypotheses on the nature of Dark Matter particles depending mainly on their spin (scalar-, vector- or fermion-like). These results are shown in Fig. 11.20.

(v) Generic measurement of the H couplings to fermions and gauge bosons

Measuring the couplings of the Higgs boson with requires additional input on constraints on its natural width, or further assumptions. A more generic approach to avoid the degeneracy in the measurement of the coupling modifiers is to probe the coupling properties of the Higgs boson through ratio of couplings. This model, is inspired by the generic model of ratios of cross sections and branching ratios discussed in Section III, where the cross section times branching fraction of the $gg \to H \to ZZ$ process is parametrized as a function of a single coupling modifier:

$$\kappa_{gZ} = \kappa_g \times \frac{\kappa_Z}{\kappa_H}$$

Then all combination signals can be parametrized with the following ratios of coupling modifiers: (i) the $\lambda_{Zg} = \kappa_Z/\kappa_g$ ratio which is mainly probed by the measurements of the VBF and ZH production; (ii) the $\lambda_{tg} = \kappa_t/\kappa_g$ ratio constrained by the ttH production process; (iii) the $\lambda_{WZ} = \kappa_W/\kappa_Z$ ratio mainly probed by the WW and ZZ decay modes;

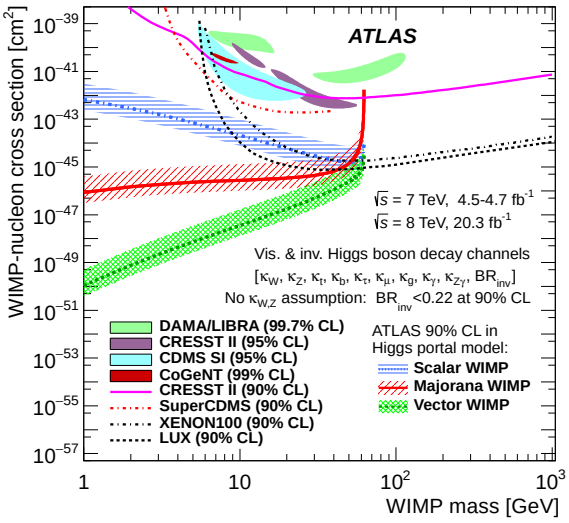

Figure 11.20: 90% CL upper limits on the WIMP-nucleon scattering cross section as a function of the Dark Matter particle mass. Spin-independent results excluded and favored regions from direct detection experiments are also shown.

(iv) the $\lambda_{\tau Z} = \kappa_\tau/\kappa_Z$ ratio constrained by the $\tau^+\tau^-$ channel; (v) the $\lambda_{bZ} = \kappa_b/\kappa_Z$ ratio probed mainly by the $VH(b\bar{b})$ channels; and (vi) the $\lambda_{\gamma Z} = \kappa_\gamma/\kappa_Z$ ratio constrained by the diphoton channel. In this parametrization the ZZ channels plays an important normalization role. This model is very general, as it makes neither assumptions on the total width of the Higgs boson or the content of the loops. The results of the combination for this general model are illustrated in Fig. 11.21.

This general model summarizes the status of a flurry of measurements of the Higgs boson that have been carried out at Run 1, in five main production and five main decay modes. Reaching unprecedented level of complexity in a combination with approximately 600 categories and several thousands of parameters for systematic uncertainties. It summarizes the legacy of the measurements of Run 1 and their main conclusions on the coupling properties of the Higgs boson, which can be summarized as follows: (i) the κ_{gZ} parameters shows that the Higgs boson has been firmly observed in a direct ZZ decay mode; (ii) the λ_{WZ} parameter illustrates the firm observation of the Higgs boson direct decays to the W-boson and measures directly the ratio of the coupling to the W- and Z-bosons a direct probe of the custodial symmetry, already very accurately measured with electroweak precision data; (iii) the $\lambda\gamma Z$ parameters shows that the coupling of the Higgs boson to photons is compatible with the SM expectation, thus providing a probe of new physics in the decay loop of the Higgs boson to two photons; (iv) the $\lambda_{\tau Z}$ parameters indicates the evidence in the direct decay of the Higgs boson to a pair of taus of the Yukawa coupling of the Higgs boson to fermions (and in particular to taus); (v) the λ_{bZ} parameter indicates that more data is needed to further establish the Yukawa coupling of the Higgs boson to b-quarks; and (vi) the λ_{tZ} similarly indicates that the more data

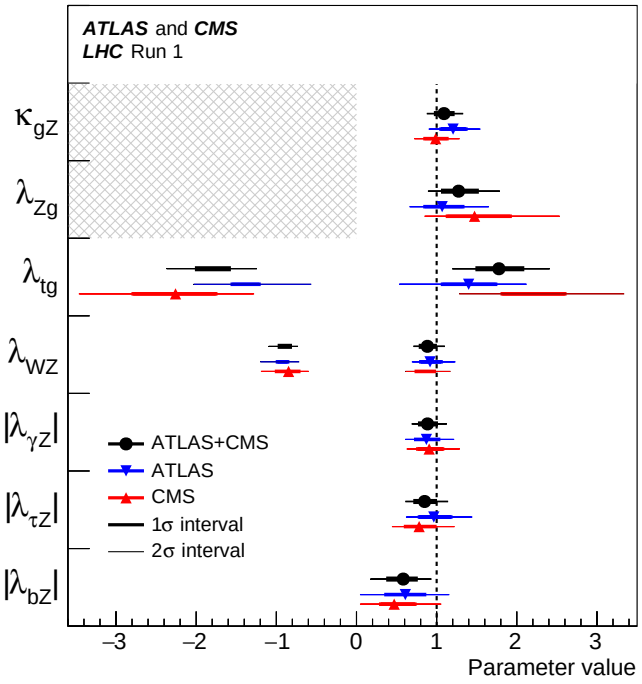

Figure 11.21: ATLAS-CMS combined measurements of ratios of coupling modifiers.

is needed to further directly constrain the Yukawa coupling of the Higgs boson to top quarks. Each measurement is consistent with the prediction within less than 2σ, except for λ_{bZ} and λ_{tZ} which show similar disagreements to those discussed in Section IV. However the probability of the overall compatibility of these measurements with the SM expectation is estimated to be 13%.

VI.2.2. Differential cross sections

To further characterize the production and decay properties of H, first measurements of fiducial and differential cross sections have been carried out by the ATLAS collaboration [240], with the 8 TeV dataset of pp collision at LHC, corresponding to an integrated luminosity of $20.3\,\text{fb}^{-1}$, in the diphoton channel. The selection criteria to define the fiducial volume are the following: the two highest transverse momentum (E_T), isolated final state photons, within $|\eta| < 2.37$ and with $105\,\text{GeV} < M_{\gamma\gamma} < 160\,\text{GeV}$ are selected (the transition region between the barrel and endcap calorimeters is not removed); after the pair is selected, the same cut on $E_T/M_{\gamma\gamma}$ as in the event selection *i.e.* in excess of 0.35 (0.25) for the two photons is applied. Several observables have been studied: the transverse momentum rapidity of the diphoton system, the production angle in the Collins–Soper frame, the jet multiplicity, the jet veto fractions for a given jet multiplicity, and the transverse momentum distribution of the leading jet. The following additional observables: the difference in azimuthal angle between the leading and the subleading jets, and the transverse component of the vector sum of the momenta of the Higgs boson and dijet system, have also been measured in two jet events. To minimize the

model dependence the differential cross sections are given within a specific fiducial region of the two photons. The observables were chosen to probe the production properties and the spin and parity of the H. The differential cross section in H transverse momentum is given in Fig. 11.22.

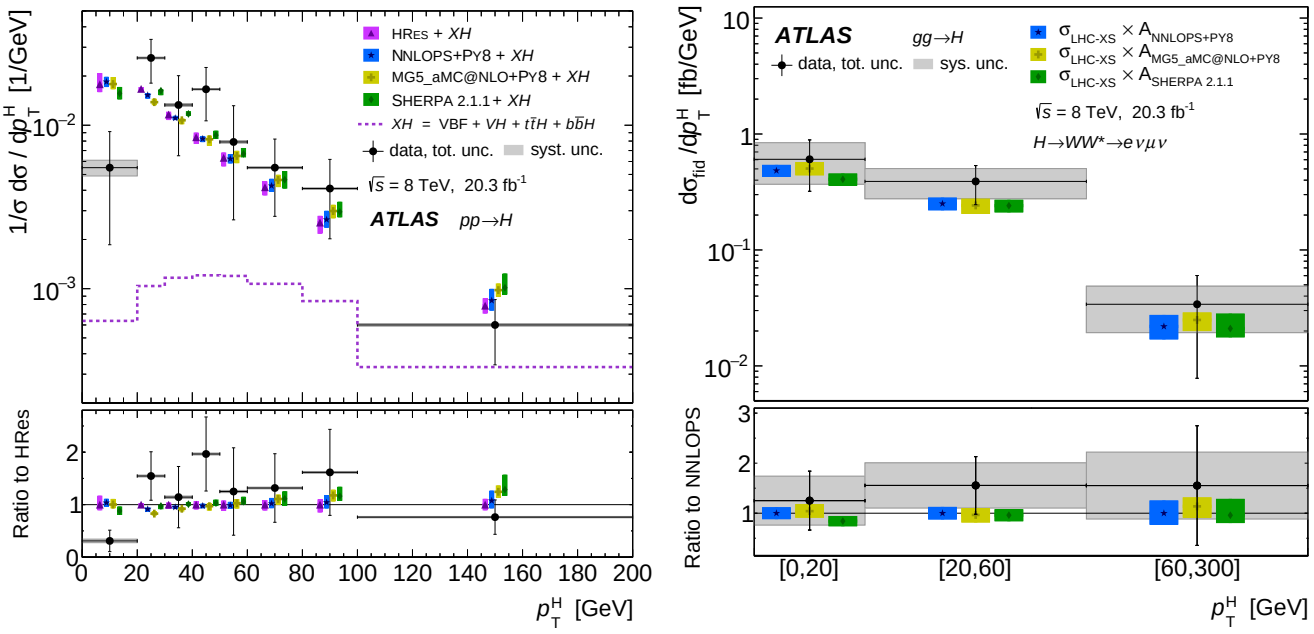

Figure 11.22: Observed differential cross sections in transverse momentum of the H in the diphoton channel, compared to the prediction of the ggF process [240].

VI.2.3. Constraints on non-SM Higgs boson interactions in an effective Lagrangian

An example of the possible use of differential cross sections in constraining non-SM Higgs boson couplings in an EFT is given by the ATLAS collaboration [241]. In this analysis, differential cross section measured in the diphoton channel are used to constrain an effective Lagrangian where the SM is supplemented by dimension six CP-even operators of the Strongly Interacting Light Higgs (SILH) formulation and corresponding CP-odd operators. The diphoton differential cross sections are mainly sensitive to the operators that affect the Higgs boson interactions with gauge bosons and the relevant terms in the effective Lagrangian can be parameterized as:

$$\begin{aligned}\mathcal{L}_{eff} =& \bar{c}_\gamma \mathcal{O}_\gamma + \bar{c}_g \mathcal{O}_g + \bar{c}_{HW} \mathcal{O}_{HW} + \bar{c}_{HB} \mathcal{O}_{HB} + \\ & \tilde{c}_\gamma \tilde{\mathcal{O}}_\gamma + \tilde{c}_g \tilde{\mathcal{O}}_g + \tilde{c}_{HW} \tilde{\mathcal{O}}_{HW} + \tilde{c}_{HB} \tilde{\mathcal{O}}_{HB}\end{aligned} \tag{11.22}$$

Where $\bar{c}_i$ and $\tilde{c}_i$ are the effective coefficients corresponding to the CP-even and CP-odd interactions, respectively.

The differential distributions used in this combination are: (i) the transverse momentum of the Higgs boson, (ii) the number of reconstructed jets produced in

association with the diphoton pair, (iii) the invariant mass of the diphoton system and (iv) the difference in azimuthal angle of the leading and sub-leading jets in events with two or more jets.

This analysis shows how differential information significantly improves the sensitivity to operators that modify the Higgs boson interaction to photons, gluons and vector bosons both from the main gluon fusion and the vector boson fusion production modes.

VII. New physics models of EWSB in the light of the Higgs boson discovery

A main theoretical motivation to add a Higgs boson to the SM is that, without it, the longitudinal components of the massive EW gauge bosons would form a strongly coupled system as their scattering amplitude would have grown with their energy, destroying all the predictive power of the model above $4\pi v \sim 3\,\text{TeV}$. The discovery of a light scalar with couplings to gauge bosons and fermions that are apparently consistent with SM predictions and the slow running of the Higgs self-coupling at high energies allows one to consider the SM as a valid perturbative description of nature all the way to the Planck scale. This picture is admittedly very attractive, but it posits that the Higgs boson is an elementary scalar field, which comes with an intrinsic instability of its mass under radiative corrections. This Higgs naturalness problem calls for new physics around the TeV scale. Supersymmetric models are the most elegant solution to maintain the perturbativity of the SM while alleviating the instability issue. Another possibility is that the Higgs boson itself has a finite size and is composite and thus never feels the UV degrees of freedom that would drag its mass to much higher scales. Both classes of models predict specific modifications from the SM Higgs properties.

The realization of supersymmetry at low energies has many good qualities that render it attractive as a model of new physics. First of all since for every fermion there is a boson of equal mass and effective coupling to the SM-like Higgs, in the case of exact supersymmetry it yields an automatic cancellation of loop corrections to the Higgs mass parameter: (analogous to Eq. (11.2)) $\delta m^2 = 0$ [9, 11]. In practice, it is known that SUSY must be broken in nature since no superpartners of the SM particles have been observed so far. The mass difference between the boson and fermion degrees of freedom is governed by the soft supersymmetry breaking parameters, generically called M_{SUSY}. Therefore, independently of the precise value of any of the particle masses and that of its corresponding superpartner, all corrections are proportional to M^2_{SUSY} times the logarithmic dependence of the ratio of energy scales as in Eq. (11.2). Hence, provided that $M_{SUSY} \simeq \mathcal{O}(<\text{few})\,\text{TeV}$, the fine-tuning problem is solved, in the sense that the low energy mass parameters of the Higgs sector become insensitive to physics at the GUT or Planck scale. Another interesting feature of SUSY theories is related to the dynamical generation of EWSB [242]. In the SM a negative Higgs mass parameter, m^2, needs to be inserted by hand to induce EWSB. In SUSY, instead, even if the relevant Higgs mass parameter is positive in the ultraviolet, it may become negative and induce electroweak symmetry breaking radiatively through the strong effect of the top quark-Higgs boson coupling in its renormalization group evolution.

In the following, the Higgs sector will be explored in specific SUSY models. In all of them there is one neutral Higgs boson with properties that resemble those of the SM Higgs boson, whereas additional neutral and charged Higgs bosons are also predicted and are intensively being sought for at the LHC (see Section VII.8). In the simplest SUSY model the lightest Higgs boson mass, that usually plays the role of the SM-like Higgs, is predicted to be less than 135 GeV for stops in the TeV to few TeV range [243] whereas, larger values of the SM-like Higgs boson mass – up to about 250 GeV – can be obtained in non-minimal SUSY extensions of the SM [243]. In general, accommodating a SM-like Higgs boson with mass of 125 GeV results in constraints on the supersymmetric parameter space of specific SUSY models. While naturalness dictates relatively light stops and gluinos, the first and second generation of squarks and sleptons couple weakly to the Higgs sector and may be heavy. Moreover, small values of the μ parameter and therefore light Higgsinos would be a signature of a natural realization of electroweak symmetry breaking. Such SUSY spectra, consisting of light stops and light Higgsinos, have been under intense scrutiny by the experimental collaborations [244] in order to derive model-independent bounds on the stop masses and to understand if such natural SUSY scenarios endure [243] and can explain why the Higgs boson remains light.

In the context of weakly coupled models of EWSB one can also consider multiple Higgs $\mathrm{SU}(2)_L$ doublets as well as additional Higgs singlets, triplets or even more complicated multiplet structures, with or without low energy supersymmetry. In general for such models one needs to take into account experimental constraints from precision measurements and flavor changing neutral currents. The LHC signatures of such extended Higgs sectors are largely shaped by the role of the exotic scalar fields in EWSB.

The idea that the Higgs boson itself could be a composite bound state emerging from a new strongly-coupled sector has regained some interest. The composite Higgs idea is an interesting incarnation of EWSB via strong dynamics that smoothly interpolates between the standard Technicolor approach and the true SM limit. To avoid the usual conflict with EW data, it is sufficient if not necessary that a mass gap separates the Higgs resonance from the other resonances of the strong sector. Such a mass gap can naturally follow from dynamics if the strongly-interacting sector exhibits a global symmetry, G, broken dynamically to a subgroup H at the scale f, such that, in addition to the three Nambu–Goldstone bosons of SO(4)/SO(3) that describe the longitudinal components of the massive W and Z, the coset G/H contains a fourth Nambu–Goldstone boson that can be identified with the physical Higgs boson. Simple examples of such a coset are SU(3)/SU(2) or SO(5)/SO(4), the latter being favored since it is invariant under the custodial symmetry (it is also possible to have non-minimal custodial cosets with extra Goldstone bosons, see for instance Ref. [245]). Attempts to construct composite Higgs models in 4D have been made by Georgi and Kaplan (see for instance Ref. [246]) and modern incarnations have been recently investigated in the framework of 5D warped models where, according to the principles of the AdS/CFT correspondence, the holographic composite Higgs boson then originates from a component of a gauge field along the 5th dimension with appropriate boundary conditions.

A last crucial ingredient in the construction of viable composite Higgs models is the concept of partial compositeness [247], i.e., the idea that there are only linear mass

mixings between elementary fields and composite states[7]. After diagonalization of the mass matrices, the SM particles, fermions and gauge bosons, are admixtures of elementary and composite states and thus they interact with the strong sector, and in particular with the Higgs boson, through their composite component. This setup has important consequences on the flavor properties, chiefly the suppression of large flavor changing neutral currents involving light fermions. It also plays an important role in dynamically generating a potential for the would-be Goldstone bosons. Partial compositeness also links the properties of the Higgs boson to the spectrum of the fermionic resonances, i.e. the partners of the top quark. As in the MSSM, these top partners are really the agents that trigger the EWSB and also generate the mass of the Higgs boson that otherwise would remain an exact Goldstone boson and hence massless. The bounds from the direct searches for the top partners in addition to the usual constraints from EW precision data force the minimal composite Higgs models into some rather unnatural corners of their parameter spaces [15, 249].

VII.1. Higgs bosons in the minimal supersymmetric standard model (MSSM)

The particle masses and interactions in a supersymmetric theory are uniquely defined as a function of the superpotential and the Kähler potential [250]. A fundamental theory of supersymmetry breaking, however, is unknown at this time. Nevertheless, one can parameterize the low-energy theory in terms of the most general set of soft supersymmetry-breaking operators [243]. The simplest realistic model of low-energy supersymmetry is the minimal supersymmetric extension of the SM (MSSM) [11, 250], that associates a supersymmetric partner to each gauge boson and chiral fermion of the SM, and provides a realistic model of physics at the weak scale. However, even in this minimal model with the most general set of soft supersymmetry-breaking terms more than 100 new parameters are introduced [243]. Fortunately, only a subset of these parameters impact the Higgs phenomenology either directly at tree-level or through quantum effects. Reviews of the properties and phenomenology of the Higgs bosons of the MSSM can be found for example in Refs. [40, 250, 251].

The MSSM contains the particle spectrum of a two-Higgs-doublet model (2HDM) extension of the SM and the corresponding supersymmetric partners. Two Higgs doublets,

$$\Phi_1 = \frac{1}{\sqrt{2}} \begin{pmatrix} \phi_1^0 + i a_1^0 \\ \sqrt{2}\phi_1^- \end{pmatrix}, \qquad \Phi_2 = \frac{1}{\sqrt{2}} \begin{pmatrix} \sqrt{2}\phi_2^+ \\ \phi_2^0 + i a_2^0 \end{pmatrix}, \tag{11.23}$$

with hypercharge $Y = -1$ and $Y = 1$, respectively, are required to ensure an anomaly-free SUSY extension of the SM and to generate mass for both up-type and down-type quarks and charged leptons [12]. In our notation $\Phi_{1(2)}$ gives mass to the down(up) type fermions.

[7] For a pedagogical introduction to models of partial compositeness, see Ref. [248].

The Higgs potential reads

$$\begin{aligned} V = {} & m_1^2 \Phi_1^\dagger \Phi_1 + m_2^2 \Phi_2^\dagger \Phi_2 - m_3^2 (\Phi_1^T i\sigma_2 \Phi_2 + \text{h.c.}) + \frac{1}{2}\lambda_1 (\Phi_1^\dagger \Phi_1)^2 + \frac{1}{2}\lambda_2 (\Phi_2^\dagger \Phi_2)^2 \\ & + \lambda_3 (\Phi_1^\dagger \Phi_1)(\Phi_2^\dagger \Phi_2) + \lambda_4 |\Phi_1^T i\sigma_2 \Phi_2|^2 + \frac{1}{2}\lambda_5 [(\Phi_1^T i\sigma_2 \Phi_2)^2 + \text{h.c.}] \\ & + [[\lambda_6 (\Phi_1^\dagger \Phi_1) + \lambda_7 (\Phi_2^\dagger \Phi_2)] \Phi_1^T i\sigma_2 \Phi_2 + \text{h.c.}] \end{aligned} \tag{11.24}$$

where $m_i^2 = \mu^2 + m_{H_i}^2$, with μ being the supersymmetric Higgsino mass parameter and m_{H_i} (for $i = 1, 2$) the soft supersymmetric breaking mass parameters of the two Higgs doublets; $m_3^2 \equiv B\mu$ is associated to the B-term soft SUSY breaking parameter; and λ_i, for $i = 1$ to 7, are all the Higgs quartic couplings. After the spontaneous breaking of the electroweak symmetry, five physical Higgs particles are left in the spectrum: one charged Higgs pair, $H^\pm$, one CP-odd neutral scalar, A, and two CP-even neutral states, H and h.

$$\begin{aligned} H^\pm &= \sin\beta \phi_1^\pm + \cos\beta \phi_2^\pm \,, \\ A &= \sin\beta \ \text{Im}\phi_1^0 + \cos\beta \ \text{Im}\phi_2^0 \,, \\ H &= \cos\alpha (\text{Re}\phi_1^0 - v_1) + \sin\alpha (\text{Re}\phi_2^0 - v_2), \\ h &= -\sin\alpha (\text{Re}\phi_1^0 - v_1) + \cos\alpha (\text{Re}\phi_2^0 - v_2), \end{aligned} \tag{11.25}$$

where $v_i = \langle \phi_i^0 \rangle$ for i=1,2 and $v^2 = v_1^2 + v_2^2 \approx (246\,\text{GeV})^2$. The angle α diagonalizes the CP-even Higgs squared-mass matrix and is given in terms of the quartic couplings, while β diagonalizes both the CP-odd and charged Higgs sectors with $\tan\beta = v_2/v_1$. The h and H denote the lightest and heaviest CP-even Higgs bosons, respectively.[8]

The supersymmetric structure of the theory imposes constraints on the Higgs sector of the model. In particular, at tree level, the parameters of the Higgs self-interaction, $\lambda_{1,\ldots,4}$, are defined in terms of the electroweak gauge coupling constants, and $\lambda_{5,6,7} = 0$. As a result, the Higgs sector at tree level depends on the electroweak gauge coupling constants and the vacuum expectation value v – or equivalently the Z gauge boson mass – and is determined by only two free parameters: $\tan\beta$ and one Higgs boson mass, conventionally chosen to be the CP-odd Higgs boson mass, m_A. The other tree-level Higgs boson masses are then given in terms of these parameters. In the large $m_A \gg M_Z$ limit, also called the decoupling limit [252 [253, $\sin\alpha \to -\cos\beta$, $\cos\alpha \to \sin\beta$, hence, $\cos(\beta - \alpha) \to 0$ and this implies that the lightest CP-even Higgs h behaves as the SM Higgs. When $m_A \geq M_Z$, the condition $\cos(\beta - \alpha) \to 0$ is also called the alignment limit [253–254]. As will be discussed below, in the MSSM the alignment limit can only occur once quantum corrections to the quartic couplings have been included. The tree level value of m_h is maximized not

[8] Observe that in the SM sections of this review, H denotes the SM Higgs, whereas in the sections about SUSY, or extensions of the SM with two Higgs doublets, H is used for the heaviest CP-even Higgs boson, since this is the standard notation in the literature, and the 125 GeV SM-like light Higgs boson will be denoted by h.

only for $m_A \gg M_Z$ but also for $\tan\beta \gg 1$. For $m_A \gg M_Z$ it acquires a maximum value $m_h = M_Z \cos 2\beta$.

Radiative corrections have a significant impact on the values of Higgs boson masses and couplings in the MSSM. The dominant radiative effects to the SM-like Higgs mass arise from the incomplete cancellation between top and scalar-top (stop) loops and at large $\tan\beta$ also from sbottom and stau loops. The loop contributions to the tree level quartic couplings depend on the SUSY spectrum, and render $\lambda_{5,6,7}$ non zero. The stop, sbottom and stau masses and mixing angles depend on the supersymmetric Higgsino mass parameter μ and on the soft-supersymmetry-breaking parameters [11, 250]: M_Q, M_U, M_D, M_L, M_E, and A_t, A_b A_τ. The first three of these are the left-chiral and the right-chiral top and bottom scalar quark mass parameters. The next two are the left-chiral stau/sneutrino and the right-chiral stau mass parameters, and the last three are the trilinear parameters that enter in the off-diagonal squark/slepton mixing elements: $X_t \equiv A_t - \mu \cot\beta$ and $X_{b,\tau} \equiv A_{b,\tau} - \mu \tan\beta$. At the two-loop level, the masses of the gluino and the electroweak gaugino also enter in the calculations.

Radiative corrections to the Higgs boson masses have been computed using a number of techniques, with a variety of approximations; see references in Ref. [243]. For large $\tan\beta$, the stau/sbottom mixing parameters and masses are also relevant. In the large m_A (decoupling) limit and for $\tan\beta \gg 1$, the m_h value can be maximized at loop level for a specific value of $X_t/M_{\rm SUSY}$ For fixed X_t, the value of m_h can change by several GeV by varying $M_{\rm SUSY}$ within a few TeV or by varying m_t within its experimental uncertainty, as well as by varying SUSY particle parameters that enter only beyond the one-loop order. Moreover, in the large $\tan\beta$ regime light staus and/or sbottoms with sizable mixing, governed by the μ parameter, yield negative radiative corrections to the mass of the lightest Higgs boson, and can lower it by several GeV [255]. Allowing for experimental and theoretical uncertainties, one finds that for $M_{\rm SUSY} \lesssim 2\,\text{TeV}$, large m_A, $\tan\beta \gg 1$ and for $X_t \simeq \sqrt{6} M_{\rm SUSY}$, the maximal value for the lightest Higgs mass is $m_h^{\rm max} = 135\,\text{GeV}$ [256–257].

The newly discovered SM-like Higgs boson, if interpreted as the lightest MSSM Higgs with a mass of about 125 GeV, provides information on the possible MSSM parameter space. In particular a sizable mixing in the stop sector is required ($|X_t/M_{\rm SUSY}| \geq 1.5$) for values of $M_{\rm SUSY} \simeq M_Q \simeq M_U \simeq M_D \simeq 1$ to a few TeV [255–269]. See for example Fig. 11.23. On the other hand, considering the third generation soft SUSY breaking parameters as independent inputs, $M_Q \neq M_U \neq M_D$, it follows that $m_h \simeq$125 GeV can be obtained for one stop that is as light as can be experimentally allowed [244] and the other one with a mass of the order of the stop mixing parameter. Considering both stops significantly above a few TeV, by varying/lowering the values of X_t and $\tan\beta$, the impact of higher loops in the computation of the Higgs mass becomes relevant [270–272]. For a given CP-odd Higgs mass m_A, the masses of the other two Higgs bosons, H and $H^\pm$, also receive radiative corrections. For a more detailed discussion of the effect of radiative corrections on the heavy Higgs masses see for example Refs. [40] and [251].

The phenomenology of the Higgs sector depends on the couplings of the Higgs bosons to gauge bosons and fermions. The couplings of the two CP-even Higgs bosons to W and

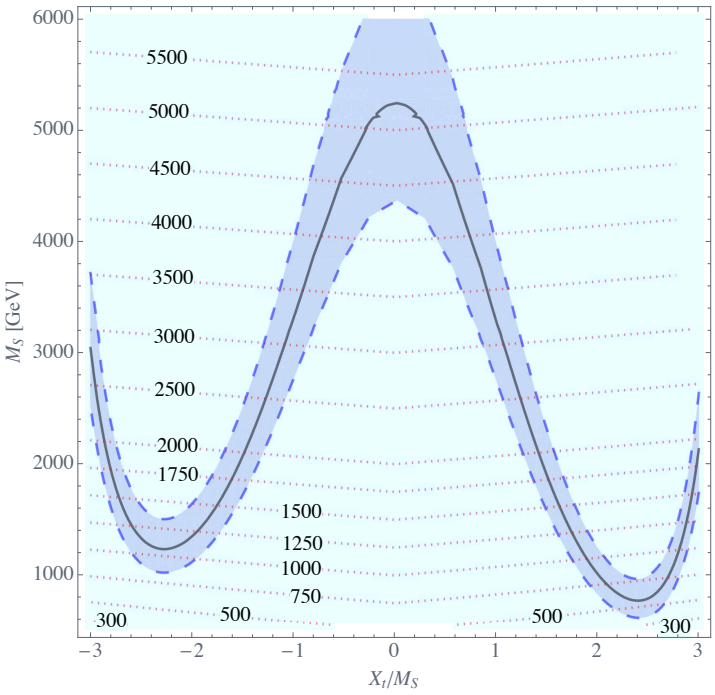

Figure 11.23: Values of the SUSY mass scale $M_{\rm SUSY} = M_S$ versus the stop mixing parameter normalized by the SUSY mass scale $X_t/M_{\rm SUSY}$, for fixed $\tan\beta = 20$, $\mu = 200\,\text{GeV}$ and $M_A = A_t = A_b = A_\tau = M_{\rm SUSY}$. The solid black line corresponds to $M_h = 125\,\text{GeV}$ while in the grey band M_h varies by $\pm 1\,\text{GeV}$. The red dotted lines are iso-values of the stop mass. This figure is based on Ref. [268].

Z bosons are given in terms of the angles α and β

$$g_{hVV} = g_V m_V \sin(\beta-\alpha), \quad g_{HVV} = g_V m_V \cos(\beta-\alpha), \tag{11.26}$$

where $g_V \equiv 2m_V/v$, for $V = \text{W}^\pm$ or Z ($g_V m_V$ is the SM hVV coupling). There are no tree-level couplings of A or $H^\pm$ to VV. The couplings of the Z boson to two neutral Higgs bosons, which must have opposite CP-quantum numbers, are given by $g_{\phi AZ}(p_\phi - p_A)$, where $\phi = H$ or h, the momenta p_ϕ and p_A point into the vertex, and

$$g_{hAZ} = g_Z \cos(\beta-\alpha)/2, \quad g_{HAZ} = -g_Z \sin(\beta-\alpha)/2\,. \tag{11.27}$$

Charged Higgs-W boson couplings to neutral Higgs bosons and four-point couplings of vector bosons and Higgs bosons can be found in Ref. [12].

The tree-level Higgs couplings to fermions obey the following property: the neutral components of one Higgs doublet, Φ_1, couple exclusively to down-type fermion pairs while the neutral components of the other doublet, Φ_2, couple exclusively to up-type fermion

pairs [12]. This Higgs-fermion coupling structure defines the Type-II 2HDM [273]. In the MSSM, fermion masses are generated when both neutral Higgs components acquire vacuum expectation values, and the relations between Yukawa couplings and fermion masses are (in third-generation notation)

$$h_{b,\tau} = \sqrt{2}\, m_{b,\tau}/(v\cos\beta), \quad h_t = \sqrt{2}\, m_t/(v\sin\beta)\,. \tag{11.28}$$

The couplings of the neutral Higgs bosons to $f\bar{f}$ relative to the SM value, $gm_f/2M_W$, are given by

$$\begin{aligned} h b\bar{b} &: -\sin\alpha/\cos\beta \qquad & h t\bar{t} &: \cos\alpha/\sin\beta\,, \\ H b\bar{b} &: \cos\alpha/\cos\beta \qquad & H t\bar{t} &: \sin\alpha/\sin\beta\,, \\ A b\bar{b} &: \gamma_5\tan\beta \qquad & A t\bar{t} &: \gamma_5\cot\beta\,. \end{aligned} \tag{11.29}$$

In each relation above, the factor listed for $b\overline{b}$ also pertains to $\tau^+\tau^-$. The charged Higgs boson couplings to fermion pairs are given by

$$\begin{aligned} g_{H^- t\bar{b}} &= \frac{g}{\sqrt{2}M_W}\left[m_t\cot\beta\frac{1+\gamma_5}{2} + m_b\tan\beta\frac{1-\gamma_5}{2}\right], \\ g_{H^-\tau^+\nu} &= \frac{g}{\sqrt{2}M_W}\left[m_\tau\tan\beta\frac{1-\gamma_5}{2}\right]. \end{aligned} \tag{11.30}$$

The non-standard neutral Higgs bosons have significantly enhanced couplings to down-type fermions at sizeable $\tan\beta$. In the alignment limit, the lightest Higgs boson behaves like the SM one and H, A have $\tan\beta$ enhanced couplings to down type fermions, and analogous enhanced couplings are in place for the charged Higgs.

Radiative corrections can modify significantly the values of the Higgs boson couplings to fermion pairs and to vector boson pairs. In a first approximation, when radiative corrections to the quartic couplings are computed, the diagonalizing angle α is shifted from its tree-level value, and hence one may compute a "radiatively-corrected" value for $\cos(\beta-\alpha)$ [255, 274]. Additional contributions from the one-loop vertex corrections to tree-level Higgs couplings [276–283] alter significantly the Higgs-fermion Yukawa couplings at large $\tan\beta$, both in the neutral and charged Higgs sector.

VII.1.1. MSSM Higgs boson phenomenology

In the MSSM, the mass, CP properties, decay and production properties of one of the neutral Higgs bosons should agree with the LHC Higgs data. Given that present data allows only for moderate departures from the SM predictions, it implies that some degree of alignment is necessary. For sufficiently heavy non-SM-like Higgs bosons, the alignment results from decoupling. If m_A is below a few hundred GeV, radiative corrections to the angle α can result in alignment for sizable values of the Higgs mass parameter $\mu > M_{\rm SUSY}$. Such radiative corrections, being proportional to ratios of mass parameters associated to the SUSY particles, do not decouple for heavy SUSY spectra.

The SM-like branching ratios of h can be modified if decays into supersymmetric particles are kinematically allowed, and, in particular, decays into a pair of the lightest

supersymmetric particles - i.e. the lightest neutralinos, $\tilde{\chi}_1^0$ - can become dominant and would be invisible if R-parity is conserved [284–286]. Moreover, if light superpartners exist that couple to photons and/or gluons, the h loop-induced coupling to gg and $\gamma\gamma$ could deviate sizably from the corresponding SM predictions [255, 287–294]

Given that some degree of alignment is necessary to agree with data, for the heavier Higgs states there are two possibilities to be considered: i) Alignment triggered by decoupling, hence $m_A \geq$ several hundred GeV: The HWW and HZZ couplings are very small. The dominant H, A decay branching ratios strongly depend on $\tan\beta$. After incorporating the leading radiative corrections to Higgs couplings, the following decay features are relevant in the MSSM: The decay modes $H, A \to b\bar{b}$, $\tau^+\tau^-$ dominate when $\tan\beta$ is large (this holds even away from decoupling). For small $\tan\beta$, the $t\bar{t}$ decay mode dominates above its kinematic threshold. For the charged Higgs boson, $H^+ \to t\bar{b}$ dominates. ii) Some degree of alignment without decoupling, hence $m_A \leq$ a few hundred GeV. The main difference with the previous case is that in the low $\tan\beta$ regime ($\tan\beta \leq 5$) additional decay channels may be allowed which involve decays into the lightest SM-like Higgs boson. For A and H, besides the $H, A \to b\bar{b}$, $\tau^+\tau^-$ decay modes, also $A \to Zh$, $H \to hh$ as well as $H \to WW/ZZ$ decay modes are available (they are suppressed in the strict alignment limit). For the charged Higgs boson, $H^+ \to \tau^+\nu_\tau$ dominates below the $t\bar{b}$ threshold, and also $H^\pm \to W^\pm h$ may be searched for. Both in i) and ii), the heavier Higgs states, H, A and $H^\pm$, are roughly mass degenerate (with masses $\pm$ 20 GeV or less apart). In cases i) and ii) the heavy Higgs boson decays into charginos, neutralinos and third-generation squarks and sleptons can be important if they are kinematically allowed [284].

The main production mechanisms for the neutral MSSM Higgs bosons at e^+e^- colliders are Higgs-strahlung ($e^+e^- \to Zh, ZH$), vector boson fusion ($e^+e^- \to \nu\bar{\nu}h, \nu\bar{\nu}H$) – with W^+W^- fusion about an order of magnitude larger than ZZ fusion – and s-channel Z boson exchange ($e^+e^- \to Ah, AH$). For the Higgs-strahlung process it is possible to reconstruct the mass and momentum of the Higgs boson recoiling against the particles from the Z boson decay, and hence sensitive searches for Higgs bosons decaying to invisible final states are possible. The main charged Higgs boson production process at e^+e^- colliders is via s-channel γ or Z boson exchange ($e^+e^- \to H^+H^-$). Charged Higgs bosons can also be produced in top quark decays via $t \to b + H^+$ if $m_H^\pm < m_t - m_b$ or via the one-loop process $e^+e^- \to W^\pm H^\mp$, which allows the production of a charged Higgs boson with $m_H^\pm > \sqrt{s}/2$, even when H^+H^- production is kinematically forbidden. Other single charged Higgs production mechanisms include $t\bar{b}H^-/\bar{t}bH^+$ production, $\tau^+\nu H^-/\tau^-\bar{\nu}H^+$ production, and a variety of processes in which $H^\pm$ is produced in association with one or two other gauge and/or Higgs bosons. For representative references on production mechanisms for the MSSM Higgs bosons at e^+e^- see [243].

At hadron colliders, the dominant neutral Higgs production mechanism at moderate values of $\tan\beta$ is gluon fusion, mediated by loops containing heavy top and bottom quarks and the corresponding supersymmetric partners [243]. The effect of light stops that may contribute to the gluon fusion production can be partially cancelled by mixing effects. Higgs boson radiation off bottom quarks becomes important for large $\tan\beta$, where at least two of the three neutral Higgs bosons have enhanced couplings to bottom-type

fermions [295, 296]. In the search for non-standard neutral Higgs bosons, A and H, the production can be via either of the above channels in the final inclusive ditau mode and via radiation off bottom quarks in the 4b's final mode. The total production rates of bottom quarks and τ pairs mediated by the production of a CP-odd Higgs boson in the large $\tan\beta$ regime are approximately given by

$$\begin{aligned}\sigma_{b\bar{b}A} \times \mathrm{BR}(A \to b\bar{b}) &\simeq \sigma^{\mathrm{SM}}_{b\bar{b}A} \;\; \frac{\tan^2\beta}{(1+\Delta_b)^2} \frac{9}{(1+\Delta_b)^2+9}, \\ \sigma_{gg\to A,b\bar{b}A} \times \mathrm{BR}(A \to \tau^+\tau^-) &\simeq \sigma^{\mathrm{SM}}_{gg\to A,b\bar{b}A} \;\; \frac{\tan^2\beta}{(1+\Delta_b)^2+9},\end{aligned} \tag{11.31}$$

where $\sigma^{\mathrm{SM}}_{b\bar{b}A}$ and $\sigma^{\mathrm{SM}}_{gg\to A,b\bar{b}A}$ denote the values of the corresponding SM Higgs boson cross sections for a SM Higgs boson mass equal to m_A. For high $\tan\beta$, the function Δ_b includes the dominant effects of the SUSY radiative corrections affecting the relation between the bottom quark mass and the bottom Yukawa coupling [259, 274, 275, 280–282], and it depends strongly on $\tan\beta$ and on the SUSY mass parameters. The production and decay rates of H, for m_A larger $m_h^{\max}$, are governed by formulas similar to the ones presented above, and given that A and H are nearly degenerate in mass, the total signal cross section is increased by roughly a factor of two. Detailed discussions of the impact of radiative corrections in these search modes are presented in Refs. [259, 297].

The vector boson fusion and Higgs-strahlung production of the CP-even Higgs bosons as well as the associated production of neutral Higgs bosons with top quark pairs have lower production cross sections by at least an order of magnitude with respect to the dominant ones, depending on the precise region of MSSM parameter space [42]. Higgs pair production of non-standard MSSM Higgs bosons has been studied in Ref. [298].

Charged Higgs bosons can be produced in several different modes at hadron colliders. If $m_{H^\pm} < m_t - m_b$, the charged Higgs boson can be produced in decays of the top quark via the decay $t \to bH^+$, which would compete with the SM process $t \to bW^+$. Relevant radiative corrections to $\mathrm{BR}(t \to H^+b)$ have been computed in Refs. [299–302]. For values of $m_{H^\pm}$ near m_t, width effects are important. If $m_{H^\pm} > m_t - m_b$, then charged Higgs boson production occurs mainly through radiation from a third generation quark. Charged Higgs bosons may also be produced singly in association with a top quark via the $2 \to 3$ partonic processes $pp \to H^+\bar{t}b + X$ and $pp \to H^-t\bar{b} + X$; via associated production with $W^\pm$ bosons through $b\bar{b}$ annihilation and gg fusion [303]; and in pairs via $q\bar{q}$ annihilation [304]. The inclusive H^+H^- cross section is less than the cross section for single charged Higgs associated production [304, 305]. For a more extensive discussion of charged Higgs boson production at LHC see Refs. [11 42, 306].

The additional Higgs bosons are sought for mainly via the channels

$$\begin{aligned}&pp \to A/H \to \tau^+\tau^- \;\; (\text{inclusive}), \\ &b\bar{b}A/H, A/H \to \tau^+\tau^- \;\; (\text{with } b\text{−tag}), \\ &b\bar{b}A/H, A/H \to b\bar{b} \;\; (\text{with } b\text{−tag}), \\ &pp \to t\bar{t} \to H^\pm W^\mp b\bar{b}, \;\; H^\pm \to \tau\nu_\tau \;\; , \\ &gb \to H^-t \quad \text{or} \quad g\bar{b} \to H^+\bar{t}, \;\; H^\pm \to \tau\nu_\tau \;\; .\end{aligned} \tag{11.32}$$

After the Higgs boson discovery, updated MSSM benchmarks scenarios have been defined, that highlight interesting conditions for MSSM Higgs searches [44, 258]. They include: i) a moderate mixing scenario in which the light CP-even Higgs boson can be interpreted as the newly discovered state in most of the $m_A - \tan\beta$ plane; ii) a light stop scenario with stop masses in the few to several hundred GeV range that can affect gluon fusion Higgs production; and iii) a tau-phobic scenario that exhibits variations of BR($h \to b\bar{b}$) and BR($h \to \tau^+\tau^-$) with respect to their SM values. In the above benchmarks it is also possible to have decays of $H \to hh$ in regions of moderate m_A and moderate $\tan\beta$ as far as one is away from precise alignment. Also for the previous benchmarks, the LHC reach in the traditional $A/H \to \tau^+\tau^-$ search channel varies depending on the values of μ and M_2, that may enable the A/H decays into electroweakinos. Lastly, varying the parameter μ in both sign and magnitude induces relevant variations in the possible discovery reach through the $4b$'s channel, and to a lesser extent through the inclusive ditau channel.

An alternative approach to reduce the large number of parameters relevant to the Higgs sector is to consider that, in the Higgs basis, the only important radiative corrections are those affecting the Higgs mass [307]. This approximation is called hMSSM and works well in large regions of parameter space but it breaks down for sizable values of μ and A_t, and moderate values of $\tan\beta$, for which the radiative corrections to the mixing between the two CP even eigenstates become relevant. The effect of such radiative corrections is to allow for alignment for small to intermediate values of $\tan\beta$, independent of the specific value of m_A [308]. In addition, the hMSSM assumption that the right value of the Higgs mass may be obtained for all values of m_A and $\tan\beta$ is in conflict with the MSSM predictions for the Higgs mass for small values of m_A and $\tan\beta \simeq \mathcal{O}(1)$.

Future precision measurements of the Higgs boson couplings to fermions and gauge bosons together with information on heavy Higgs searches will provide powerful information on the SUSY parameter space [309, 308–311]. If no other new states beyond the current Higgs candidate are discovered at the LHC, it becomes mandatory to understand what would be the required precision of the Higgs rate measurements to distinguish the MSSM from the SM.

Improvements in our understanding of B-physics observables put indirect constraints on additional Higgs bosons in mass ranges that would be accessible in direct LHC searches. In particular, BR($B_s \to \mu^+\mu^-$), BR($b \to s\gamma$), and BR($B_u \to \tau\nu$) play an important role within minimal flavor-violating (MFV) models [312], in which flavor effects proportional to the CKM matrix elements are induced, as in the SM. For example, see references in [243]. The supersymmetric contributions to these observables come both at the tree and loop level, and have a different parametric dependence, but share the property that they become significant for large values of $\tan\beta$, which is also the regime in which searches for non-standard MSSM Higgs bosons at hadron colliders are the most powerful.

VII.2. Higgs bosons in singlet extensions of the MSSM

In the MSSM, the Higgs mass parameter μ is a supersymmetric parameter, and as such, it should naturally be of order M_{GUT} or M_{Planck}. The fact that phenomenologically

it is required that μ be at the electroweak/TeV scale is known as the μ problem [313]. Supersymmetric models with additional singlets can provide a solution to the μ problem, by promoting the μ parameter to a dynamical singlet superfield S that only interacts with the MSSM Higgs doublets through a coupling λ_S at the level of the superpotential. An effective μ is generated when the real scalar component of S acquires a vacuum expectation value $\langle S \rangle$

$$\mu_{\mathit{eff}} = \lambda_S \langle S \rangle. \tag{11.33}$$

After the minimization of the Higgs potential the vacuum state relates the vacuum expectation values of the three CP-even neutral scalars, ϕ_1^0, ϕ_2^0 and S, to their soft supersymmetry breaking masses, hence, one expects that these VEVs should all be of order $M_{\rm SUSY}$ and therefore the μ problem is solved.

The solution of the μ problem through the addition of a singlet superfield to the MSSM comes along with the existence of an extra global U(1) symmetry, known as the Peccei–Quinn (PQ) symmetry [314]. This PQ symmetry is broken explicitly in realistic models. For that purpose one can consider a discrete Z_3 symmetry that allows the existence of a PQ odd S^3 term in the superpotential. This model extension has been called the next-to-minimal supersymmetric SM (NMSSM) (the NMSSM was first introduced in Ref. [315], see the 2014 edition of this review for an extensive list of subsequent references). It is known however that discrete symmetries may come along with the existence of domain wall structures that imply that our universe would consist of disconnected domains with different ground states, creating unacceptably large anisotropies in the cosmic microwave background [316]. To avoid the problem of domain walls one can consider the existence of non-renormalizable operators that would lead to the preferred vacuum state. However, the same operators in turn may generate quadratically divergent tadpole contributions [243] that could shift the VEV of S to be much larger, order M_{GUT}, and ruin the singlet solution to the μ problem. To cure the problem of destabilizing tadpoles, discrete R-symmetries have been proposed that ensure that tadpoles would only appear at very high order loops and be safely suppressed. Depending on the symmetries imposed on the theory, different models with singlet extensions of the MSSM (xMSSM) have been proposed. In Table 11.16 we show the most studied examples: the NMSSM, the Nearly-Minimal Supersymmetric SM (nMSSM) [317], and the U(1)$'$-extended MSSM (UMSSM) [318], specifying the new parameters appearing in the superpotential and the respective symmetries. A Secluded U(1)$'$-extended MSSM (sMSSM) [319] contains three singlets in addition to the standard UMSSM Higgs singlet; this model is equivalent to the nMSSM in the limit that the additional singlet VEV's are large, and the trilinear singlet coupling, λ_S, is small [320].

Based on the extended models defined in Table 11.16, we write the most generic supersymmetric and soft supersymmetry breaking scalar potentials for the three scalar

Table 11.16: Symmetries associated to various models with singlet extensions, the corresponding terms in the superpotential that only involve Higgs and singlet fields, and the number of neutral states in the Higgs sector for the case of CP conservation.

Model	MSSM	NMSSM	nMSSM	UMSSM
Symmetry	-	Z_3	Z_5^R, Z_7^R	$U(1)'$
Superpotential	$\mu\Phi_2\cdot\Phi_1$	$\lambda_S S\Phi_2\cdot\Phi_1+\frac{\kappa}{3}S^3$	$\lambda_S S\Phi_2\cdot\Phi_1+t_F S$	$\lambda_S S\Phi_2\cdot\Phi_1$
H_i^0	2	3	3	3
A_i^0	1	2	2	1

fields: Φ_1, Φ_2 and S:

$$\begin{aligned} V_{xMSSM} = &\left|\lambda_S\Phi_2\cdot\Phi_1+t_F+\kappa S^2\right|^2+|\lambda_S S|^2\left(|\Phi_1|^2+|\Phi_2|^2\right)\\ &+\frac{g'^2+g^2}{8}\left(|\Phi_1|^2-|\Phi_2|^2\right)^2+\frac{g^2}{2}\left(|\Phi_1|^2|\Phi_2|^2-|\Phi_2\cdot\Phi_1|^2\right)\\ &+\frac{g_1'^2}{2}\left(Q_{\Phi_1}|\Phi_1|^2+Q_{\Phi_2}|\Phi_2|^2+Q_S|S|^2\right)^2 \end{aligned} \tag{11.34}$$

$$V_{\rm soft}=m_{H_1}^2|\Phi_1|^2+m_{H_2}^2|\Phi_2|^2+m_s^2|S|^2+\left(A_s\lambda_S S H_u\cdot H_d+\frac{\kappa}{3}A_\kappa S^3+t_S S+h.c.\right). \tag{11.35}$$

where $\Phi_2\cdot\Phi_1=\epsilon_{ij}\Phi_2^i\Phi_1^j$ and the couplings g', g, and g_1' are associated to the $U(1)_Y$, $SU(2)_L$, and $U(1)'$ gauge symmetries, respectively. t_F and t_S are supersymmetric and SUSY breaking tadpole terms, respectively, m_s is a SUSY breaking mass term for the scalar component of the field S, and A_s and A_κ are the trilinear soft SUSY breaking mass parameters associated with the new terms $\lambda_S S\Phi_2\cdot\Phi_1$ and $\kappa S^3/3$ in the superpotential, with the B-term of the MSSM expressed as $B\mu\equiv A_s\mu_{eff}$. In particular, κ and A_κ are the parameters for the NMSSM model, while t_F and t_S are those of the nMSSM. The UMSSM depends on the new coupling g_1' as well as on the $U(1)'$ charges of the Higgs fields, Q_{Φ_1}, Q_{Φ_2} and Q_S, that are free parameters with the restriction that they have to add to zero for the superpotential $\lambda_3 S\Phi_2\Phi_1$ to be gauge invariant. In a given $U(1)'$ construction the charges are specified. The addition of the singlet scalar field(s) imply that additional CP-even and CP-odd Higgs bosons will appear in the spectra, whereas the charged Higgs sector remains the same as in the MSSM given that the number of Higgs doublets remains unchanged. The mixing with the extra scalar S alters the masses and properties of the physical Higgs bosons, that in general can differ significantly from the SM or the MSSM. A detailed discussion of typical mass spectra and decay properties in these models can be found for example in Refs. [321, 320]. Moreover, these models have extra neutralinos and in some cases extra neutral gauge bosons, Z'. The extra gauge boson sector is constrained by experimental data through direct Z' searches as well as the $Z-Z'$ mixing angle $\alpha_{ZZ'}$ constrained to be less that $\mathcal{O}(10^{-3})$ by precision electroweak data .

In singlet extensions of the MSSM the lightest CP-even Higgs mass at tree level, $m_{H_1}^{tree}$ receives a contribution from the singlet scalar that renders it larger than the MSSM

value, in particular for small values of $\tan\beta$. The tree level upper bound reads[9]

$$m_{H_1}^{tree} \leq M_Z^2 \cos^2 2\beta + \frac{1}{2}\lambda_S^2 v^2 \sin^2 2\beta\,. \tag{11.36}$$

At the one-loop level, the top and stop loops (as well as sbottom and stau loops for large $\tan\beta$) are the dominant contributions, that are common to the MSSM and to all the singlet extensions. Gauge couplings in the UMSSM are small compared to the top quark Yukawa coupling, hence the one-loop gauge contributions are negligible. Corrections exclusive to the NMSSM and the nMSSM enter only at the two loop level. Therefore, there are no significant model-dependent contributions at one loop order, and as a result, for large $\tan\beta$ the lightest CP-even Higgs mass does not differ in any significant way from the MSSM one. In the decoupling limit, a value of the lightest SM Higgs mass of about 125 GeV is achievable in all these MSSM extensions, and this remains the case even after higher order corrections are implemented.

A singlet extended supersymmetric Higgs sector opens new avenues for discovery. Since the singlet pseudoscalar particle may be identified as the pseudo-Goldstone boson of a spontaneously broken Peccei–Quinn symmetry, it may become naturally light [322, 323]. Generally, there is mixing of the singlet sector with the MSSM Higgs sector, and for a sufficiently light, singlet dominated scalar or pseudoscalar, h_S or A_S, respectively, the SM-like Higgs boson h may decay to pairs of h_S or A_S. The light scalar and/or pseudoscalar may subsequently decay to $\tau\tau$ or $b\bar{b}$ pairs. Such cascade decays are more difficult to detect than standard searches due to the potentially soft decay products. There is also a rich phenomenology for the decays of the heavy CP-even and CP-odd doublets, A and H into two lighter Higgs bosons such as $H \to hh_S$, hh, h_Sh_S or $A \to A_Sh_S$, A_Sh as well as into a light Higgs boson and a gauge boson: $H \to A_SZ$; $A \to h_SZ$, hZ. If kinematically allowed the heavy Higgs bosons decay into $t\bar{t}$. If the singlet dominated scalar or pseudoscalar are somewhat heavier, the decays $h_S \to WW$ or $A_S \to h_SZ$ will be allowed.

In addition, the light singlet scenario in the NMSSM or nMSSM is typically associated with a light singlino-dominated neutralino. The recently discovered SM-like Higgs boson can then decay to pairs of this neutralino [324, 320], opening an invisible decay mode that is not excluded by present data. All of the Higgs bosons can decay into electroweakinos depending on kinematics and the singlino or higgsino composition of the electroweakinos.

In models with extended singlets, at low $\tan\beta$ it is possible to trade the requirement of a large stop mixing by a sizeable trilinear Higgs-singlet Higgs coupling λ_S, rendering more freedom on the requirements for gluon fusion production. As in the MSSM, mixing in the Higgs sector -additionally triggered by the extra new parameter λ_S - can produce variations in the Higgs–$b\bar{b}$ and Higgs–$\tau^-\tau^+$ couplings that can alter the Higgs to ZZ/WW and diphoton rates. Light charginos at low $\tan\beta$ can independently contribute to enhance the di-photon rate, without altering any other of the Higgs decay rates [290, 325].

[9] Additional gauge interactions in the UMSSM contribute to this increase with a term of $\mathcal{O}(g_1'^2 v^2 (Q_{\phi_2}^2 \cos^2\beta + Q_{\phi_1}^2 \sin^2\beta))$.

There is much activity in exploring the NMSSM phenomenology in the light of the 125 GeV Higgs boson [326], as well as in defining benchmark scenarios with new topologies including Higgs decay chains [291]. An analytic understanding of the alignment condition in the NMSSM is presented in Ref. [292]. The NMSSM with a Higgs boson of mass 125 GeV can be compatible with stop masses of order of the electroweak scale, thereby reducing the degree of fine tuning necessary to achieve electroweak symmetry breaking (see Fig. 11.24). The alignment conditions point toward a more natural region of parameter space for electroweak symmetry breaking, while allowing for perturbativity of the theory up to the Planck scale and yielding a rich and interesting Higgs boson phenomenology at the LHC.

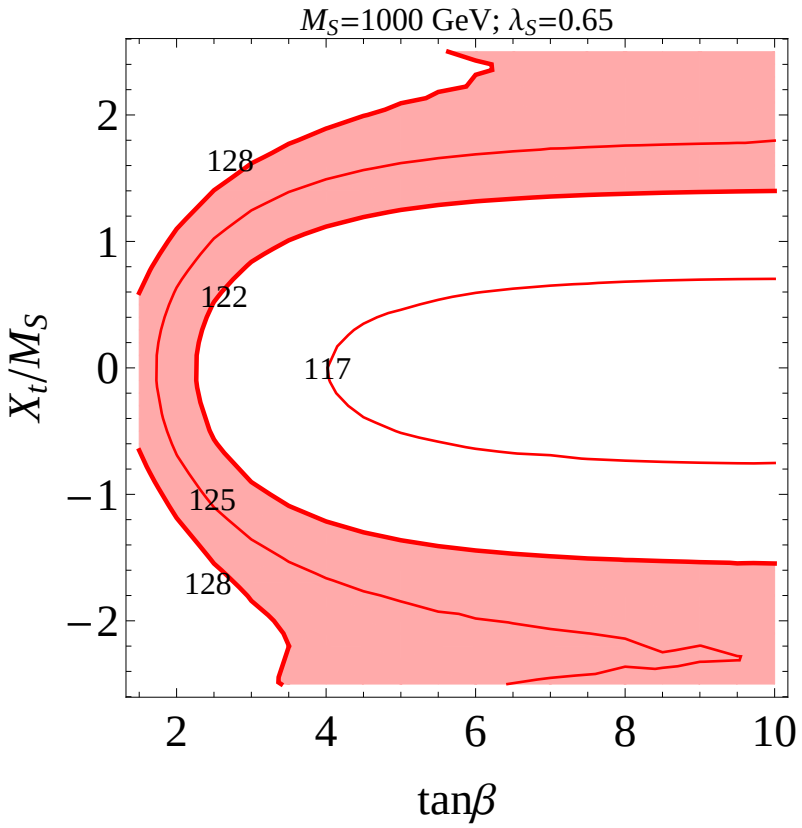

Figure 11.24: Values of the stop mixing parameter normalized to the SUSY mass scale $X_t/M_{\rm SUSY}$, as a function of $\tan\beta$, for $M_{\rm SUSY} \equiv M_S = 1000\,\text{GeV}$, $\lambda_S = 0.65$, and contours of constant values of the Higgs mass $m_h = 125 \pm 3\,\text{GeV}$ shaded in red [327].

VII.3. Supersymmetry with extended gauge sectors

In the MSSM, the tree-level value of the lightest CP-even Higgs mass originates from the D-term dependence of the scalar potential that comes from the supersymmetric kinetic terms in the Kähler potential. The D-terms lead to tree-level quartic couplings which are

governed by the squares of the gauge couplings of the weak interactions, under which the Higgs has non-trivial charges and hence the lightest Higgs mass is bounded to be smaller than M_Z. If new gauge interactions were present at the TeV scale, and the Higgs bosons would have non-trivial charges under them, there would be new D-term contributions that would lead to an enhancement of the tree-level Higgs mass value. Since the low energy gauge interactions reduce to the known $\mathrm{SU}(3)_c \times \mathrm{SU}(2)_L \times \mathrm{U}(1)_Y$ ones, in order for this mechanism to work, the extended gauge and Higgs sectors should be integrated out in a non-supersymmetric way. This means that there must be supersymmetry breaking terms that are of the order of, or larger than, the new gauge boson masses. The tree-level quartic couplings would then be enhanced through their dependence on the square of the gauge couplings of the extended Higgs sector. This effect will be suppressed when the heavy gauge boson masses are larger than the supersymmetry breaking scale and will acquire its full potential only for large values of this scale.

One of the simplest possibilities is to extend the weak interactions to a $\mathrm{SU}(2)_1 \times \mathrm{SU}(2)_2$ sector, such that the known weak interactions are obtained after the spontaneous breaking of these groups to $\mathrm{SU}(2)_L$ [328]. This may be achieved by introducing a bi-doublet Σ under the two SU(2) gauge groups, which acquires a non-trivial vacuum expectation value u in the diagonal direction. The heavy gauge boson masses are therefore given by $M^2_{W'} = (g_1^2 + g_2^2)u^2/2$, and the weak coupling $g^2 = g_1^2 g_2^2/(g_1^2 + g_2^2)$. To obtain a new tree-level contribution to the Higgs potential, the Higgs bosons must be charged under the new gauge interactions. One possibility is to assume that the third generation quarks and leptons as well as the Higgs doublets have charges under the $\mathrm{SU}(2)_1$ group, while the second and first generations have charges under $\mathrm{SU}(2)_2$. This provides a natural explanation of the largeness of the third generation couplings compared to the first and second generation ones.

Under the above conditions, the D-term contributions to the neutral Higgs effective potential are given by

$$V_D = \frac{g^2\Delta + g'^2}{8}\left(|H_2^0|^2 - |H_1^0|^2\right)^2 \tag{11.37}$$

with

$$\Delta = \left(1 + \frac{4m_\Sigma^2}{g_2^2 u^2}\right)\left(1 + \frac{4m_\Sigma^2}{(g_1^2 + g_2^2)u^2}\right)^{-1}, \tag{11.38}$$

where m_Σ is the supersymmetry breaking term associated with the bi-doublet Σ. It is easy to see that while the MSSM D-term is recovered when $m_\Sigma \to 0$, it is replaced by the $\mathrm{SU}(2)_1 \times \mathrm{U}(1)_Y$ D-term when m_Σ becomes much larger than $M_{W'}$. The tree-level mass now reads

$$m_h^2|_{\mathrm{tree}} = \frac{g^2\Delta + g'^2}{4} v^2 \cos^2 2\beta, \tag{11.39}$$

and reduces to the MSSM value, $M_Z^2 \cos^2 2\beta$, for $\Delta = 1$.

Assuming $g_1 \simeq g_2$, values of $g_{1,2}$ of order one are necessary to obtain the proper value of the weak gauge coupling. In addition, if values of m_Σ of order $M_{W'}$ are assumed, enhancements of order 50 percent of the MSSM D-term contribution to the Higgs mass

may be obtained. Such enhancements are sufficient to obtain the measured Higgs mass value without the need for very heavy stops or large stop mixing parameters.

The gauge extension described above leads to new, heavy gauge and Higgs bosons, as well as new neutralinos and charginos. Constraints from precision measurements put bounds of the order of a few TeV on the mass of these gauge bosons, which may be probed at the higher energy run of the LHC collider. If the new gaugino supersymmetry breaking masses are smaller than the gauge boson masses, the new electroweakinos will have masses of the order of a few TeV and therefore the weak scale phenomenology reduces to the MSSM one. Similar gauge extensions, including also new abelian gauge groups have been considered, for instance, in Ref. [329].

Gauge extensions of the MSSM can also lead to an enhancement of the Higgs mass value by modifying the renormalization group evolution of the Higgs quartic coupling to low energies. In the MSSM, the evolution of the quartic coupling is governed by the top-quark Yukawa interactions and depends on the fourth power of the top-quark Yukawa coupling. The neutralino and chargino contributions, which depend on the fourth power of the weak gauge couplings, are small due to the smallness of these couplings. Depending on the values of the soft supersymmetry breaking parameters in the gaugino and Higgsino sectors, the $\mathrm{SU}(2)_1$ gauginos may become light, with masses of the order of the weak scale. Since the $\mathrm{SU}(2)_1$ coupling may be significantly larger than the $\mathrm{SU}(2)_L$ one, for small values of the Higgsino mass parameter μ, the associated charginos and neutralinos may modify the evolution of the quartic coupling in a significant way [330]. This may lead to a significant increase of the lightest CP-even Higgs mass, even for small values of $\tan\beta \simeq 1$ for which the D-term contributions become small. In addition, under these conditions, light charginos may lead to a significant modification of the Higgs diphoton decay rate, which may be as large as 50% of the SM [330–334].

VII.4. Effects of CP violation

SUSY scenarios with CP-violation (CPV) phases are theoretically appealing, since additional CPV beyond that observed in the K, D, and B meson systems is required to explain the observed cosmic matter-antimatter asymmetry. In the MSSM, CP-violation effects in the Higgs sector appear at the quantum level, while in singlet extensions of the MSSM CP-violation effects can already be effective at tree level. In general, CP-violation effects in the Higgs sector have significant constraints from electric dipole moments data [243].

In the MSSM, the gaugino mass parameters ($M_{1,2,3}$), the Higgsino mass parameter, μ, the bilinear Higgs squared-mass parameter, m_{12}^2, and the trilinear couplings of the squark and slepton fields to the Higgs fields, A_f, may carry non-trivial phases. The two parameter combinations $\arg[\mu A_f (m_{12}^2)^*]$ and $\arg[\mu M_i (m_{12}^2)^*]$ are invariant under phase redefinitions of the MSSM fields [335, 261]. Therefore, if one of these quantities is non-zero, there would be new sources of CP-violation, which affects the Higgs sector through radiative corrections [260, 261, 336–340]. The mixing of the neutral CP-odd and CP-even Higgs boson states is no longer forbidden. Hence, m_A is no longer a physical parameter. However, the charged Higgs boson mass $m_{H^\pm}$ is still physical and can be

used as an input for the computation of the neutral Higgs spectrum of the theory. For large values of $m_{H^\pm}$, corresponding to the decoupling limit, the properties of the lightest neutral Higgs boson state approach those of the SM Higgs boson. In particular, the upper bound on the lightest neutral Higgs boson mass, takes the same value as in the CP-conserving case [261]. Nevertheless, there still can be significant mixing between the two heavier neutral mass eigenstates. For a detailed study of the Higgs boson mass spectrum and parametric dependence of the associated radiative corrections, see Refs. [336, 339].

Major variations to the MSSM Higgs phenomenology occur in the presence of explicit CPV phases. In the CPV case, vector boson pairs couple to all three neutral Higgs boson mass eigenstates, H_i $(i = 1, 2, 3)$, with couplings

$$g_{H_iVV} = \cos\beta\mathcal{O}_{1i} + \sin\beta\mathcal{O}_{2i}\,, \tag{11.40}$$

$$g_{H_iH_jZ} = \mathcal{O}_{3i}\left(\cos\beta\mathcal{O}_{2j} - \sin\beta\mathcal{O}_{1j}\right) - \mathcal{O}_{3j}\left(\cos\beta\mathcal{O}_{2i} - \sin\beta\mathcal{O}_{1i}\right)\,, \tag{11.41}$$

where the g_{H_iVV} couplings are normalized to the analogous SM coupling and the $g_{H_iH_jZ}$ have been normalized to $g_Z^{\rm SM}/2$. The orthogonal matrix $\mathcal{O}_{ij}$ is relating the weak eigenstates to the mass eigenstates. It has non-zero off-diagonal entries mixing the CP-even and CP-odd components of the weak eigenstates. The above couplings obey the relations

$$\sum_{i=1}^{3} g^2_{H_iZZ} = 1 \quad \text{and} \quad g_{H_kZZ} = \varepsilon_{ijk}\, g_{H_iH_jZ}\,, \tag{11.42}$$

where ε_{ijk} is the Levi-Civita symbol. Moreover, CPV phases imply that all neutral Higgs bosons can couple to both scalar and pseudoscalar fermion bilinear densities. The couplings of the mass eigenstates H_i to fermions depend on the loop-corrected fermion Yukawa couplings (similarly to the CPC case), on $\tan\beta$ and on the $\mathcal{O}_{ji}$ [336, 341].

The production processes of neutral MSSM Higgs bosons in the CPV scenario are similar to those in the CPC scenario. Regarding the decay properties, the lightest mass eigenstate, H_1, predominantly decays to $b\bar{b}$ if kinematically allowed, with a smaller fraction decaying to $\tau^+\tau^-$, similar to the CPC case. If kinematically allowed, a SM-like neutral Higgs boson, H_2 or H_3 can decay predominantly to H_1H_1 leading to many new interesting signals both at lepton and hadron colliders; otherwise it will decay preferentially to $b\bar{b}$.

The discovery of a 125 GeV Higgs boson has put strong constraints on the realization of the CPV scenario within the MSSM. This is partly due to the fact that the observed Higgs rates are close to the SM values, and a large CP-violating component would necessarily induce a large variation in the rate of the SM-like Higgs decay into the weak gauge bosons $W^\pm$ and Z. The measured Higgs mass imposes additional constraints on the realization of this scenario. Once all effects are considered, the CP-odd Higgs A component of the lightest Higgs tends to be smaller than about 10%. This restriction can be alleviated in the NMSSM or more general two Higgs doublet models. CP-violating effects can still be significant in the heavy Higgs sector. For instance, the Higgs bosons

H_2 and H_3 may be admixtures of CP-even and CP-odd scalars, and therefore both may be able to decay into pairs of weak gauge bosons. The observation of such decays would be a clear signal of CP-violation. In the MSSM the proximity of the masses of H_2 and H_3 makes the measurement of such effect quite challenging, but in generic two Higgs doublet models, the mass splitting between the two heavy mass eigenstates may become larger, facilitating the detection of CP-violating effects at collider experiments. For a recent studies see for example [342].

VII.5. Non-supersymmetric extensions of the Higgs sector

There are many ways to extend the minimal Higgs sector of the SM. In the preceding sections the phenomenology of SUSY Higgs sectors is considered, which at tree level implies a constrained type-II 2HDM (with restrictions on the Higgs boson masses and couplings). In the following discussion, more generic 2HDM's [12, 273, 343, 344] are presented. These models are theoretically less compelling since they do not provide an explanation for the SM Higgs naturalness problem, but can lead to different patterns of Higgs-fermion couplings, hence, to different phenomenology. It is also possible to consider models with a SM Higgs boson and one or more additional scalar SU(2) doublets that acquire no VEV and hence play no role in the EWSB mechanism. These models are dubbed Inert Higgs Doublet Models (IHD) [345]. Without a VEV associated to it, a Higgs boson from an inert doublet has no tree-level coupling to gauge bosons and hence cannot decay into a pair of them. And imposing a Z_2 symmetry that prevents them from coupling to the fermions, it follows that, if the lightest inert Higgs boson is neutral, it becomes a good dark matter candidate with interesting associated collider signals. Recent studies of IHD models in the light of a 125 GeV Higgs have been performed [346], showing that there can be non-negligible enhancement or suppression of Higgs to diphotons or Higgs to $Z\gamma$. This may be due to the presence of a light charged Higgs, as light as 100 GeV, that is not in conflict with collider or flavor constraints, because it has no couplings to fermions. It is interesting to study the interplay between collider and direct dark matter detection signals in these models.

Other extensions of the Higgs sector can include [321, 347] multiple copies of $\mathrm{SU}(2)_L$ doublets, additional Higgs singlets [348], triplets or more complicated combinations of Higgs multiplets. It is also possible to enlarge the gauge symmetry beyond $\mathrm{SU}(2)_L \times \mathrm{U}(1)_Y$ along with the necessary Higgs structure to generate gauge boson and fermion masses. There are two main experimental constraints on these extensions: *(i)* precision measurements which constrain $\rho = m_W^2/(m_Z^2 \cos^2\theta_W)$ to be very close to 1 and *(ii)* flavor changing neutral current (FCNC) effects. In electroweak models based on the SM gauge group, the tree-level value of ρ is determined by the Higgs multiplet structure. By suitable choices for the hypercharges, and in some cases the mass splitting between the charged and neutral Higgs sector or the vacuum expectation values of the Higgs fields, it is possible to obtain a richer combination of singlets, doublets, triplets and higher multiplets compatible with precision measurements [349]. Concerning the constraints coming from FCNC effects, the Glashow–Weinberg (GW) criterion [350] states that, in the presence of multiple Higgs doublets the tree-level FCNC's mediated by neutral Higgs bosons will be absent if all fermions of a given electric charge couple to no

more than one Higgs doublet. An alternative way of suppressing FCNC in a two Higgs doublet model has been considered in Ref. [351], where it is shown that it is possible to have tree level FCNC completely fixed by the CKM matrix, as a result of an abelian symmetry.

VII.5.1. Two-Higgs-doublet models

Supersymmetry demands the existence of two Higgs doublets such that one doublet couples to up-type quarks and the other to down-type quarks and charged leptons. This Higgs-fermion coupling structure is the one identified as type-II 2HDM [273] and assures that masses for both up and down-type quarks can be generated in a supersymmetric and gauge invariant way. Two Higgs doublet models [343], however, can have a more diverse Higgs-fermion coupling structure and can be viewed as a simple extension of the SM to realize the spontaneous breakdown of $\mathrm{SU}(2)_L \times \mathrm{U}(1)_Y$ to $\mathrm{U}(1)_{\mathrm{em}}$. Quite generally, if the two Higgs doublets contain opposite hypercharges, the scalar potential will contain mixing mass parameters of the kind $m_{12}^2 \Phi_1^T i\sigma_2 \Phi_2 + h.c.$. In the presence of such terms, both Higgs doublets will acquire vacuum expectation values, $v_1/\sqrt{2}$ and $v_2/\sqrt{2}$, respectively, and the gauge boson masses will keep their SM expressions with the Higgs vacuum expectation value v replaced by $v = \sqrt{v_1^2 + v_2^2}$. Apart from the mass terms, the most generic renormalizable and gauge invariant scalar potential contains seven quartic couplings, which are defined in Eq. (11.24).

Considering two doublets with hypercharges, with $Y_{\Phi_1} = -1$ and $Y_{\Phi_2} = 1$ as in Eq. (11.23), and the most general, renormalizable Higgs potential will be given by Eq. (11.24). Just as in the MSSM case, after electroweak symmetry breaking and in the absence of CP-violation, the physical spectrum contains a pair of charged Higgs bosons $H^{\pm}$, a CP-odd Higgs boson A and two neutral CP-even Higgs bosons, h and H. The angles α and β diagonalize the CP-even, and the CP-odd and Charged Higgs sectors, respectively.

The complete 2HDM is defined only after considering the interactions of the Higgs fields to fermions. Yukawa couplings of the generic form

$$-h_{ij}^a \bar{\Psi}_L^i H_a \Psi_R^j + h.c. \tag{11.43}$$

may be added to the renormalizable Lagrangian of the theory. Contrary to the SM, the two Higgs doublet structure does not ensure the alignment of the fermion mass terms $m_{ij} = h_{ij}^a v_a/\sqrt{2}$ with the Yukawa couplings h_{ij}^a. This implies that quite generally, the neutral Higgs boson will mediate flavor changing interactions between the different mass eigenstates of the fermion fields. Such flavor changing interactions should be suppressed in order to describe properly the Kaon, D and B meson phenomenology. Based on the Glashow–Weinberg criterion, it is clear that the simplest way of avoiding such transitions is to assume the existence of a symmetry that ensures the couplings of the fermions of each given quantum number (up-type and down-type quarks, charged and neutral leptons) to only one of the two Higgs doublets. Different models may be defined depending on which of these fermion fields couple to a given Higgs boson, see Table 11.17. Models of type-I [344] are those in which all SM fermions couple to a single Higgs field. In type-II

Table 11.17: Higgs boson couplings to up, down and charged lepton-type $SU(2)_L$ singlet fermions in the four discrete types of 2HDM models that satisfy the Glashow–Weinberg criterion, from Ref. [352].

Model	2HDM I	2HDM II	2HDM III	2HDM IV
u	Φ_2	Φ_2	Φ_2	Φ_2
d	Φ_2	Φ_1	Φ_2	Φ_1
e	Φ_2	Φ_1	Φ_1	Φ_2

models [273] down-type quarks and charged leptons couple to a common Higgs field, while the up-type quarks and neutral leptons couple to the other. In models of type-III (lepton-specific) quarks couple to one of the Higgs bosons, while leptons couple to the other. Finally, in models of type-IV (flipped), up-type quarks and charged leptons couple to one of the Higgs fields while down-quarks and neutral leptons couple to the other.

The two Higgs doublet model phenomenology depends strongly on the size of the mixing angle α and therefore on the quartic couplings. For large values of m_A, $\sin\alpha \to -\cos\beta$, $\cos\alpha \to \sin\beta$, $\cos(\beta-\alpha) \to 0$, and the lightest CP-even Higgs h behaves as the SM Higgs. The same behavior is obtained if the quartic couplings are such that $\mathcal{M}_{12}^2 \sin\beta = -(\mathcal{M}_{11}^2 - m_h^2)\cos\beta$. The latter condition represents a situation in which the coupling of h to fermions and weak gauge bosons become the same as in the SM, without decoupling the rest of the non-standard scalars and it is of particular interest due to the fact that the recently discovered Higgs boson has SM-like properties. This situation will be referred to as alignment, as in the MSSM case.

In type-II Higgs doublet models, at large values of $\tan\beta$ and moderate values of m_A, the non-standard Higgs bosons H, A and $H^\pm$ couple strongly to bottom quarks and τ leptons. Hence the decay modes of the non-standard Higgs bosons tend to be dominated by b-quark and tau-lepton modes, including top quarks or neutrinos in the case of the charged Higgs. However, for large and negative values of λ_4, the charged Higgs boson mass may be sufficiently heavy to allow on-shell decays

$$\begin{aligned} H^\pm &\to W^\pm + (H, A), \\ g_{H^\pm W^\mp H,A} &\simeq \frac{M_W}{v}\sin(\beta-\alpha)(p_{H^+} - p_{H,A})\,, \end{aligned} \tag{11.44}$$

where p_{H^+} and $p_{H,A}$ are the charged and neutral scalar Higgs momenta pointing into the vertex. On the other hand, for large and positive values of λ_5, the above charged Higgs decay into a $W^\pm$ and the CP-odd Higgs boson may be allowed, but the heavy Higgs H may be sufficiently heavy to decay into a CP-odd Higgs boson and an on-shell Z.

$$H \to Z + A, \quad g_{HZA} \simeq \frac{M_Z}{v}\sin(\beta-\alpha)(p_H - p_A). \tag{11.45}$$

The decay $H^\pm \to W^\pm + H$, on the other hand may be allowed only if $\lambda_4 < -\lambda_5$. The couplings controlling all the above decay modes are proportional to $\sin(\beta-\alpha)$ and therefore they are unsuppressed in the alignment limit. Moreover, these could still be the

dominant decay modes at moderate values of $\tan\beta$, offering a way to evade the current bounds obtained assuming a dominant decay into bottom quarks or τ leptons.

The quartic couplings are restricted by the condition of stability of the effective potential as well as by the restriction of obtaining the proper value of the lightest CP-even Higgs mass. Close to the alignment limit, the lightest CP-even Higgs mass becomes approximately independent of m_A and is given by

$$\begin{aligned} m_h^2 \simeq & v^2(\lambda_1 \cos^4\beta + \lambda_2 \sin^4\beta + 2\tilde{\lambda}_3 v^2 \cos^2\beta \sin^2\beta) \\ & + v^2(4\lambda_6 \cos^3\beta \sin\beta + 4\lambda_7 \sin^3\beta \cos\beta)\,, \end{aligned} \tag{11.46}$$

where $\tilde{\lambda}_3 = \lambda_3 + \lambda_4 + \lambda_5$.

The stability conditions imply the positiveness of all masses, as well as the avoidance of run-away solutions to large negative values of the fields in the scalar potential. These conditions imply

$$\begin{aligned} & \lambda_1 \geq 0, \quad \lambda_2 \geq 0, \quad \lambda_3 + \lambda_4 - |\lambda_5| \geq -\sqrt{\lambda_1 \lambda_2}, \\ & \lambda_3 \geq -\sqrt{\lambda_1 \lambda_2}, \quad 2|\lambda_6 + \lambda_7| < \frac{\lambda_1 + \lambda_2}{2} + \tilde{\lambda}_3, \end{aligned} \tag{11.47}$$

where the first four are necessary and sufficient conditions in the case of $\lambda_6 = \lambda_7 = 0$, while the last one is a necessary condition in the case all couplings are non-zero. Therefore, to obtain the conditions that allow the decays $H^\pm \to W^\pm H, A$ and $H \to ZA$, λ_3 should take large positive values in order to compensate for the effects of λ_4 and λ_5. For recent detailed discussions about 2HDM phenomenology see Refs [309, 254, 347, 353–356, 357].

VII.5.2. Higgs triplets

Electroweak triplet scalars are the simplest non-doublet extension of the SM that can participate in the spontaneous breakdown of $\mathrm{SU}(2)_L \times \mathrm{U}(1)_Y$ to $\mathrm{U}(1)_{\mathrm{em}}$. Two types of model have been developed in enough detail to make a meaningful comparison to LHC data: the Higgs triplet model (HTM) [358, 359] and the Georgi–Machacek model [360–362].

The Higgs triplet model extends the SM by the addition of a complex $\mathrm{SU}(2)_L$ triplet scalar field Δ with hypercharge $Y = 2$, and a general gauge-invariant renormalizable potential $V(\Phi, \Delta)$ for Δ and the SM Higgs doublet Φ. The components of the triplet field can be parameterized as

$$\Delta = \frac{1}{\sqrt{2}} \begin{pmatrix} \Delta^+ & \sqrt{2}\Delta^{++} \\ v_\Delta + \delta + i\xi & -\Delta^+ \end{pmatrix}. \tag{11.48}$$

where Δ^+ is a singly-charged field, Δ^{++} is a doubly-charged field, δ is a neutral CP-even scalar, ξ is a neutral CP-odd scalar, and v_Δ is the triplet VEV. The general scalar potential mixes the doublet and triplet components. After electroweak symmetry breaking there are seven physical mass eigenstates, denoted $H^{\pm\pm}$, $H^\pm$, A, H, and h.

A distinguishing feature of the HTM is that it violates the custodial symmetry of the SM; thus the ρ parameter deviates from 1 even at tree level. Letting x denote the ratio of triplet and doublet VEVs, the tree level expression [363] is:

$$\rho = \frac{1+2x^2}{1+4x^2} \,. \tag{11.49}$$

The measured value of the ρ parameter then limits [364] the triplet VEV to be quite small, $x \lesssim 0.03$, or $v_\Delta < 8\,\text{GeV}$. This constraint severely limits the role of the triplet scalar in the EWSB mechanism.

The small VEV of the Higgs triplet in the HTM is a virtue from the point of view of generating neutrino masses without the necessity for introducing right-handed neutrino fields. The gauge invariant dimension four interaction

$$h_{\nu_{ij}}\, \ell_i^T C^{-1} i\sigma_2\, \Delta\, \ell_j \,, \tag{11.50}$$

where ℓ_i are the lepton doublets, C is the charge conjugation matrix, and $h_{\nu_{ij}}$ is a complex symmetric coupling matrix, generates a Majorana mass matrix for the neutrinos:

$$m_{\nu_{ij}} = \sqrt{2} h_{\nu_{ij}} v_\Delta \,. \tag{11.51}$$

This can be combined with the usual neutrino seesaw to produce what is known as the type-II seesaw [365].

The HTM suggests the exciting possibility of measuring parameters of the neutrino mass matrix at the LHC. If the doubly-charged Higgs is light enough and/or its couplings to W^+W^+ are sufficiently suppressed, then its primary decay is into same-sign lepton pairs: $H^{++} \to \ell_i^+ \ell_j^+$; from Eq. (11.50) and Eq. (11.51) it is apparent that these decays are in general lepton-flavor violating with branchings proportional to elements of the neutrino mass matrix [366].

Precision electroweak data constrain the mass spectrum as well as the triplet VEV of the HTM [363, 367, 368]. As described in Ref. [368], these constraints favor a spectrum where H^{++} is the lightest of the exotic bosons, and where the mass difference between H^+ and H^{++} is a few hundred GeV. The favored triplet VEV is a few GeV, which also favors H^{++} decays into W^+W^+ over same-sign dileptons.

The Georgi–Machacek model addresses the ρ parameter constraint directly by building in custodial symmetry. Writing the complex scalar doublet of the SM as a $(2,2)$ under $\text{SU}(2)_L \times \text{SU}(2)_R$, it is obvious that the next simplest construction respecting custodial symmetry is a scalar transforming like a $(3,3)$ [369]. These nine real degrees of freedom correspond to a complex electroweak triplet combined with a real triplet, with the scalar potential required to be invariant under $\text{SU}(2)_R$. Under the custodial $\text{SU}(2)_{L+R}$, they transform as $1 \oplus 3 \oplus 5$, with a CP-even neutral scalar as the custodial singlet (thus matching the SM Higgs boson), a CP-odd neutral scalar in the custodial triplet, and another CP-even neutral scalar in the custodial 5-plet.

The scalar components can be decomposed as [370]

$$\Xi = \begin{pmatrix} \chi_3^* & \xi_1 & \chi_1 \\ -\chi_2^* & \xi_2 & \chi_2 \\ \chi_1^* & -\xi_1^* & \chi_3 \end{pmatrix}, \tag{11.52}$$

where ξ_2 is a real scalar and the others are complex scalars. Linear combinations of these account for the neutral custodial singlet, a neutral and singly-charged field making up the custodial triplet, and neutral, singly-charged, and doubly-charged fields making up the custodial 5-plet.

When combined with the usual SM doublet field Φ, the electroweak scale v is now related to the doublet and triplet VEVs by

$$v^2 = v_\Phi^2 + 8v_\Xi^2 \, . \tag{11.53}$$

Note that the GM triplets by themselves are sufficient to explain electroweak symmetry breaking and the existence of a 125 GeV neutral boson along with a custodial triplet of Goldstone bosons; the complex doublet field in the GM model is required to generate fermion masses via the usual dimension four Yukawa couplings. This raises the question of whether one can rule out the possibility that the 125 GeV boson is the neutral member of a custodial 5-plet rather than a custodial singlet, without invoking decays to fermions. A conclusive answer is given by observing that the ratio of the branching fractions to W versus Z bosons is completely determined by the custodial symmetry properties of the boson. For a custodial 5-plet, the ratio of the signal strength to WW over that to ZZ is predicted to be 1/4 that of a SM Higgs boson [369, 371], and thus already ruled out by the experimental results presented in Section VI.

Another interesting general feature of Higgs triplet models is that, after mixing, the SM-like neutral boson can have stronger couplings to WW and ZZ than predicted by the SM [362, 372]; this is in contrast to mixing with additional doublets and singlet, which can only reduce the WW and ZZ couplings versus the SM. This emphasizes that LHC Higgs data cannot extract model independent coupling strengths for the Higgs boson [230, 373].

Because of the built-in custodial symmetry, the triplet VEV in the GM model can be large compared to the doublet VEV. The custodial singlet neutral boson from the triplets mixes with the neutral boson from the doublet. Two interesting special cases are (i) the triplet VEV is small and the 125 GeV boson is SM-like except for small deviations, and (ii) the 125 GeV boson is mostly the custodial singlet neutral boson from the electroweak triplets. The phenomenology of the doubly-charged and singly-charged bosons is similar to that of the HTM. The constraints on the GM model from precision electroweak data, LEP data, and current LHC data are described in Refs. [370, 374–377].

VII.6. Composite Higgs models

Within the SM, EWSB is posited but has no dynamical origin. Furthermore, the Higgs boson appears to be unnaturally light. A scenario that remedies these two catches is to consider the Higgs boson as a bound state of new dynamics becoming strong

around the weak scale. The Higgs boson can be made significantly lighter than the other resonances of the strong sector if it appears as a pseudo-Nambu–Goldstone boson, see Refs. [15, 16, 378] for recent reviews.

VII.6.1. Little Higgs models

The idea behind the Little Higgs models [379, 380] is to identify the Higgs doublet as a (pseudo) Nambu–Goldstone boson while keeping some sizable non-derivative interactions, in particular a largish Higgs quartic interaction. By analogy with QCD where the pions $\pi^{\pm,0}$ appear as Nambu–Goldstone bosons associated to the breaking of the chiral symmetry $\mathrm{SU}(2)_\mathrm{L} \times \mathrm{SU}(2)_\mathrm{R}/\mathrm{SU}(2)$, switching on some interactions that break explicitly the global symmetry will generate masses for the would-be massless Nambu–Goldstone bosons of the order of $g\Lambda_{G/H}/(4\pi)$, where g is the coupling of the symmetry breaking interaction and $\Lambda_{G/H} = 4\pi f_{G/H}$ is the dynamical scale of the global symmetry breaking G/H. In the case of the Higgs boson, the top Yukawa interaction or the gauge interactions themselves will certainly break explicitly (part of) the global symmetry since they act non-linearly on the Higgs boson. Therefore, obtaining a Higgs mass around 100 GeV would demand a dynamical scale $\Lambda_{G/H}$ of the order of 1 TeV, which is known to lead to too large oblique corrections. Raising the strong dynamical scale by at least one order of magnitude requires an additional selection rule to ensure that a Higgs mass is generated at the 2-loop level only

$$m_H^2 = \frac{g^2}{16\pi^2}\Lambda_{G/H}^2 \to m_H^2 = \frac{g_1^2 g_2^2}{(16\pi^2)^2}\Lambda_{G/H}^2 \tag{11.54}$$

The way to enforce this selection rule is through a "collective breaking" of the global symmetry:

$$\mathcal{L} = \mathcal{L}_{G/H} + g_1\mathcal{L}_1 + g_2\mathcal{L}_2. \tag{11.55}$$

Each interaction $\mathcal{L}_1$ or $\mathcal{L}_2$ individually preserves a subset of the global symmetry such that the Higgs remains an exact Nambu–Goldstone boson whenever either g_1 or g_2 is vanishing. A mass term for the Higgs boson can be generated only by diagrams involving simultaneously both interactions. At one-loop, such diagram are not quadratically divergent, so the Higgs mass is not UV sensitive. Explicitly, the cancellation of the SM quadratic divergences is achieved by a set of new particles around the Fermi scale: gauge bosons, vector-like quarks, and extra massive scalars, which are related, by the original global symmetry, to the SM particles with the same spin. Contrary to supersymmetry, the cancellation of the quadratic divergences is achieved by same-spin particles. These new particles, with definite couplings to SM particles as dictated by the global symmetries of the theory, are perfect goals for the LHC.

The simplest incarnation of the collective breaking idea, the so-called littlest Higgs model, is based on a non-linear σ-model describing the spontaneous breaking SU(5) down to SO(5). A subgroup $\mathrm{SU}(2)_1 \times \mathrm{U}(1)_1 \times \mathrm{SU}(2)_2 \times \mathrm{U}(1)_2$ is weakly gauged. This model contains a weak doublet, that is identified with the Higgs doublet, and a complex weak triplet whose mass is not protected by collective breaking. Other popular little Higgs models are based on different coset spaces: minimal moose $(\mathrm{SU}(3)^2/\mathrm{SU}(3))$ [381], the

simplest little Higgs ($SU(3)^2/SU(2)^2$) [382], the bestest little Higgs ($SO(6)^2/SO(6)$) [383] *etc.* For comprehensive reviews, see Refs. [384, 385].

Generically, oblique corrections in Little Higgs models are reduced either by increasing the coupling of one of the gauge groups (in the case of product group models) or by increasing the masses of the W and Z partners, leading ultimately to a fine-tuning of the order of a few percents (see for instance Ref. [386] and references therein). The compatibility of Little Higgs models with experimental data is significantly improved when the global symmetry involves a custodial symmetry as well as a T-parity [387] under which, in analogy with R-parity in SUSY models, the SM particles are even and their partners are odd. Such Little Higgs models would therefore appear in colliders as jet(s) with missing transverse energy [388] and the ATLAS and CMS searches for squarks and gluinos [389] can be recast to obtain limits on the masses of the heavy vector-like quarks. The T-even top partner, with an expected mass below 1 TeV to cancel the top loop quadratic divergence without too much fine-tuning, would decay dominantly into a $t + Z$ pair or into a $b + W$ pair or even into $t + H$. The latest CMS and ATLAS direct searches [390] for vector-like top partners put a lower bound around 700 GeV on their mass, excluding the most natural region of the parameter space of these models, i.e., there is still fine-tuning at the per cent level.

The motivation for Little Higgs models is to solve the little hierarchy problem, i.e., to push the need for new physics (responsible for the stability of the weak scale) up to around 10 TeV. Per se, Little Higgs models are effective theories valid up to their cutoff scale $\Lambda_{G/H}$. Their UV completions could either be weakly or strongly coupled.

VII.6.2. Models of partial compositeness

The Higgs boson is a special object. Even in composite models, it cannot appear as a regular resonance of the strong sector without endangering the viability of the setup when confronted to data. The way out is that the Higgs appears as a pseudo Nambu–Goldstone boson: the new strongly coupled sector is supposed to be invariant under a global symmetry G spontaneously broken to a subgroup H at the scale f. To avoid conflict with EW precision measurements, it is better if the strong interactions themselves do not break the EW symmetry, hence the SM gauge symmetry itself should be contained in H. See Table 11.18 for a few examples of coset spaces.

The SM (light) fermions and gauge bosons cannot be part of the strong sector itself since LEP data have already put stringent bounds on the compositeness scale of these particles far above the TeV scale. The gauge bosons couple to the strong sector by a weak gauging of an $SU(2)\times U(1)$ subgroup of the global symmetry G. Inspiration for the construction of such models comes from the AdS/CFT correspondence: the components of a gauge field along extra warped space dimension can be interpreted as the Goldstone boson resulting from the breaking of global symmetry of the strong sector. The couplings of the SM fermions to the strong sector could a priori take two different forms: (i) a bilinear coupling of two SM fermions to a composite scalar operator, $\mathcal{O}$, of the form $\mathcal{L} = y\,\bar{q}_L u_R \mathcal{O} + \text{hc}$ in simple analogy with the SM Yukawa interactions. This is the way fermion masses were introduced in Technicolor theories and it generically comes with severe flavor problems and calls for extended model building gymnastics [391]

Table 11.18: Global symmetry breaking patterns and the corresponding Goldstone boson contents of the SM, the minimal composite Higgs model, the next to minimal composite Higgs model, and the minimal composite two Higgs doublet model. Note that the SU(3) model does not have a custodial invariance. a denotes a CP-odd scalar while h and H are CP-even scalars.

Model	Symmetry Pattern	Goldstone's
SM	SO(4)/SO(3)	W_L, Z_L
–	SU(3)/SU(2)×U(1)	W_L, Z_L, H
MCHM	SO(5)/SO(4)	W_L, Z_L, H
NMCHM	SO(6)/SO(5)	W_L, Z_L, H, a
MC2HM	SO(6)/SO(4)×SO(2)	$W_L, Z_L, h, H, H^\pm, a$

to circumvent them; (ii) a linear mass mixing with fermionic vector-like operators: $\mathcal{L} = \lambda_L\, \bar{q}_L \mathcal{Q}_R + \lambda_R \bar{\mathcal{U}}_L u_R$. $\mathcal{Q}$ and $\mathcal{U}$ are two fermionic composite operators of mass M_Q and M_U. Being part of the composite sector, they can have a direct coupling of generic order Y_* to the Higgs boson. In analogy with the photon-ρ mixing in QCD, once the linear mixings are diagonalized, the physical states are a linear combination of elementary and composite fields. Effective Yukawa couplings are generated and read for instance for the up-type quark

$$y = Y_* \sin\theta_L \sin\theta_R \tag{11.56}$$

where $\sin\theta_i = \lambda_i/\sqrt{M_U^2 + \lambda_i^2}$, $i = L, R$, measure the amount of compositeness of the SM left- and right-handed up-type quark. If the strong sector is flavor-anarchic, i.e., if the couplings of the Higgs to the composite fermions does not exhibit any particular flavor structure, the relation Eq. (11.56) implies that the light fermions are mostly elementary states ($\sin\theta_i \ll 1$), while the third generation quarks need to have a sizable degree of compositeness. The partial compositeness paradigm offers an appealing dynamical explanation of the hierarchies in the fermion masses. In fact, assuming the strong sector to be almost conformal above the confinement scale, the low-energy values of the mass-mixing parameters $\lambda_{L,R}$ are determined by the (constant) anomalous dimension of the composite operator they mix with. If the UV scale at which the linear mixings are generated is large, then $\mathcal{O}(1)$ differences in the anomalous dimensions can generate naturally large hierarchies in the fermion masses via renormalization group running [392]. While the introduction of partial compositeness greatly ameliorated the flavor problem of the original composite Higgs models, nevertheless it did not solve the issue completely, at least in the case where the strong sector is assumed to be flavor-anarchic [393]. While the partial compositeness set-up naturally emerges in models built in space-times with extra dimensions, no fully realistic microscopic realization of partial compositeness has been proposed in the literature.

Another nice aspect of the partial compositeness structure is the dynamical generation of the Higgs potential. The Higgs being a pseudo-Nambu–Goldstone boson, its mass does not receive any contribution from the strong sector itself but it is generated at the one-loop level via the couplings of the SM particles to the strong sector since these

interactions are breaking the global symmetries under which the Higgs doublet transforms non-linearly. The leading contribution to the potential arises from top loops and it takes the form

$$V(H) = m_\rho^4 \frac{\sin\theta_{tL}\sin\theta_{tR}}{16\pi^2}\left(\alpha\cos(H/f) + \beta\sin^2(H/f) + \gamma\sin^4(H/f)\right), \tag{11.57}$$

where α, β, γ are numbers of order 1 subject to selection rules following the transformation properties of the top quark under the global symmetries of the strong sector[10], and $m_\rho \approx g_\rho f$ is the typical mass scale of the strong sector resonances. The gauge contribution to the potential takes the form (g denotes the SU(2) gauge coupling)

$$m_\rho^4 \frac{g^2/g_\rho^2}{16\pi^2}\sin^2(H/f), \tag{11.58}$$

which is parametrically suppressed with respect to the top contribution by $g^2/(g_\rho y_t)$. The gauge term is always positive, and cannot trigger EWSB by itself. When $\alpha = 0$, the minimization condition of the potential simply reads

$$\sin^2\frac{\langle H\rangle}{f} = -\frac{\beta}{2\gamma}, \tag{11.59}$$

which implies that the natural expectation is that the scale f is generically of the order of the weak scale. Obtaining $v \ll f$, as required phenomenologically, requires some degree of tuning, which scales like $\xi \equiv v^2/f^2$. A mild tuning of the order of 10% ($\xi \approx 0.1$) is typically enough to comply with electroweak precision constraints. This is an important point: in partial compositeness models, the entire Higgs potential is generated at one loop, therefore the separation between v and f can only be obtained at a price of a tuning. This marks a difference with respect to the Little Higgs models, which realize a parametric hierarchy between the quartic and mass terms through the collective symmetry breaking mechanism. In fact in Little Higgs models, the quartic coupling is a tree-level effect, leading to a potential

$$V(H) \approx \frac{g_{\rm SM}^2}{16\pi^2} m_\rho^2 H^2 + g_{\rm SM}^2 H^4, \tag{11.60}$$

where $g_{\rm SM}$ generically denotes the SM couplings. The minimization condition now reads $v^2/f^2 \sim g_\rho^2/(16\pi^2)$, therefore v is formally loop suppressed with respect to f. This is the major achievement of the Little Higgs constructions, which however comes at the price

[10] For instance in the SO(5)/SO(4) composite models, when the top quark is embedded into a spinorial representation of SO(5), then $\gamma = 0$ and when it is part of a **5**, **10** or **14** representation, $\alpha = 0$ as it can be inferred by looking at the structure of the H-dependent invariants built out of these representations [394]. The coefficient γ also generically comes with an extra power of the top compositeness fractions.

of the presence of sub-TeV vectors carrying EW quantum numbers and therefore giving rise generically to large oblique corrections to the propagators of the W and the Z gauge bosons.

After minimization, the potential Eq. (11.57) leads to an estimate of the Higgs mass as

$$m_H^2 \approx g_\rho^3\, y_t 2\pi^2 v^2. \tag{11.61}$$

It follows that the limit $f \to \infty$, i.e. $\xi \to 0$, is a true decoupling limit: all the resonances of the strong sector become heavy but the Higgs whose mass is protected by the symmetries of the coset G/H. When compared to the experimentally measured Higgs mass, this estimate puts an upper bound on the strength of the strong interactions: $g_\rho \lesssim 2$. In this limit of not so large coupling, the Higgs potential receives additional contributions. In particular, the fermionic resonances in the top sector which follow from the global symmetry structure of the new physics sector can help raising the Higgs mass. For instance in the minimal SO(5)/SO(4) model, using some dispersion relation techniques, one obtains [395]

$$m_H^2 \approx \frac{6}{\pi^2}\frac{m_t^2}{f^2}\frac{m_{Q_4}^2 m_{Q_1}^2}{m_{Q_1}^2 - m_{Q_4}^2}\log\left(\frac{m_{Q_1}}{m_{Q_4}}\right) \tag{11.62}$$

where Q_4 and Q_1 are fermionic color resonances transforming as a weak bi-doublet of hypercharge $Y = 1/6$ and $Y = 7/6$ and a weak singlet with hypercharge $Y = -1/3$. Therefore a 125 GeV mass can be obtained if at least one of the fermionic resonances is lighter than $\sim 1.4\, f$. As in supersymmetric scenarios, the top sector is playing a crucial role in the dynamics of EWSB and can provide the first direct signs of new physics. The direct searches for these top partners, in particular the ones with exotic electric charges 5/3, are already exploring the natural parameter spaces of these models [390, 396, 397].

The main physics properties of a pseudo Nambu–Goldstone Higgs boson can be captured in a model-independent way by a few number of higher-dimensional operators. Indeed, the strong dynamics at the origin of the composite Higgs singles out a few operators among the complete list presented earlier in Section VI: these are the operators that involve extra powers of the Higgs doublets and they are therefore generically suppressed by a factor $1/f^2$ as opposed to the operators that involve extra derivatives or gauge bosons and are suppressed by a factor $1/(g_\rho^2 f^2)$. The relevant effective Lagrangian describing a strongly interacting light Higgs is:

$$\begin{aligned}\mathcal{L}_{\rm SILH} =& \frac{c_H}{2f^2}\left(\partial_\mu\left(\Phi^\dagger\Phi\right)\right)^2 + \frac{c_T}{2f^2}\left(\Phi^\dagger \overleftrightarrow{D}^\mu \Phi\right)^2 - \frac{c_6\lambda}{f^2}\left(\Phi^\dagger\Phi\right)^3 \\ &+ \left(\sum_f \frac{c_f\, y_f}{f^2}\Phi^\dagger\Phi\bar{f}_L\Phi f_R + \text{h.c.}\right).\end{aligned} \tag{11.63}$$

Typically, these new interactions induce deviations in the Higgs couplings that scale like $\mathcal{O}(v^2/f^2)$, hence the measurements of the Higgs couplings can be translated into some

constraints on the compositeness scale, $4\pi f$, of the Higgs boson. The peculiarity of these composite models is that, due to the Goldstone nature of the Higgs boson, the direct couplings to photons and gluons are further suppressed and generically the coupling modifiers defined in Section VI scale like

$$\begin{aligned} \kappa_{W,Z,f} &\sim 1 + \mathcal{O}\left(\frac{v^2}{f^2}\right) , \\ \kappa_{Z\gamma} &\sim \mathcal{O}\left(\frac{v^2}{f^2}\right) , \\ \kappa_{\gamma,g} &\sim \mathcal{O}\left(\frac{v^2}{f^2} \times \frac{y_t^2}{g_\rho^2}\right) , \end{aligned} \tag{11.64}$$

where g_ρ denotes the typical coupling strength among the states of the strongly coupled sector and y_t is the top Yukawa coupling, the largest interaction that breaks the Goldstone symmetry. The $\kappa_{Z\gamma,\gamma,g}$ coupling modifiers are not generated by the strong coupling operators of Eq. (11.63) but some subleading form-factor operator generated by loops of heavy resonances of the strong sector. The coupling modifiers also receive additional contributions from the other resonances of the strong sector, in particular the fermionic resonances of the top sector that are required to be light to generate a 125 GeV Higgs mass. Some indirect information on the resonance spectrum could thus be inferred by a precise measurement of the Higgs coupling deviations. However, it was realized [398] that the task is actually complicated by the fact that, in the minimal models, these top partners give a contribution to both κ_t (resulting from a modification of the top Yukawa coupling) and κ_γ and κ_g (resulting from new heavy particles running into the loops) and the structure of interactions are such that the net effect vanishes for inclusive quantities like $\sigma(gg \to H)$ or $\Gamma(H \to \gamma\gamma)$ as a consequence of the Higgs low energy theorem [24, 25, 231]. So one would need to rely on differential distribution, like the Higgs p_T distribution [399], to *see* the top partner effects in Higgs data [400]. The off-shell channel $gg \to h^* \to 4\ell$ [401] and the double Higgs production $gg \to hh$ [402] can also help to resolve the gluon loop and separate the top and top-partner contributions.

VII.6.3. Minimal composite Higgs models

The minimal composite Higgs models (MCHM) are concrete examples of the partial compositeness paradigm. The Higgs doublet is described by the coset space SO(5)/SO(4) where a subgroup $\mathrm{SU}(2)_L \times \mathrm{U}(1)_Y$ is weakly gauged under which the four Goldstone bosons transform as a doublet of hypercharge 1. There is some freedom on how the global symmetry is acting on the SM fermions: in MCHM4 [394] the quarks and leptons are embedded into spinorial representations of SO(5), while in MHCM5 [403] they are part of fundamental representations (it might also be interesting phenomenologically to consider larger representations like MCHM14 [404] with the SM fermions inside a representation of dimension 14). The non-linearly realized symmetry acting on the Goldstone bosons leads to general predictions of the coupling of the Higgs boson to the EW gauge bosons. For instance, it can be shown that the quadratic terms in the W and Z bosons read

$$m_W^2(H)\left(W_\mu W^\mu + \frac{1}{2\cos^2\theta_W} Z_\mu Z^\mu\right)$$

with $m_W(H) = \frac{gf}{2}\sin\frac{H}{f}$. Expanding around the EW vacuum, the expression of the weak scale is:

$$v = f\sin(\langle H\rangle/f), \tag{11.65}$$

and the values of the modified Higgs couplings to the W and Z:

$$g_{HVV} = \frac{2m_V^2}{v}\sqrt{1-v^2/f^2}\,, \quad g_{HHVV} = \frac{2m_V^2}{v^2}(1-2v^2/f^2)\,. \tag{11.66}$$

Note that the Higgs couplings to gauge bosons is always suppressed compared to the SM prediction. This is a general result [405] that holds as long as the coset space is compact.

The Higgs couplings to the fermions depend on the representation which the SM fermions are embedded into. For the most commonly used embeddings, they take the following forms

$$\begin{aligned}
\text{MCHM4}: g_{Hff} &= \frac{m_f}{v}\sqrt{1-v^2/f^2}\,,\\
\text{MCHM5}: g_{Hff} &= \frac{m_f}{v}\frac{1-2v^2/f^2}{\sqrt{1-v^2/f^2}}\,,\\
\text{MCHM14}: g_{Hff} &= \frac{m_f}{v}\left(1+A(M_{1,4,9})\frac{v^2}{f^2}+O(v^4/f^4)\right)\,,\\
&\text{with } A(M_{1,4,9}) = \frac{3M_1M_4-11M_1M_9+8M_4M_9}{2M_9(M_1-M_4)}\,.
\end{aligned} \tag{11.67}$$

While, in MHCM4 and MCHM5, the modifications of the couplings depend only on the Higgs compositeness scale, in MCHM14 the leading corrections depend also on the mass spectrum of the resonances parametrized by M_1, M_4 and M_9 [404]. This is due to the fact that more than one SO(5) invariant gives rise to SM fermion masses. The (κ_V, κ_f) experimental fit of the Higgs couplings can be used to derive a lower bound on the Higgs compositeness scale $4\pi f \gtrsim 9\,\text{TeV}$, which is less stringent than the indirect bound obtained from EW precision data, $4\pi f \gtrsim 15\,\text{TeV}$ [406] but more robust and less subject on assumptions [407].

VII.6.4. Twin Higgs models

In all composite models presented above, the particles responsible for canceling the quadratic divergences in the Higgs mass are charged under the SM gauge symmetries. In particular, the top partner carries color charge, implying a reasonably large minimal production cross section at the LHC. An alternative scenario, which is experimentally quite challenging and might explain the null result in various new physics searches, is the case nowadays referred to as "neutral naturalness" [20, 21], where the particles canceling the 1-loop quadratic divergences are neutral under the SM. The canonical example for such theories is the Twin Higgs model of [20]. This is an example of a pseudo-Goldstone boson Higgs theory, with an approximate global $SU(4)$ symmetry broken to $SU(3)$. The Twin Higgs model is obtained by gauging the $SU(2)_A \times SU(2)_B$ subgroup of $SU(4)$,

where $SU(2)_A$ is identified with the SM $SU(2)_L$, while $SU(2)_B$ is the twin $SU(2)$ group. Gauging this subgroup breaks the $SU(4)$ symmetry explicitly, but quadratically divergent corrections given do not involve the Higgs boson when the gauge couplings of the two SU(2) subgroups are equal, $g_A = g_B$. The $SU(4) \to SU(3)$ breaking will also result in the breaking of the twin $SU(2)_B$ group and as a result three of the seven Goldstone bosons will be eaten, leaving 4 Goldstone bosons corresponding to the SM Higgs doublet h. In fact imposing the Z_2 symmetry on the full model will ensure the cancellation of all 1-loop quadratic divergences to the Higgs mass. Logarithmically divergent terms can however arise for example from gauge loops, leading to a Higgs mass of order $g^2 f/4\pi$, which is of the order of the physical Higgs mass for $f \sim 1\,\text{TeV}$. The quadratic divergences from the top sector can be eliminated if the Z_2 protecting the Higgs mass remains unbroken by the couplings that result in the top Yukawa coupling. This can be achieved by introducing top partners charged under a twin $SU(3)_c$. In this case the quadratic divergences are cancelled by top partners that are neutral under the SM gauge symmetries.

Twin Higgs models are low-energy effective theories valid up to a cutoff scale of order $\Lambda \sim 4\pi f \sim$ 5–10 TeV, beyond which a UV completion has to be specified. The simplest such possibility is to also make the Higgs composite, and UV complete the twin-Higgs model via gauge and top partners at masses of the order of a few TeV. A concrete implementation is the holographic twin Higgs model [408], which also incorporates a custodial symmetry to protect the T-parameter from large corrections. It is based on a warped extra dimensional theory with a bulk SO(8) gauge group, which incorporates the $SU(4)$ global symmetry discussed above enlarged to contain the $\text{SU}(2)_L \times \text{SU}(2)_R$ custodial symmetry. In addition the bulk contains either a full $SU(7)$ group or an $SU(3) \times SU(3) \times U(1) \times U(1) \times Z_2$ subgroup of it to incorporate QCD, its twin, and hypercharge. The breaking on the UV brane is to the SM and the twin SM symmetries, while on the IR brane $SO(8) \to SO(7)$, giving rise to the 7 Goldstone bosons, three of which will be again eaten by the twin W, Z. The main difference compared to ordinary composite Higgs models is that in composite twin Higgs models the cancellation of the one-loop quadratic divergences is achieved by the twin partners of order 700 GeV– 1 TeV, which are uncharged under the SM gauge group. This allows the IR scale of the warped extra dimension to be raised to the multi-TeV range without reintroducing the hierarchy problem. The role of the composite partners is to UV complete the theory, rather than the cancellation of the one-loop quadratic divergences. For more details about the composite twin Higgs models, see Refs. [409].

VII.7. The Higgs boson as a dilaton

The possibility that the new particle H^0 discovered at the LHC is in fact the Goldstone boson associated to the spontaneous breaking of scale invariance at a scale f attracted some attention [18, 19] but is now challenged by the fact that all its properties are in good agreement with those predicted for the SM Higgs. And this scenario now requires rather involved model-building engineering. The first issue is the fact that the observed scalar couplings are close to their SM values. In a generic theory of spontaneously broken scale invariance, order one shifts are possible, and indeed expected in most models. Also, the apparent hierarchy between the light scalar and the cutoff of the dilaton effective theory

is not reconcilable with the general walking technicolor (or Higgsless) type scenario unless a tuning is imposed.

The general couplings of a wide class of dilaton models are given (at leading order in a low-energy theorem limit for dilatons) by

$$\begin{aligned}\mathcal{L}_{dilaton} = \frac{\sigma}{f}\left[2M_W^2 W_\mu^\pm W^{\pm\mu} + M_Z^2 Z_\mu Z^\mu + \sum_{ij}\sqrt{m_f^i m_f^j}\Gamma^{ij}\bar{\psi}^i\psi^j\right] \\ + \frac{\sigma}{f}\left[\frac{2}{e}\Delta\beta^{\rm em}F_{\mu\nu}^2 + \frac{2}{g_3}\Delta\beta^{\rm QCD}G_{\mu\nu}^{a\ 2}\right]\end{aligned} \tag{11.68}$$

where Γ^{ij} is a matrix that depends upon anomalous dimensions of operators in the conformal theory that give rise to fermion masses, and the terms $\Delta\beta$ are the differences in the beta functions of electromagnetism or QCD at scales above and below the scale at which conformal symmetry is spontaneously broken. The SM low energy theorem limit for the SM Higgs is obtained from this expression by taking

$$f = v, \quad \Gamma^{ij} = I_{3\times 3}, \quad \Delta\beta^{em} = \beta_{top}^{em} + \beta_W^{em}, \quad \Delta\beta^{\rm QCD} = \beta_{top}^{\rm QCD}. \tag{11.69}$$

It is unclear why these relations should be approximately realized in a generic conformal field theory, as must be the case to be consistent with current data and allow for a scalar with mass of about 125 GeV. For example, in warped models of electroweak symmetry breaking (AdS/CFT duals to theories with spontaneously approximate broken conformal invariance), the ratio v/f is a function of the geometry, and is suppressed when the 5D theory is perturbative, contrary to the experimental result that the v/f ratio should be close to 1, implying that the underlying CFT may not be a large N CFT.

An additional complication is that the mass of the dilaton is expected to be, along with many other resonances, around the cutoff scale of the strongly interacting theory responsible for breaking the scale invariance spontaneously. Suppression of the dilation mass either requires a tuning of order $v^2/\Lambda^2 \sim$ percent, or a very special conformal dynamics where the beta function of the interaction leading to the scale invariance breaking remains small over a large region of couplings [410].

VII.8. Searches for signatures of extended Higgs sectors

The measurements described in Section III have established the existence of one state of the electroweak symmetry breaking sector, compatible with a SM Higgs boson, but not that it is the only one.

Various classes of models beyond the SM discussed above require extended Higgs sectors. These models, and in particular the MSSM and the NMSSM serve as guiding principle of the experimental searches for additional scalar states beyond the SM. However these searches are made as model-independent as possible and can be summarized in the following classes: (i) the search for an additional CP-even state mostly in the high mass domain decaying to vector bosons, which would correspond to the heavy CP-even state in

a generic 2HDM where the light state would be the discovered H or a generic additional singlet; (ii) the search for a state in the high mass domain decaying to pairs of fermions, which would correspond a CP-odd A and the heavy CP-even state H in a generic 2HDM; (iii) the search for charged Higgs bosons, which also appear in generic 2HDMs; (iv) the search for a CP-odd state a in the low mass region which appears in the NMSSM; and (v) doubly charged Higgs which are motivated in extensions of the Higgs sector with triplets.

(i) Searches for an additional CP-even state

(a) Exclusion limits from LEP

The LEP searches for the SM Higgs boson put a lower limit of 114 GeV on its mass, but also have relevance for non-SM Higgs bosons. These searches were also interpreted as 95% CL upper bounds on the ratio of the coupling g_{HZZ} to its SM prediction as a function of the Higgs boson mass [125]. Among the MSSM new benchmarks, the low-m_H is one example which is disfavored by these searches at low mass, and nearly ruled out by current direct constraints and charged Higgs limits from LHC. Another example is the light CP-even Higgs boson of the NMSSM which is constrained to project predominantly onto the EW singlet component. An additional motivation for these scenarios is given by the slight excess observed at LEP [125] at a Higgs boson mass hypothesis of approximately 98 GeV. The light CP-even Higgs boson h was also searched for in association with the CP-odd A, these searches are described in Section III.

(b) Searches at the LHC

The searches for the SM Higgs boson before the discovery covered a wide range of mass hypotheses. Until recently the range of investigation at LHC was from 100 GeV to 600 GeV. It has been extended to masses of up to 1 TeV. At the Tevatron this mass range was limited to up to 200 GeV. Since the discovery, the SM Higgs boson searches are reappraised to search for a heavy CP-even state. This state could be the heavy CP-even Higgs boson of a 2HDM, or a generic additional singlet. In both cases the natural width of the additional H state can be very different from that of the SM Higgs boson. To preserve unitarity of the longitudinal vector boson scattering and the longitudinal vector boson scattering into fermion pairs, the couplings of the additional CP-even Higgs boson to gauge bosons and fermions should not be too large and should constrain the natural width to be smaller than that of a unique Higgs boson at high mass with couplings to fermions and gauge bosons as predicted by the SM (and provided that trilinear and quartic couplings are not too large and that no new state affects the heavy state total width). It is therefore reasonable to consider total widths for the high mass CP-even state smaller than the equivalent SM width. For the sake of generality these searches should be done as a function of Higgs boson mass and total width. Until recently only two cases have been investigated: (i) the SM width using the complex pole scheme (CPS), and (ii) the narrow width approximation.

Searches for the Higgs boson in the $H \to \gamma\gamma$, $H \to Z\gamma$, $H \to W^{(*)}W^{(*)}$ in the $\ell\nu\ell\nu$ and $\ell\nu q\overline{q}$ channels, and the $H \to Z^{(*)}Z^{(*)}$ searches in the 4ℓ, $\ell\ell q\overline{q}$ and $\ell\ell\nu\nu$ channels have

Table 11.19: Summary of references to searches for additional states from extended Higgs sectors, where (BBr) denotes the BaBar experiment, (TeV) the Tevatron experiments.

	ATLAS	CMS	Other experiments
CP-even H			
$H \to \gamma\gamma$	—	[415]	—
$H \to Z\gamma$	[171]	[170]	—
$H \to ZZ \to 4\ell$	[470]	[471]	—
$H \to ZZ \to \ell\ell\nu\nu$	[472]	[473]	—
$H \to ZZ \to \ell\ell q\overline{q}$	[474, 475]	[476]	—
$H \to WW \to \ell\nu\ell\nu$	[477]	[471]	—
$H \to WW \to \ell\nu\ell\nu$ (2HDM)	[414]	[471]	—
$H \to WW \to \ell\nu q\overline{q'}$	[478]	[479, 480]	—
$H \to hh \to b\overline{b}\tau\tau, b\overline{b}\gamma\gamma, 4b, \gamma\gamma WW^*$	[412]	[413, 411]	—
CP-odd A (and/or CP-even H)			
$H, A \to \tau^+\tau^-$	[429]	[430]	[427, 428]-TeV [481]-LHCb
$H, A \to \mu^+\mu^-$	[429]	—	—
$H, A \to t\overline{t}$	[435]	—	
$H, A \to b\overline{b}$	—	[431]	[425, 426]-TeV
$A \to hZ \to b\overline{b}\ell\ell, \ell\ell\tau\tau, \nu\overline{\nu}b\overline{b}$	[438]	[411]	—
Charged $H^\pm$			
$H^\pm \to \tau^\pm\nu$	[447]	[449]	—
$H^\pm \to cs$	[451]	[452]	—
$H^\pm \to tb$	[450]	[449]	—
$H^\pm \to W^\pm Z$	[453]	[449]	—
CP-odd NMSSM a			
$a \to \mu^+\mu^-$	[464]	[465]	—
$h \to aa \to 4\mu, 4\tau, 2\mu 2\tau, 4\gamma$	[482, 466]	[467, 468]	[456]-TeV, [469]-LEP
$\Upsilon_{1s,3s} \to a\gamma$	—	—	[461, 462]-BBr
Doubly Charged $H^\pm$	[483]	[484]	—

also been done, but in most cases are simple reinterpretations of the SM Higgs search in the CPS scheme. Recent references are summarized in Table 11.19.

(d) Searches for an additional resonance decaying to a pair of h

In addition to the rare and expected Higgs pair production mode, high mass CP-even Higgs bosons can be searched for in the resonant double Higgs mode. Searches for such processes, where the Higgs boson is used as a tool for searches for new phenomena beyond the SM, have been carried out in four distinct modes depending on the subsequent decays of each Higgs boson. The ATLAS and CMS Collaborations have searched for the $H \to hh \to b\bar{b}\tau\tau$ [411, 412] and $b\bar{b}\gamma\gamma$ [413, 412] final states. The ATLAS Collaboration has also searched for the $H \to hh \to 4b$ and $\gamma\gamma WW^*$ final states [412]. For masses hypotheses of an additional Higgs boson below 500 GeV, the two dominant search channels are the $b\bar{b}\gamma\gamma$ and the $b\bar{b}\tau\tau$. For masses above 500 GeV, the most powerful search channel is the $4b$ final state. The ATLAS Collaboration has also performed a combination of these search results assuming that the Higgs boson has standard decay rates [412].

(d) Searches for an additional state with the presence of h

In the post-discovery era, analyses in general need to take into account the presence of the newly discovered state. For searches with sufficiently high resolution of additional states non degenerate in mass, the strength of the observed state and limits on the signal strength of a potential additional state can be set independently, as discussed in the next section. However in some cases, such as when a channel does not have a sufficiently fine mass resolution or when the states are nearly degenerate in mass, specific analyses need to be designed. There are two examples of such analyses: (i) the search for an additional state in the $H \to W^{(*)}W^{(*)} \to \ell\nu\ell\nu$ channel in ATLAS and (ii) the search for nearly degenerate states in the $H \to \gamma\gamma$ channel with the CMS detector.

The search in the $H \to W^{(*)}W^{(*)} \to \ell\nu\ell\nu$ channel, for an additional state is done using a boosted decision tree combining several discriminating kinematic characteristics to separate the signal from the background and a high mass signal H from the lower mass state h [414]. A simultaneous fit of the two states h and H is then made to test the presence of an additional state. In this case, the usual null hypothesis of background includes including the SM signal.

The CMS search for nearly degenerate mass states decaying to a pair of photons [415] is more generic and could for instance apply to CP-odd Higgs bosons as well. It consists of a fit to the diphoton mass spectrum using two nearly degenerate mass templates.

(e) Type I 2HDM and fermiophobia

The measurements of coupling properties of H indirectly exclude that the discovered state is fermiophobic. However, the presence of an additional fermiophobic state, as predicted by Type I 2HDMs, is not excluded. Prior to the discovery, ATLAS and CMS have performed searches for a fermiophobic Higgs boson, *i.e.* produced through couplings with vector bosons only (VBF and VH) and decaying in $h_f \to \gamma\gamma$, optimized for fermiophobic signatures in the diphoton channel [416, 417]. CMS has further combined these results with searches for $h_f \to W^+W^-$ and $h_f \to ZZ$ assuming fermiophobic production and decay [418]. CMS excludes a fermiophobic Higgs boson in the range $110\,\text{GeV} < m_H < 188\,\text{GeV}$ at the 95% C.L.

(f) Interpretation benchmarks in the light of the discovered Higgs boson

Two specific benchmark scenarios driven by unitarity relations are proposed in Ref. [44], assuming the existence of an additional state h' with coupling scale factors, i.e., deviations from the couplings predicted for the SM Higgs at the same mass, denoted κ'_V and κ'_F for the couplings of h' to vector bosons and fermions respectively. The gauge boson scattering unitarity then yields the following sum rule

$$\kappa_V^2 + \kappa_V'^2 = 1 \tag{11.70}$$

and the unitarization of the gauge boson scattering to fermions yields

$$\kappa_V \cdot \kappa_F + \kappa'_V \cdot \kappa'_F = 1 \tag{11.71}$$

The two benchmark scenarios are then defined as follows: (i) a single coupling scale factor is assumed for the gauge bosons and the fermions, with an additional parameter to take into account decays to new states; (ii) two parameters are used to describe independently the couplings to fermions and the couplings to vector bosons. A direct application of the latter can be done in the CP-even sector of the type-I 2HDM.

(ii) Searches for additional neutral states ($\phi \equiv h$, H, A) decaying to fermions

(a) Exclusion limits from LEP

In e^+e^- collisions at LEP centre-of-mass energies, the main production mechanisms of the neutral MSSM Higgs bosons were the Higgs-strahlung processes $e^+e^- \to hZ$, HZ and the pair production processes $e^+e^- \to hA$, HA, while the vector boson fusion processes played a marginal role. Higgs boson decays to $b\bar{b}$ and $\tau^+\tau^-$ were used in these searches.

The searches and limits from the four LEP experiments are described in Refs. [419, 420]. The combined LEP data did not contain any excess of events which would imply the production of a Higgs boson, and combined limits were derived [421]. For $m_A \gg M_Z$ the limit on m_h is nearly that of the SM searches, as $\sin^2(\beta-\alpha) \approx 1$. For high values of $\tan\beta$ and low m_A ($m_A \leq m_h^{max}$), the $e^+e^- \to hA$ searches become the most important, and the lightest Higgs h is non SM-like. In this region, the 95% CL mass bounds are $m_h > 92.8\,\text{GeV}$ and $m_A > 93.4\,\text{GeV}$. In the m_h-max. scenario, values of $\tan\beta$ from 0.7 to 2.0 are excluded taking $m_t = 174.3\,\text{GeV}$, while a much larger $\tan\beta$ region is excluded for other benchmark scenarios such as the no-mixing one.

A flavor-independent limit for Higgs bosons in the Higgs-strahlung process at LEP has also been set at 112 GeV [422].

Neutral Higgs bosons may also be produced by Yukawa processes $e^+e^- \to f\overline{f}\phi$, where the Higgs particle $\phi \equiv h$, H, A, is radiated off a massive fermion ($f \equiv b$ or $\tau^\pm$). These processes can be dominant at low masses, and whenever the $e^+e^- \to h\text{Z}$ and hA processes are suppressed. The corresponding ratios of the $f\overline{f}h$ and $f\overline{f}A$ couplings to the SM coupling are $\sin\alpha/\cos\beta$ and $\tan\beta$, respectively. The LEP data have been used to search for $b\overline{b}\,b\overline{b}$, $b\overline{b}\tau^+\tau^-$, and $\tau^+\tau^-\,\tau^+\tau^-$ final states [423, 424]. Regions of low mass and high enhancement factors are excluded by these searches.

The searches for the Higgs boson at LEP also included the case where it does not predominantly decay to a pair of b quarks. All four collaborations conducted dedicated searches for the Higgs boson with reduced model dependence, assuming it is produced via the Higgs-strahlung process, and not addressing its flavor of decay, a lower limit on the Higgs mass of 112.9 GeV is set by combining the data of all four experiments [422].

Using an effective Lagrangian approach and combining results sensitive to the $h\gamma\gamma$, $hZ\gamma$ and hZZ couplings, an interpretation of several searches for the Higgs boson was made and set a lower limit of 106.7 GeV on the mass of a Higgs boson that can couple anomalously to photons [422].

(b) Searches at the Tevatron and LHC

The best sensitivity is in the regime with low to moderate m_A and with large $\tan\beta$ which enhances the couplings of the Higgs bosons to down-type fermions. The corresponding limits on the Higgs boson production cross section times the branching ratio of the Higgs boson into down-type fermions can be interpreted in MSSM benchmark scenarios [259]. If $\phi = A, H$ for $m_A > m_h^{\max}$, and $\phi = A, h$ for $m_A < m_h^{\max}$, the most promising channels at the Tevatron are the inclusive $p\overline{p} \to \phi \to \tau^+\tau^-$ process, with contributions from both $gg \to \phi$ and $b\overline{b}\phi$ production, and $b\overline{b}\phi, \phi \to \tau^+\tau^-$ or $\phi \to b\overline{b}$, with $b\tau\tau$ or three tagged b-jets in the final state, respectively. Although Higgs boson production via gluon fusion has a higher cross section in general than via associated production, it cannot be used to study the $\phi \to b\overline{b}$ decay mode since the signal is overwhelmed by the QCD background.

The CDF and D0 collaborations have searched for neutral Higgs bosons produced in association with bottom quarks and which decay into $b\overline{b}$ [425, 426], or into $\tau^+\tau^-$ [427,428]. The most recent searches in the $b\overline{b}\phi$ channel with $\phi \to b\overline{b}$ analyze approximately 2.6 fb^{-1} of data (CDF) and 5.2 fb^{-1} (D0), seeking events with at least three b-tagged jets. The cross section is defined such that at least one b quark not from ϕ decay is required to have $p_T > 20$ GeV and $|\eta| < 5$. The invariant mass of the two leading jets as well as b-tagging variables are used to discriminate the signal from the backgrounds. The QCD background rates and shapes are inferred from data control samples, in particular, the sample with two b-tagged jets and a third, untagged jet. Separate-signal hypotheses are tested and limits are placed on $\sigma(p\overline{p} \to b\overline{b}\phi) \times \text{BR}(\phi \to b\bar{b})$. A local excess of approximately 2.5σ significance has been observed in the mass range of 130–160 GeV, but D0's search is more sensitive and sets stronger limits. The D0 result had an $\mathcal{O}(2\sigma)$ local upward fluctuation in the 110 to 125 GeV mass range. These results have been superseded by the LHC searches and the excess seen in the D0 experiment has not been confirmed elsewhere.

ATLAS and CMS also search for $\phi \to \tau^+\tau^-$ in pp collisions at $\sqrt{s} = 7$ TeV. ATLAS seeks tau pairs in 4.7–4.8 fb^{-1} of data [429], and the search by CMS uses the full 4.9 fb^{-1} of 7 TeV data 4.9 fb^{-1} of 8 TeV data [430] and bb [431]. The searches are performed in categories of the decays of the two tau leptons: $e\tau_{\text{had}}$, $\mu\tau_{\text{had}}$, $e\mu$, and $\mu\mu$, where τ_{had} denotes a tau lepton which decays to one or more hadrons plus a tau neutrino, e denotes $\tau \to e\nu\nu$, and μ denotes $\tau \to \mu\nu\nu$. The dominant background comes from $Z \to \tau^+\tau^-$ decays, although $t\overline{t}$, W+jets and Z+jets events contribute as well. Separating events into

categories based on the number of b-tagged jets improves the sensitivity in the MSSM. The $b\bar{b}$ annihilation process and radiation of a Higgs boson from a b quark gives rise to events in which the Higgs boson is accompanied by a $b\bar{b}$ pair in the final state. Requiring the presence of one or more b jets reduces the background from Z+jets. Data control samples are used to constrain background rates. The rates for jets to be identified as a hadronically decaying tau lepton are measured in dijet samples, and W+jets samples provide a measurement of the rate of events that, with a fake hadronic tau, can pass the signal selection requirements. Lepton fake rates are measured using samples of isolated lepton candidates and same-sign lepton candidates. Constraints from the CMS searches for $h \to \tau^+\tau^-$ and $h \to b\overline{b}$ are shown in Fig. 11.25 in the m_h-mod+ scenario defined in [258] and in the hMSSM approximation defined in [307] . The neutral Higgs boson searches consider the contributions of both the CP-odd and CP-even neutral Higgs bosons with enhanced couplings to bottom quarks, similarly as it was done for the Tevatron results. In Fig. 11.25, decays of the charged Higgs into $\tau\nu$ and of the heavy Higgs H decaying into a pair of SM-like Higgs bosons or gauge bosons, or of A decaying into hZ are also being constrained. In addition, decays of the neutral Higgs bosons into muon pairs are also being explored. Observe that in the $m_h$mod+ scenario the region of $\tan\beta$ lower than 5 does not allow for a Higgs mass m_h close to 125 GeV, as shown in the figure. For the hMSSM scenario, instead, the SM-like Higgs mass is fixed as an input and hence the requirement that it is close to 125 GeV is always fulfilled, although this may imply other limitations as discussed in section VII.1.1.

A search for $\phi \to \mu^+\mu^-$ has also been performed by the ATLAS collaboration [429]. The exclusion limits obtained are given in terms of cross section times branching fraction and combined with those of $\phi \to \tau^+\tau^-$ [429].

A search for pseudoscalar Higgs bosons at intermediate to low masses, below the Z mass (in the 25 GeV to 80 GeV mass range) has been performed by the CMS collaboration [433]. A light pseudoscalar in this mass range is excluded by current direct constraints in the MSSM but not in general 2HDMs [434]. This search is done in the decay channel where the pseudoscalar Higgs boson decays to a pair of taus and is produced in association with a pair of b-quarks.

Finally searches for a resonance decaying to a top quark pair were already done by ATLAS [435] and CMS [436]. These searches were interpreted as searches for scalar resonances by ATLAS [435], however an important missing component of these searches is an accurate treatment of the interference effects between the signal and the continuum background, that may have a non-conventional pure dip structure and can be non-negligible for a high mass state decaying to top quarks[357, 437].

The LHC has the potential to explore a broad range of SUSY parameter space through the search for non-SM-like Higgs bosons. Nevertheless, Fig. 11.25 shows a broad region with intermediate $\tan\beta$ and large values of m_A that is not tested by present neutral or charged Higgs boson searches, and which cannot be covered completely via these searches, even with much larger data sets. In this region of parameter space it is possible that only the SM-like Higgs boson can be within the LHC's reach. If no other state of the EWSB sector than H is discovered, it may be challenging to determine only from the Higgs sector whether there is a supersymmetric extension of the SM in nature.

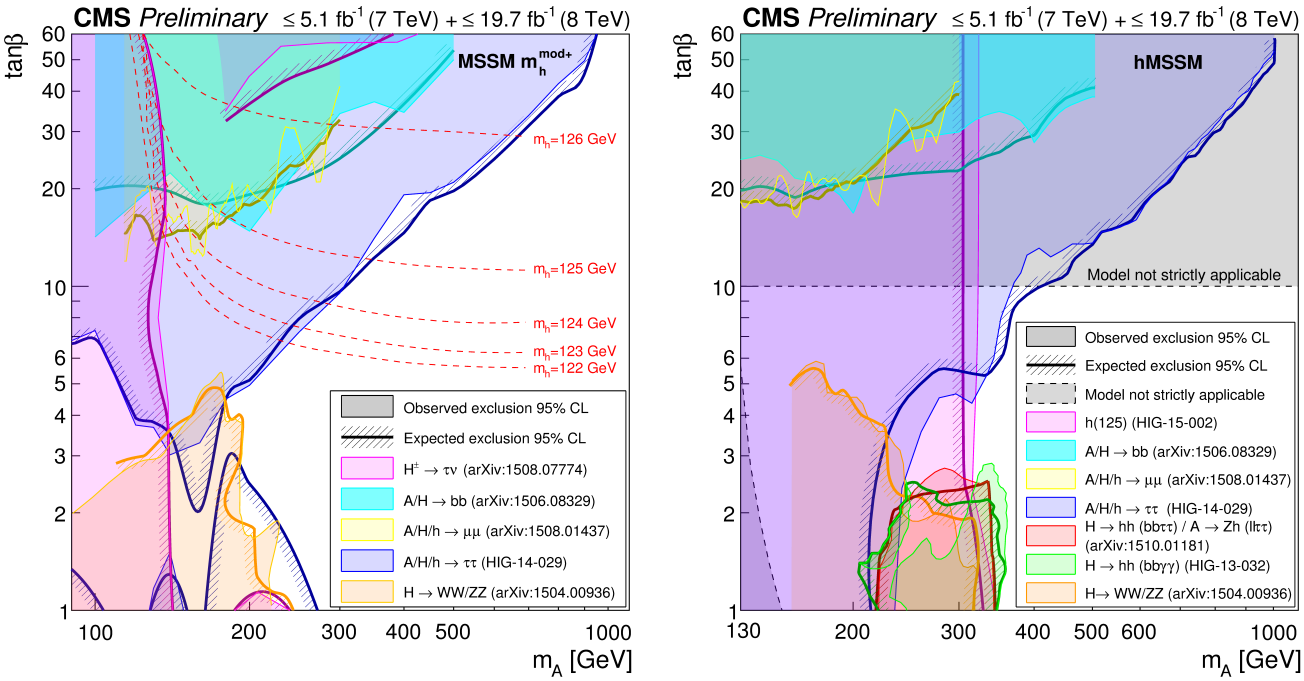

Figure 11.25: The 95% CL exclusion contours in the $(M_A, \tan\beta)$ parameter space for the hMSSM scenario (right panel) and for the m_h-mod+ scenario (left panel), for several search channels [432].

(iii) Searches for a CP-odd state decaying to hZ

Similarly to the search for a CP-even high mass Higgs boson decaying to a pair of Higgs bosons, the search for a CP-odd states decaying hZ was carried out at the LHC by the ATLAS and CMS experiments. The ATLAS Collaboration has performed the search in three main final states corresponding to the following subsequent decays of the Higgs and Z bosons [438]: $(Z \to \ell\ell)(h \to b\bar{b})$, $(Z \to \nu\nu)(h \to b\bar{b})$ and $(Z \to \ell\ell)(h \to \tau\tau)$; and their combination assuming SM Higgs decay branching fractions. The CMS Collaboration has performed a search in the $(Z \to \ell\ell)(h \to \tau\tau)$ final state [411]. These searches have been used to constrain the parameter space of 2HDMs. In the MSSM these searches place limits on small values of $tan\beta$ for masses of A comprised between 220 GeV and 360 GeV as illustrated in Fig. 11.25.

(iv) Searches for charged Higgs bosons $H^\pm$

At e^+e^- colliders charged Higgs bosons can be pair produced in the s-channel via γ or Z boson exchange. This process is dominant in the LEP centre-of-mass energies range *i.e.* up to 209 GeV. At higher centre-of-mass energies, other processes can play an important role such as the production in top quark decays via $t \to b + H^+$ if $m_H^\pm < m_t - m_b$ or via the one-loop process $e^+e^- \to W^\pm H^\mp$ [439, 440], which allows the production of a charged Higgs boson with $m_H^\pm > \sqrt{s}/2$, even when H^+H^- production is kinematically forbidden. Other single charged Higgs production mechanisms include $t\bar{b}H^-/\,\bar{t}bH^+$ production [107], $\tau^+\nu H^-/\,\tau^-\bar{\nu}H^+$ production [441], and a variety of processes in which $H^\pm$ is produced

in association with a one or two other gauge and/or Higgs bosons [442].

At hadron colliders, Charged Higgs bosons can be produced in several different modes. If $m_{H^\pm} < m_t - m_b$, the charged Higgs boson can be produced in decays of the top quark via the decay $t \to bH^\pm$. Relevant QCD and SUSY-QCD corrections to BR($t \to H^\pm b$) have been computed [299–302]. For values of $m_{H^\pm}$ near m_t, width effects are important. In addition, the full $2 \to 3$ processes $pp/p\bar{p} \to H^+\bar{t}b + X$ and $pp/p\bar{p} \to H^-t\bar{b} + X$ must be considered. If $m_{H^\pm} > m_t - m_b$, then charged Higgs boson production occurs mainly through radiation from a third generation quark. Charged Higgs bosons may also be produced singly in association with a top quark via the $2 \to 3$ partonic processes gg, $q\bar{q} \to t\bar{b}H^-$. For charged Higgs boson production cross section predictions for the Tevatron and the LHC, see Refs. [11, 44, 43]. Charged Higgs bosons can also be produced via associated production with $W^\pm$ bosons through $b\overline{b}$ annihilation and gg-fusion [303] and in pairs via $q\overline{q}$ annihilation [304].

(a) Exclusion limits from LEP

Charged Higgs bosons have been searched for at LEP, where the combined data of the four experiments, ALEPH, DELPHI, L3, and OPAL, were sensitive to masses of up to about 90 GeV [421] in two decay channels, the $\tau\nu$ and $c\overline{s}$. The exclusion limit independent of the admixture of the two above mentioned branching fractions was 78.6 GeV.

(b) Exclusion limits from Tevatron

Compared to the mass domain covered by LEP searches, the Tevatron covered a complementary range of charged Higgs masses. The CDF and D0 collaborations have also searched for charged Higgs bosons in top quark decays with subsequent decays to $\tau\nu$ or to $c\bar{s}$ [443–445]. For the $H^+ \to c\bar{s}$ channel, the limits on BR($t \to H^+b$) from CDF and D0 are $\approx 20\%$ in the mass range $90\,\text{GeV} < m_{H^+} < 160\,\text{GeV}$ and assuming a branching fraction of 100% in this specific final state. $H^+ \to \tau^+\nu_\tau$ channel, D0's limits on BR($t \to H^+b$) are also $\approx 20\%$ in the same mass range and assuming a branching fraction of 100% in this final state. These limits are valid in general 2HDMs, and they have also been interpreted in terms of the MSSM [443–445].

(c) Exclusion limits from LHC

Similarly to the Tevatron, at the LHC light charged Higgs bosons can be searched for in the decays of top quarks. The main initial production mode for light charged Higgs bosons ($m_{H^\pm} < m_t - m_b$) is top pair production. The subsequent decay modes of the charged Higgs boson for these searches are $\tau\nu$ and $c\overline{s}$. More recently ATLAS and CMS have also searched for higher mass charged Higgs bosons ($m_{H^\pm} > m_t + m_b$) in $H^+ \to t\overline{b}$. The main production modes are the associated production of a charged Higgs boson in association with a top and a bottom quark or in association with a top quark only.

ATLAS has searched for the decay $H^+ \to \tau^+\nu_\tau$ in three final state topologies [446]: (i) lepton+jets: with $t\bar{t} \to \overline{b}WH^+ \to b\overline{b}(q\bar{q}')(\tau_{\text{lep}}\nu)$, i.e., the W boson decays hadronically and the tau decays into an electron or a muon, with two neutrinos; (ii) τ +lepton:

with $t\bar{t} \to \bar{b}WH^+ \to b\bar{b}(l\nu)(\tau_{\rm had}\nu)$ i.e., the W boson decays leptonically (with $\ell = e,\ \mu$) and the tau decays hadronically; (iii) τ+jets: $t\bar{t} \to \bar{b}WH^+ \to b\bar{b}(q\bar{q}')(\tau_{\rm had}\nu)$, i.e., both the W boson and the τ decay hadronically [447]. Assuming BR($H^+ \to \tau^+\nu_\tau$) = 100%, ATLAS sets upper limits on BR($t \to H^+b$) between 0.24% and 2.1% for charged Higgs boson masses between 90 GeV to 160 GeV. When interpreted in the context of the $m_h^{\rm max}$ scenario of the MSSM, these bounds exclude a large fraction of the ($m_{H^\pm}$,tan β) plane.

The CMS collaboration has searched for the charged Higgs boson in the decay products of top quark pairs: $t\bar{t} \to H^\pm W^\mp b\bar{b}$ and $t\bar{t} \to H^+H^-b\bar{b}$ [448, 449] as well. Three types of final states with large missing transverse energy and jets originating from b-quark hadronization have been analyzed: the fully-hadronic channel with a hadronically decaying tau in association with jets, the dilepton channel with a hadronically decaying tau in association with an electron or muon and the dilepton channel with an electron-muon pair. Combining the results of these three analyses and assuming BR($H^\pm \to \tau\nu$)=1, the upper limits on BR($t \to H^+b$) are less than 2% to 3% depending on the charged Higgs boson mass in the interval 80 GeV $< m_{H^+} <$160 GeV.

Both the ATLAS [450] and CMS [449] experiments have also searched for high mass charged Higgs bosons decaying to a top and bottom quarks. The main production mode for this search is the associated production with one top quark (5-flavour scheme) or a top quark and and bottom quark (4-flavour scheme) in the final state. The s-channel production mode where the charged Higgs boson is produced alone in the final state at tree level is also considered. This search is particularly intricate and it is sensitive to the modeling of the top pair production background produced in association with additional partons and in particular b-quarks. No excess was found and the results are expressed in terms of exclusion limits of cross section times branching fractions. The CMS collaboration has combined the results of this search with the $H^+ \to \tau^+\nu_\tau$ search in the framework of an updated mhmax MSSM scenario [449].

ATLAS and CMS have also searched for charged Higgs bosons in top quark decays assuming BR($H^+ \to c\bar{s}$) = 100% [451, 452], and sets limits of $\approx$ 20% on BR($t \to H^+b$) in the 90 GeV $< m_{H^+} <$ 160 GeV mass range.

In two Higgs doublet models the decay of the Charged Higgs boson to a W- and a Z-boson is allowed only at loop level and is therefore suppressed. However the $H^\pm \to W^\pm Z$ decay channel is allowed in Higgs triplet models. The ATLAS experiment [453] has searched for such decays, requiring that the Charged Higgs boson is produced through the fusion of vector bosons. No excess with respect to the SM backgrounds has been observed in this channel, and the results are interpreted in the Georgi–Machacek model [360–362] discussed in Section VII.5.2.

At the LHC various other channels still remain to be explored, in particular searches involving additional neutral scalars in particular in WH, WA where A is the pseudo scalar MSSM Higgs boson, and Wa where a is the light CP-odd scalars of the NMSSM.

(v) Searches for a light CP-odd Higgs boson a

A light pseudoscalar boson a is present in any two Higgs doublet mode enhanced with an additional singlet field. A prominent example is the NMSSM. The theoretical motivations for singlet extensions of the MSSM are discussed in Section VII.2. In the

NMSSM, the searches now focus on the low mass pseudo-scalar boson a region for several reasons: (i) in the NMSSM, the light pseudo-scalar a boson can, as a pseudo-Goldstone boson, be a natural candidate for an axion; (ii) scenarios where $m_a > 2m_b$ and a CP-even state h decaying to a pair of a ($m_h > 2m_a$) are excluded by direct searches at LEP in the four b channel [421, 455, 456]; (iii) in the pre-discovery era, LEP limits on a CP-even Higgs boson resulted in fine tuning MSSM constraints [457] which could be evaded through non standard decays of the Higgs to aa; (iv) an NMSSM CP-odd a boson with a mass in the range 9.2–12 GeV can also account for the difference observed between the measured anomalous muon magnetic moment and its prediction [458]. A scenario that has drawn particular attention was motivated by a small excess of events 2.3σ in the SM Higgs search at LEP at Higgs boson mass of around 98 GeV. Speculative interpretations of this excess as a signal of a Higgs boson with reduced couplings to b-quarks were given [457]. Complete reviews of the NMSSM phenomenology can be found in Refs. [459, 456].

The potential benchmark scenarios have changed in the light of the H discovery. The discovered state could be the lightest or the next-to-lightest of the three CP-even states of the NMSSM. Light pseudoscalar scenarios are still very interesting in particular for the potential axion candidate. There are three main types of direct searches for the light a boson: (i) for masses below the Υ resonance, the search is for radiative decays $\Upsilon \to a\gamma$ at B-factories; (ii) the inclusive search for in high energy pp collisions at the LHC; (iii) the search for decays of a CP-even Higgs h boson to a pair of a bosons.

Radiative decays $\Upsilon \to a\gamma$, have been searched for in various colliders, the most recent results are searches for radiative decays of the $\Upsilon(1s)$ to $a\gamma$ with a subsequent decay of the a boson to a pair of taus at CLEO [460] and the radiative decays of the $\Upsilon(1s, 2s, 3s)$ to $a\gamma$ with subsequent decays to a pair of muons or taus by the BaBar collaboration [461, 462].

Direct inclusive searches for the light pseudo scalar a boson were performed in the $a \to \mu\mu$ channel at the Tevatron by the D0 experiment [463] and by the ATLAS [464] and CMS [465] collaborations at the LHC.

Finally searches for the decays of the Higgs boson to a pair of a bosons where performed with subsequent decays to four photons by the ATLAS experiment [466], in the four muons final state by the CMS and D0 experiments [456, 467], in the two muons and two taus final state by the ATLAS [466] and D0 [456] collaborations, and in the four taus final state by the CMS [468] ALEPH collaboration at LEP [469].

No significant excess in the searches for a light CP-odd a boson were found and limits on the production times branching fractions of the a boson have been set.

(vi) Searches for doubly charged Higgs bosons $H^{\pm\pm}$

As discussed in Section VII.5, the generation of small neutrino masses via the standard EWSB mechanism described in Section II requires unnaturally small Yukawa couplings, provided that neutrinos are Dirac-type fermions. A Majorana mass term with a see-saw mechanism for neutrinos, would allow for naturally small masses and yield a framework for the appealing scenario of leptogenesis. However within the SM Majorana mass terms correspond to (non-renomalizable) dimension-5 operators. Such effective interactions can be generated via renormalizable interactions with an electroweak triplet of complex scalar fields (corresponding to a type-II see-saw mechanism). Other models such as the

Zee–Babu model, with the introduction of two $SU(2)_L$ singlets, also generate Majorana mass terms. The signature of such models would be the presence of doubly charged Higgs bosons $H^{\pm\pm}$.

The main production mechanisms of $H^{\pm\pm}$ bosons at hadron colliders are the pair production in the s-channel through the exchange of a Z boson or a photon and the associated production with a Charged Higgs boson through the exchange of a W boson.

VII.8.1. Searches for non-standard production processes of the Higgs boson

The discovery of the Higgs boson has also allowed for searches of BSM (beyond the SM) processes involving standard decays of the Higgs boson. One example directly pertaining to the search for additional states of the EWSB sector is the search for Higgs bosons in the cascade decay of a heavy CP-even Higgs boson decaying to charged Higgs boson and a W boson, and the charged Higgs boson subsequently decaying to H and another W boson. This search has been performed by the ATLAS collaboration in $b\overline{b}$ decays of the H particle [485].

Another example of searches for non standard processes through the presence of the H particle is the search for large flavor changing neutral current decays of the top quark to H and a charm quark. This search has been performed with the ATLAS experiment in the $H \to \gamma\gamma$ channel [486].

VII.8.2. Outlook of searches for additional states

The LHC program of searches for additional states covers a large variety of decay and production channels. Since the last review on the *Status of Higgs boson physics* [243] many new channels have been explored at the LHC, *e.g.* the searches for additional states decaying into hh or Zh. The search for charged Higgs bosons has been extended to include the WZ and the very difficult $t\overline{b}$ decay channel. There are however more channels to cover, *e.g.* the search for charged Higgs bosons in the HW and AW channels.

VIII. Summary and outlook

Summary– The discovery of the Higgs boson is an important milestone in the history of particle physics as well as an extraordinary success of the LHC machine and the ATLAS and CMS experiments. Since its discovery, substantial progress in the field of Higgs boson physics has been accomplished and a significant number of measurements probing its nature have been made. They are revealing an increasingly precise profile of the Higgs boson. All experimental measurements are consistent with the EWSB mechanism of the Standard Model (SM).

Since the last review [487], the ATLAS and CMS experiments have made a combined measurement of the mass of the Higgs boson in the diphoton and the four-lepton channels at per mille precision, $m_H = 125.09 \pm 0.24\,\text{GeV}$. The quantum numbers of the Higgs boson have been probed in greater detail and show an excellent consistency with the $J^{PC} = 0^{++}$ hypothesis. Anomalous CP-even and CP-odd couplings have also been probed, mostly using angular distributions in diboson events. Higgs boson production

and decay mechanisms have been further characterized through the measurement of various differential and fiducial cross sections.

The ATLAS and CMS collaborations have produced a detailed combined measurement of the properties of the Higgs boson. This combination establishes the direct observation of the VBF production process with a significance of 5.4σ and the observation of the $H \to \tau^+\tau^-$ with a significance of 5.5σ. This combination also provides the most precise probes of the coupling structure of the Higgs boson, with a 10%-20% accuracy. This precision could not have been reached without the rapid and profound theoretical developments on many fronts: higher order calculations, Monte Carlo simulations, and new ideas on how to extract further informations on the nature of the Higgs boson. A particularly important breakthrough has been the recent calculation at the next-to-next-to-next-to-leading order of the Higgs production by gluon fusion, the dominant production channel at the LHC. All measurements are consistent with the SM predictions and provide stringent constraints on a large number of scenarios of new physics predicting sizeable deviations in the couplings of the Higgs boson.

Without assumptions on or a measurement of the Higgs boson width, the measurements at the LHC do not provide constraints on the absolute couplings of the Higgs boson. In the SM, the total Higgs width is approximately 4.2 MeV. The direct experimental measurements using the Higgs boson mass lineshape yield an upper bound still three orders of magnitude above its SM value. However, new ideas have emerged through the study of the Higgs couplings away from its mass shell. Under the specific assumption that the running of the Higgs couplings to vector bosons and gluons is small, the total width of the Higgs boson is constrained to be smaller than 25 MeV at 95% CL. Another interesting new idea, in the diphoton channel, is the observation that the interference between the signal and the continuum background induces shifts in the mass. Constraints on the width of the Higgs boson can then be inferred from precise measurements of its mass.

Further useful information on the components of the width of the Higgs boson can also be obtained from searches for rare and exotic decay modes, including invisible decays. Insights on the couplings of the Higgs boson are also obtained from the searches for rare production modes. No significant deviation from the SM Higgs boson expectations has been found in the channels analyzed so far.

Finally, all extensions of the SM at higher energies call for an enlargement of the EWSB sector. Therefore invaluable insights can also be acquired from searches for new additional scalar states. Since the last review [487], an ample number of new searches for CP-even and CP-Odd neutral Higgs bosons, and charged Higgs bosons have been carried out. No significant deviations from the minimal SM Higgs sector has been found in the ranges of mass and couplings of the additional states that have been explored so far.

Outlook– The unitarization of the vector boson scattering (VBS) amplitudes, dominated at high energies by their longitudinal polarizations, has been the basis of the *no lose* theorem at the LHC and was one of the main motivations to build the accelerator and the detectors. It motivated the existence of a Higgs boson or the observability of manifestations of strong dynamics at TeV scale. Now that a Higgs boson has been found and that its couplings to gauge bosons comply with the SM predictions, perturbative unitarity is preserved to a large amount with the sole exchange of the Higgs boson and

without the need for any additional states. It is, however, still an important channel to investigate further in order to better understand the nature of the Higgs sector and the possible completion of the SM at the TeV scale. In association with the double Higgs boson production channel by vector boson fusion, VBS could, for instance, confirm that the Higgs boson is part of a weak doublet and also establish whether it is an elementary object or a composite state that could emerge as a pseudo-Nambu–Goldstone boson from a new underlying broken symmetry.

The Higgs boson couplings are not dictated by any local gauge symmetry. Thus, in addition to a new particle, the LHC has also discovered a new force, different in nature from the other fundamental interactions since it is non-universal and distinguishes between the three families of quarks and leptons. The existence of the Higgs boson embodies the problem of an unnatural cancellation among the quantum corrections to its mass, if new physics is present at scale significantly higher than the EW scale. The non-observation of additional states which could stabilize the Higgs mass is a challenge for natural scenarios like supersymmetry or models with a new strong interaction in which the Higgs boson is not a fundamental particle. This increasingly pressing paradox starts questioning the principle of naturalness which underlies the hypothesis that phenomena at different scales do not influence each other.

The search for the Higgs boson has occupied the Particle physics community for the last 50 years. Its discovery has shaped and sharpened the physics programs of the LHC and of future accelerators. The experimental data together with the progress in theory mark the beginning of a new era of precision Higgs boson measurements.

Acknowledgements

We would like to thank many of our colleagues for proofreading parts of the review, for useful criticism and their input in general: W. Altmannshofer, G. Branco, J. Campbell, F. Cerutti, C. Csáki, R. Contino, J. Conway, N. Craig, J.B. De Vivie, J.R. Espinosa, A. Falkowski, W. Fischer, M. Grazzini, H. Haber, S. Heinemeyer, J. Hubisz, A. Korytov, B. Jäger, H. Ji, T. Junk, P. Langacker, J. Lykken, F. Maltoni, R. Mishra, M. Mühlleitner, B. Murray, M. Neubert, G. Perez, G. Petrucciani, A. Pomarol, E. Pontón, D. Rebuzzi, E. Salvioni, N. Shah, G. Shaughnessy, M. Spira, O. Stål, A. Strumia, R. Tanaka, J. Terning, A. Vartak, C. Wagner, and A. Weiler. We are also most grateful to the ATLAS, CDF, CMS and D0 collaborations for their help with this review.

M.C. is supported by Fermilab, that is operated by Fermi Research Alliance, LLC under Contract No. DE–AC02–07CH11359 with the United States Department of Energy. C.G. is supported by the European Commission through the Marie Curie Career Integration Grant 631962 and by the Helmholtz Association. M.K. is supported by the ANR HiggsNet grant. V.S. is supported by the grant DE–SC0009919 of the United States Department of Energy.

References

1. G. Aad *et al.*, [ATLAS Collab.], Phys. Lett. **B716**, 1 (2012).
2. S. Chatrchyan *et al.*, [CMS Collab.], Phys. Lett. **B716**, 30 (2012).
3. S.L. Glashow, Nucl. Phys. **20**, 579 (1961);
   S. Weinberg, Phys. Rev. Lett. **19**, 1264 (1967);
   A. Salam, *Elementary Particle Theory*, eds.: Svartholm, Almquist and Wiksells, Stockholm, 1968;
   S. Glashow, J. Iliopoulos, and L. Maiani, Phys. Rev. **D2**, 1285 (1970).
4. F. Englert and R. Brout, Phys. Rev. Lett. **13**, 321 (1964);
   P.W. Higgs, Phys. Rev. Lett. **13**, 508 (1964) and Phys. Rev. **145**, 1156 (1966);
   G.S. Guralnik, C.R. Hagen, and T.W. Kibble, Phys. Rev. Lett. **13**, 585 (1964).
5. J.M. Cornwall, D.N. Levin, and G. Tiktopoulos, Phys. Rev. Lett. **30**, 1286 (1973) and Phys. Rev. **D10**, 1145 (1974);
   C.H. Llewellyn Smith, Phys. Lett. **B46**, 233 (1973).
6. B.W. Lee, C. Quigg, and H.B. Thacker, Phys. Rev. **D16**, 1519 (1977).
7. K. Wilson, Phys. Rev. D 3,1818(1971);
   G. t'Hooft, in *Proc. of 1979 Cargèse Institute on Recent Developments in Gauge Theories,* p. 135 Press, New York 1980;
   For a recent review, see G.F. Giudice, PoS EPS **-HEP2013**, 163 (2013).
8. J. Parsons, and A. Pomarol, *Extra Dimenions*, in this volume.
9. J. Wess and B. Zumino, Nucl. Phys. **B70**, 39 (1974) and Phys. Lett. **49B**, 52 (1974);
   H.P. Nilles, Phys. Rev. **C110**, 1 (1984);
   S.P. Martin, `arXiv:hep-ph/9709356` (1997);
   P. Fayet, Phys. Lett. **B69**, 489 (1977), Phys. Lett. **B84**, 421 (1979), Phys. Lett. **B86**, 272 (1979) and Nucl. Phys. **B101**, 81 (2001).
10. E. Witten, Nucl. Phys. **B188**, 513 (1981);
    R.K. Kaul, Phys. Lett. **B109**, 19 (1982) and Pramana **19**, 183 (1982);
    L. Susskind, Phys. Rev. **104**, 181 (1984).
11. H.E. Haber and G.L. Kane, Phys. Rev. **C117**, 75 (1985).
12. J. F. Gunion *et al.*, *The Higgs Hunter's Guide*, Addison-Wesley (1990).
13. S. Weinberg, Phys. Rev. **D13**, 974 (1979) and Phys. Rev. **D19**, 1277 (1979);
    L. Susskind, Phys. Rev. **D20**, 2619 (1979);
    for a recent review, see C.T. Hill and E.H. Simmons, Phys. Reports **381**, 235 (2003) [E: **390**, 553 (2004)].
14. D. B. Kaplan and H. Georgi, Phys. Lett. **B136**, 183 (1984).
15. G. Panico and A. Wulzer, Lect. Notes Phys. **913**, 1 (2016).
16. C. Csaki, C. Grojean and J. Terning, `arXiv:1512.00468 [hep-ph]` (2015).
17. C. Csaki *et al.*, Phys. Rev. **D69**, 055006 (2004);
    C. Csaki *et al.*, Phys. Rev. Lett. **92**, 101802 (2004).
18. C. Csaki *et al.*, Phys. Rev. **D62**, 045015 (2000);
    for other references, see the 2014 edition of this review.
19. W. D. Goldberger, B. Grinstein, and W. Skiba, Phys. Rev. Lett. **100**, 111802 (2008);

J. Fan *et al.*, Phys. Rev. **D79**, 035017 (2009);
B. Bellazzini *et al.*, Eur. Phys. J. **C73**, 2333 (2013);
Z. Chacko and R.K. Mishra, Phys. Rev. **D87**, 115006 (2013);
Z. Chacko, R. Franceschini, and R.K. Mishra, JHEP **1304**, 015 (2013).

20. Z. Chacko, H.S. Goh and R. Harnik, Phys. Rev. Lett. **96**, 231802 (2006) and JHEP **0601**, 108 (2006).
21. N. Craig, A. Katz, M. Strassler and R. Sundrum, JHEP **1507**, 105 (2015);
N. Craig, S. Knapen and P. Longhi, Phys. Rev. Lett. **114**, 061803 (2015).
22. P.W. Graham, D. E. Kaplan and S. Rajendran, Phys. Rev. Lett. **115**, 221801 (2015);
J.R. Espinosa *et al.*, Phys. Rev. Lett. **115**, 251803 (2015).
23. T. van Ritbergen and R.G. Stuart, Phys. Rev. Lett. **82**, 488 (1999) and Nucl. Phys. **B564**, 343 (2000);
M. Steinhauser and T. Seidensticker, Phys. Lett. **B467**, 271 (1999);
D.M. Webber *et al.*, [MuLan Collab.], Phys. Rev. Lett. **106**, 041803 (2011).
24. J. Ellis, M.K. Gaillard, and D.V. Nanopoulos, Nucl. Phys. **B106**, 292 (1976).
25. M.A. Shifman *et al.*, Sov. J. Nucl. Phys. **30**, 711 (1979) [Yad. Fiz. **30**, 1368 (1979)].
26. P. Sikivie *et al.*, Nucl. Phys. **B173**, 189 (1980);
H. Georgi, Ann. Rev. Nucl. and Part. Sci. **43**, 209 (1993).
27. M.J.G. Veltman, Nucl. Phys. **B123**, 89 (1977).
28. R.S. Chivukula *et al.*, Ann. Rev. Nucl. and Part. Sci. **45**, 255 (1995).
29. S. Willenbrock, `arXiv:0410370 [hep-ph]` (2004).
30. I.V. Krive and A.D. Linde, Nucl. Phys. **B117**, 265 (1976);
for other references, see the 2014 edition of this review.
31. J. Elias-Miro *et al.*, Phys. Lett. **B709**, 222 (2012);
G. Degrassi *et al.*, JHEP **1208**, 098 (2012);
D. Buttazzo *et al.*, JHEP **1312**, 089 (2013);
J.R. Espinosa *et al.*, JHEP **1509**, 174 (2015).
32. J.R. Espinosa and M. Quiros, Phys. Lett. **B353**, 257 (1995);
G. Isidori, G. Ridolfi, and A. Strumia, Nucl. Phys. **B609**, 387 (2001).
33. V. Branchina, E. Messina and M. Sher, Phys. Rev. **D91**, 013003 (2015).
34. A. Hook *et al.*, JHEP **1501**, 061 (2015);
J. Kearney, H. Yoo and K.M. Zurek, Phys. Rev. **D91**, 123537 (2015).
35. C.D. Froggatt and H.B. Nielsen, Phys. Lett. **B368**, 96 (1996);
M. Shaposhnikov and C. Wetterich, Phys. Lett. **B683**, 196 (2010);
M. Holthausen, K.S. Lim, and M. Lindner, JHEP **1202**, 037 (2012).
36. F.L. Bezrukov and M. Shaposhnikov, Phys. Lett. **B659**, 703 (2008);
F.L. Bezrukov, A. Magnin, and M. Shaposhnikov, Phys. Lett. **B675**, 88 (2009).
37. A. Salvio, Phys. Lett. **B727**, 234 (2013).
38. B.A. Kniehl, Phys. Reports **240**, 211 (1994).
39. M. Spira, Fortsch. Phys. **46**, 203 (1998).
40. M. Carena and H.E. Haber, Prog. in Part. Nucl. Phys. **50**, 152 (2003).
41. A. Djouadi, Phys. Reports **457**, 1 (2008).

42. S. Dittmaier *et al.*, [LHC Higgs Cross Section Working Group], arXiv:1101.0593 [hep-ph] (2011).
43. S. Dittmaier *et al.*, [LHC Higgs Cross Section Working Group], arXiv:1201.3084 [hep-ph] (2012).
44. S. Heinemeyer *et al.*, [LHC Higgs Cross Section Working Group], arXiv:1307.1347 [hep-ph] (2013).
45. C. Anastasiou *et al.*, [LHC Higgs Cross Section Working Group], CERN Report, to appear (2016).
46. LHC Higgs Cross Section Working Group, https://twiki.cern.ch/twiki/bin/view/LHCPhysics/LHCHXSWG.
47. T. Aaltonen *et al.*, [CDF and D0 Collaborations], Phys. Rev. **D88**, 052014 (2013).
48. H.M. Georgi *et al.*, Phys. Rev. Lett. **40**, 692 (1978).
49. D. Graudenz, M. Spira, and P.M. Zerwas, Phys. Rev. Lett. **70**, 1372 (1993).
50. M. Spira *et al.*, Nucl. Phys. **B453**, 17 (1995).
51. S. Dawson, Nucl. Phys. **B359**, 283 (1991);
    A. Djouadi, M. Spira, and P.M. Zerwas, Phys. Lett. **B264**, 440 (1991).
52. R.V. Harlander and W.B. Kilgore, Phys. Rev. Lett. **88**, 201801 (2002);
    C. Anastasiou and K. Melnikov, Nucl. Phys. **B646**, 220 (2002);
    V. Ravindran, J. Smith, and W.L. van Neerven, Nucl. Phys. **B665**, 325 (2003).
53. C. Anastasiou *et al.*, Phys. Rev. Lett. **114**, 212001 (2015);
    C. Anastasiou *et al.*, JHEP **1605**, 058 (2016).
54. R.V. Harlander and K.J. Ozeren, JHEP **0911**, 088 (2009);
    A. Pak, M. Rogal, and M. Steinhauser, JHEP **1002**, 025 (2010).
55. A. Djouadi and P. Gambino, Phys. Rev. Lett. **73**, 2528 (1994);
    S. Actis *et al.*, Phys. Lett. **B670**, 12 (2008);
    U. Aglietti *et al.*, Phys. Lett. **B595**, 432 (2004);
    G. Degrassi and F. Maltoni, Phys. Lett. **B600**, 255 (2004).
56. C. Anastasiou, R. Boughezal, and F. Petriello, JHEP **0904**, 003 (2009).
57. S. Catani *et al.*, JHEP **0307**, 028 (2003);
    S. Moch and A. Vogt, Phys. Lett. **B631**, 48 (2005);
    E. Laenen and L. Magnea, Phys. Lett. **B632**, 270 (2006);
    A. Idilbi *et al.*, Phys. Rev. **D73**, 077501 (2006);
    V. Ravindran, Nucl. Phys. **B752**, 173 (2006);
    V. Ahrens *et al.*, Eur. Phys. J. **C62**, 333 (2009).
58. V. Ahrens *et al.*, Phys. Lett. **B698**, 271 (2011);
    D. de Florian and M. Grazzini, Phys. Lett. **B718**, 117 (2012);
    C. Anastasiou *et al.*, JHEP **1204**, 004 (2012).
59. M. Bonvini *et al.*, arXiv:1603.08000 [hep-ph] (2016).
60. J.C. Collins, D.E. Soper and G.F. Sterman, Nucl. Phys. **B250**, 199 (1985).
61. D. de Florian *et al.*, JHEP **1111**, 064 (2011);
    T. Becher and M. Neubert, Eur. Phys. J. **C71**, 1665 (2011);
    J.Y. Chiu *et al.*, JHEP **1205**, 084 (2012);
    J. Wang *et al.*, Phys. Rev. **D86**, 094026 (2012);
    T. Becher, M. Neubert and D. Wilhelm, JHEP **1305**, 110 (2013).

62. S. Catani and M. Grazzini, Eur. Phys. J. **C72**, 2013 (2012) [E: **C72**, 2132 (2012)].
63. W.Y. Keung and F.J. Petriello, Phys. Rev. **D80**, 01007 (2009);
S. Buhler *et al.*, JHEP **1207**, 115 (2012).
64. H. Mantler and M. Wiesemann, Eur. Phys. J. **C73**, 2467 (2013).
65. M. Grazzini and H. Sargsyan, JHEP **1309**, 129 (2013).
66. R.V. Harlander, T. Neumann, K.J. Ozeren and M. Wiesemann, JHEP **1208**, 139 (2012);
T. Neumann and M. Wiesemann, JHEP **1411**, 150 (2014).
67. R.V. Harlander, S. Liebler, and H. Mantler, Comp. Phys. Comm. **184**, 1605 (2013).
68. D. de Florian, M. Grazzini, and Z. Kunszt, Phys. Rev. Lett. **82**, 5209 (1999);
C.J. Glosser and C. R. Schmidt, JHEP **0212**, 016 (2002);
V. Ravindran, J. Smith and W. L. Van Neerven, Nucl. Phys. **B634**, 247 (2002);
X. Liu and F. Petriello, Phys. Rev. **D87**, 014018 (2013).
69. J.M. Campbell, R.K. Ellis, and G. Zanderighi, JHEP **0610**, 028 (2006);
J.M. Campbell, R.K. Ellis, and C. Williams, Phys. Rev. **D81**, 074023 (2010).
70. R. Boughezal *et al.*, JHEP **1306**, 072 (2013);
R. Boughezal *et al.*, Phys. Rev. Lett. **115**, 082003 (2015);
X. Chen *et al.*, Phys. Lett. **B740**, 147 (2015) and `arXiv:1604.04085 [hep-ph]` (2016).
71. C.F. Berger *et al.*, JHEP **1104**, 092 (2011);
A. Banfi, G.P. Salam, and G. Zanderighi, JHEP **1206**, 159 (2012);
T. Becher and M. Neubert, JHEP **1207**, 108 (2012);
A. Banfi *et al.*, Phys. Rev. Lett. **109**, 202001 (2012);
F.J. Tackmann, J.R. Walsh, and S. Zuberi, Phys. Rev. **D86**, 053011 (2012);
T. Becher, M. Neubert, and L. Rothen, JHEP **1310**, 125 (2013).
72. A. Banfi *et al.*, JHEP **1604**, 049 (2016).
73. I. Moult and I. W. Stewart, JHEP **1409**, 129 (2014).
74. M. Duhrssen *et al.*, Phys. Rev. **D70**, 113009 (2004).
75. T. Han, G. Valencia, and S. Willenbrock, Phys. Rev. Lett. **69**, 3274 (1992);
T. Figy, C. Oleari, and D. Zeppenfeld, Phys. Rev. **D68**, 073005 (2003);
T. Figy and D. Zeppenfeld, Phys. Lett. **B591**, 297 (2004);
E.L. Berger and J. Campbell, Phys. Rev. **D70**, 073011 (2004);
M. Ciccolini, A. Denner, and S. Dittmaier, Phys. Rev. Lett. **99**, 161803 (2007);
M. Ciccolini, A. Denner, and S. Dittmaier, Phys. Rev. **D77**, 103002 (2008);
A. Denner, S. Dittmaier, and A. Muck, `HAWK`,
`http://omnibus.uni-freiburg.de/~sd565/programs/hawk/hawk.html`;
K. Arnold *et al.*, `VBFNLO`, Comp. Phys. Comm. **180**, 1661 (2009);
M. Spira, `VV2H`, `http://people.web.psi.ch/spira/vv2h`;
N. Adam *et al.*, `arXiv:0803.1154 [hep-ph]` (2008);
T. Figy, S. Palmer, and G. Weiglein, JHEP **1202**, 105 (2012).
76. P. Nason and C. Oleari, JHEP **1002**, 037 (2010);
S. Frixione, P. Torrielli, and M. Zaro, Phys. Lett. **B726**, 273 (2013);
F. Maltoni, K. Mawatari, and M. Zaro, Eur. Phys. J. **C74**, 2710 (2014).

77. P. Bolzoni *et al.*, Phys. Rev. Lett. **105**, 011801 (2010);
P. Bolzoni *et al.*, Phys. Rev. **D85**, 035002 (2012).
78. M. Cacciari *et al.*, Phys. Rev. Lett. **115**, 082002 (2015).
79. S.L. Glashow, D.V. Nanopoulos, and A. Yildiz, Phys. Rev. **D18**, 1724 (1978);
T. Han and S. Willenbrock, Phys. Lett. **B273**, 167 (1991);
T. Han, G. Valencia, and S. Willenbrock, Phys. Rev. Lett. **69**, 3274 (1992);
H. Baer, B. Bailey, and J.F. Owens, Phys. Rev. **D47**, 2730 (1993);
J. Ohnemus and W.J. Stirling, Phys. Rev. **D47**, 2722 (1993).
80. A. Stange, W. Marciano, and S. Willenbrock, Phys. Rev. **D49**, 1354 (1994).
81. A. Stange, W. Marciano, and S. Willenbrock, Phys. Rev. **D50**, 4491 (1994).
82. M.L. Ciccolini, S. Dittmaier, and M. Kramer, Phys. Rev. **D68**, 073003 (2003);
A. Denner, S Dittmaier, and S. Kalweit, JHEP **1203**, 075 (2012).
83. R. Hamberg, W.L. van Neerven, and T. Matsuura, Nucl. Phys. **B359**, 343 (1991).
84. O. Brein, A. Djouadi, and R. Harlander, Phys. Lett. **B579**, 149 (2004);
L. Altenkamp *et al.*, JHEP **1302**, 078 (2013).
85. O. Brein *et al.*, Eur. Phys. J. **C72**, 1868 (2012).
86. O. Brein, R.V. Harlander, and T.J. Zirke, Comp. Phys. Comm. **184**, 998 (2013).
87. A. Denner *et al.*, JHEP **1203**, 075 (2012).
88. G. Ferrera, M. Grazzini, and F. Tramontano, Phys. Rev. Lett. **107**, 152003 (2011).
89. G. Ferrera, M. Grazzini and F. Tramontano, Phys. Lett. **B740**, 51 (2015).
90. J.M. Campbell, R.K. Ellis and C. Williams, JHEP **1606**, 179 (2016).
91. W. Astill *et al.*, `arXiv:1603.01620 [hep-ph]` (2016).
92. R. Raitio and W.W. Wada, Phys. Rev. **D19**, 941 (1979);
J.N. Ng and P. Zakarauskas, Nucl. Phys. **B247**, 339 (1984);
J.F. Gunion, Phys. Lett. **B261**, 510 (1991);
W.J. Marciano and F.E. Paige, Phys. Rev. Lett. **66**, 2433 (1991).
93. W. Beenakker *et al.*, Phys. Rev. Lett. **87**, 201805 (2001);
L. Reina and S. Dawson, Phys. Rev. Lett. **87**, 201804 (2001);
S. Dawson *et al.*, Phys. Rev. **D67**, 071503 (2003);
W. Beenakker *et al.*, Nucl. Phys. **B653**, 151 (2003).
94. R. Frederix *et al.*, Phys. Lett. **B701**, 427 (2011);
M. Garzelli *et al.*, Europhys. Lett. **96**, 11001 (2011).
95. F. Demartin *et al.*, Eur. Phys. J. **C75**, 267 (2015).
96. K.A. Assamagan *et al.*, [Higgs Working Group, "Physics at TeV Colliders" workshop, Les Houches, 2003], `arXiv:hep-ph/0406152` (2004).
97. R.V. Harlander and W.B. Kilgore, Phys. Rev. **D68**, 013001 (2003);
J. M. Campbell *et al.*, Phys. Rev. **D67**, 095002 (2003);
S. Dawson *et al.*, Phys. Rev. Lett. **94**, 031802 (2005);
S. Dittmaier, M. Kramer, and M. Spira, Phys. Rev. **D70**, 074010 (2004);
S. Dawson *et al.*, Phys. Rev. **D69**, 074027 (2004).
98. W.J. Stirling and D.J. Summers, Phys. Lett. **B283**, 411 (1992);
F. Maltoni *et al.*, Phys. Rev. **D64**, 094023 (2001).
99. S. Dawson, S. Dittmaier and M. Spira, Phys. Rev. **D58**, 115012 (1998).
100. D. de Florian and J. Mazzitelli, Phys. Rev. Lett. **111**, 201801 (2013).

101. S. Borowka *et al.*, Phys. Rev. Lett. **117**, 012001 (2016).
102. B.L. Ioffe and V.A. Khoze, Sov. J. Nucl. Phys. **9**, 50 (1978).
103. D.R.T. Jones and S. Petcov, Phys. Lett. **B84**, 440 (1979);
R.N. Cahn and S. Dawson, Phys. Lett. **B136**, 196 (1984);
G.L. Kane, W.W. Repko, and W.B. Rolnick, Phys. Lett. **B148**, 367 (1984);
G. Altarelli, B. Mele, and F. Pitolli, Nucl. Phys. **B287**, 205 (1987);
W. Kilian, M. Kramer, and P.M. Zerwas, Phys. Lett. **B373**, 135 (1996).
104. B.A. Kniehl, Z. Phys. **C55**, 605 (1992).
105. J. Fleischer and F. Jegerlehner, Nucl. Phys. **B216**, 469 (1983);
A. Denner *et al.*, Z. Phys. **C56**, 261 (1992).
106. B.A. Kniehl, Int. J. Mod. Phys. **A17**, 1457 (2002).
107. K.J. Gaemers and G.J. Gounaris, Phys. Lett. **B77**, 379 (1978);
A. Djouadi, J. Kalinowski, and P. M. Zerwas, Z. Phys. **C54**, 255 (1992);
B.A. Kniehl, F. Madricardo, and M. Steinhauser, Phys. Rev. **D66**, 054016 (2002).
108. S. Dittmaier *et al.*, Phys. Lett. **B441**, 383 (1998);
S. Dittmaier *et al.*, Phys. Lett. **B478**, 247 (2000);
S. Dawson and L. Reina, Phys. Rev. **D59**, 054012 (1999).
109. S. Dawson *et al.*, [Higgs Working Group, "Snowmass on the Mississippi" workshop] `arXiv:1310.8361 [hep-ex]` (2013).
110. D.M. Asner *et al.*, [ILC Higgs white paper, "Snowmass on the Mississippi" workshop] `arXiv:1310.0763 [hep-ph]` (2013).
111. A. Denner *et al.*, Eur. Phys. J. **C71**, 1753 (2011).
112. A. Djouadi, J. Kalinowski, and M. Spira, Comp. Phys. Comm. **108**, 56 (1998);
A. Djouadi *et al.*, `arXiv:1003.1643 [hep-ph]` (2010).
113. S. Gorishnii *et al.*, Mod. Phys. Lett. **A5**, 2703 (1990);
S. Gorishnii *et al.*, Phys. Rev. **D43**, 1633 (1991);
A.L. Kataev and V.T. Kim, Mod. Phys. Lett. **A9**, 1309 (1994);
L.R. Surguladze, Phys. Lett. **B341**, 60 (1994);
S. Larin, T. van Ritbergen, and J. Vermaseren, Phys. Lett. **B362**, 134 (1995);
K. Chetyrkin and A. Kwiatkowski, Nucl. Phys. **B461**, 3 (1996);
K. Chetyrkin, Phys. Lett. **B390**, 309 (1997);
P.A. Baikov, K.G. Chetyrkin, and J.H. Kuhn, Phys. Rev. Lett. **96**, 012003 (2006).
114. J. Fleischer and F. Jegerlehner, Phys. Rev. **D23**, 2001 (1981);
D. Bardin, B. Vilensky, and P. Khristova, Sov. J. Nucl. Phys. **53**, 152 (1991);
A. Dabelstein and W. Hollik, Z. Phys. **C53**, 507 (1992);
B.A. Kniehl, Nucl. Phys. **B376**, 3 (1992);
A. Djouadi *et al.*, *Proceedings* e^+e^- *collisions at 500 GeV* (1991).
115. T. Inami, T. Kubota, and Y. Okada, Z. Phys. **C18**, 69 (1983);
K.G. Chetyrkin, B.A. Kniehl, and M. Steinhauser, Phys. Rev. Lett. **79**, 353 (1997);
P.A. Baikov and K.G. Chetyrkin, Phys. Rev. Lett. **97**, 061803 (2006).
116. H.Q. Zheng and D.D. Wu, Phys. Rev. **D42**, 3760 (1990);
A. Djouadi *et al.*, Phys. Lett. **B257**, 187 (1991);
S. Dawson and R. Kauffman, Phys. Rev. **D47**, 1264 (1993);
A. Djouadi, M. Spira, and P. Zerwas, Phys. Lett. **B311**, 255 (1993);

K. Melnikov and O.I. Yakovlev, Phys. Lett. **B312**, 179 (1993);
M. Inoue *et al.*, Mod. Phys. Lett. **A9**, 1189 (1994).
117. P. Maierhofer and P. Marquard, Phys. Lett. **B721**, 131 (2013).
118. U. Uglietti *et al.*, Phys. Lett. **B595**, 432 (2004);
G. Degrassi and F. Maltoni, Phys. Lett. **B600**, 255 (2004);
S. Actis *et al.*, Phys. Lett. **B670**, 12 (2008);
U. Aglietti *et al.*, Phys. Lett. **B600**, 57 (2004);
G. Degrassi and F. Maltoni, Nucl. Phys. **B724**, 183 (2005);
U. Aglietti *et al.*, [Tevatron for LHC report: Higgs] `arXiv:hep-ph/0612172` (2006).
119. A. Abbasabadi *et al.*, Phys. Rev. **D55**, 5647 (1997);
A. Abbasabadi and W.W. Repko, Phys. Rev. **D71**, 017304 (2005);
A. Abbasabadi and W.W. Repko, JHEP **0608**, 048 (2006);
D.A. Dicus and W.W. Repko, Phys. Rev. **D87**, 077301 (2013);
L.B. Chen, C.F. Qiao, and R.L. Zhu, Phys. Lett. **B726**, 306 (2013);
Y. Sun, H.R. Chang, and D.N. Gao, JHEP **1305**, 061 (2013);
G. Passarino, Phys. Lett. **B727**, 424 (2013).
120. M. Spira, A. Djouadi, and P.M. Zerwas, Phys. Lett. **B276**, 350 (1992).
121. A. Bredenstein *et al.*, Phys. Rev. **D74**, 013004 (2006);
A. Bredenstein *et al.*, JHEP **0702**, 080 (2007);
A. Bredenstein *et al.*, `Prophecy4f`: A Monte Carlo generator for a proper description of the Higgs decay into 4 fermions, `http://omnibus.uni-freiburg.de/~sd565/programs/prophecy4f/prophecy4f.html`.
122. A. Ghinculov, Phys. Lett. **B337**, 137 (1994) [E: **B346**, 426 (1995)];
L. Durand, B.A. Kniehl, and K. Riesselmann, Phys. Rev. **D51**, 5007 (1995);
L. Durand, K. Riesselmann, and B.A. Kniehl, Phys. Rev. Lett. **72**, 2534 (1994) [E: **74**, 1699 (1995)].
123. E. Braaten and J.P. Leveille, Phys. Rev. **D22**, 715 (1980);
L. Durand, K. Riesselmann, and B.A. Kniehl, Phys. Rev. Lett. **72**, 2534 (1994);
E. Gross, G. Wolf, and B.A. Kniehl, Z. Phys. **C63**, 417 (1994) [E: *ibid.*, **C66**, 32 (1995)];
A. Ghinculov, Phys. Lett. **B337**, 137 (1994) and Nucl. Phys. **B455**, 21 (1995);
A. Djouadi, M. Spira, and P.M. Zerwas, Z. Phys. **C70**, 427 (1996);
A. Frink *et al.*, Phys. Rev. **D54**, 4548 (1996);
K.G. Chetyrkin and M. Steinhauser, Phys. Lett. **B408**, 320 (1997);
R. Harlander and M. Steinhauser, Phys. Rev. **D56**, 3980 (1997);
A.L. Kataev, Sov. Phys. JETP Lett. **66**, 327 (1997);
S. Actis *et al.*, Nucl. Phys. **B811**, 182 (2009).
124. J. Erler and A. Freitas, *Electroweak Model and Constraints on New Physics*, in this volume.
125. R. Barate *et al.*, [LEP Working Group for Higgs boson searches and ALEPH, DELPHI, L3, and OPAL Collaborations], Phys. Lett. **B565**, 61 (2003).
126. CDF and D0 Collaborations, Phys. Rev. **D88**, 052014 (2013).
127. G. Aad *et al.*, [ATLAS Collab.], Phys. Rev. **D90**, 112015 (2014).

128. S. Chatrchyan *et al.*, [CMS Collab.], Phys. Rev. **D89**, 092007 (2014).
129. S. Chatrchyan *et al.*, [CMS Collab.], Eur. Phys. J. **C74**, 3076 (2014).
130. G. Aad *et al.*, [ATLAS Collab.], Phys. Rev. **D91**, 012006 (2015).
131. S. Chatrchyan *et al.*, [CMS Collab.], JHEP **12**, 034 (2012).
132. G. Aad *et al.*, [ATLAS Collab.], Phys. Rev. **D90**, 052004 (2014).
133. S. Chatrchyan *et al.*, [CMS Collab.], Eur. Phys. J. **C75**, 212 (2015).
134. G. Aad *et al.*, [Atlas and CMS Collaborations], Phys. Rev. Lett. **114**, 191803 (2015).
135. G. Aad *et al.*, [ATLAS Collab.], Phys. Rev. **D92**, 012006 (2015).
136. S. Chatrchyan *et al.*, [CMS Collab.], JHEP **01**, 096 (2014).
137. G. Aad *et al.*, [ATLAS Collab.], JHEP **08**, 137 (2015).
138. S. Chatrchyan *et al.*, [CMS Collab.], JHEP **05**, 104 (2014).
139. G. Aad *et al.*, [ATLAS Collab.], JHEP **04**, 117 (2015).
140. S. Chatrchyan *et al.*, [CMS Collab.], Phys. Rev. **D89**, 012003 (2014).
141. ATLAS and CMS Collaborations, ATLAS-CONF-2015-044 and CMS-PAS-HIG-15-002 (2015).
142. T. Aaltonen *et al.*, [CDF and D0 Collaborations], Phys. Rev. Lett. **109**, 071804 (2012).
143. J.M. Butterworth *et al.*, Phys. Rev. Lett. **100**, 242001 (2008).
144. G. Aad *et al.*, [ATLAS Collab.], JHEP **01**, 069 (2015).
145. S. Chatrchyan *et al.*, [CMS Collab.], Phys. Rev. **D92**, 032008 (2015).
146. ATLAS Collab., ATLAS-CONF-2015-060 (2015).
147. CMS Collab., CMS-PAS-HIG-15-005 (2016).
148. ATLAS Collab., ATLAS-CONF-2015-059 (2015).
149. CMS Collab., CMS-PAS-HIG-15-004 (2016).
150. ATLAS Collab., ATLAS-CONF-2015-069 (2015).
151. CMS Collab., CMS-PAS-HIG-15-003 (2016).
152. CMS Collab., CMS-PAS-HIG-16-003 (2016).
153. S. Chatrchyan *et al.*, [CMS Collab.], JHEP **09**, 087 (2014).
154. S. Chatrchyan *et al.*, [CMS Collab.], Eur. Phys. J. **C75**, 215 (2015).
155. G. Aad *et al.*, [ATLAS Collab.], Phys. Lett. **B740**, 222 (2012).
156. G. Aad *et al.*, [ATLAS Collab.], Eur. Phys. J. **C75**, 349 (2015).
157. G. Aad *et al.*, [ATLAS Collab.], Phys. Lett. **B749**, 519 (2015).
158. G. Aad *et al.*, [ATLAS Collab.], Phys. Lett. **B740**, 222 (2015).
159. G. Aad *et al.*, [ATLAS Collab.], JHEP **12**, 061 (2015).
160. S. Chatrchyan *et al.*, [CMS Collab.], Phys. Rev. **D90**, 112013 (2014).
161. G. Aad *et al.*, [ATLAS Collab.], Phys. Rev. Lett. **114**, 081802 (2015).
162. G. Aad *et al.*, [ATLAS Collab.], Phys. Rev. **D92**, 092004 (2015).
163. G. Aad *et al.*, [ATLAS Collab.], Eur. Phys. J. **C75**, 412 (2015).
164. S. Chatrchyan *et al.*, [CMS Collab.], Phys. Rev. **D90**, 112013 (2014).
165. S. Chatrchyan *et al.*, [CMS Collab.], Phys. Lett. **B755**, 220 (2016).
166. S. Chatrchyan *et al.*, [CMS Collab.], Phys. Lett. **B749**, 560 (2015).
167. ATLAS Collab., ATL-PHYS-PUB-2015-046 (2015).
168. CMS Collab., CMS-PAS-FTR-15-002 (2015).

169. ATLAS Collab., ATL-PHYS-PUB-2014-019 (2014).
170. S. Chatrchyan *et al.*, [CMS Collab.], Phys. Lett. **B726**, 587 (2013).
171. G. Aad *et al.*, [ATLAS Collab.], Phys. Lett. **B753**, 341 (2016).
172. G. Aad *et al.*, [ATLAS Collab.], Phys. Lett. **B738**, 68 (2014).
173. S. Chatrchyan *et al.*, [CMS Collab.], Phys. Lett. **B744**, 184 (2015).
174. S. Chatrchyan *et al.*, [CMS Collab.], Phys. Lett. **B749**, 137 (2015).
175. G. Aad *et al.*, [ATLAS Collab.], JHEP **1511**, 211 (2015).
176. G. Aad *et al.*, [ATLAS Collab.], CERN-EP-2016-055(2016).
177. C. Delaunay *et al.*, Phys. Rev. **D89**, 033014 (2014).
178. G. T. Bodwin *et al.*, Phys. Rev. **D88**, 053003 (2013).
179. G. Aad *et al.*, [ATLAS Collab.], Phys. Rev. Lett. **114**, 121801 (2015).
180. ATLAS Collab., CERN-EP-2016-130 (2016).
181. A. Djouadi *et al.*, Eur. Phys. J. **C73**, 2455 (2013).
182. G. Aad *et al.*, [ATLAS Collab.], Eur. Phys. J. **C75**, 337 (2015).
183. G. Aad *et al.*, [ATLAS Collab.], Phys. Rev. Lett. **112**, 201802 (2014).
184. G. Aad *et al.*, [ATLAS Collab.], JHEP **01**, 172 (2016).
185. G. Aad *et al.*, [ATLAS Collab.], JHEP **11**, 206 (2015).
186. S. Chatrchyan *et al.*, [CMS Collab.], Eur. Phys. J. **C74**, 2980 (2014).
187. S. Chatrchyan *et al.*, [CMS Collab.], CMS-PAS-HIG-15-012 (2015).
188. S. Chatrchyan *et al.*, [CMS Collab.], CMS-PAS-HIG-16-009 (2016).
189. S. Chatrchyan *et al.*, [CMS Collab.], CMS-PAS-HIG-16-008 (2016).
190. M.J. Strassler and K.M. Zurek, Phys. Lett. **B651**, 374 (2007).
191. M.J. Strassler and K.M. Zurek, Phys. Lett. **B661**, 263 (2008).
192. T. Han *et al.*, JHEP **0807**, 008 (2008).
193. A. Falkowski *et al.*, JHEP **1005**, 077 (2010) and Phys. Rev. Lett. **105**, 241801 (2010).
194. G. Aad *et al.*, [ATLAS Collab.], New J. Phys. **15**, 043009 (2013).
195. G. Aad *et al.*, [ATLAS Collab.], Phys. Lett. **B721**, 32 (2013).
196. G. Aad *et al.*, [ATLAS Collab.], Phys. Rev. Lett. **108**, 251801 (2012).
197. D. Tucker-Smith and N. Weiner, Phys. Rev. **D64**, 043502 (2001).
198. S. Chatrchyan *et al.*, [CMS Collab.], Phys. Lett. **B726**, 564 (2013).
199. G. Aad *et al.*, [ATLAS Collab.], Eur. Phys. J. **C76**, 6 (2016).
200. L.D. Landau, Dokl. Akad. Nauk Ser. Fiz. **60**, 207 (1948);
C.N. Yang, Phys. Rev. **D77**, 242 (1950).
201. G. Aad *et al.*, [ATLAS Collab.], Eur. Phys. J. **C75**, 476 (2015).
202. V. Khachatryan *et al.*, [CMS Collab.], Phys. Rev. **D92**, 012004 (2015).
203. ATLAS Collab., Phys. Lett. **B726**, 120 (2013).
204. P. Artoisenet *et al.*, JHEP **1311**, 043 (2013);
A. Alloul, B. Fuks, and V. Sanz, JHEP **1404**, 110 (2014);
A. Falkowski *et al.*, Eur. Phys. J. **C75**, 583 (2015).
205. J. Ellis *et al.*, JHEP **1211**, 134 (2012).
206. D0 Collab., Note 6387-CONF (2013).
207. D0 Collab., Note 6406-CONF (2013).
208. A. De Rujula *et al.*, Phys. Rev. **D82**, 013003 (2010).

209. ATLAS Collab., Eur. Phys. J. **C75**, 335 (2015).
210. V. Khachatryan *et al.*, [CMS Collab.], Phys. Rev. **D92**, 072010 (2015).
211. V. Khachatryan *et al.*, [CMS Collab.], CERN-EP-2016-054.
212. L. Dixon and S. Siu, Phys. Rev. Lett. **90**, 252001 (2003);
S. P. Martin, Phys. Rev. **D86**, 073016 (2012);
L. Dixon and Y. Li, Phys. Rev. Lett. **111**, 111802 (2013).
213. ATLAS Collab., ATL-PHYS-PUB-2016-009 (2016).
214. ATLAS Collab., ATL-PHYS-PUB-2013-014 (2013).
215. N. Kauer and G. Passarino, JHEP **08**, 116 (2012);
F. Caola and K. Melnikov, Phys. Rev. **D88**, 054024 (2013);
J.M. Campbell, R.K. Ellis, and C. Williams, JHEP **04**, 060 (2014);
J.M. Campbell, R.K. Ellis, and C. Williams, Phys. Rev. **D89**, 053011 (2014);
C. Englert and M. Spannowsky, Phys. Rev. **D90**, 053003 (2014).
216. ATLAS Collab., ATL-PHYS-PUB-2015-024 (2015).
217. M. Gonzalez-Alonso *et al.*, Eur. Phys. J. **C75**, 128 (2015);
A. Greljo *et al.*, Eur. Phys. J. **C76**, 158 (2016).
218. G. Buchalla, O. Cata and C. Krause, Nucl. Phys. **B880**, 552 (2014);
I. Brivio *et al.*, JHEP **1403**, 014 (2014).
219. W. Buchmuller and D. Wyler, Nucl. Phys. **B268**, 621 (1986).
220. C.J. C. Burges and H.J. Schnitzer, Nucl. Phys. **B288**, 464 (1983);
C.N. Leung, S.T. Love and S. Rao, Z. Phys. **C31**, 433 (1986).
221. B. Grzadkowski *et al.*, JHEP **1010**, 085 (2010).
222. L. Lehman and A. Martin, JHEP **1602**, 081 (2016);
B. Henning *et al.*, `arXiv:1512.03433 [hep-ph]` (2015).
223. R. Alonso *et al.*, JHEP **1404**, 159 (2014).
224. G.F. Giudice *et al.*, JHEP **0706**, 045 (2007).
225. R. Contino *et al.*, JHEP **1307**, 035 (2013).
226. J. Elias-Miro *et al.*, JHEP **1311**, 066 (2013);
R.S. Gupta, A. Pomarol and F. Riva, Phys. Rev. **D91**, 035001 (2015);
E. Masso, JHEP **1410**, 128 (2014).
227. A. Falkowski and F. Riva, JHEP **1502**, 039 (2015).
228. A. Falkowski *et al.*, Phys. Rev. Lett. **116**, 011801 (2016).
229. C. Degrande *et al.*, JHEP **1207**, 036 (2012);
J.F. Kamenik, M. Papucci, and A. Weiler, Phys. Rev. **D85**, 071501 (2012).
230. A. David *et al.*, [LHC Higgs Cross Section Working Group], `arXiv:1209.0040 [hep-ph]` (2012).
231. B.A. Kniehl and M. Spira, Z. Phys. **C69**, 77 (1995).
232. G. Isidori, A.V. Manohar, and M. Trott, Phys. Lett. **B728**, 131 (2014);
G. Isidori and M. Trott, JHEP **1402**, 082 (2014).
233. A. Pomarol and F. Riva, JHEP **1401**, 151 (2014).
234. R. Godbole *et al.*, Phys. Lett. **B730**, 275 (2014).
235. M. Reece, New J. Phys. **15**, 043003 (2013).
236. S. Biswas, E. Gabrielli, and B. Mele, JHEP **1301**, 088 (2013);
S. Biswas *et al.*, JHEP **07**, 073 (2013).

237. M. Farina *et al.*, JHEP **1305**, 022 (2013).
238. ATLAS Collab., JHEP **11**, 206 (2015).
239. A. Djouadi *et al.*, Eur. Phys. J. **C73**, 2455 (2013).
240. ATLAS Collab., ATLAS-CONF-2013-072 (2013).
241. ATLAS Collab., Phys. Lett. **B753**, 69 (2016).
242. L.E. Ibanez and G.G. Ross, Phys. Lett. **B110**, 215 (1982);
L.E. Ibanez, Phys. Lett. **B118**, 73 (1982);
J. Ellis, D.V. Nanopoulos, and K. Tamvakis, Phys. Lett. **B121**, 123 (1983);
L. Alvarez-Gaume, J. Polchinski, and M.B. Wise, Nucl. Phys. **B221**, 495 (1983).
243. See the list of references in the corresponding section of the 2014 edition of this review.
244. ATLAS Collab.,
`https://twiki.cern.ch/twiki/bin/view/AtlasPublic/Publications`;
CMS Collab.,
`http://cms-results.web.cern.ch/cms-results/public-results/publications/SUS/STO`
245. J. Mrazek *et al.*, Nucl. Phys. **B853**, 1 (2011).
246. H. Georgi and D. B. Kaplan, Phys. Lett. **B145**, 216 (1984).
247. D.B. Kaplan, Nucl. Phys. **B365**, 259 (1991).
248. E. Savioni, PhD thesis, `http://paduaresearch.cab.unipd.it/6166/` (2013).
249. G. Panico *et al.*, JHEP **1303**, 051 (2013).
250. H.E. Haber, *Supersymmetry*, in this volume.
251. A. Djouadi, Phys. Reports **459**, 1 (2008).
252. H.E. Haber and Y. Nir, Nucl. Phys. **B335**, 363 (1990);
A. Dabelstein, Nucl. Phys. **B456**, 25 (1995);
S. Heinemeyer, W. Hollik, and G. Weiglein, Eur. Phys. J. **C16**, 139 (2000);
A. Dobado, M. J. Herrero, and S. Penaranda, Eur. Phys. J. **C17**, 487 (2000).
253. J.F. Gunion and H.E. Haber, Phys. Rev. **D67**, 075019 (2003).
254. N. Craig, J. Galloway, and S. Thomas, `arXiv:1305.2424 [hep-ph]` (2013).
255. M. Carena *et al.*, JHEP **1203**, 014 (2012);
M. Carena *et al.*, JHEP **1207**, 175 (2012).
256. G. Degrassi *et al.*, Eur. Phys. J. **C28**, 133 (2003).
257. S. Heinemeyer *et al.*, JHEP **0808**, 087 (2008).
258. M. Carena *et al.*, Eur. Phys. J. **C26**, 601 (2003);
M. Carena *et al.*, Eur. Phys. J. **C73**, 2552 (2013).
259. M. Carena *et al.*, Eur. Phys. J. **C45**, 797 (2006).
260. S.Y. Choi, M. Drees, and J.S. Lee, Phys. Lett. **B481**, 57 (2000);
M. Carena *et al.*, Nucl. Phys. **B625**, 345 (2002).
261. A. Pilaftsis and C.E.M. Wagner, Nucl. Phys. **B553**, 3 (1999).
262. A. Arbey *et al.*, Phys. Lett. **B708**, 162 (2012);
A. Arbey *et al.*, JHEP **1209**, 107 (2012).
263. L.J. Hall, D. Pinner, and J.T. Ruderman, JHEP **1204**, 131 (2012).
264. H. Baer, V. Barger, and A. Mustafayev, Phys. Rev. **D85**, 075010 (2012).
265. P. Draper *et al.*, Phys. Rev. **D85**, 095007 (2012).
266. S. Heinemeyer, O. Stal, and G. Weiglein, Phys. Lett. **B710**, 201 (2012).

267. M. Kadastik *et al.*, JHEP **1205**, 061 (2012).
268. P. Draper, G. Lee and C.E.M. Wagner, Phys. Rev. **D89**, 055023 (2014).
269. J.P. Vega and G. Villadoro, JHEP **1507**, 159 (2015).
270. S.P. Martin, Phys. Rev. **D75**, 055005 (2007);
P. Kant *et al.*, JHEP **1008**, 104 (2010);
J.L. Feng *et al.*, Phys. Rev. Lett. **111**, 131802 (2013).
271. M. Carena *et al.*, Nucl. Phys. **B580**, 29 (2000).
272. T. Hahn *et al.*, Phys. Rev. Lett. **112**, 141801 (2014).
273. T.D. Lee, Phys. Rev. **D8**, 1226 (1973);
P. Fayet, Nucl. Phys. **B78**, 14 (1974);
R.D. Peccei and H.R. Quinn, Phys. Rev. Lett. **38**, 1440 (1977);
P. Fayet and S. Ferrara, Phys. Reports **32**, 249 (1977);
L.J. Hall and M.B. Wise, Nucl. Phys. **B187**, 397 (1981);
V.D. Barger, J.L. Hewett, and R.J.N. Phillips, Phys. Rev. **D41**, 3421 (1990).
274. M. Carena, S. Mrenna, and C.E.M. Wagner, Phys. Rev. **D60**, 075010 (1999) and Phys. Rev. **D62**, 055008 (2000).
275. D.M. Pierce *et al.*, Nucl. Phys. **B491**, 3 (1997).
276. A. Dabelstein, Nucl. Phys. **B456**, 25 (1995);
F. Borzumati *et al.*, Nucl. Phys. **B555**, 53 (1999);
H. Eberl *et al.*, Phys. Rev. **D62**, 055006 (2000).
277. J.A. Coarasa, R.A. Jimenez, and J. Sola, Phys. Lett. **B389**, 312 (1996);
R.A. Jimenez and J. Sola, Phys. Lett. **B389**, 53 (1996);
A. Bartl *et al.*, Phys. Lett. **B378**, 167 (1996).
278. S. Heinemeyer, W. Hollik, and G. Weiglein, Eur. Phys. J. **C16**, 139 (2000).
279. H. E. Haber *et al.*, Phys. Rev. **D63**, 055004 (2001).
280. L. Hall, R. Rattazzi, and U. Sarid, Phys. Rev. **D50**, 7048 (1994);
R. Hempfling, Phys. Rev. **D49**, 6168 (1994).
281. M.S. Carena *et al.*, Nucl. Phys. **B426**, 269 (1994).
282. J. Guasch, P. Hafliger, and M. Spira, Phys. Rev. **D68**, 115001 (2003);
D. Noth and M. Spira, Phys. Rev. Lett. **101**, 181801 (2008) and JHEP **1106**, 084 (2011);
L. Mihaila and C. Reisser, JHEP **1008**, 021 (2010).
283. M.S. Carena *et al.*, Phys. Lett. **B499**, 141 (2001).
284. A. Djouadi, J. Kalinowski, and P.M. Zerwas, Z. Phys. **C57**, 569 (1993);
H. Baer *et al.*, Phys. Rev. **D47**, 1062 (1993);
A. Djouadi *et al.*, Phys. Lett. **B376**, 220 (1996);
A. Djouadi *et al.*, Z. Phys. **C74**, 93 (1997);
S. Heinemeyer and W. Hollik, Nucl. Phys. **B474**, 32 (1996).
285. J.F. Gunion, Phys. Rev. Lett. **72**, 199 (1994);
D. Choudhury and D.P. Roy, Phys. Lett. **B322**, 368 (1994);
O.J. Eboli and D. Zeppenfeld, Phys. Lett. **B495**, 147 (2000);
B.P. Kersevan, M. Malawski, and E. Richter-Was, Eur. Phys. J. **C29**, 541 (2003).
286. E.L. Berger *et al.*, Phys. Rev. **D66**, 095001 (2002).

287. A. Brignole *et al.*, Nucl. Phys. **B643**, 79 (2002);
R. Dermisek and I. Low, Phys. Rev. **D77**, 035012 (2008).
288. A. Djouadi, Phys. Lett. **B435**, 101 (1998).
289. M.R. Buckley and D. Hooper, Phys. Rev. **D86**, 075008 (2012);
for other references, see the 2014 edition of this review.
290. J.J. Cao *et al.*, JHEP **1203**, 086 (2012);
R. Benbrik *et al.*, Eur. Phys. J. **C72**, 2171 (2012);
Z. Kang, J. Li, and T. Li, JHEP **1211**, 024 (2012);
J.F. Gunion, Y. Jiang, and S. Kraml, Phys. Lett. **B710**, 454 (2012);
U. Ellwanger, JHEP **1203**, 044 (2012).
291. LHC Cross Section Working Group for Beyond the Satndard Model Higgs: NMSSM
`https://twiki.cern.ch/twiki/bin/view/LHCPhysics/LHCHXSWGNMSSM`.
292. M. Carena *et al.*, Phys. Rev. **D93**, 035013 (2016).
293. T. Kitahara, JHEP **1211**, 021 (2012);
M. Carena *et al.*, JHEP **1302**, 114 (2013).
294. B. Batell, S. Jung, and C.E.M. Wagner, JHEP **1312**, 075 (2013).
295. D. Dicus *et al.*, Phys. Rev. **D59**, 094016 (1999).
296. C. Balazs, H.-J. He, and C.P. Yuan, Phys. Rev. **D60**, 114001 (1999).
297. E. Boos *et al.*, Phys. Rev. **D66**, 055004 (2002);
E. Boos, A. Djouadi, and A. Nikitenko, Phys. Lett. **B578**, 384 (2004);
E. Boos *et al.*, Phys. Lett. **B622**, 311 (2005);
M. Carena *et al.*, JHEP **1207**, 091 (2012).
298. A.A. Barrientos Bendezu and B.A. Kniehl, Phys. Rev. **D64**, 035006 (2001).
299. J.A. Coarasa Perez *et al.*, Eur. Phys. J. **C2**, 373 (1998);
J.A. Coarasa Perez *et al.*, Phys. Lett. **B425**, 329 (1998).
300. C.S. Li and T.C. Yuan, Phys. Rev. **D42**, 3088 (1990) [E: **D47**, 2156 (1993)];
A. Czarnecki and S. Davidson, Phys. Rev. **D47**, 3063 (1993);
C.S. Li, Y.-S. Wei, and J.-M. Yang, Phys. Lett. **B285**, 137 (1992).
301. J. Guasch, R.A. Jimenez, and J. Sola, Phys. Lett. **B360**, 47 (1995).
302. M.S. Carena *et al.*, Nucl. Phys. **B577**, 88 (2000).
303. A.A. Barrientos Bendezu and B.A. Kniehl, Phys. Rev. **D59**, 015009 (1999), Phys. Rev. **D61**, 015009 (2000) and Phys. Rev. **D63**, 015009 (2001).
304. A.A. Barrientos Bendezu and B.A. Kniehl, Nucl. Phys. **B568**, 305 (2000).
305. A. Krause *et al.*, Nucl. Phys. **B519**, 85 (1998);
O. Brein and W. Hollik, Eur. Phys. J. **C13**, 175 (2000).
306. R.M. Barnett, H.E. Haber, and D.E. Soper, Nucl. Phys. **B306**, 697 (1988);
for other references, see the 2014 edition of this review.
307. L. Maiani, A. D. Polosa and V. Riquer, New J. Phys. **14**, 073029 (2012) and Phys. Lett. **B718**, 465 (2012);
A. Djouadi and J. Quevillon, JHEP **1310**, 028 (2013);
A. Djouadi *et al.*, Eur. Phys. J. **C73**, 2650 (2013).
308. M. Carena *et al.*, Phys. Rev. **D91**, 035003 (2015).
309. M. Carena *et al.*, JHEP **1404**, 015 (2014).

310. K. Blum, R.T. D'Agnolo, and J. Fan, JHEP **1301**, 057 (2013);
A. Azatov *et al.*, Phys. Rev. **D86**, 075033 (2012);
J.R. Espinosa *et al.*, JHEP **1212**, 077 (2012);
R.S. Gupta, M. Montull, and F. Riva, JHEP **1304**, 132 (2013);
R.T. D'Agnolo, PhD thesis, Scuola Normale Superiore, Pisa, 2013.
311. A. Djouadi *et al.*, JHEP **1506**, 168 (2015).
312. G. D'Ambrosio *et al.*, Nucl. Phys. **B645**, 155 (2002);
R.S. Chivukula and H. Georgi, Phys. Lett. **B188**, 99 (1987);
L.J. Hall and L. Randall, Phys. Rev. Lett. **65**, 2939 (1990);
A.J. Buras *et al.*, Phys. Lett. **B500**, 161 (2001).
313. L.J. Hall, J. Lykken, and S. Weinberg, Phys. Rev. **D27**, 2359 (1983);
J.E. Kim and H.P. Nilles, Phys. Lett. **B138**, 150 (1984);
G.F. Giudice and A. Masiero, Phys. Lett. **B206**, 480 (1988);
E.J. Chun, J.E. Kim, and H.P. Nilles, Nucl. Phys. **B370**, 105 (1992);
I. Antoniadis *et al.*, Nucl. Phys. **B432**, 187 (1994).
314. R.D. Peccei and H.R. Quinn, Phys. Rev. Lett. **38**, 1440 (1977).
315. P. Fayet, Phys. Lett. **B90**, 104 (1975).
316. Y.B. Zeldovich, I.Y. Kobzarev, and L.B. Okun, Zh. Eksp. Teor. Fiz. **67**, 3 (1974);
A. Vilenkin, Phys. Reports **121**, 263 (1985).
317. C. Panagiotakopoulos and K. Tamvakis, Phys. Lett. **B469**, 145 (1999);
A. Dedes *et al.*, Phys. Rev. **D63**, 055009 (2001);
A. Menon, D. Morrissey, and C.E.M. Wagner, Phys. Rev. **D70**, 035005 (2004).
318. M. Cvetic *et al.*, Phys. Rev. **D56**, 2861 (1997) [E: **D58**, 119905 (1998)];
P. Langacker and J. Wang, Phys. Rev. **D58**, 115010 (1998) and references therein.
319. J. Erler, P. Langacker, and T.J. Li, Phys. Rev. **D66**, 015002 (2002);
T. Han, P. Langacker and B. McElrath, Phys. Rev. **D70**, 115006 (2004);
V. Barger *et al.*, Phys. Rev. **D73**, 115010 (2006).
320. V. Barger *et al.*, Phys. Rev. **D73**, 115010 (2006);
V. Barger, P. Langacker, and G. Shaughnessy, Phys. Rev. **D75**, 055013 (2007).
321. E. Accomando, *et al.*, `hep-ph/0608079` (2006).
322. B. A. Dobrescu, G. L. Landsberg, and K. T. Matchev, Phys. Rev. **D63**, 075003 (2001).
323. R. Dermisek and J. F. Gunion, Phys. Rev. Lett. **95**, 041801 (2005).
324. O.J.P. Eboli and D. Zeppenfeld, Phys. Lett. **B495**, 147 (2000);
H. Davoudiasl, T. Han, and H.E. Logan, Phys. Rev. **D71**, 115007 (2005).
325. L. Wang and X.F. Han, Phys. Rev. **D87**, 015015 (2013);
K. Schmidt-Hoberg and F. Staub JHEP **1210**, 195 (2012);
H. An, T. Liu, and L.T. Wang, Phys. Rev. **D86**, 075030 (2012);
D.A. Vasquez *et al.*, Phys. Rev. **D86**, 035023 (2012);
S.F. King, M. Muhlleitner, and R. Nevzorov, Nucl. Phys. **B860**, 207 (2012).
326. N.D. Christensen, T. Han, Z. Liu and S. Su, JHEP **1308**, 019 (2013);
T. Han, Z. Liu and S. Su, JHEP **1408**, 093 (2014);
S.F. King *et al.*, Phys. Rev. **D90**, 095014 (2014);
N.E. Bomark *et al.*, JHEP **1502**, 044 (2015);

P. Athron *et al.*, JHEP **1501**, 153 (2015);
N.E. Bomark, S. Moretti and L. Roszkowski, arXiv:1503.04228 [hep-ph] (2015);
T. Li and S. Su, JHEP **1511**, 068 (2015);
G. Belanger *et al.*, JHEP **1509**, 151 (2015);
J. Baglio *et al.*, JHEP **1510**, 024 (2015);
M. Guchait and J. Kumar, Int. J. Mod. Phys. **A31**, 1650069 (2016);
D. Barducci *et al.*, JHEP **1601**, 050 (2016);
M. Carena *et al.*, Phys. Rev. **D93**, 035013 (2016);
P. Bandyopadhyay, K. Huitu and S. Niyogi, JHEP **1607**, 015 (2016);
U. Ellwanger and M. Rodriguez-Vazquez, JHEP **1602**, 096 (2016);
R. Costa *et al.*, JHEP **1606**, 034 (2016);
E. Conte *et al.*, JHEP **1605**, 100 (2016).

327. Courtesy of Marcin Barziak based on the public code NMSSMTools, www.th.u-psud.fr/NMHDECAY/nmssmtools.html.
328. P. Batra *et al.*, JHEP **0402**, 043 (2004).
329. P. Batra *et al.*, JHEP **0406**, 032 (2004);
A. Maloney, A. Pierce, and J.G. Wacker, JHEP **0606**, 034 (2006);
Y. Zhang *et al.*, Phys. Rev. **D78**, 011302 (2008);
C.W. Chiang *et al.*, Phys. Rev. **D81**, 015006 (2010);
A.D. Medina, N.R. Shah, and C.E.M. Wagner, Phys. Rev. **D80**, 015001 (2009);
M. Endo *et al.*, Phys. Rev. **D85**, 095006 (2012);
C. Cheung and H.L. Roberts, JHEP **1312**, 018 (2013).
330. R. Huo *et al.*, Phys. Rev. **D87**, 055011 (2013).
331. R.T. D'Agnolo, E. Kuflik, and M. Zanetti, JHEP **1303**, 043 (2013).
332. A. Azatov and J. Galloway, Int. J. Mod. Phys. **A28**, 1330004 (2013).
333. N. Craig and A. Katz, JHEP **1305**, 015 (2013).
334. T.F. Feng *et al.*, Nucl. Phys. **B871**, 223 (2013).
335. S. Dimopoulos and S. Thomas, Nucl. Phys. **B465**, 23 (1996);
S. Thomas, Int. J. Mod. Phys. **A13**, 2307 (1998).
336. M.S. Carena *et al.*, Nucl. Phys. **B586**, 92 (2000).
337. A. Pilaftsis, Phys. Rev. **D58**, 096010 (1998) and Phys. Lett. **B435**, 88 (1998);
K.S. Babu *et al.*, Phys. Rev. **D59**, 016004 (1999).
338. G.L. Kane and L.T. Wang, Phys. Lett. **B488**, 383 (2000);
S.Y. Choi, M. Drees, and J.S. Lee, Phys. Lett. **B481**, 57 (2000);
S.Y. Choi and J.S. Lee, Phys. Rev. **D61**, 015003 (2000);
S.Y. Choi, K. Hagiwara, and J.S. Lee, Phys. Rev. **D64**, 032004 (2001) and Phys. Lett. **B529**, 212 (2002);
T. Ibrahim and P. Nath, Phys. Rev. **D63**, 035009 (2001);
T. Ibrahim, Phys. Rev. **D64**, 035009 (2001);
S. Heinemeyer, Eur. Phys. J. **C22**, 521 (2001);
S.W. Ham *et al.*, Phys. Rev. **D68**, 055003 (2003).
339. M. Frank *et al.*, JHEP **0702**, 047 (2007);
S. Heinemeyer *et al.*, Phys. Lett. **B652**, 300 (2007);
T. Hahn *et al.*, arXiv:0710.4891 (2007).

340. D.A. Demir, Phys. Rev. **D60**, 055006 (1999);
S.Y. Choi, M. Drees, and J.S. Lee, Phys. Lett. **B481**, 57 (2000);
K. E. Williams, H. Rzehak, and G. Weiglein, Eur. Phys. J. **C71**, 1669 (2011).
341. E. Christova *et al.*, Nucl. Phys. **B639**, 263 (2002) [E: Nucl. Phys. **B647**, 359 (2002)].
342. M.D. Goodsell and F. Staub, `arXiv:1604.05335 [hep-ph]` (2016);
A. Chakraborty *et al.*, Phys. Rev. **D90**, 055005 (2014);
M. Carena *et al.*, JHEP **1602**, 123 (2016).
343. J.F. Gunion and H.E. Haber, Phys. Rev. **D67**, 075019 (2003);
G.C. Branco *et al.*, Phys. Reports **516**, 1 (2012).
344. S.L. Glashow and S. Weinberg, Phys. Rev. **D15**, 1958 (1977);
E.A. Paschos, Phys. Rev. **D15**, 1966 (1977);
H. Georgi, Hadronic J. **1,** 1227 (1978);
H. Haber, G. Kane, and T. Sterling, Nucl. Phys. **B161**, 493 (1979);
A.G. Akeroyd, Phys. Lett. **B368**, 89 (1996);
A.G. Akeroyd, Nucl. Phys. **B544**, 557 (1999);
A.G. Akeroyd, A. Arhrib, and E. Naimi, Eur. Phys. J. **C20**, 51 (2001).
345. N.G. Deshpande and E. Ma, Phys. Rev. **D18**, 2574 (1978);
R. Barbieri, L.J. Hall, and V. Rychkov, Phys. Rev. **D74**, 015007 (2006);
L. Lopez Honorez *et al.*, JCAP **0702**, 028 (2007);
E. Lundstrom, M. Gustafsson, and J. Edsjo, Phys. Rev. **D79**, 035013 (2009);
E. Dolle *et al.*, Phys. Rev. **D8**, 035003 (2010);
X. Miao, S. Su, and B. Thomas, Phys. Rev. **D82**, 035009 (2010);
L. Lopez-Honorez and C. Yaguna, JCAP **1101**, 002 (2011).
346. A. Arhrib, R. Benbrik, and N. Gaur, Phys. Rev. **D85**, 095021 (2012);
B. Swiezewska and M. Krawczyk, Phys. Rev. **D88**, 035019 (2013);
A. Goudelis, B. Herrmann, and O. Stoel, JHEP **1309**, 106 (2013).
347. V. Barger, H.E. Logan, and G. Shaughnessy, Phys. Rev. **D79**, 115018 (2009).
348. D. O'Connell, M.J. Ramsey-Musolf, and M.B. Wise, Phys. Rev. **D75**, 037701 (2007);
V. Barger *et al.*, Phys. Rev. **D77**, 035005 (2008);
V. Barger *et al.*, Phys. Rev. **D79**, 015018 (2009).
349. H.E. Haber, *Proceedings of the 1990 Theoretical Advanced Study Institute in Elementary Particle Physics,* edited by M. Cvetič and Paul Langacker (World Scientific, Singapore, 1991) pp. 340–475 and references therein.
350. S. Glashow and S. Weinberg, Phys. Rev. **D15**, 1958 (1977).
351. G.C. Branco, W. Grimus, and L. Lavoura, Phys. Lett. **B380**, 119 (1996);
F.J. Botella, G.C. Branco, M.N. Rebelo Phys. Lett. **B687**, 194 (2010).
352. N. Craig and S. Thomas, JHEP **1211**, 083 (2012).
353. G.C. Branco *et al.*, Phys. Reports **516**, 1 (2012).
354. C.Y. Chen, S. Dawson, and M. Sher, Phys. Rev. **D88**, 015018 (2013).
355. B. Swiezewska and M. Krawczyk, Phys. Rev. **D88**, 035019 (2013).
356. B. Coleppa, F. Kling and S. Su, JHEP **1409**, 161 (2014);
J. Cao *et al.*, JHEP **1412**, 026 (2014);

B. Coleppa, F. Kling and S. Su, JHEP **1412**, 148 (2014);
D. Curtin, R. Essig and Y.M. Zhong, JHEP **1506**, 025 (2015);
F. Kling, A. Pyarelal and S. Su, JHEP **1511**, 051 (2015);
J. Hajer *et al.*, JHEP **1511**, 124 (2015);
W. Bernreuther *et al.*, Phys. Rev. **D93**, 034032 (2016);
S. Gori *et al.*, Phys. Rev. **D93**, 075038 (2016);
F. Kling, J.M. No and S. Su, `arXiv:1604.01406 [hep-ph]` (2016);
N. Craig *et al.*, `arXiv:1605.08744 [hep-ph]` (2016).
357. N. Craig *et al.*, JHEP **1506**, 137 (2015).
358. J. Schechter and J. W. F. Valle, Phys. Rev. **D22**, 2227 (1980).
359. T.P. Cheng and L.F. Li, Phys. Rev. **D22**, 2860 (1980).
360. H. Georgi and M. Machacek, Nucl. Phys. **B262**, 463 (1985).
361. M.S. Chanowitz and M. Golden, Phys. Lett. **B165**, 105 (1985).
362. H.E. Logan and M.A. Roy, Phys. Rev. **D82**, 115011 (2010).
363. H.E. Haber and H.E. Logan, Phys. Rev. **D62**, 015011 (2000).
364. A.G. Akeroyd, M. Aoki, and H. Sugiyama, Phys. Rev. **D77**, 075010 (2008).
365. P. Nath *et al.*, Nucl. Phys. (Proc. Supp.) **B200**, 185 (2010).
366. J. Garayoa and T. Schwetz, JHEP **0803**, 009 (2008).
367. J.F. Gunion, R. Vega, and J. Wudka, Phys. Rev. **D43**, 2322 (1991).
368. S. Kanemura and K. Yagyu, Phys. Rev. **D85**, 115009 (2012).
369. I. Low and J. Lykken, JHEP **1010**, 053 (2010).
370. C. Englert, E. Re, and M. Spannowsky, Phys. Rev. **D87**, 095014 (2013).
371. I. Low, J. Lykken, and G. Shaughnessy, Phys. Rev. **D86**, 093012 (2012).
372. A. Falkowski, S. Rychkov, and A. Urbano, JHEP **1204**, 073 (2012).
373. B.A. Dobrescu and J.D. Lykken, JHEP **1302**, 073 (2013).
374. D. Carmi *et al.*, JHEP **1210**, 196 (2012).
375. C.W. Chiang and K. Yagyu, JHEP **1301**, 026 (2013).
376. G. Belanger *et al.*, Phys. Rev. **D88**, 075008 (2013).
377. C. Englert, E. Re, and M. Spannowsky, Phys. Rev. **D88**, 035024 (2013).
378. B. Bellazzini, C. Csaki and J. Serra, Eur. Phys. J. **C74**, 2766 (2014).
379. N. Arkani-Hamed *et al.*, JHEP **0207**, 034 (2002).
380. N. Arkani-Hamed, A.G. Cohen, and H. Georgi, Phys. Lett. **B513**, 232 (2001).
381. N. Arkani-Hamed *et al.*, JHEP **0208**, 021 (2002).
382. M. Schmaltz, JHEP **0408**, 056 (2004).
383. M. Schmaltz, D. Stolarski, and J. Thaler, JHEP **1009**, 018 (2010).
384. M. Perelstein, Prog. in Part. Nucl. Phys. **58**, 247 (2007).
385. M. Schmaltz and D. Tucker-Smith, Ann. Rev. Nucl. and Part. Sci. **55**, 229 (2005).
386. J.A. Casas, J.R. Espinosa, and I. Hidalgo, JHEP **0503**, 038 (2005).
387. H.C. Cheng and I. Low, JHEP **0309**, 051 (2003).
388. M.S. Carena *et al.*, Phys. Rev. **D75**, 091701 (2007).
389. ATLAS Collab., ATLAS-CONF-2012-147, ATLAS-CONF-2012-109 and ATLAS-CONF-2013-024 (2012);
CMS Collab., CMS-PAS-EXO-12-048 and CMS-SUS-12-028 (2012).

390. CMS Collab., CMS-PAS-B2G-12-015 (2012);
ATLAS Collab., ATLAS-CONF-2013-060 (2013).

391. R.S. Chivukula, M. Narain, and J. Womersley, *Dynamical Electroweak Symmetry Breaking*, in this volume.

392. H. Georgi, A.E. Nelson, and A. Manohar, Phys. Lett. **B126**, 169 (1983);
A.E. Nelson and M.J. Strassler, JHEP **0009**, 030 (2000);
S. Davidson, G. Isidori, and S. Uhlig, Phys. Lett. **B663**, 73 (2008).

393. C. Csaki, A. Falkowski, and A. Weiler, JHEP **0809**, 008 (2008);
B. Keren-Zur *et al.*, Nucl. Phys. **B867**, 429 (2013).

394. K. Agashe, R. Contino, and A. Pomarol, Nucl. Phys. **B719**, 165 (2005).

395. O. Matsedonskyi, G. Panico, and A. Wulzer, JHEP **1301**, 164 (2013);
M. Redi and A. Tesi, JHEP **1210**, 166 (2012);
D. Marzocca, M. Serone, and J. Shu, JHEP **1208**, 013 (2012);
A. Pomarol and F. Riva, JHEP **1208**, 135 (2012).

396. R. Contino and G. Servant, JHEP **0806**, 026 (2008);
J. Mrazek and A. Wulzer, Phys. Rev. **D81**, 075006 (2010).

397. A. De Simone *et al.*, JHEP **1304**, 004 (2013);
A. Azatov *et al.*, Phys. Rev. **D89**, 075001 (2014).

398. A. Falkowski, Phys. Rev. **D77**, 055018 (2008);
I. Low and A. Vichi, Phys. Rev. **D84**, 045019 (2011);
A. Azatov and J. Galloway, Phys. Rev. **D85**, 055013 (2012);
C. Delaunay, C. Grojean, and G. Perez, JHEP **1309**, 090 (2013).

399. R.K. Ellis *et al.*, Nucl. Phys. **B297**, 221 (1988);
U. Baur and E.W.N. Glover, Nucl. Phys. **B339**, 38 (1990);
O. Brein and W. Hollik, Phys. Rev. **D68**, 095006 (2003);
U. Langenegger *et al.*, JHEP **0606**, 035 (2006).

400. A. Banfi, A. Martin, and V. Sanz, JHEP **1408**, 053 (2014);
A. Azatov and A. Paul, JHEP **1401**, 014 (2014);
C. Grojean *et al.*, JHEP **1405**, 022 (2014);
M. Schlaffer *et al.*, Eur. Phys. J. **C74**, 3120 (2014);
M. Buschmann *et al.*, Phys. Rev. **D90**, 013010 (2014);
M. Buschmann *et al.*, JHEP **1502**, 038 (2015);
U. Langenegger, M. Spira and I. Strebel, `arXiv:1507.01373 [hep-ph]` (2015).

401. A. Azatov *et al.*, J. Exp. Theor. Phys. **120**, 354 (2015).

402. A. Azatov *et al.*, Phys. Rev. **D92**, 035001 (2015).

403. R. Contino, L. Da Rold, and A. Pomarol, Phys. Rev. **D75**, 055014 (2007).

404. D. Pappadopulo, A. Thamm, and R. Torre, JHEP **1307**, 058 (2013);
M. Montull *et al.*, Phys. Rev. **D88**, 095006 (2013).

405. I. Low, R. Rattazzi, and A. Vichi, JHEP **1004**, 126 (2010).

406. M. Ciuchini *et al.*, JHEP **1308**, 106 (2013).

407. C. Grojean, O. Matsedonskyi, and G. Panico, JHEP **1310**, 160 (2013).

408. M. Geller and O. Telem, Phys. Rev. Lett. **114**, 191801 (2015).

409. P. Batra and Z. Chacko, Phys. Rev. D 79,095012(2009);
R. Barbieri *et al.*, JHEP **1508**, 161 (2015);
M. Low, A. Tesi and L. T. Wang, Phys. Rev. **D91**, 095012 (2015).
410. B. Bellazzini *et al.*, Eur. Phys. J. **C74**, 2790 (2014);
F. Coradeschi *et al.*, JHEP **1311**, 057 (2013).
411. CMS Collab., *Submitted to Phys. Lett. B*, CERN-PH-EP-2015-211 (2015).
412. ATLAS Collab., Phys. Rev. **D92**, 092004 (2015).
413. CMS Collab., CMS-PAS-HIG-13-032 (2013).
414. ATLAS Collab., ATLAS-CONF-2013-027 (2013).
415. CMS Collab., CMS-PAS-HIG-13-016 (2013).
416. ATLAS Collab., ATLAS-CONF-2012-013 (2012).
417. CMS Collab., CMS-PAS-HIG-12-002 (2012).
418. CMS Collab., CMS-HIG-12-013 (2013), CERN-PH-EP/2013-011.
419. ALEPH Collab., Phys. Lett. **B526**, 191 (2002).
420. L3 Collab., Phys. Lett. **B545**, 30 (2002).
421. S. Schael *et al.*, [ALEPH, DELPHI, L3 and OPAL Collaborations and LEP Working Group for Higgs Boson Searches], Eur. Phys. J. **C47**, 547 (2006).
422. M.M. Kado and C.G. Tully, Ann. Rev. Nucl. and Part. Sci. **52**, 65 (2002).
423. OPAL Collab., Eur. Phys. J. **C23**, 397 (2002).
424. DELPHI Collab., Eur. Phys. J. **C38**, 1 (2004).
425. V.M. Abazov *et al.*, [D0 Collab.], Phys. Lett. **B698**, 97 (2011).
426. T. Aaltonen *et al.*, [CDF Collab.], Phys. Rev. **D85**, 032005 (2012).
427. V.M. Abazov *et al.*, [D0 Collab.], Phys. Rev. Lett. **104**, 151801 (2010).
428. D0 Collab., D0 Note 5974-CONF (2011).
429. ATLAS Collab., ATLAS-CONF-2012-094 (2012).
430. CMS Collab., CMS-PAS-HIG-13-021 (2013).
431. S. Chatrchyan *et al.*, [CMS Collab.], Phys. Lett. **B722**, 207 (2013).
432. CMS Collab., CMS-PAS-HIG-16-007 (2016).
433. CMS Collab., *Submitted to Phys. Lett. B*, CERN-PH-EP/2015-284 (2015).
434. J. Bernon *et al.*, Phys. Rev. **D91**, 075019 (2015).
435. ATLAS Collab., JHEP **08**, 148 (2015).
436. S. Chatrchyan *et al.*, [CMS Collab.], JHEP **09**, 029 (2012).
437. A. Djouadi, J. Ellis and J. Quevillon, `arXiv:1605.00542 [hep-ph]`(2016);
M Carena and Zhen Liu, to appear.
438. ATLAS Collab., Phys. Lett. **B744**, 163 (2015).
439. S.H. Zhu, `hep-ph/9901221` (1999).
440. H.E. Logan and S. Su, Phys. Rev. **D66**, 035001 (2002).
441. A. Gutierrez-Rodriguez and O.A. Sampayo, Phys. Rev. **D62**, 055004 (2000).
442. S. Kanemura, S. Moretti, and K. Odagiri, JHEP **0102**, 011 (2001).
443. B. Abbott *et al.*, [D0 Collab.], Phys. Rev. Lett. **82**, 4975 (1999).
444. A. Abulencia *et al.*, [CDF Collab.], Phys. Rev. Lett. **96**, 042003 (2006).
445. V.M. Abazov *et al.*, [D0 Collab.], Phys. Lett. **B682**, 278 (2009).
446. ATLAS Collab., JHEP **1206**, 039 (2012).
447. ATLAS Collab., JHEP **03**, 088 (2015).

448. CMS Collab., CMS-PAS-HIG-11-019.
449. CMS Collab., *Submitted to JHEP*, CERN-PH-EP-2015-221 (2015).
450. ATLAS Collab., *Submitted to JHEP*, CERN-PH-EP-2015-290 (2015).
451. ATLAS Collab., ATLAS-CONF-2012-010 (2012).
452. CMS Collab., *Submitted to JHEP*, CERN-PH-EP-2015-266 (2015).
453. ATLAS Collab., Phys. Rev. Lett. **114**, 231801 (2015).
454. J.F. Gunion, R. Vega, and J. Wudka, Phys. Rev. **D42**, 1673 (1990).
455. J. Abdallah *et al.*, [DELPHI Collab.], Eur. Phys. J. **C54**, 1 (2008) [E: **C56**, 165 (2008)].
456. V.M. Abazov *et al.*, [D0 Collab.], Phys. Rev. Lett. **103**, 061801 (2009).
457. R. Dermisek, Mod. Phys. Lett. **A24**, 1631 (2009).
458. J.F. Gunion, JHEP **0908**, 032 (2009).
459. U. Ellwanger, Eur. Phys. J. **C71**, 1782 (2011).
460. W. Love *et al.*, [CLEO Collab.], Phys. Rev. Lett. **101**, 151802 (2008).
461. B. Aubert *et al.*, [BaBar Collab.], Phys. Rev. Lett. **103**, 081803 (2009).
462. B. Aubert *et al.*, [BaBar Collab.], Phys. Rev. Lett. **103**, 181801 (2009).
463. V.M. Abazov *et al.*, [D0 Collab.], Phys. Rev. Lett. **103**, 061801 (2009).
464. ATLAS Collab., ATLAS-CONF-2011-020 (2011).
465. S. Chatrchyan *et al.*, [CMS Collab.], Phys. Rev. Lett. **109**, 121801 (2012).
466. ATLAS Collab., ATLAS-CONF-2012-079 (2012).
467. CMS Collab., Phys. Lett. **B752**, 146 (2016).
468. CMS Collab., JHEP **01**, 079 (2016).
469. S. Schael *et al.*, [ALEPH Collab.], JHEP **1005**, 049 (2010).
470. ATLAS Collab., ATLAS-CONF-2013-013 (2013).
471. S. Chatrchyan *et al.*, [CMS Collab.], Eur. Phys. J. **C73**, 2469 (2013).
472. ATLAS Collab., ATLAS-CONF-2012-016 (2012).
473. CMS Collab., CMS-PAS-HIG-13-014 (2013).
474. ATLAS Collab., ATLAS-CONF-2012-017 (2012).
475. ATLAS Collab., ATLAS-CONF-2012-163 (2012).
476. CMS Collab., CMS-PAS-HIG-12-024 (2012).
477. ATLAS Collab., ATLAS-CONF-2013-067 (2013).
478. ATLAS Collab., ATLAS-CONF-2012-018 (2012).
479. CMS Collab., CMS-PAS-HIG-13-008 (2013).
480. CMS Collab., CMS-PAS-HIG-12-046 (2012).
481. R. Aaij *et al.*, [LHCb Collab.], JHEP **1305**, 132 (2013).
482. ATLAS Collab., Phys. Rev. **D92**, 052002 (2015).
483. G. Aad *et al.*, [ATLAS Collab.], Eur. Phys. J. **C72**, 2244 (2012).
484. S. Chatrchyan *et al.*, [CMS Collab.], Eur. Phys. J. **C72**, 2189 (2012).
485. ATLAS Collab., CERN-PH-EP-2013-172 (2013).
486. ATLAS Collab., ATLAS-CONF-2013-081 (2013).
487. M. Carena, C. Grojean, M. Kado, and V. Sharma, *Status of Higgs boson physics*, in Review of Particle Physics, Chin. Phys. **C38** (2014) 090001.